



**Novel optical methods to monitor G-protein-coupled receptor activation in  
microtiter plates**

**Neue optische Methoden zur Messung der Aktivierung von G-Protein-gekoppelten  
Rezeptoren in Mikrotiter-Platten**

Doctoral thesis for a Doctoral degree  
at the Graduate School of Life Sciences,  
Julius-Maximilians-Universität Würzburg,  
Section Biomedicine  
submitted by

**Hannes Schihada**  
from Pasewalk, Germany

Würzburg, 2018





**Novel optical methods to monitor G-protein-coupled receptor activation in  
microtiter plates**

**Neue optische Methoden zur Messung der Aktivierung von G-Protein-gekoppelten  
Rezeptoren in Mikrotiter-Platten**

Doctoral thesis for a Doctoral degree  
at the Graduate School of Life Sciences,  
Julius-Maximilians-Universität Würzburg,  
Section Biomedicine  
submitted by

**Hannes Schihada**  
from Pasewalk, Germany

Würzburg, 2018

Submitted on: .....

Office stamp

Members of the Promotionskomitee:

Chairperson:           **Prof. Dr. Dr. Lorenz Meinel**

Primary Supervisor:   **Prof. Dr. Martin J. Lohse**

Supervisor (Second):  **Prof. Dr. Michael Decker**

Supervisor (Third):   **Prof. Dr. Michel Bouvier**

Supervisor (Fourth):  **Dr. Isabella Maiellaro**

Date of Public Defence: .....

Date of Receipt of Certificates: .....

## Affidavit

I hereby confirm that my thesis entitled “**Novel optical methods to monitor G-protein-coupled receptor activation in microtiter plates**” is the result of my own work. I did not receive any help or support from commercial consultants. All sources and / or materials applied are listed and specified in the thesis.

Furthermore, I confirm that this thesis has not yet been submitted as part of another examination process neither in identical nor in similar form.

Place, Date

Signature

## Eidesstattliche Erklärung

Hiermit erkläre ich an Eides statt, die Dissertation „**Neue optische Methoden zur Messung der Aktivierung von G-Protein-gekoppelten Rezeptoren in Mikrotiter-Platten**” eigenständig, d.h. insbesondere selbständig und ohne Hilfe eines kommerziellen Promotionsberaters, angefertigt und keine anderen als die von mir angegebenen Quellen und Hilfsmittel verwendet zu haben.

Ich erkläre außerdem, dass die Dissertation weder in gleicher noch in ähnlicher Form bereits in einem anderen Prüfungsverfahren vorgelegen hat.

Ort, Datum

Unterschrift

# **Novel optical methods to monitor G-protein-coupled receptor activation in microtiter plates**

Doctoral thesis by  
Hannes Schihada

## Abstract

G-protein-coupled receptors (GPCRs) regulate diverse physiological processes in the human body and represent prime targets in modern drug discovery. Engagement of different ligands to these membrane-embedded proteins evokes distinct receptor conformational rearrangements that facilitate subsequent receptor-mediated signalling and, ultimately, enable cellular adaptation to altered environmental conditions. Since the early 2000s, the technology of resonance energy transfer (RET) has been exploited to assess these conformational receptor dynamics in living cells and real time. However, to date, these conformational GPCR studies are restricted to single-cell microscopic setups, slowing down the discovery of novel GPCR-directed therapeutics.

In this work, we present the development of a novel generalizable high-throughput compatible assay for the direct measurement of GPCR activation and deactivation.

By screening a variety of energy partners for fluorescence (FRET) and bioluminescence resonance energy transfer (BRET), we identified a highly sensitive design for an  $\alpha_{2A}$ -adrenergic receptor conformational biosensor. This biosensor reports the receptor's conformational change upon ligand binding in a 96-well plate reader format with the highest signal amplitude obtained so far. We demonstrate the capacity of this sensor prototype to faithfully quantify efficacy and potency of GPCR ligands in intact cells and real time. Furthermore, we confirm its universal applicability by cloning and validating five further equivalent GPCR biosensors. To prove the suitability of this new GPCR assay for screening purposes, we measured the well-accepted Z-factor as a parameter for the assay quality. All tested biosensors show excellent Z-factors indicating outstanding assay quality. Furthermore, we demonstrate that this assay provides excellent throughput and presents low rates of erroneous hit identification (false positives and false negatives). Following this phase of assay development, we utilized these biosensors to understand the mechanism and consequences of the postulated modulation of parathyroid hormone receptor 1 (PTH1R) through receptor activity-modifying protein 2 (RAMP2). We found that RAMP2 desensitizes PTH1R, but not the  $\beta_2$ -adrenergic receptor ( $\beta_2$ AR), for agonist-induced structural changes.

This generalizable sensor design offers the first possibility to upscale conformational GPCR studies, which represents the most direct and unbiased approach to monitor receptor activation and deactivation. Therefore, this novel technology provides substantial advantages over currently established methods for GPCR ligand screening. We feel confident that this technology will aid the discovery of novel types of GPCR ligands, help to identify the endogenous ligands of so-called orphan GPCRs and deepen our understanding of the physiological regulation of GPCR function.

## Table of Contents

List of Figures

List of Tables

1. Introduction	12
1.1. G-protein-coupled receptors and their physiological relevance	12
1.2. Architecture of G-protein-coupled receptors	12
1.3. GPCR activation	13
1.4. GPCR classification	14
1.5. GPCR signaling and desensitization	16
1.5.1. Classical G protein-dependent GPCR signaling	16
1.5.2. Arrestin-mediated GPCR signaling & internalization	18
1.5.3. GPCR signaling from endosomal compartments	19
1.6. GPCR ligand classification	20
1.7. Physiological modulators of GPCR activation	20
1.8. GPCRs as drug targets	22
1.9. Methods in GPCR drug discovery	25
1.9.1. GPCR binding assays	26
1.9.2. Functional GPCR assays	26
1.9.3. Computer-aided GPCR drug discovery	33
1.10. Resonance energy transfer – based techniques	34
1.10.1. Principle of fluorescence resonance energy transfer	34
1.10.2. Bioluminescence resonance energy transfer	35
1.10.3. Techniques to measure RET	36
1.11. Relevance of FRET and BRET for life sciences	38
1.11.1. GPCR studies with FRET and BRET biosensors	38
1.11.2. RET-based studies of GPCR conformational dynamics	39
1.11.3. Limitations and challenges of conformational GPCR biosensors	40
1.12. Techniques for intracellular GPCR labeling	41
1.12.1. Fluorescent proteins	41
1.12.2. Bioluminescent enzymes – luciferases	42
1.12.3. Fluorescence-Arsenical-Hairpin-binder	43
1.12.4. Self-labeling protein tags	44
1.12.5. Labeling with unnatural amino acids	46
1.13. Objective of the study	47
2. Material and Methods	48
2.1. Materials	48
2.1.1. Cell lines	48

2.1.2.	Cell culture media and supplements	48
2.1.3.	Plasmids	49
2.1.4.	Primers	49
2.1.5.	Cloning enzymes	49
2.1.6.	Fluorescent antibodies	50
2.1.7.	Fluorescent SNAP-tag and HaloTag dyes and luciferase substrate	50
2.1.8.	GPCR ligands	50
2.1.9.	Comercially available kits	50
2.1.10.	Other consumables	50
2.1.11.	Plate readers	51
2.2.	Methods	51
2.2.1.	Molecular Biology	51
2.2.2.	Cell Biology	54
2.2.3.	Radioligand binding	56
2.2.4.	Biophysical methods	56
2.2.5.	Data analysis and statistics	58
3.	Results	59
3.1.	Designing an $\alpha_2AAR$ biosensor suitable for microtiter plate experiments	59
3.1.1.	Selected labeling techniques and chromophores	59
3.1.2.	Basal energy transfer of $\alpha_2AAR$ sensors	60
3.1.3.	Sensitivity of $\alpha_2AAR$ sensors to agonist stimulation	61
3.2.	Validation of the $\alpha_2AAR_{Nluc/Halo(618)}$ assay	63
3.2.1.	Ligand binding properties of $\alpha_2AAR_{Nluc/Halo(618)}$	63
3.2.2.	Optimization of the $\alpha_2AAR_{Nluc/Halo(618)}$ assay	64
3.2.3.	Kinetics of $\alpha_2AAR_{Nluc/Halo(618)}$ BRET signals	65
3.2.4.	$\alpha_2AAR_{Nluc/Halo(618)}$ reports distinct ligand efficacies and potencies	66
3.2.5.	Signaling capacity of $\alpha_2AAR_{Nluc/Halo(618)}$	68
3.3.	Transferability of the novel sensor design	69
3.3.1.	Characterization of $\beta_2AR_{Nluc/Halo}$ conformational biosensor	70
3.3.2.	Characterization of $PTHR1_{Nluc/Halo}$ conformational biosensor	73
3.4.	Evaluation of High-throughput screening suitability of GPCR biosensors	75
3.4.1.	Quality of GPCR conformational biosensor assays	76
3.4.2.	Stability of BRET signals over time	77
3.4.3.	Miniaturization of the GPCR conformation assay	78
3.4.4.	False positive screening hit rate	79
3.5.	Extending the toolbox of GPCR conformational biosensors	80
3.5.1.	Generation of the angiotensin-II-type 1 receptor biosensor	81
3.5.2.	Generation of the chemokine CXCR4 receptor biosensor	82



3.5.3.	Generation of the sphingosine-1-phosphate receptor 1 biosensor	83
3.6.	Application of GPCR biosensors to study modulatory effects of receptor activity-modifying proteins	85
4.	Discussion	88
4.1.	GPCR <sub>Nluc/Halo(618)</sub> constitutes the optimal sensor design among currently available conformational GPCR sensors	88
4.1.1.	Impact of tag positioning on results of $\alpha_{2A}AR_{\text{donor/acceptor}}$ sensor comparison	89
4.2.	BRET-based GPCR <sub>Nluc/Halo(618)</sub> biosensors constitute functional GPCR variants	90
4.2.1.	$\alpha_{2A}AR_{\text{Nluc/Halo}}$ shows wildtype-like ligand binding characteristics	90
4.2.2.	BRET-based GPCR <sub>Nluc/Halo</sub> biosensors retain signaling capacity	92
4.3.	GPCR <sub>Nluc/Halo(618)</sub> biosensors reliably report ligand efficacy and potency	94
4.3.1.	GPCR <sub>Nluc/Halo(618)</sub> faithfully reveal ligand efficacies	94
4.3.2.	GPCR <sub>Nluc/Halo(618)</sub> faithfully reveal ligand potencies	96
4.4.	Studying GPCR (de-) activation kinetics with GPCR <sub>Nluc/Halo(618)</sub> biosensors	97
4.4.1.	Stimulation of basal-state $\alpha_{2A}AR_{\text{Nluc/Halo(618)}}$	97
4.4.2.	Deactivation of active-state $\alpha_{2A}AR_{\text{Nluc/Halo(618)}}$	98
4.5.	High-throughput screening suitability of GPCR <sub>Nluc/Halo(618)</sub> biosensors	99
4.5.1.	GPCR <sub>Nluc/Halo(618)</sub> biosensors provide excellent screening windows	99
4.5.2.	GPCR <sub>Nluc/Halo(618)</sub> facilitate high data throughput	99
4.5.3.	GPCR <sub>Nluc/Halo(618)</sub> biosensors display low false positive rates	100
4.5.4.	False negative hits of GPCR <sub>Nluc/Halo(618)</sub> biosensors	101
4.6.	GPCR <sub>Nluc/Halo(618)</sub> represent reliable tools to study receptor modulators	102
4.7.	Conclusion	103
4.8.	Outlook	103
5.	Summary	104
6.	Zusammenfassung	105
7.	Annex	106
8.	Abbreviations	111
9.	References	114
10.	Curriculum vitae	140
11.	Acknowledgements	142

## List of Figures

Figure 1.1: Two-dimensional scheme of a G-protein-coupled receptor.	13
Figure 1.2: Conformational changes involved in GPCR activation.	14
Figure 1.3: GPCR-mediated G protein signaling and activation.	17
Figure 1.4: $\beta$ -arrestin-mediated GPCR regulation.	19
Figure 1.5: GPCR ligand classification.	20
Figure 1.6: Schematic structure of RAMPs.	22
Figure 1.7: Drug approvals in four major target families since 1990.	23
Figure 1.8: The current GPCR target space.	24
Figure 1.9: Refining GPCR-targeting treatments with allosteric modulators.	25
Figure 1.10: Non-imaging based $\beta$ -arrestin recruitment assays used in GPCR drug discovery.	30
Figure 1.11: Label-free assays in GPCR drug discovery.	32
Figure 1.12: Principle of the PathHunter™ assay for the study of receptor heteromerization.	33
Figure 1.13: Jablonski Diagram.	34
Figure 1.14: Excitation and emission spectra of two exemplary FRET pairs.	35
Figure 1.15: Typical FRET traces.	37
Figure 1.16: Principle of intramolecular RET-based GPCR sensors.	40
Figure 1.17: Mechanism of self-labeling protein tags.	45
Figure 1.18: Dimensions of protein tags.	46
Figure 3.1: Design of conformational $\alpha_2$ AR RET sensors.	59
Figure 3.2: Spectra of applied RET partners.	60
Figure 3.3: Basal energy transfer in conformational $\alpha_2$ AR biosensors.	61
Figure 3.4: Workflow of ratiometric RET experiments in 96-well plates.	61
Figure 3.5: Sensitivity of $\alpha_2$ AR sensors to agonist stimulation.	62
Figure 3.6: Effect of inverting donor/acceptor positions within the $\alpha_2$ AR <sub>Nluc/Halo(618)</sub> biosensor.	63
Figure 3.7: Ligand binding properties of $\alpha_2$ AR <sub>Nluc/Halo</sub> in the presence of GTP.	64
Figure 3.8: $\alpha_2$ AR <sub>Nluc/Halo(618)</sub> assay optimization.	65
Figure 3.9: Kinetics of $\alpha_2$ AR <sub>Nluc/Halo(618)</sub> BRET signals.	66
Figure 3.10: $\alpha_2$ AR <sub>Nluc/Halo(618)</sub> reports ligand- and concentration-dependent BRET signals.	67
Figure 3.11: Comparison of BRET EC <sub>50</sub> values with binding properties of $\alpha_2$ AR <sub>Nluc/Halo(618)</sub> .	68
Figure 3.12: Principle of FRET-based $G\alpha_i$ -sensor.	68
Figure 3.13: Functionality of $\alpha_2$ AR <sub>Nluc/Halo(618)</sub> .	69
Figure 3.14: Characterization of $\beta_2$ AR <sub>Nluc/Halo(618)</sub> .	71
Figure 3.15: Principle of EPAC-based H187 FRET sensor.	72
Figure 3.16: Functionality of $\beta_2$ AR <sub>Nluc/Halo(618)</sub> .	73
Figure 3.17: Characterization of PTHR1 <sub>Nluc/Halo(618)</sub> .	74
Figure 3.18: Antagonistic effect of (dW)-PTH(7-34).	74

Figure 3.19: Functionality of PTHR1 <sub>Nluc/Halo(618)</sub> .	75
Figure 3.20: Z-factors of GPCR conformational biosensor assays.	77
Figure 3.21: Time-stability of $\alpha_2$ AR <sub>Nluc/Halo(618)</sub> BRET changes.	78
Figure 3.22: Downscaling the $\alpha_2$ AR <sub>Nluc/Halo(618)</sub> assay to 384-well plates.	79
Figure 3.23: False positive screening hits generated by $\alpha_2$ AR <sub>Nluc/Halo(618)</sub> .	80
Figure 3.24: Two-dimensional illustration of wildtype AT1R.	81
Figure 3.25: Validation of the AT1R <sub>Nluc/Halo(618)</sub> biosensor.	82
Figure 3.26: Two-dimensional illustration of wildtype CXCR4.	82
Figure 3.27: Validation of the CXCR4 <sub>Nluc/Halo(618)</sub> biosensor.	83
Figure 3.28: Two-dimensional illustration of wildtype S1PR1.	84
Figure 3.29: Comparison of S1PR1 <sub>Nluc/Halo(618)</sub> biosensors.	85
Figure 3.30: Modulatory effect of RAMP2 on PTHR1 <sub>Nluc/Halo(618)</sub> dynamics.	86
Figure 3.31: Modulatory effect of RAMP2 on $\beta_2$ AR <sub>Nluc/Halo(618)</sub> dynamics.	86
Figure 3.32: Control of PTHR1 <sub>Nluc/Halo(618)</sub> expression and localization.	87
Figure 4.1: Structures of $\alpha_2$ AR ligands tested in radioligand binding experiments.	91
Figure 4.2: Model for steric effects of BRET tags on $\alpha_2$ AR conformation.	93
Figure 4.3: Technical setup for kinetic measurement with RET-based GPCR biosensors.	98
Figure 4.4: Chemical structures of false positive hits in $\alpha_2$ AR <sub>Nluc/Halo(618)</sub> assay.	101
Figure 4.5: Concept of RAMP-mediated GPCR trans-inactivation.	102

## List of tables

Table 1.1: Classification of G-protein-coupled receptors based on homology and functional properties.	15
Table 1.2: GRAFS classification of G-protein-coupled receptors based on phylogenetics.	15
Table 1.3: Classification of G proteins, involved effector proteins and intracellular implications.	16
Table 1.4: Endogenous GPCR modulators.	21
Table 2.1: Plasmids used in the course of this study.	49
Table 3.1 Analysis of ligand-dependent $\alpha_2\text{AR}_{\text{Nluc/Halo}(618)}$ BRET kinetics.	66
Table 3.2: Comparison of BRET $\text{EC}_{50}$ values with binding properties of $\beta_2\text{AR}$ wildtype.	71
Table 3.3: Comparison of BRET $\text{EC}_{50}$ values with binding properties of PTHR1 wildtype.	74
Table 3.4: Maximum BRET changes reported by $\text{AT1R}_{\text{Nluc/Halo}(618)}$ and comparison of ligand potencies reported by $\text{AT1R}_{\text{Nluc/Halo}(618)}$ with ligand binding affinities to wildtype AT1R.	82
Table 3.5: Maximum BRET changes reported by $\text{CXCR4}_{\text{Nluc/Halo}(618)}$ and comparison of ligand potencies reported by $\text{CXCR4}_{\text{Nluc/Halo}(618)}$ with ligand binding affinities to wildtype CXCR4.	83
Table 3.6: HaloTag and Nluc insertion sites in S1PR1 conformational BRET sensors.	84
Table 7.1: Resolved structures of GPCRs.	106
Table 7.2: GPCR-RAMP interactions.	108
Table 7.3: RET-based GPCR conformational biosensors.	109
Table 7.4: Pharmacological classification of GPCR ligands applied in this study.	110

## 1. Introduction

### 1.1. G-protein-coupled receptors and their physiological relevance

The ability to communicate with other individuals and respond to changing framework conditions represents the hallmark of all living things. To do so, entire organisms down to subcellular compartments of individual cells within a specific tissue need to perceive and translate external information and subsequently initiate distinct biological processes to adapt to altered environmental influences.

The plasma membrane constitutes the interface between the cell and the extracellular milieu. While the phospholipid bilayer of the plasma membrane isolates the cell interior from its surroundings, the proteins embedded in this bilayer play a key role in the communication and interaction processes between cells and their environment. These membrane proteins act like biological antennas by relaying numerous ambient stimuli to intracellular signaling cascades to provoke a global adjustment of the cell phenotype. Among the various types of membrane proteins such as ligand-gated ion channels and receptor tyrosine kinases, G-protein-coupled receptors (GPCRs) comprise one of the largest family of integral membrane proteins with more than 800 expressed genes all over the human body. They regulate a multiplicity of highly diverse cellular processes as for instance cell proliferation, differentiation and migration (Fredriksson et al., 2003). Furthermore, GPCRs play a vital role in the regulation of almost every human compartment including the central nervous system, cardiovascular system, respiratory system, immune system and skeletal system. Therefore, their malfunction or mal-regulation is implicated in genesis of myriad human disease states and scientists realized soon that restoring physiological GPCR function represents a milestone in modern medicine.

The human genome encodes at least 800 GPCRs. About half of them are olfactory GPCRs that are mainly expressed in sensory neurons of the olfactory system to facilitate the perception of odor and pheromone signaling ( $\approx 400$ ) (Mombaerts, 2004). The residual non-olfactory GPCRs act as receptors for a set of strikingly diverse physiological ligands including ions, small molecular chemical entities, lipids, peptides and even large proteins (Southan et al., 2016). However, more than 140 GPCRs ( $\approx 40\%$  of all non-olfactory GPCRs) could not yet be linked to any endogenous ligand leaving the physiological function and involvement in pathological processes of these receptors mainly in doubt. These are the so-called orphan GPCRs (Tang et al., 2012).

### 1.2. Architecture of G-protein-coupled receptors

Despite differences in function and localization within the cell, GPCRs share a common architecture. The hallmark of GPCRs is their particular structure comprising an extracellular N-terminus, 7 membrane-spanning  $\alpha$ -helices (TM1 – TM7) connected by three extra- (ecl1 – ecl3) and three intracellular loops (icl1 – icl3), and an intracellular C-terminus (**Figure 1.1**). The length of the loops or the receptors' termini can vary significantly among different GPCRs and constitutes a characteristic feature within specific GPCR families (see also section 1.4). The site of interaction between GPCRs and their endogenous ligands is called the orthosteric ligand binding pocket, a dynamic cleft allowing the engagement of structurally diverse chemical entities from the extracellular side. In most GPCRs this binding pocket is formed through interhelical interactions (such as salt bridges or dipole-dipole interactions) but it might also involve parts of the extracellular N-terminus or membrane connecting loops. The intracellular C-terminus in contrast, is important for receptor trafficking and further involved in the interplay of GPCRs with their signaling partners.

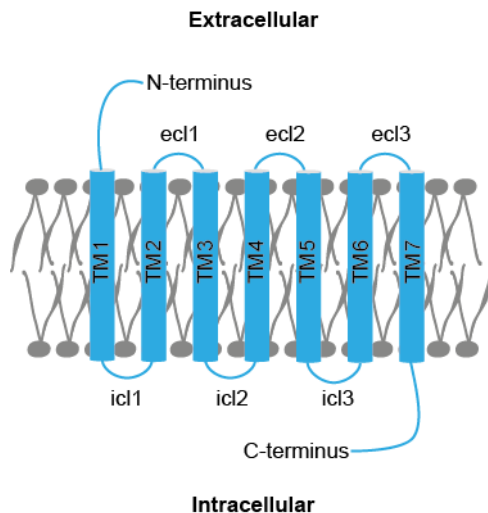


**Figure 1.1: Two-dimensional scheme of a G-protein-coupled receptor.** GPCRs are embedded in the plasma membrane of living cells and constituted of an extracellular N-terminus, seven transmembrane helices (TM1 – TM7) and an intracellular C-terminus. TM1 – TM7 are connected via three extracellular (ecl1 – ecl3) and three intracellular loops (icl1 – icl3).

### 1.3. GPCR activation

The essential role of GPCRs is to perceive extracellular stimuli and translate them to a specific cellular outcome through intracellular signaling cascades (e.g. elevation of heart rate and contractility upon  $\beta_1$ -adrenergic receptor,  $\beta_1$ AR, activation in cardiomyocytes).

Binding of a ligand (small molecules, peptides, phospholipids, etc.) present in the extracellular fluid to its cognate GPCR initiates the receptor activation process and represents the first step in the GPCR-mediated signal transduction. The GPCR ligand occupies a specific receptor binding site (also termed the binding pocket) and interacts with distinct key amino acids. This interaction locks the binding site in a specific state and subsequently triggers a global GPCR reorganization. Certain GPCRs however, exhibit unique mechanisms of interaction with their respective ligands. For instance, the well-studied ‘light receptor’ rhodopsin is covalently linked to a non-active isoform of retinal (*11-cis* retinal) at the receptor’s transmembrane bundle. Photons induce the isomerization of the *11-cis* to the *all-trans* form, the active ligand that provokes the conformational rearrangement of rhodopsin (Zhou et al., 2012).

Much effort has been made in the last decades to resolve the ensemble of conformational modifications occurring during receptor activation. In particular crystallographic GPCR studies have provided valuable insights into the movements of individual transmembrane helices. To date, more than 50 different GPCRs have been resolved in about 250 unique crystal structures – mainly of rhodopsin-like receptors (Isberg et al., 2016) (**Annex Table 7.1**). One limitation of these X-ray structures is that they reflect rather static snapshots of the examined crystalline complex but do not display possible intermediate changes that the receptor undergoes in the course of the activation process. However, comparing the structure of the same receptor bound to distinct ligands or stabilized under differential experimental conditions has deepened our understanding of the GPCR activation process and its modulation (Carpenter et al., 2016; Wacker et al., 2017b; Yao and Kobilka, 2005). For example, four different GPCRs ( $\beta_2$ -adrenergic receptor,  $\beta_2$ AR; muscarinic acetylcholine receptor 2, mAChR<sub>2</sub>;  $\mu$ -opioid receptor, MOR; adenosine A<sub>2A</sub> receptor, A<sub>2A</sub>R) have already been crystallized in both, the inactive (i.e. antagonist bound) and active (agonist bound) receptor state providing paramount knowledge on the general mechanism of GPCR activation (Carpenter and Tate, 2017; Huang et al., 2015b; Rasmussen et al., 2011). Thanks to these studies we know that GPCR activation involves a pronounced outward movement of TM3 and TM6 (TM6 movement  $\approx 14$  Å for  $\beta_2$ AR; 5Å for A<sub>2A</sub>R) resulting in a disruption of the so-called *ionic lock* (Rasmussen et al., 2011) (Carpenter and Tate, 2017) (**Figure 1.2**). This *ionic lock* is formed through intrahelical and interhelical electrostatic interactions within TM3 and between TM6 / TM3, respectively, and constrains the receptor in its inactive conformation (Ballesteros et al., 2001; Hofmann et al., 2009; Palczewski et al., 2000). The relative rearrangement of the transmembrane helices further affects the architecture of the connecting loops, especially the three intracellular loops icl1-3, and opens the receptor’s cytosolic face to create a crevice for the association of intracellular effector proteins (Choe et al., 2011).

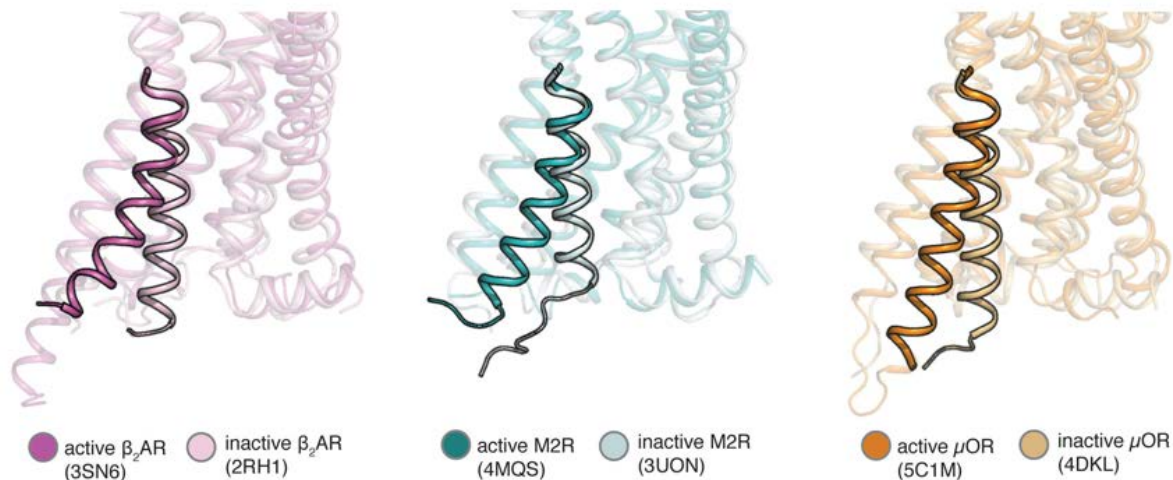


**Figure 1.2: Conformational changes involved in GPCR activation.**

Crystallographic structures of three distinct members of the rhodopsin-like GPCR superfamily depicted in both, their inactive and active conformation reveal a similar pronounced outward movement of transmembrane helix 6 (highlighted) involved in the activation process.  $\beta_2AR$  abbreviates  $\beta_2$ -adrenergic receptor, M2R is the muscarinic acetylcholine receptor 2 and  $\mu OR$  the  $\mu$ -opioid receptor (image taken and modified from (Latorraca et al., 2017) with permission from the American Chemical Society (ACS); further permissions related to the material excerpted should be directed to the ACS <https://pubs.acs.org/doi/abs/10.1021%2Facs.chemrev.6b00177>).

Initially, the scientific community envisioned a simple two-state model of GPCRs switching from a fully *inactive state*, without signaling, into a fully *active* conformation. However, the development of new outstanding biophysical methods such as nuclear magnetic resonance (NMR) spectroscopy and single-molecule microscopy have expanded this simplified concept. It is clear today that GPCRs can adopt multiple functionally distinct receptor conformations (Gregorio et al., 2017; Latorraca et al., 2017; Manglik and Kobilka, 2014). Furthermore, the discovery of the significant role of the transducer protein (e.g. the heterotrimeric G protein) in stabilizing the active conformation of the GPCR in addition to the extracellular ligand has added further complexity to the concept of GPCR activation (DeVree et al., 2016; Manglik et al., 2015).

Besides the efforts to understand its molecular mechanism, another important aspect of GPCR activation attracting wide attention from the scientific community concerns the kinetics of these processes. The majority of kinetical GPCR studies focused on rhodopsin due to several unique physiological and biochemical attributes making it a readily accessible and directly examinable GPCR. For rhodopsin's activation process, a time constant of 1.9 ms has been found for the movement of TM6 (Knierim et al., 2007). However, conformational transition of other class A GPCRs occurs in the range of 30 – 50 ms (Lohse et al., 2014) and some class B receptors require even longer time frames to complete their structural rearrangement (Castro et al., 2005; Vilardaga et al., 2003). This significant difference can either be accounted to rhodopsin's exemplary function as a sensor for fast light stimuli or be due to technical limitations in ligand delivery in the study of non-rhodopsin GPCRs. The activation process of rhodopsin can directly be triggered with a short light pulse in an experimental setup whereas cells expressing other GPCR require superfusion with ligand-containing media adding factors for sample delivery and ligand diffusion speed on the entire kinetic outcome.

#### 1.4. GPCR classification

GPCRs can be classified based on either homology and functional properties (classes A-F) (**Table 1.1**) (Attwood and Findlay, 1994) or on phylogenetic analysis of the human GPCR encoding genome (GRAFS system) (**Table 1.2**) (Fredriksson et al., 2003). In the further course of this work, the classification system based on GPCR homology and functionality is employed for simplicity.

Class	Attribution
A	Rhodopsin-like family
B	Secretin receptor family
C	Metabotropic glutamate receptor family
D	Fungal mating pheromone receptor family
E	Cyclic AMP receptor family

**Table 1.1: Classification of G-protein-coupled receptors based on homology and functional properties.**

Class	Attribution
G	Glutamate family
R	Rhodopsin family
A	Adhesion family
F	Frizzled/Taste2 family
S	Secretin family

**Table 1.2: GRAFS classification of G-protein-coupled receptors based on phylogenetics.**

In the following paragraph, class-specific features of the different GPCR families are described. **Class A GPCRs:** Rhodopsin-like receptors (class A or R, respectively) represent by far the biggest family of GPCRs with more than 700 individual proteins, about 240 of them non-olfactory receptors (Fredriksson et al., 2003). Eponym of this family is rhodopsin, a light-sensitive receptor responsible for visual photo-transduction. Rhodopsin is the first GPCR whose complete amino acid sequence has been disclosed back in the 1980s, highlighting the conjunction of seven individual transmembrane domains, and probably still represents the most extensively studied GPCR (Hargrave et al., 1983). This discovery triggered a rally of structural studies that significantly deepened our understanding of GPCRs and resulted in the first high-resolution crystal structures of this protein family in the 2000s, representing milestones in GPCR research (Jaakola et al., 2008; Palczewski et al., 2000; Rasmussen et al., 2007).

Class A GPCRs predominantly respond to small chemical entities such as adrenaline or adenosine.

**Class B GPCRs:** The family of class B GPCRs, also known as the secretin receptor family, comprises 15 distinct receptor proteins. They typically display a bulky N-terminal extracellular domain that substantially controls the ligand recognition and binding process (Castro et al., 2005; Hollenstein et al., 2014). This feature of an outwardly exposed binding pocket clearly differentiates these receptors from rhodopsin-like GPCRs that usually bind their ligands within the transmembrane region (Kratochwil et al., 2011). In contrast to class A GPCRs, Class B bind rather large peptide ligands that often exert their physiological actions in a paracrine manner.

**Class C GPCRs:** A large N-terminus involved in ligand recognition is also characteristic for class C GPCRs. This family, also known as the glutamate receptor family, comprises 15 distinct receptors that typically occur as constitutive homo- (i.e. a complex of two identical GPCRs) or heterodimers (i.e a complex of two different GPCRs) resulting in unique activation modes as compared to other GPCRs (Rondard et al., 2011).

**Class F GPCRs:** This GPCR family, also called the Frizzled/Taste2 family, has only been described in the GRAFS classification system and represents a quite exotic group of GPCRs in several aspects. 24 different receptors form this GPCR family that is activated by a unique class of GPCR ligands, the secreted lipoglycoprotein growth factors WNTs. Intriguingly, Frizzled/Taste2 receptors (FZD) are able to signal via the transcription regulator  $\beta$ -catenin (canonical WNT/FZD signaling) in addition to the classical G protein-dependent /  $\beta$ -catenin-independent pathway (non-canonical WNT/FZD signaling). Thereby, Class F receptors regulate rather GPCR-unusual signaling cascades (Katanaev, 2010).

**Adhesion GPCRs:** The adhesion GPCR family comprises 24 distinct receptors. Initially, its members have been assigned to the class B superfamily (Baud et al., 1995; Hamann et al., 1995). However in 2003, phylogenetic analysis revealed that these membrane proteins are distinct from all other G-protein-coupled receptors in several aspects (Fredriksson et al., 2003). The class owes its name to the physiological relevance for cell-cell and cell-matrix adhesion. All adhesion GPCRs display relatively large extracellular N-termini possessing multiple different functional domains (Hamann et al., 2015). Most prominent is the GPCR autoproteolysis-inducing (GAIN) domain located close to the first transmembrane helix. This region has



been identified in the great majority of adhesion GPCRs and postulated to be involved in the activation process (Arac et al., 2012).

## 1.5. GPCR signaling and desensitization

Transition of GPCRs from inactive to active states entails major conformational reorganization of the cytoplasmic side. This rearrangement gives space for the engagement of G proteins, G-protein-coupled receptor kinases (GRKs) and  $\beta$ -arrestins to couple to the receptor and transfer the encoded stimulus to further cellular signaling complexes.

### 1.5.1. Classical G protein-dependent GPCR signaling

G protein-dependent signaling is accountable for the majority of the GPCR-mediated cellular implications. Heterotrimeric G proteins consist of an  $\alpha$ - (45 kDa),  $\beta$ - (35 kDa) and  $\gamma$ -subunit (8-10 kDa) and derive from 35 different human genes (16 encoding  $\alpha$ -subunits, five  $\beta$  and 14  $\gamma$ ) (Gilman, 1987; Milligan and Kostenis, 2006; Simon et al., 1991).

G proteins transduce the information through distinct intracellular signaling pathways. According to their specific effector proteins, four major  $G\alpha$  families have been postulated:  $G\alpha_s$ ,  $G\alpha_{i/o}$ ,  $G\alpha_{q/11}$  and  $G\alpha_{12/13}$  (Downes and Gautam, 1999) (**Table 1.3**).

<b><math>G\alpha</math> class</b>	<b>Effector protein</b>	<b>Signaling outcome</b>
$G_s$	Adenylyl cyclase (AC)	Activation of AC; increase of intracellular cAMP production
$G_{i/o}$	AC	Inhibition of AC; decrease of intracellular cAMP production
$G_{q/11}$	Phospholipase C (PLC $\beta$ )	Activation of PLC $\beta$ ; production of DAG and inositol phosphates; release of $Ca^{2+}$ from intracellular stores
$G_{12/13}$	Rho-GTPase	Regulation of intracellular kinase activity

**Table 1.3: Classification of G proteins, involved effector proteins and intracellular implications.**

$G\alpha_s$  activates, whereas  $G\alpha_{i/o}$  inhibits membrane-embedded adenylyl cyclases (AC) which in turn catalyze the cyclization of intracellular adenosine triphosphate (ATP) to the second messenger cyclic adenosine monophosphate (cAMP).  $G\alpha_{q/11}$  stimulates phospholipase C (PLC $\beta$ ) and Rho guanine nucleotide exchange factors (RhoGEFs) (Kristiansen, 2004; Milligan and Kostenis, 2006) leading to consequent production of inositol-1,4,5-trisphosphat (IP $_3$ ) and its metabolites. IP $_3$  further binds to its intracellular receptor and promotes  $Ca^{2+}$  release from intracellular stores (Berridge, 1993; Hill et al., 2010; Naor, 2009; Patel et al., 2001).  $G\alpha_{12/13}$  is a well-established regulator of the GTPase RhoA that in turn controls a variety of cellular events including the formation of actin stress fibers and cell growth (Suzuki et al., 2009).

In contrast, the other constituent of the heterotrimeric G protein, the  $G\beta\gamma$ -subunit regulates other intracellular process. Collaborating as one functional protein,  $G\beta\gamma$  recruits GRKs to the membrane and regulates G-protein-coupled inwardly rectifying potassium channels (GIRKs), voltage-dependent  $Ca^{2+}$  channels, adenylyl cyclases, phospholipase C, phosphoinositide 3 kinase and mitogen-activated protein kinases (Khan et al., 2013; Smrcka, 2008).

Ultimately, GPCR activation can modulate gene transcription through elevated second messenger and stimulated effector proteins levels (Ho et al., 2009). For instance, stimulation of cAMP-activated protein kinase A (PKA) catalyzes phosphorylation of nuclear cAMP-responsive element (CRE) that in turn associates with p300/CREB-binding protein and modulates transcription of various genes (Andrisani, 1999). Despite their involvement in differential intracellular pathways, all types of G proteins share the same mechanism of activation.

Inactive-state G proteins bind guanosine diphosphate (GDP) in the guanine-nucleotide binding site within the  $G\alpha$ -subunit. This binding site is encompassed by two domains, a Ras-like GTPase domain and an  $\alpha$ -

helical domain (AHK) (Oldham and Hamm, 2006; Sprang, 1997). GPCR mediated G protein activation separates these two domains and opens an exit pathway for GDP (Noel et al., 1993; Rasmussen et al., 2011; Van Eps et al., 2011). Upon rapid GDP release, GTP engages the nucleotide-binding site due to its high intracellular concentration. This results in a rearrangement of the G protein subunits  $G\alpha$ -GTP and  $G\beta\gamma$  (Higashijima et al., 1987). The process from GPCR-G protein coupling to subunit rearrangement has been measured with about 10-times slower kinetics ( $\tau \approx 500$  ms) compared to receptor activation (Hein et al., 2006). This raises the question whether G protein activation is intrinsically slow or the rate of GPCR-G protein encounters is low (Lohse et al., 2014).

Upon G protein activation, the individual G protein subunits further modulate specific effector proteins to initiate different signaling cascades. Once the intrinsic GTPase activity of the  $G\alpha$  subunit hydrolyses GTP to GDP,  $G\alpha$  and  $G\beta\gamma$  transition back to the inactive complex resulting in the termination of G protein-mediated signaling (Hilger et al., 2018) (**Figure 1.3**). Reassembly of heterotrimeric G proteins can be accelerated by GTPase activating proteins (GAPs), such as regulators of G protein signaling (RGS), that increase the intrinsic GTPase activity of dissociated  $G\alpha$ -subunits (Kimple et al., 2011).

It is assumed that GPCRs can only bind one heterotrimeric G protein at a time. However, dissociation of the activated G protein subunits makes room for subsequent coupling of GDP-bound G proteins to the active-state receptor and leads to amplification of the agonist-mediated stimulus – a process known as signal amplification.

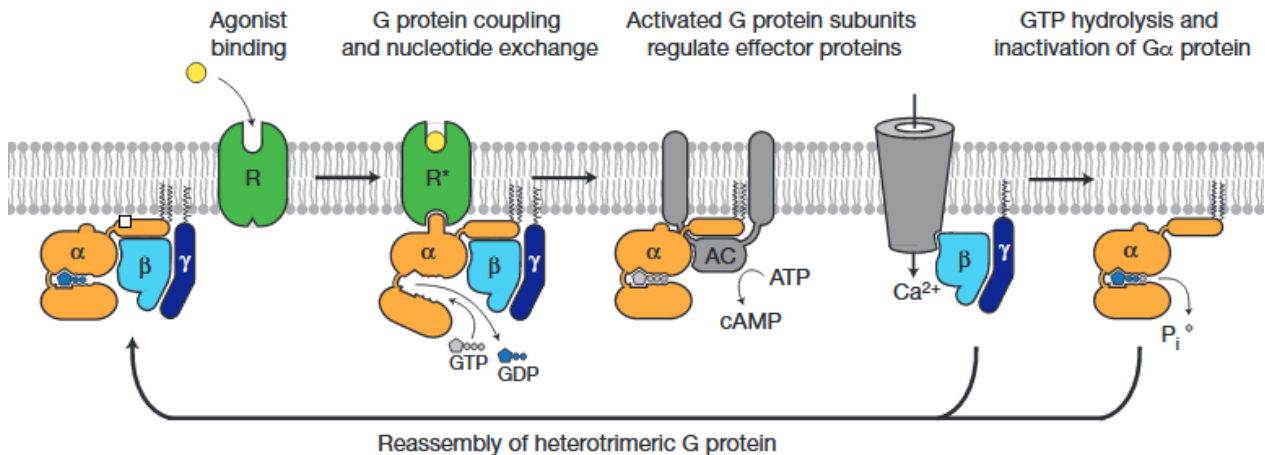


**Figure 1.3: GPCR-mediated G protein signaling and activation.**

Upon receptor coupling, conformational changes within the  $G\alpha$ -subunit of the G protein (orange) trigger the exchange of GDP for GTP and the subsequent rearrangement of the heterotrimeric G protein. The resulting  $G\alpha$  and  $G\beta\gamma$  subunits signal through different effector proteins such as adenylyl cyclases and resemble to the inactive complex upon GTP hydrolysis (extracted and modified from (Rasmussen et al., 2011) with permission from Springer Nature; license number: 4390811231504).

Up to today the dynamics of GPCR-G protein interaction and its regulation via GPCR agonists are not entirely clear and two main contrary models describing the underlying mechanisms have been postulated. First, Hein et al. hypothesized the so-called *rapid collision coupling model*. This concept claims that the ligand-free GPCR and its cognate G protein localize in distinct spots of the plasma membrane without significant precoupling and only receptor activation upon agonist binding triggers association of the two entities (Hein et al., 2005). In contrast, the *precoupling model* introduced by Galés and co-workers postulates pre-existing GPCR-G protein complexes that undergo conformational reorganization upon receptor-agonist binding (Gales et al., 2006). Both models agree that receptor ligand binding represents the central event inducing G protein activation and intracellular signaling cascades. Recent data supports a concept of GPCR-G protein interaction that can be considered a mix of those two models (Sungkaworn et al., 2017). By simultaneously recording the single-molecule trajectories of fluorescently tagged G proteins and GPCRs, Sungkaworn et al. found both, short- and long-lived complexes in agonist-free experimental conditions and that these complexes are mainly regulated by agonists at the level of  $k_{on}$  (the time constant for complex assembly).

Recent cryo-EM and crystal structures of four distinct receptors in complex with heterotrimeric G proteins

or an engineered mini-G $\alpha_s$  subunit, namely the class A receptors  $\beta_2$ AR (Rasmussen et al., 2011) and A $_2$ AR (Carpenter et al., 2016), as well as the class B calcitonin receptor (CTR) (Liang et al., 2017) and glucagon-like peptide receptor 1 (GLP1) (Zhang et al., 2017), helped understanding which protein domains are involved in the interaction of the receptor with its classical effector protein. These studies highlighted the important role of the C-terminal  $\alpha$ 5-helix of G $\alpha$  in forming an extensive interface between the G protein and mainly TM3, TM5, TM6, and intracellular loops icl2 and icl3 of the receptor and indicate a conserved interaction mechanism among class A and class B GPCRs (Hilger et al., 2018; Zhou et al., 2017b). Further analysis of receptor-G protein structures revealed specific ‘selectivity barcodes’ (that are, patterns of amino acids) presented at the different G proteins subtypes that are recognized by distinct GPCR regions and confer coupling selectivity to these GPCR-G protein pairs (Flock et al., 2017). Intriguingly, different receptors identify these barcodes through distinct amino acid residues mainly residing in the receptor’s TM5 extension and icl3, “like multiple keys (receptors) opening the same lock (G protein) using non-identical cuts” (Flock et al., 2017).

### 1.5.2. Arrestin-mediated GPCR signaling & internalization

G-protein-coupled receptors not only convey the extracellular stimulus via G protein-dependent pathways but also control a second major class of effector proteins named  $\beta$ -arrestins (Luttrell and Lefkowitz, 2002). While there are several G protein isoforms, only four arrestin family members exist. On the one hand, visual arrestin (arrestin1) (Benovic et al., 1987) and cone arrestin (arrestin4) (Craft et al., 1994) are solely expressed in rod and cone photoreceptors whereas two non-visual proteins  $\beta$ -arrestin1 (arrestin2) (Lohse et al., 1990) and  $\beta$ -arrestin2 (arrestin3) (Attramadal et al., 1992) display ubiquitous expression and regulate the function of the many hundreds of non-visual GPCRs. These four arrestin isoforms constitute a superfamily of structurally and functionally related cytosolic scaffolding proteins of  $\approx$  45 kDa. All arrestins present a distinctive organization in  $\beta$ -stranded N- and C-lobes linked by a hinge region containing the so-called gate loop (Aubry et al., 2009; Vishnivetskiy et al., 2002).

To promote GPCR- $\beta$ -arrestin coupling, GRKs initially need to associate with activated receptors and phosphorylate specific intracellular serine and threonine residues, mainly at the receptor C-terminus and icl3 (**Figure 1.4**) (Komolov and Benovic, 2018; Krasel et al., 2005; Liggett et al., 1992; Ohguro et al., 1995; PalsRylaarsdam and Hosey, 1997; Yang et al., 2015; Zhou et al., 2017a). There are seven isoforms of GRKs, each of them imprinting distinct “phosphorylation barcodes” (the specific phosphoserine-phosphothreonine pattern at the receptor) onto the receptor that favor diverse GPCR- $\beta$ -arrestin interaction patterns and elevate  $\beta$ -arrestin affinity to the GPCR (Butcher et al., 2011; Premont and Gainetdinov, 2007; Tobin et al., 2008).

A set of characteristic  $\beta$ -arrestin conformational changes upon receptor coupling have been identified. Initial breaking of  $\beta$ -arrestin’s polar core (a network of buried charged residues at the interface of the N- and C-lobe) is accompanied by a movement of the gate loop. This, in-turn facilitates subsequent wide-spread conformational changes and a  $\approx$  20° interdomain rotation. The ensemble of these modifications ultimately increases the flexibility of  $\beta$ -arrestin’s finger loop region, the key receptor binding motif, allowing it to engage the cytoplasmic crevice of the active receptor (Lee et al., 2016; Nuber et al., 2016; Scheerer and Sommer, 2017).

A wealth of biophysical studies suggests that  $\beta$ -arrestins are able to couple to the receptor in different ways. In particular, two unique GPCR- $\beta$ -arrestin complexes aroused attention in the last years due to their high relevance for intracellular signaling: In the “tail” complex,  $\beta$ -arrestins primarily interact with the phosphorylated receptor C-terminus and mediate receptor internalization but not desensitization of G protein signaling. In the “core” complex in contrast,  $\beta$ -arrestins are additionally engaged to the receptor transmembrane core where they sterically block the classical G protein binding sites within icl2 and icl3. Thereby  $\beta$ -arrestins desensitize the receptor within a timeframe of seconds to minutes for new stimulation pulses (Cahill et al., 2017; DeGraff et al., 2002; Kang et al., 2015; Lohse et al., 1990; Marion et al., 2006; Shukla et al., 2014).

In contrast to the relatively fast process of GPCR desensitization, receptor internalization represents another regulatory process that reduces GPCR signaling but occurs over minutes upon GPCR stimulation.  $\beta$ -arrestin binding to clathrin adaptor protein 2 (AP2) promotes concentration of the GPCR- $\beta$ -arrestin complex in clathrin-coated pits. Subsequently, receptors are internalized to intracellular compartments through a dynamin-dependent process (Ferguson et al., 1998; Goodman et al., 1998; Lohse, 1993). From these intracellular compartments, receptors can either initiate signaling, traffic back to the plasma membrane or

be degraded (Goodman et al., 1996; Laporte et al., 1999; von Zastrow and Kobilka, 1992) (**Figure 1.4**). In addition to their role as endocytic adaptor proteins,  $\beta$ -arrestins mediate further processes including the modulation of various kinases and regulatory proteins. For instance,  $\beta$ -arrestins promote the mitogen-activated protein kinase cascade, receptor de-/ubiquitination or route GPCRs to particular cellular loci (Berthouze et al., 2009; Chen et al., 2003; Hicke and Dunn, 2003; Kovacs et al., 2008; Lefkowitz and Shenoy, 2005; Shenoy and Lefkowitz, 2011; Shenoy et al., 2001).

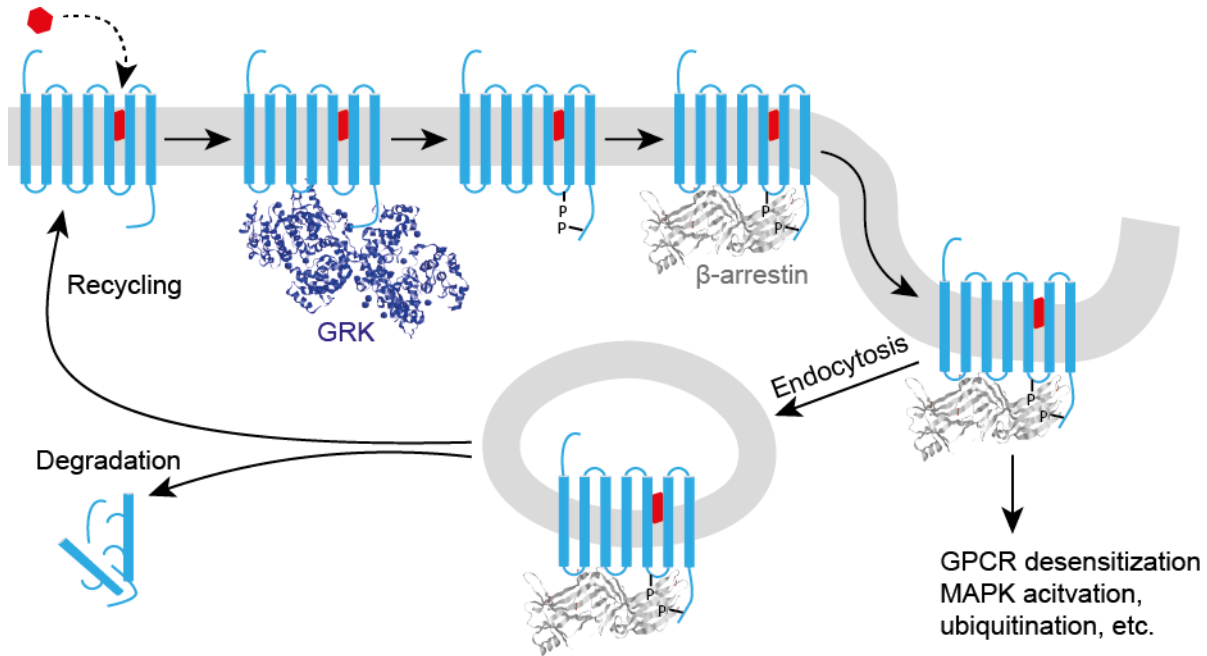


**Figure 1.4:  $\beta$ -arrestin-mediated GPCR regulation.**

GRKs phosphorylate specific receptor residues and trigger  $\beta$ -arrestin-recruitment to the active GPCR. After GPCR concentration in clathrin-coated pits, the receptor- $\beta$ -arrestin complex is internalized to intracellular membrane compartments from where they are degraded or trafficked back to the plasma membrane.

### 1.5.3. GPCR signaling from endosomal compartments

Over the last decade, the paradigm that GPCR-G protein signaling solely originates from the cell surface has been challenged by different groups.

Initial findings of persistent, internalization-dependent cAMP production mediated by some GPCRs, e.g. the thyroid stimulating hormone receptor (TSHR) and the parathyroid hormone receptor (PTHr), boosted deeper investigations questioning the classical model (Calebiro et al., 2009; Ferrandon et al., 2009; Mullershausen et al., 2009). More recently, an elegant study combining novel biosensors with structural and biophysical methods provides direct evidence for the formation of so called “megaplexes” in endosomal compartments (Namkung et al., 2016). These complexes are composed of a GPCR engaging the G protein to the receptor transmembrane core and  $\beta$ -arrestin bound to the GPCR C-terminal tail and present a physical basis for G protein signaling arising from internalized GPCRs. Moreover, the biological relevance of endosomal GPCR signaling has already been proven for two different GPCRs that regulate gene transcription and hormone function via a second wave of cyclic AMP production (Lyga et al., 2016; Tsvetanova and von Zastrow, 2014).

Taken together, these different observations elucidate that many aspects of GPCR signaling yet need to be unraveled and researchers should not hesitate to scrutinize traditional and well-accepted opinions of the scientific community.

## 1.6. GPCR ligand classification

GPCR ligands with intrinsic efficacy modulate the extent of receptor-mediated signaling through engagement of specific binding sites and stabilization of distinct receptor conformations. Full agonists induce the maximal signaling response whereas partial agonists evoke submaximal effects. In contrast, neutral antagonists solely stabilize the receptor in its basal conformation without measurable effects on signaling. Of note, the basal receptor conformation can already exhibit a certain degree of GPCR-mediated signaling – a concept termed constitutive activity - which can vary significantly between different GPCRs. Inverse agonists inhibit this constitutive receptor activity and thereby reduce the level of receptor mediated downstream signaling (Wacker et al., 2017a) (**Figure 1.5**).

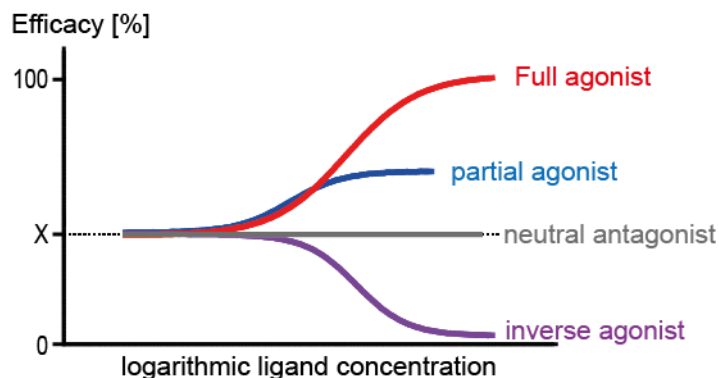


**Figure 1.5: GPCR ligand classification.**

GPCRs can occupy multiple distinct conformations and are able to signal through their effector proteins already in the basal state where no compound is bound at the extracellular side – a concept called constitutive activity. Binding of agonists increases the activity to maximal (full agonists) or submaximal (partial agonists) levels. Neutral antagonists stabilize the basal conformation of the receptor whereas inverse agonists induce a transition to a more inactive receptor conformation, thereby decreasing GPCR activity and signaling extent.

Other criteria often considered for GPCR ligand classification base on the targeted receptor binding site. Compounds engaging the same site as the endogenous agonist are so-called orthosteric ligands. By contrary, molecules engaging any receptor pocket other than the orthosteric site are termed allosteric ligands that can further be distinguished with regards to their positive (positive allosteric modulator, PAM) or negative (negative allosteric modulator, NAM) modulatory effects on affinity and efficacy of orthosteric ligands (Clark and Mitchelson, 1976; Foster and Conn, 2017; Wootten et al., 2013a). Bitopic ligands possess chemical moieties with affinities to both, the orthosteric and allosteric binding site within one chemical entity (Fronik et al., 2017; Holzgrabe and Decker, 2017; Huang et al., 2015a; Mohr et al., 2013).

Further classification of GPCR ligands refers to the different signaling pathways downstream of the receptor promoted upon binding of distinct ligands. As described in the previous section 1.5, many GPCRs are able to stimulate more than just one effector protein and thus, multiple independent intracellular signaling cascades can originate from the same receptor. Balanced ligands (such as most of the endogenous agonists) trigger the even activation of the entire signaling capacity linked to this receptor. By contrast, binding of so-called biased or functionally selective ligands increases the probability of a receptor to adapt a conformation that favors one pathway over the other(s) (Luttrell, 2014; Roth and Chuang, 1987; Smith et al., 2018). The receptor conformation stabilized by the ligand constitutes the key determinant defining whether a compound exhibits a balanced or biased signaling profile through its cognate receptor (Liu et al., 2012; Okude et al., 2015).

## 1.7. Physiological modulators of GPCR activation

Ligand-induced G-protein-coupled receptor activation can be regulated by endogenous biomolecules working as so-called GPCR modulators. These modulators control receptor function at distinct points of

intervention and have therefore emerged as potential new therapeutic targets.

Many G-protein-coupled receptors show abundant expression levels in more than one organ but, intriguingly, many receptors do not mediate the identical signaling pattern or cellular effect when stimulated in a distinct environment. For instance, stimulation of endogenous class C calcium-sensing receptors (CaSR) leads to  $G_{i/o}$ -dependent phosphorylation of the transcription factor CREB in human parathyroid cells but not in control HEK cells overexpressing CaSR (Avlani et al., 2013). Endogenous GPCR modulators that co-exist with their cognate receptors in some but not all tissues can form the basis for these tissue- and cell type-specific GPCR effects. Therefore, targeting a specific GPCR modulator might represent a beneficial strategy for the development of better-tolerated or more efficacious medical treatments.

The most obvious and best-characterized modulators of GPCRs are their cognate effectors - G proteins and  $\beta$ -arrestins. However, considerably more specific GPCR-modulator pairs have been detected with the progress in GPCR research. **Table 1.4** lists the main types of such endogenous GPCR modulators but owing to the practical relevance for this study, only the interaction of PTHR1 with receptor activity-modifying proteins (RAMPs) is described in more detail.

Type of modulator	Example	Effect of GPCR-modulator interaction	Reference
GPCR	$\beta_2$ AR + Angiotensin-II-type 1 receptor (AT1R)	Altered pharmacology, signaling and trafficking	(Prinster et al., 2005)
G protein	$\beta_2$ AR + $G_s$	Enhanced affinity of GPCR agonists	(De Lean et al., 1980)
$\beta$ -arrestin	$\beta_2$ AR + $\beta$ -arrestin2	Altered ligand affinity, GPCR de-sensitization and internalization	(Lohse et al., 1990)
Receptor activity-modifying proteins (RAMPs)	Calcitonin-like receptor (CLR) + RAMP1	Altered GPCR trafficking pattern, ligand specificity and signaling	(McLatchie et al., 1998)
Melanocortin receptor accessory proteins	MRAP1 + Melanocortin receptor 2 (MCR2)	Modulation of GPCR expression, trafficking and signaling	(Novoselova et al., 2013)
Ions	$\beta_2$ AR + $Zn^{2+}$	Altered GPCR ligand affinities	(Schetz and Sibley, 1997)
Lipids	Cannabinoid receptor 1 (CB1) + Lipoxin A4	Altered GPCR ligand affinities and receptor signaling	(van der Westhuizen et al., 2015)
Amino acids and their metabolites	CaSR + L-Phenylalanin	Alteration of agonist effects	(Agnati et al., 2006; Conigrave et al., 2000)
Peptides	mAChR <sub>2</sub> + dynorphin-A (1-13)	Alteration of GPCR ligand affinities	(van der Westhuizen et al., 2015)
GPCR-directed autoantibodies (AAB)	AT1R + anti-AT1-AAB	Stimulation or inhibition of GPCR signaling	(Venter et al., 1980)

**Table 1.4: Endogenous GPCR modulators.**

*Classification adjusted to (van der Westhuizen et al., 2015)*

RAMPs are an example of ubiquitously expressed accessory proteins that globally coevolved with GPCRs (Barbash et al., 2017). Three different subtypes, RAMP1, RAMP2 and RAMP3 have been identified. They share the same overall composition characterized by a relatively large extracellular N-terminus (91 – 95 amino acids), a single transmembrane-spanning helix and a short intracellular C-terminus (9 or 10 amino acids) (**Figure 1.6**).

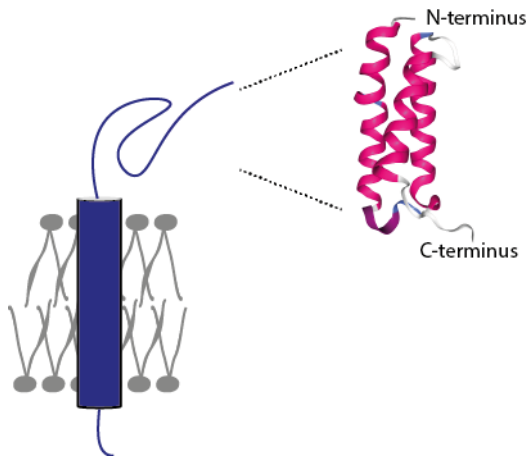


**Figure 1.6: Schematic structure of RAMPs.**

Membrane-embedded RAMPs are composed of an extracellular N-terminus, a single transmembrane helix and a short intracellular C-terminus. The inset shows the crystal structure of RAMP1's extracellular domain forming four (three vertically, one horizontally displayed) prominent  $\alpha$ -helices (purple) (PDB code: 2YX8).

Four main modulatory mechanisms of RAMPs have been postulated (Hay and Pioszak, 2016): 1) RAMPs can act as chaperones enabling correct folding and transport of GPCRs to the cell surface after protein biosynthesis. 2) GPCR-RAMP interaction can alter ligand selectivity of the receptor (so-called pharmacological switch). 3) GPCRs coupled to RAMPs can exhibit modified signaling patterns, for instance enhanced G protein but not  $\beta$ -arrestin signaling (biased signaling). 4) RAMPs can ultimately control the fate of the receptor after internalization by inducing GPCR degradation or recycling.

Under pathological conditions, any of these processes can be maladjusted and targeting clinically relevant RAMP-GPCR interactions might represent an advantageous approach to restore the physiological phenotype compared to GPCR-targeting pharmaceuticals (Sexton et al., 2012).

Initially, RAMPs were discovered as essential coupling partners for the secretin family member calcitonin-like receptor (CLR) conferring unique pharmacological properties to the particular GPCR-RAMP complex (McLatchie et al., 1998). Following this, numerous studies extended the map of GPCR-RAMP interactions to a number of 11 specific pairs as of 2016 – primarily RAMPs in complex with a secretin family GPCR (nine) (Hay and Pioszak, 2016) (**Annex Table 7.2**).

One of these secretin family GPCRs controlled via RAMPs is PTHR1. Co-expression of this target for the endogenous peptide parathyroid hormone (PTH) results in RAMP2, but not RAMP1 or RAMP3 translocation to the plasma membrane and elevation of its total cellular level (Christopoulos et al., 2003). Vice versa, absence of RAMP2 in mouse placenta diminishes PTHR1 expression, blunts response to systemic PTH administration and impairs placental development providing *in vivo* evidence for the substantial implications of GPCR-RAMP interactions for (patho-)physiology (Kadmiel et al., 2017). Despite these fascinating findings underlying the clinical relevance and mutual consequences of PTHR1-RAMP2 interaction, little is known about the mechanism of this modulation and its consequences for ligand selectivity, signaling or recycling and degradation of PTHR1.

## 1.8. GPCRs as drug targets

GPCRs have been of long-standing interest as targets for therapeutic interventions due to the extensive physiological and pathophysiological implications of GPCR-mediated signaling. Their expression at the cell surface exposes ligand binding sites to the extracellular milieu and the feature to interact with a plethora of different kinds of ligands makes them targetable by many applied pharmaceuticals. Additionally, GPCRs regulate a diverse array of intracellular signaling pathways and thus operate at the center stage in multiple different pathological processes.

In 2017, 475 ( $\approx 34\%$ ) drugs approved by the US Food and Drug Administration (FDA) exert their pharmacological effects through G-protein-coupled receptors. This accounts for a global market share of  $\approx 27\%$  (Hauser et al., 2017). The endeavor of major research institutions and pharmaceutical companies in

GPCRs as drug targets is further exemplified by the approval of 24 new GPCR addressing compounds from 2011 to 2015 (**Figure 1.7**) and 60 agents in clinical trials targeting GPCRs for which no pharmacological treatment was available by 2017 (Hauser et al., 2017; Santos et al., 2017).

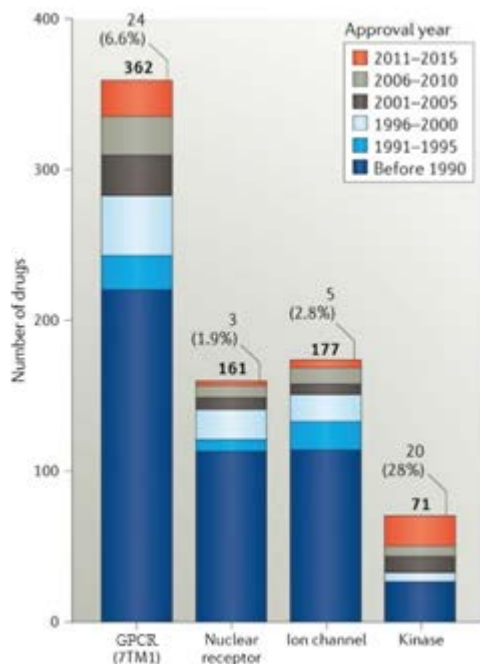


**Figure 1.7: Drug approvals in four major target families since 1990.** With 24 novel GPCR-targeting chemical entities approved between 2011 and 2015, the GPCR target family keeps attracting highest attention in drug discovery and development (extracted from (Santos et al., 2017) with permission from Springer Nature; license number: 4363631082854).

In order to launch new drugs to the healthcare market, pharmaceutical companies have to prove the superiority of novel treatment regimens over established pharmaceuticals to get the approval by healthcare authorities like FDA and EMA (European Medicines Agency; healthcare authority of the European Union). Achieving superior treatments often poses a major obstacle. Therefore, research institutions and pharmaceutical companies follow different strategies to develop beneficial drug candidates. The four major strategies in GPCR drug discovery aim to either 1) target yet untapped GPCRs, 2) reveal the pathophysiological roles of orphan GPCRs, or improve treatments addressing established GPCRs through development of 3) drugs with biased pharmacological activity or 4) allosteric modulators.

Addressing yet untapped GPCRs:

Today 475 approved drugs modulate 100 – 140 unique GPCRs, which gives an average of three to five drugs per GPCR and indicates a near saturation of the current GPCR target space (Hauser et al., 2017; Sriram and Insel, 2018). However, more than 50% of all non-olfactory GPCRs remain unexploited as pharmaceutical targets and therefore provide great potential for the discovery of novel, superior GPCR drugs. Thus, many research institutions already shifted their focus on these yet untapped receptors.

Interestingly, especially peptide- and protein-binding receptors moved into the spotlight of modern drug discovery campaigns exemplified by 37 of 66 candidates in clinical trials targeting these GPCRs (Hauser et al., 2017). This progress would not have been possible without magnificent improvements in the field of pharmaceutical technology and drug delivery (Lagasse et al., 2017) (**Figure 1.8**).



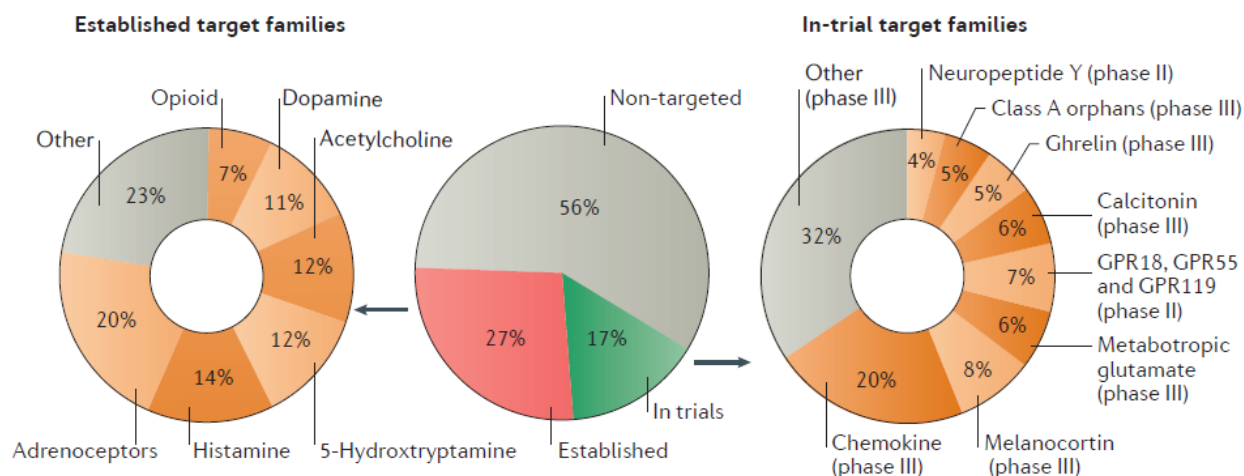


**Figure 1.8: The current GPCR target space.**

108 of all 398 non-olfactory GPCRs are targeted by approved drugs (middle, red) and further 66 have agents in clinical trials (middle, green) leaving 224 receptors yet unexploited (middle, grey). The majority of current GPCR drug targets (left) are regulated by small molecular agents whereas peptide-binding receptors are in the main focus of current clinical trials (right) (extracted and modified from (Hauser et al., 2017); reuse of article content is available under the terms of Creative Commons Attribution License).

#### Understanding the pathophysiological role of orphan GPCRs:

Related to the approach of tackling yet untouched receptors is the subject dealing with so-called orphan GPCRs – receptors for which the endogenous ligand is unknown leaving the physiological relevance of these GPCRs in doubt. The more than 140 non-olfactory orphan GPCRs encoded in the human genome are subject to fundamental research rather than drug discovery campaigns (Tang et al., 2012). Identifying their endogenous activators and understanding their biological conjunction to pathophysiological processes *in vivo* implies a significant advancement in GPCR drug discovery.

#### Establishing new drug-types – biased GPCR ligands:

Improving existing therapies by designing novel types of agents for the established GPCR target space represents another approach towards superior therapeutics.

One way to do this is to exploit the concept of GPCR biased signaling and functional selectivity. As introduced above, the concept of biased agonism describes the ability of a ligand to favor one signaling pathway over others upon binding to a G-protein-coupled receptor. Designing innovative drugs that initiate specific GPCR-mediated signaling pathways could elevate the desired pharmacological effects on the one hand, and prevent the occasion of undesired side effects on the other.

A typical illustration of such beneficial profiles of biased ligands is offered by the  $\mu$ -opioid receptor (MOR). MOR is widely distributed in the central nervous system and mainly involved in pain signaling and antinociception. Opiates (the ligands of MOR) such as morphine have been used for centuries to manage pain. Unfortunately, these traditional pharmaceuticals not only work as effective analgesics but also elicit severe side effects including tolerance and dependence, constipation and respiratory suppression. Several lines of evidence suggest that in case of MOR, analgesia is mainly G protein-mediated whereas the undesired effects are dependent on  $\beta$ -arrestin2 signaling (Bohn et al., 2000; Raehal et al., 2005). Developing compounds that selectively promote G protein over  $\beta$ -arrestin signaling could yield superior painkillers that present enhanced efficacies and reduced side effects as compared to the class-typical opioid morphine (Chen et al., 2013; Groer et al., 2007; Violin and Lefkowitz, 2007).

#### Establishing new drug-types – allosteric GPCR modulators:

Another strategy to improve established GPCR-targeting pharmacological treatments has emerged with the discovery and rising significance of allosteric modulators (Foster and Conn, 2017; Gao and Jacobson, 2013; Topiol, 2018). Synthetic allosteric modulators induce global GPCR structural transformations that yield structurally altered binding pockets and thereby positively (PAM) or negatively (NAM) fine-tune affinity and efficacy of orthosteric ligands (Figure 1.9) (May et al., 2007; Wild et al., 2014).

Allosteric modulators are of special interest for GPCRs since high selectivity of the pharmacological agent to its primary target minimizes undesired side effects. For instance, the rhodopsin-like GPCR subfamily of muscarinic acetylcholine receptors (mAChR<sub>1</sub> – mAChR<sub>5</sub>) features a large degree of homology between the five receptor subtypes - particularly in the orthosteric binding site for the endogenous ligand acetylcholine.

This fact extremely hampers the development of well-tolerated therapeutics because traditionally designed orthosteric ligands will most likely bind and regulate all five receptor subtypes, resulting in a conglomerate of desired and undesired physiological effects. However, the structure of the allosteric binding sites among the five muscarinic acetylcholine receptors is way less conserved laying the foundation for the development of subtype-selective allosteric modulators. These chemical controllers allow the specific activation or inactivation of one receptor subtype but not the others when applied alone or in combination with low doses of traditional orthosteric ligands (Bock et al., 2017; Ellis and Seidenberg, 1992). Intriguingly, recent studies show that novel bitopic ligands, composed of an allosteric and an orthosteric moiety connected by flexible linkers are able to yield subtype-selective activation of muscarinic acetylcholine receptors (Messerer et al., 2017).

Allosteric modulators can find their implications in the treatment of various types of diseases linked to GPCRs from different receptor families. For instance, the approved PAM of the class C calcium-sensing receptor cincalcet is applied to treat patients suffering from hyperparathyroidism. In contrast, maraviroc is an approved NAM of the class A chemokine CCR5 receptor used to block the entry of HIV-1 in patients with acquired immune deficiency syndrome (AIDS) (Dorr et al., 2005; Shoback et al., 2003). Moreover, allosteric modulators have been suggested as potential valuable therapeutics targeting Class B GPCRs that are difficult to modulate with classical small molecular orthosteric GPCR ligands (Wooten et al., 2017). The fact that almost 30,000 unique chemical entities are listed in the allosteric database with several PAMs and NAMs currently investigated in clinical trials raises immense hope for the future of GPCR allosteric modulators and it will be exciting to observe how this new compound class finds its way to the patient (Hauser et al., 2017; Shen et al., 2016).

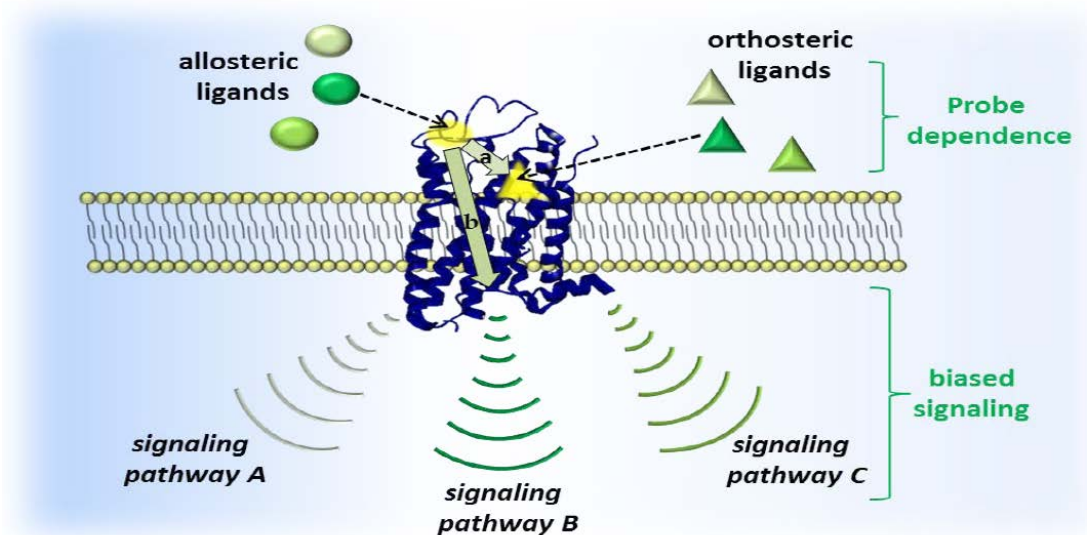


**Figure 1.9: Refining GPCR-targeting treatments with allosteric modulators.**

Allosteric ligands (spheres) bind to sites topographically distinct from the binding site for orthosteric ligands (triangles). Allosteric modulation alters affinity and/or efficacy of orthosteric ligands and potentially favors promotion of certain signaling pathways over others (biased signaling) (image taken and modified from (Wild et al., 2014) with permission from Austin Publishing Group).

## 1.9. Methods in GPCR drug discovery

Since GPCRs represent outstanding target structures for potential medical treatments, assay development and ligand screening campaigns for these proteins remain the top priority of drug discovery efforts worldwide. Two major events are currently exploited by modern GPCR screening assays: either the ligand-GPCR binding process or the intracellular downstream signals arising from receptor activation.

### 1.9.1. GPCR binding assays

Historically, the first method established to identify and quantify interaction between a molecule and a G-protein-coupled receptor was based on radioactively labeled compounds that occupy specific binding sites of a given receptor but can be displaced by non-radiative ligands with affinity to the same GPCR region (Lefkowitz et al., 1970). Initially conducted *in vivo* and with isolated organs, these experiments can also be performed in whole cell or membrane preparations with endogenous or overexpressed GPCRs.

This approach features important upsides such as its applicability to theoretically any GPCR and suitability for high-throughput formats (Glickman et al., 2008), but suffers from some significant drawbacks and limitations. Appropriate radioligands with high affinity do not exist for all GPCRs making this method practically useless for GPCR de-orphanization. Furthermore, binding assays do not directly reveal whether a compound exerts agonistic or antagonistic activity at the affiliated receptor and, most importantly, experimenters are exposed to harmful radiation. Compliance with associated regulations assuring the safety levels and environmentally friendly disposal of radioactive consumables occasions high costs and expenditure of human labor.

To overcome these drawbacks caused by the usage of radioactive material, fluorescence and luminescence based assays have been developed and up-scaled to high-throughput screening (HTS) formats (see also section 1.11) (Stoddart et al., 2015b; Zwier et al., 2010). Here, association of fluorescently labeled ligands with receptors carrying luminescent or fluorescent tags is assessed through monitoring the relative emission intensities. However, also these assays require specifically labeled ligands and, additionally, GPCRs need to be tagged with fluorescent or luminescent reporters limiting the applicability of these techniques and raising questions of how faithfully these methods report affinities of the original compounds to wildtype receptors.

### 1.9.2. Functional GPCR assays

Once a compound has been confirmed to bind to the receptor of interest, further actions are necessary to complete its pharmacodynamical picture and unveil the compound's intrinsic activity. As introduced before, ligand induced GPCR conformational changes can promote multiple distinct signaling pathways. Thus, monitoring the downstream consequences of receptor stimulation presents another approach to quantify detect GPCR-targeting compounds. These methods include the activation of effector proteins (e.g. G protein), fluctuations in second-messenger concentrations (e.g. cAMP, IP<sub>3</sub>, Ca<sup>2+</sup>) or GPCR-mediated gene transcription (e.g. through cAMP response element, CRE).

#### 1.9.2.1. G protein-dependent functional GPCR assays

##### 1.9.2.1.1. G protein activation assays

Studying the activation of the G protein itself represents a very proximal readout in GPCR drug discovery. In GTPγS binding assays, the guanine nucleotide exchange during G protein activation is directly measured by applying the radioactively labeled, non-hydrolysable GTP analogue [<sup>35</sup>S]-GTPγS to membrane preparations containing the GPCR of interest and its associated G protein (Ferrer et al., 2003; Johnson et al., 2008; Milligan, 2003). In theory, GTPγS assays can be employed to study any G protein isoform since all subtypes rely on a common activation principle. However, all GTPγS binding assays established so far exhibit relatively low signal-to-noise ratios, especially for Gα<sub>s</sub> and Gα<sub>q</sub> proteins, limiting their applicability for high-throughput screening (Zhang and Xie, 2012).

With the aim to avoid radioactive material, fluorescence-based alternatives have been developed to study this early step in GPCR signal transduction and validated for different receptors (Frang et al., 2003; Koval et al., 2010). Fluorescence (FRET) and bioluminescence resonance energy transfer (BRET) technology have been employed to develop G protein-based biosensors for Gα<sub>i</sub> and Gα<sub>s</sub> (Bunemann et al., 2003; Gales et al., 2005). These sensors rely on a combination of a fluorescent or luminescent donor transferring energy to a fluorescent acceptor as a function of the inter-fluorophore distance and relative orientation (see also section 1.10 and 1.11). Overexpression of Gα- and Gβγ-subunits tagged with these FRET-/BRET-partners allows to temporally resolve the G protein activation process in living cells. The HTS-compatibility of these

sensors has not been evaluated to date, which restricts their use mainly for fundamental research. A detailed description of the underlying principle and characteristics of these biosensors is provided in a later section of this work that is particularly devoted to FRET and BRET techniques.

#### 1.9.2.1.2. cAMP assays

Going one step further in the G protein-dependent signaling cascade, activated  $G\alpha_s$ - and  $G\alpha_i$ -subunits stimulate ( $G\alpha_s$ ) or inhibit ( $G\alpha_i$ ) membrane-bound adenylyl cyclases that in turn produce the intracellular second-messenger cAMP (Patel et al., 2001). Many commercially available kits for the assessment of cAMP capitalize on the competition between AC-derived cAMP and an exogenously introduced labeled form of cAMP for binding to an anti-cAMP antibody. These labels can be either radiometric (Butcher et al., 1965), fluorescent / luminescent (Degorce et al., 2009; Wigdal et al., 2008) or composed of a protein fragment that complements to a functional enzyme unless the labeled cAMP is not bound to the applied antibody (Weber et al., 2004).

In addition, FRET cAMP sensors have been developed. These sensors possess cAMP binding sites (e.g. based on exchange protein directly activated by cAMP, EPAC or PKA) sandwiched between two fluorophores and report variations in cAMP concentration as a change in fluorescence emission. In-depth description of the fundamental principle of FRET-based cAMP biosensors can be found in a later section of this work. These sensors resolve both, temporal as well as spatial aspects of GPCR-mediated cAMP alterations (Evellin et al., 2004; Nikolaev et al., 2004; Ponsioen et al., 2004).

Owing to the significant signal amplification generated in each step of the signaling cascade, measuring increases in cAMP concentration represents a very straightforward assay characterized by high signal-to-noise ratio. In contrast, investigation of  $G\alpha_i$ -coupled receptors through cAMP assays can be extremely difficult and often requires direct AC prestimulation (e.g. with forskolin). However, promising improvements have been made with the refinement of FRET cAMP probes that led to a new generation of superior cAMP indicators. This new sensor generation has proven valuable to directly (without forskolin prestimulation) detect decreases of basal cAMP levels in consequence of  $G_{i/o}$ -coupled receptor activation (Klarenbeek et al., 2015).

#### 1.9.2.1.3. $IP_{3/1}$ assays

$G\alpha_q$ -mediated stimulation of phospholipase C ( $PLC\beta$ ) promotes hydrolysis of phosphatidylinositol-4,5-bisphosphate ( $PIP_2$ ) and generation of the second-messengers diacylglycerine (DAG) and inositol-1,4,5-trisphosphat ( $IP_3$ ). While DAG further stimulates protein kinase C (PKC),  $IP_3$  activates the  $IP_3$  receptor localized in the endosomal membrane inducing efflux of  $Ca^{2+}$  ions from the endoplasmic reticulum (ER) and consequent elevation of intracellular  $Ca^{2+}$  levels. However,  $IP_3$  is also substrate to rapid enzymatically catalyzed degradation resulting in the intermediate products  $IP_2$ ,  $IP_1$  and finally inositol (Berridge, 1993). Radioactive assays have first been developed to assess  $IP_3$  accumulation based on [ $^3H$ ]inositol incorporation (Berridge, 1993) but this method does not allow high-throughput in its original version and advanced assay modifications still suffered from low practicability (Brandish et al., 2003). To overcome these limitations, a fluorescence-based alternative that makes use of a specific antibody in combination with the inhibitory action of lithium on  $IP_1$  degradation through inositol monophosphatase has been developed and optimized to HTS-compatibility (Trinquet et al., 2006).

#### 1.9.2.1.4. $Ca^{2+}$ assays

Assays to measure intracellular  $Ca^{2+}$  levels constitute one of the most common methods in GPCR drug discovery due to their high sensitivity and HTS-suitability. In general, there are two major types of  $Ca^{2+}$  indicators.

1) Fluorescent dyes such as FURA-2AM are loaded to the sample and display alterations of their spectral properties as a function of  $Ca^{2+}$  concentration whereas 2) genetically encoded photoproteins like aequorin and GCaMPs can be targeted to specific subcellular compartments and exhibit strong luminescent signals

upon  $\text{Ca}^{2+}$  binding (Eglen and Reisine, 2008; Tsien, 1980). Both techniques facilitate robust and easily amenable calcium measurements. Unfortunately, the rapid and transient nature of the calcium signal impedes the investigation of slow-binding agonists and one should consider an  $\text{IP}_{3/1}$  assay as the preferred readout for such kind of ligands (Zhang and Xie, 2012).

#### 1.9.2.1.5. Reporter gene assays

G-protein-coupled receptor signaling ultimately modulates gene expression through distinct pathways. Therefore, scientists have developed so-called reporter gene assays (e.g. One-Glo™ Luciferase Assay from Promega, Twinlite Reporter Gene Assay from Perkin Elmer) to quantify altered gene expression upon GPCR stimulation. This technique couples GPCR-mediated elevation of protein expression to simultaneous promotion of cellular reporter enzyme biosynthesis (Cheng et al., 2010; Conway and Demarest, 2002; Fan and Wood, 2007; Kunapuli et al., 2003). Subsequently, activity of the reporter enzyme is quantitated through luminescence or fluorescence emission intensity. These assays provide high sensitivity and signal-to-noise ratio allowing the identification of even weak partial agonistic responses and scalability to 1536- and 3456-well formats (Conway and Demarest, 2002; Kornienko et al., 2004). However, recoding such a distal signaling event bears important weaknesses that should be taken into consideration. First, antagonistic effects are often difficult to detect due to reporter gene accumulation in the cell. Additionally, long incubation times required to finalize the gene translation process reduce assay throughput and, most importantly, the rate of false positives resulting from the compound's involvement in other signaling pathways is often much higher compared to more proximal readouts.

#### 1.9.2.1.6. Limitations of G protein-dependent functional GPCR assays

A more general issue of second-messenger and reporter gene assays is that one needs to know which signaling pathways are associated with this specific GPCR of interest. This prerequisite excludes their applicability for the investigation of many orphan GPCRs. Additionally, measuring effects of a compound at the second-messenger level of one specific signaling cascade downstream the receptor entails an increased risk of false negative results due to biased signaling. For example, an industrial drug discovery campaign that aims to identify lead compounds stimulating AT1R initially applies an assay reporting intracellular accumulation of the second-messenger  $\text{IP}_3$ . However, during this first screening cycle, biased agonists that result in stimulation of  $\beta$ -arrestin or  $\text{G}\alpha_i$  but not  $\text{G}\alpha_q$ -mediated signaling are mistakenly considered as “non-activators” and eventually no more examined in subsequent screenings (Holloway et al., 2002; Ikeda et al., 2015). On the contrary, biased ligands can also serve as superior drugs with less side effects and pharmaceutical companies might be interested in exclusively detecting compounds that solely modulate one specific pathway downstream the receptor. In this case, combining e.g. a basic binding assay to a specific second-messenger readout provides a straightforward approach towards identification of novel biased GPCR agonists.

#### 1.9.2.2. G protein-independent functional GPCR assays

In addition to G protein-dependent assays, techniques that report GPCR activation as a function of G protein-independent cellular effects constitute the second important pillar of GPCR screening assays.

##### 1.9.2.2.1. $\beta$ -arrestin recruitment assays

As described earlier, GRKs phosphorylate agonist-occupied GPCRs resulting in  $\beta$ -arrestin recruitment to the plasma membrane, interaction with the phosphate-labeled receptors and  $\beta$ -arrestin-mediated receptor desensitization, internalization and/or signaling.

The event of  $\beta$ -arrestin recruitment to the membrane represents an early step within the  $\beta$ -arrestin signaling cascade and downregulation of GPCR signaling that can be monitored using several imaging-and non-

imaging-based approaches.

Imaging-based  $\beta$ -arrestin recruitment assays: Historically, the first commercialized  $\beta$ -arrestin recruitment assay requires the expression of  $\beta$ -arrestin tagged with the green fluorescent protein (GFP) (Oakley et al., 2002). Upon GPCR agonist binding, redistribution of fluorescently labeled  $\beta$ -arrestin can be visualized and quantitated using different high-content imaging systems (Eggeling et al., 2003; Garippa et al., 2006; Haasen et al., 2006b). Due to strict requirements of employed cell lines (strong adherence and large cytosol-to-nucleus ratio (Zhang and Xie, 2012) alternative assays that do not necessitate image-based monitoring of  $\beta$ -arrestin translocation have been developed.

Non-Imaging-based  $\beta$ -arrestin recruitment assays: The Tango™ GPCR Assay System, for instance, correlates increases in reporter gene expression with elevated GPCR- $\beta$ -arrestin interaction upon compound treatment (**Figure 1.10A**) (Barnea et al., 2008; Hanson et al., 2009). In order to make this possible,  $\beta$ -arrestin is fused to tobacco etch virus (TEV) protease and artificially expressed in cells. Additionally, the GPCR of interest is extended at its C-terminus with a specific protease cleavage site followed by the transcription factor Gal-VP16. Once the protease-tagged  $\beta$ -arrestin and the receptor come into close proximity, the TEV protease releases the transcription factor that is ready to enter the nucleus and induce reporter gene transcription.

Another example for a non-imaging-based  $\beta$ -arrestin recruitment method is the PathHunter™ assay marketed by DiscoverX (Yin et al., 2009; Zhao et al., 2008). Here, the recovery of  $\beta$ -galactosidase enzyme functionality upon association of tagged  $\beta$ -arrestin / GPCR fusion proteins results in complementation of two  $\beta$ -galactosidase fragments (**Figure 1.10B**). Subsequently, the functional  $\beta$ -galactosidase catalyzes cleavage of an exogenously applied substrate resulting in chemiluminescent emission. This assay has been applied for the study of various GPCRs and found its way into both, academic and industrial GPCR research (Zhang and Xie, 2012).

Further assays that allow the quantification of  $\beta$ -arrestin recruitment rely on two fluorophore partners fused to interacting proteins that are able to exchange energy as a function of their relative distance and orientation. This principle represents the main background of this doctoral thesis and is described in a separate chapter in particular detail.

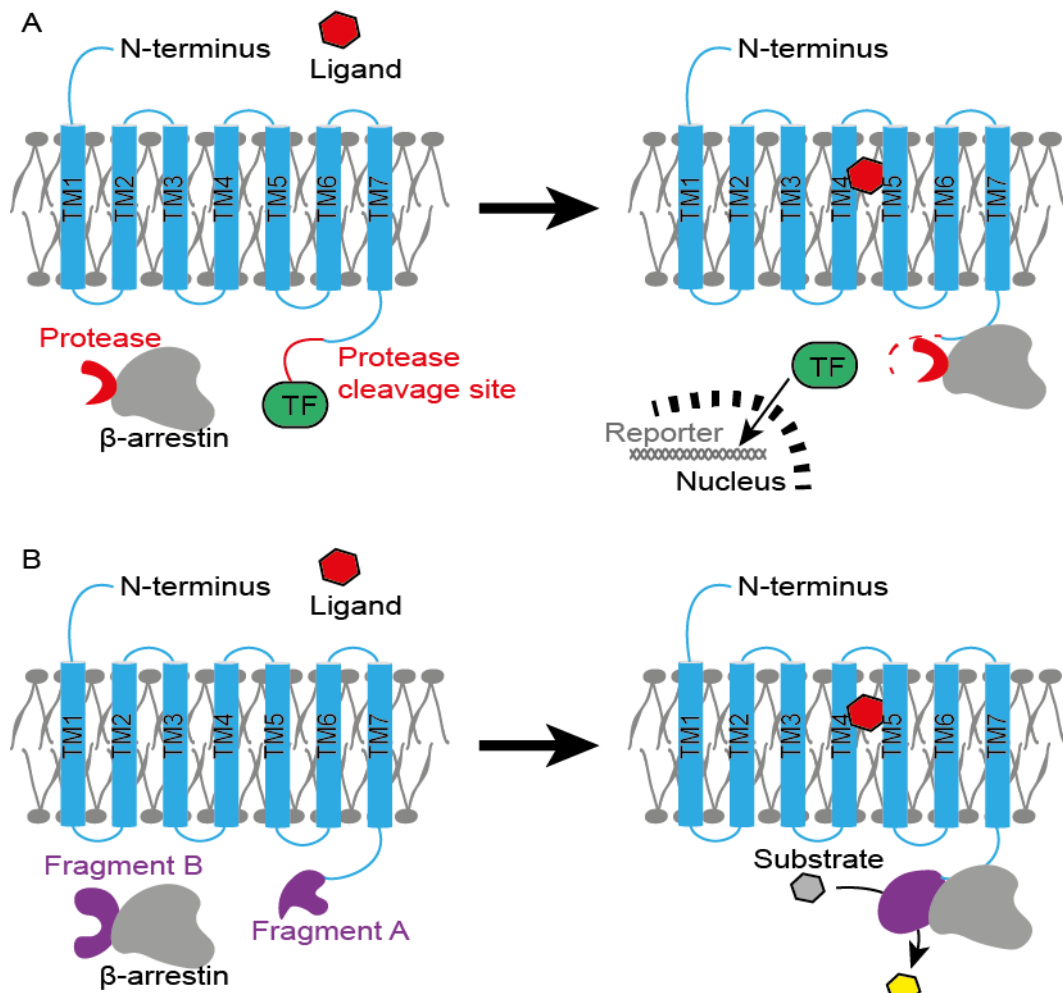


**Figure 1.10: Non-imaging based  $\beta$ -arrestin recruitment assays used in GPCR drug discovery.**

A) A  $\beta$ -arrestin-protase fusion protein translocates to the plasma membrane upon GPCR activation and cleaves the transcription factor (TF) from the tagged GPCR. Subsequently, TF enters the nucleus to promote transcription of a reporter gene. B)  $\beta$ -arrestin and the GPCR are conjugated to complementary fragments of  $\beta$ -galactosidase. Upon GPCR- $\beta$ -arrestin interaction, the fragments resemble to a functional enzyme that cleaves the enzyme substrate and generates a chemiluminescent signal (adapted from (Zhang and Xie, 2012)).

#### 1.9.2.2.2. Receptor trafficking assays

GPCR- $\beta$ -arrestin interaction promotes specific signaling cascades and, moreover, represents an essential mechanism to prevent GPCR-mediated overstimulation of the cell by pulling activated receptors from the cell surface to intracellular compartments, a concept defined as receptor trafficking.

Owing to the G protein-independent nature of this process, receptor trafficking assays can be applied to monitor receptor activation without any prior knowledge about further – mainly G protein-dependent – signaling events mediated by the GPCR of interest. This feature makes internalization assays an indispensable technique for GPCR de-orphanization (Zhang and Xie, 2012). Similarly to the recruitment of  $\beta$ -arrestin, receptor trafficking is monitored using either imaging-based or non-imaging-based techniques.

**Imaging-based GPCR trafficking assays:** For imaging-based approaches, actions need to be taken to stain the receptor of interest. The emergence of fluorescent GPCR ligands in the 1970s and ongoing improvements in ligand affinity and specificity have provided useful tools to visualize the internalization of ligand-bound receptors (Kuder and Kiec-Kononowicz, 2008; Middleton and Kellam, 2005). Immunofluorescence labeling with receptor-specific antibodies represents an alternative, however time consuming and expensive approach to visualize receptors of interest if e.g. no specific fluorescent ligands are available (Hislop and von Zastrow, 2011). Therefore, a primary antibody directed against an extracellular

epitope of the receptor is co-internalized upon agonist binding and visualized with the use of a fluorescent secondary antibody. In contrast, tagging the receptor with fluorescent proteins provides the most convenient method to visualize GPCR internalization processes and is therefore commonly used in large library screening campaigns (Haasen et al., 2006a). For instance, unsaturated long-chain free fatty acids have been identified as the endogenous ligands of GPR120 by applying a fusion protein of this receptor with the fluorescent protein enhanced green fluorescent protein (EGFP) (Hirasawa et al., 2005).

Comparable to methods used to monitor  $\beta$ -arrestin recruitment, non-imaging-based systems for GPCR internalization rely on either energy transfer between two fluorophores or complementation of two protein fragments yielding functional enzymes (Hammer et al., 2007; Namkung et al., 2016). In either case, one of the partnering structures is fused to the receptor under investigation whereas the other has to be anchored to a specific cellular compartment. For example, the FYVE domain of endofin is able to target fluorescent proteins or enzyme fragments to early endosomes – a very common destination of GPCRs during the internalization processes (Burd and Emr, 1998; Irannejad and von Zastrow, 2014).

### 1.9.2.3. Label-free GPCR assays

Label-free assays cover a greatly different chapter of whole-cell GPCR assays. These methods have emerged over the last decade and follow a different strategy to detect GPCR activation. Whereas all previously described methods focus on individual cellular events (e.g. increases in intracellular cAMP levels), label-free assays detect the ensemble of GPCR-mediated intracellular responses by measuring global cellular properties such as cell adhesion and morphology (Scott and Peters, 2010). To this end, biosensors are employed that convert the summation of intracellular effects into quantifiable, most commonly electrical or optical signals. Hereafter, the two main types of label-free biosensors frequently employed for GPCR drug discovery are described.

**Impedance-based biosensors:** These biosensors provide an electrical readout that requires culturing of cells on small gold electrodes (**Figure 1.11**). Following this, cells impede the flow of a weak alternating current (0.1 V at 4 kHz) as a function of cellular motion or morphological modifications (Giaever and Keese, 1984; Giaever and Keese, 1991). This method has been successfully utilized to study the pharmacological modulation of different G-protein-coupled receptors including proteinase-activated receptor 1 (PAR1) and sphingosine-1-phosphate receptor 1 (S1PR1) (McLaughlin et al., 2005; Waters et al., 2006).

**Optic-based biosensors:** On the other hand, resonant waveguide grating (RWG) biosensors convert the summation of cellular events into an optical response. Grating surfaces embedded in the bottom of microtiter plates reflect narrow bands of light that are characteristic for the refractive index of the attached sample upon illumination with white light (**Figure 1.11**). Alterations of intracellular concentrations of biomolecules (also referred to as “dynamic mass distribution”) within the penetration depth of the biosensor ( $\approx 150$  nm), as well as morphological adaptations of cultured cells affect the refractive index of the sample and lead to hypsochromic or bathochromic shifts of the reflected light (Cunningham et al., 2004). This optic-based, label-free whole cell assay has been shown to be capable to monitor the activation of different endogenously expressed GPCRs and intriguingly, the optical signature provides information on the preferred G protein-coupling of the receptor of interest (Fang et al., 2007).

A great advantage of label-free whole-cell assays is that they do not require artificial modification of the GPCR and allow the investigation of activation / modulation without receptor overexpression warranting a more natural environment. Although sensitivity and precision of label-free assays support their utilization for high-throughput campaigns, high costs for consumables and comparably great numbers of false positives and false negatives due to GPCR signaling through pathways that neutralize each other might limit their broader application (Peters et al., 2010).



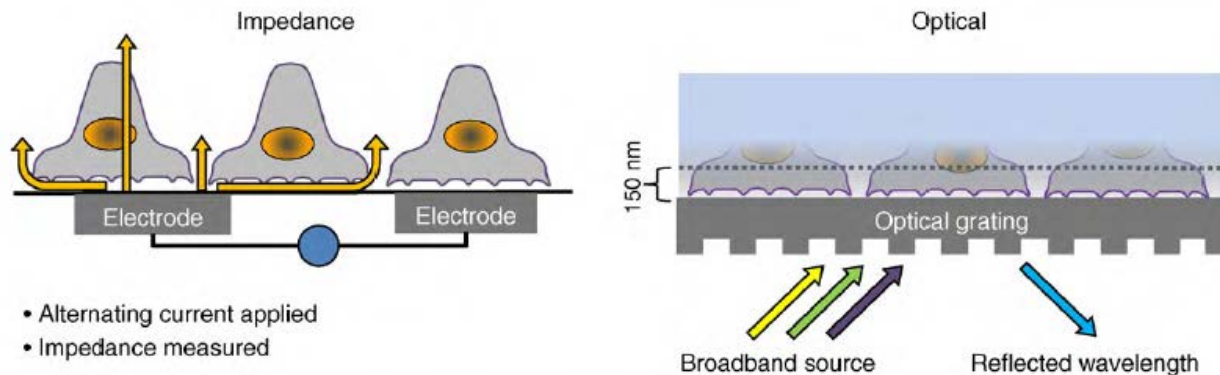


**Figure 1.11: Label-free assays in GPCR drug discovery.**

Concept of label-free impedance- and optic-based biosensors. Cells cultured on impedance biosensors (left) impede the current flow across two electrodes mounted in the bottom of the microtiter well as a function of e.g. cell morphology and adhesion. Optical biosensors (right) detect hypsochromic and bathochromic shifts of light reflected by a grating surface at the bottom of the microtiter well (extracted from (Scott and Peters, 2010) with permission from Elsevier; license number: 4363650406075).

#### 1.9.2.4. GPCR dimerization assays

Many G-protein-coupled receptors have been shown to form dimers and even higher-order oligomers at the surface of living cells and some of them (e.g. all class C members; see also section 1.4) are only functional when occurring in a well-defined aggregate with an interacting protomer (Bouvier, 2001; Milligan, 2004). These complexes constitute distinct biological entities that play significant roles in diverse (patho-) physiological processes and thus, should be considered as unique potential drug targets (Rozenfeld and Devi, 2011; Rozenfeld et al., 2011).

In order to identify a potential drug candidate modulating dimerization or oligomerization of a specific GPCR, assays that uncover the assembling and disassembling process are required. FRET- and BRET-based approaches are commonly used to study GPCR dimerization patterns and described in a separate chapter devoted for these techniques.

Another method to monitor receptor dimerization events combines the aforementioned enzyme-fragment-complementation based  $\beta$ -arrestin recruitment with the application of receptor subtype selective GPCR ligands (**Figure 1.12**). Significant chemiluminescent emission upon selective pharmacological stimulation of untagged GPCR proofs the direct interaction between the co-expressed GPCR protomers via a transactivation mechanism (Zhang and Xie, 2012).

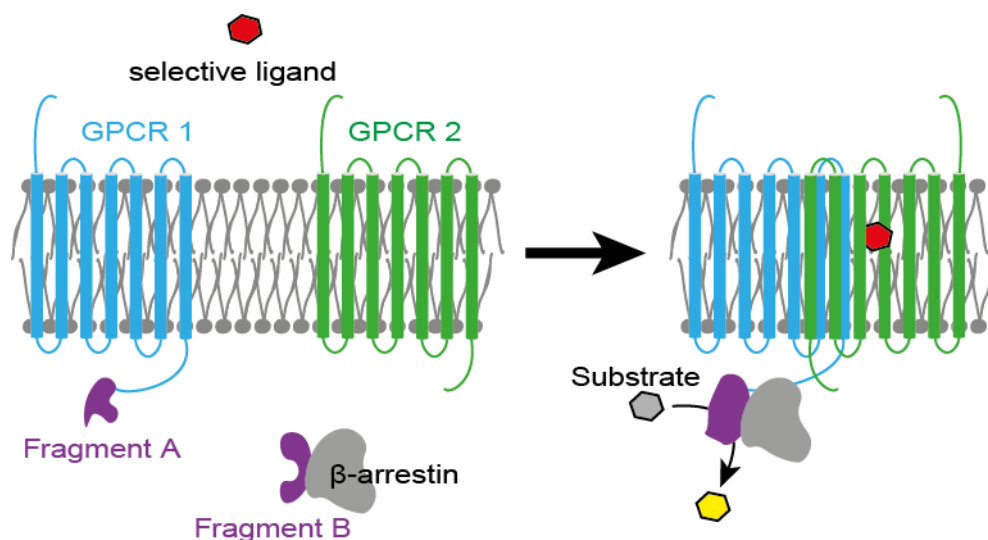


**Figure 1.12: Principle of the PathHunter™ assay for the study of receptor heteromerization.**

The enzyme  $\beta$ -galactosidase is split into two fragments (purple) that are fused to  $\beta$ -arrestin and one of the GPCRs (blue), respectively. Upon stimulation of the second untagged receptor (green) with a selective GPCR ligand (red), both protomers associate and the transactivation process promotes  $\beta$ -arrestin recruitment to the tagged GPCR and subsequent enzyme fragment complementation resulting in emission of chemiluminescent light.

### 1.9.3. Computer-aided GPCR drug discovery

GPCR drug discovery usually bases on the employment of primary biochemical and pharmacological assays in high-throughput formats for initial hit identification and subsequent lead optimization (i.a. improvement of critical physicochemical and pharmacological properties such as water solubility and off-target affinities, respectively) to develop potential drug candidates (Keseru and Makara, 2006). However, the emergence and maturation of computational methods facilitates their progressive application in early-stage compound screening. Combining laboratory and computational techniques reduces time and costs for the entire screening campaign since probable positive or negative compounds can be identified beforehand reducing the number of compounds that remain to be experimentally tested.

Structure-based *in silico* screening relies on 3-dimensional information on the target receptor (Heifetz et al., 2016). Significant advances in protein engineering, X-ray crystallography and - most recently – cryo-EM have provided an enormous growth of knowledge on GPCR structure and receptor-ligand interactions (Chun et al., 2012; Serrano-Vega et al., 2008; Thal et al., 2018). Additionally, in the absence of detailed structural information on the receptor under investigation, homology modeling based on sequence alignments to a template GPCR structure can be performed to establish reliable model systems for molecular simulations (Ciancetta et al., 2015). Once an appropriate receptor structure has been selected, interaction patterns between the virtual ligand and the amino acid residues or water molecules within the receptor binding site can be explored through molecular dynamics (MD) simulations and can be further used to score the tested molecule and estimate its binding affinity and efficacy (Heifetz et al., 2016; Kolb et al., 2009). However, it has to be noted that these approaches are subject to certain restrictions. Any model applied for the computational simulations can only be as good as the experimental structural data that it relies on. Thus, not only homology models but also X-ray crystal structures may introduce large degrees of error probability since these structures have been achieved through significant protein modifications (e.g. insertion of fusion proteins that allow for crystallization) and solely represent snapshots of the receptor structure but do not depict its conformational dynamics (Rosenbaum et al., 2009).

In the absence of sufficient structural data to create adequate models serving as templates for MD simulations (which is an issue arising for many GPCRs), ligand-based computational approaches remain the method of choice to evaluate large libraries of potential GPCR ligands. This technique capitalizes on the knowledge of chemical entities that evidentially bind to the target structure. These molecules are explored to identify key chemical moieties (the pharmacophores) accounting for receptor affinity and to correlate these chemical descriptors with the pharmacological activities of the ligands – a procedure termed quantitative structure activity relationship (QSAR) (Acharya et al., 2011; Aparoy et al., 2012). Subsequently,

these findings are combined to generate predictive models allowing for virtual design of novel GPCR ligands.

## 1.10. Resonance energy transfer – based techniques

### 1.10.1. Principle of fluorescence resonance energy transfer

Fluorescence resonance energy transfer (FRET) has first been described by Theodor Förster in 1946 and is therefore often also referred to as *Förster* resonance energy transfer (Forster, 1946). As indicated, FRET is a fluorescence-based physical phenomenon. Fluorescence relies on the capability of a ground singlet state ( $S_0$ ) electron in the highest occupied molecular orbital (HOMO) to transition to the excited state ( $S_1$ ) lowest unoccupied molecular orbital (LUMO) of a fluorescent molecule while maintaining its singlet nature (singlet-singlet transition). This electron relaxes from higher energy  $S_1$  states ( $S_1$ ) via internal relaxation until it falls back to the ground state by delivering the excessive energy as light of a characteristic wavelength. In FRET however, the  $S_1$  donor electron transfers energy to a proximally situated ground-state acceptor fluorophore via dipole-dipole interaction (**Figure 1.13**). The resonance energy transfer (RET) results in concerted quenching of the donor fluorescence intensity and excitation of the acceptor that can but does not has to emit photons of a characteristic wavelength.

The efficiency of energy transfer ( $E$ ) of a given donor-acceptor fluorophore pair is a quantitative measure of the transferred energy from donor to acceptor and determined by several parameters (Clegg, 1995).

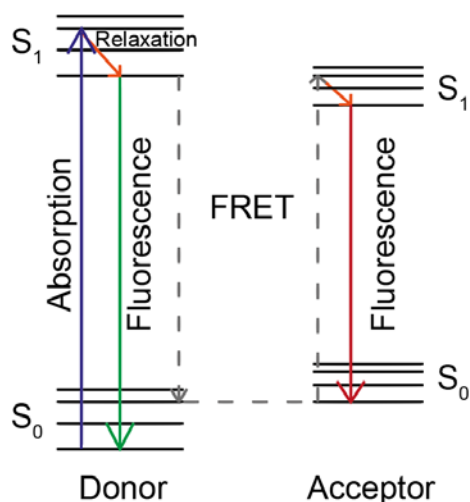


**Figure 1.13: Jablonski Diagram.**

Energy absorption of an orbital electron of the donor fluorophore lifts it from the ground state ( $S_0$ ) to the first excited singlet state ( $S_1$ ). After relaxation to a lower energy  $S_1$ -state, the electron can come back to the ground state by emission of photons (fluorescence) or transfer energy to the ground state acceptor molecule ( $S_0$ ) via FRET. The excited acceptor electron reaches  $S_1$  and emits photons of a specific longer wavelength.

Resonance energy transfer (RET) only occurs if the distance between the interacting partners ranges from 1 to 10 nm (Wu and Brand, 1994). Furthermore, the spectral overlap of donor emission and acceptor excitation spectra represents an essential requirement for RET to occur and highly affects the RET efficiency of a given donor-acceptor pair (**Figure 1.14**). Due to the broad emission spectra of most donor fluorophores applied in biological research, a plethora of different donor-acceptor combinations should in theory result in detectable RET efficiencies. Further properties that influence RET efficiency are the donor's quantum yield ( $Q_D$ ) - a measure of the efficacy of a fluorophore to convert absorbed to emitted photons - and the acceptor's extinction coefficient ( $\epsilon_A$ ) that quantifies the ability to absorb energy (Clegg, 1995).

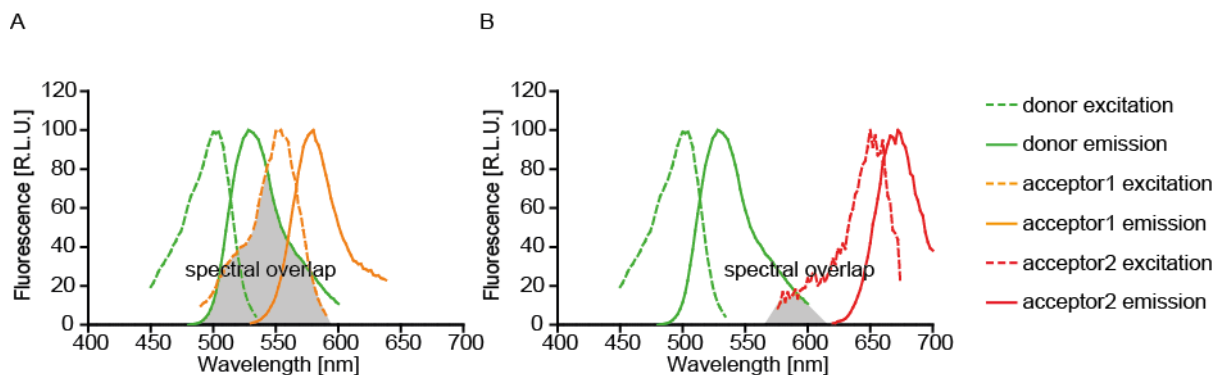


**Figure 1.14: Excitation and emission spectra of two exemplary FRET pairs.**

A) The combination of a green-light emitting donor with an orange-light emitting acceptor fluorophore results in large overlap of donor emission and acceptor excitation (gray area). B) The combination of the same green-light emitting donor to a more-red shifted fluorescent acceptor substantially decreases the spectral overlap of donor emission and acceptor excitation resulting in reduced resonance energy transfer.

These physical properties in combination with the relative dipole-dipole orientation ( $\kappa^2$ ) of combined RET partners determine the Förster radius  $R_0$ .  $R_0$  describes the distance between donor and acceptor that results in half-maximal non-radiative energy transfer and can be calculated from the physicochemical properties as follows (Sapsford et al., 2006):

$$R_0 = 9.78 * 10^3 * \sqrt[6]{[\kappa^2 n^{-4} Q_D J(\lambda)]} \text{ (in \AA)} \quad (1)$$

The orientation factor  $\kappa^2$  ranges in value from 0 (perpendicular orientation of RET partners) to 4 (parallel orientation). Although there is no reliable method to precisely assess  $\kappa^2$  values of RET probes in biological samples and predict its outcome on RET efficiency, accumulated evidence shows that  $\kappa^2$  approximates 2/3 in biological samples with fluorescent dyes that rotate freely in timescales significantly shorter than the excited state lifetime of the RET donor (Stryer, 1978). The factor  $n$  defines the refractive index of the medium and equals 1.4 for biomolecules in aqueous solution.  $J(\lambda)$  describes the overlap integral that increases with higher  $\epsilon_A$  and spectral overlap of donor emission and acceptor excitation (Sapsford et al., 2006).

The knowledge of  $R_0$  for a particular donor-acceptor combination allows the exact calculation of the RET efficiency as a function of the distance between the interacting fluorophores:

$$E = \frac{1}{1 + \left(\frac{R}{R_0}\right)^6} \quad (2)$$

Equation 2 highlights that RET efficiency is proportional to the inverse sixth power of the distance between the fluorophores. Owing to the sigmoidal relationship between FRET efficiency and inter-fluorophore distance  $R$ , the dynamic range of the RET efficiency is highest when  $R$  approximates  $R_0$  – an observation that should be considered when RET-based sensors for biological research are designed (Bajar et al., 2016).

### 1.10.2. Bioluminescence resonance energy transfer

Bioluminescence resonance energy transfer (BRET) describes the luminescent, naturally occurring analogue of FRET and has been discovered in a variety of organisms such as *Aequorea*, *Obelia*, *Phialidium* and *Renilla* (Lorenz et al., 1991; Morin and Hastings, 1971). Here, an enzyme named luciferase serves as the energy donor (Hastings, 1983). In contrast to the fluorescent donor in FRET, the luciferase does not require an exogenous light source but instead catalyzes the oxidation of specific substrates with the concurrent emission of a photon and resonance energy transfer to the BRET acceptor (Marullo and Bouvier, 2007). All further, previously introduced physicochemical characteristics of FRET (e.g. requirement of

spectral overlap) do also apply to BRET.

The major disadvantage of BRET compared to FRET is that visualization of single-cell and subcellular events via BRET requires highly sensitive microscopic setups to compensate for the drastically lower photon output (Goyet et al., 2016). However compared to FRET, no sample illumination through an external light source is necessary. This feature prevents “contamination” of the RET signal resulting from direct acceptor excitation, cellular autofluorescence or fluorophore photobleaching and thus simplifies the analysis of raw BRET data (Boute et al., 2002).

### 1.10.3. Techniques to measure RET

Several techniques requiring distinct instrumentation have been developed to quantify RET. In general, there are three major strategies to detect changes in resonance energy transfer.

#### 1.10.3.1. Indirect RET measurements

In indirect RET measurements, RET efficiency is indirectly inferred from spectral imaging (siRET), acceptor photobleaching (apRET) or fluorescence lifetime imaging (FLIM) (Bajar et al., 2016).

In siRET, RET efficiencies of different donor-acceptor pairs are determined by fitting the spectral data of a RET probe with its theoretical spectrum created from the fluorophore’s physicochemical properties and the underlying Förster equations (Lam et al., 2012; Zimmermann et al., 2002). Unfortunately, these methods require the knowledge of the donor-acceptor stoichiometry and are thus limited to studies that guarantee a fixed and known expression ratio of the two RET partners.

The apRET-based approach however, makes use of the phenomenon that the donor emission intensity is diminished as a result of energy transfer to the RET acceptor. By monitoring the recovery of donor emission intensity (also called donor-dequenching) upon photo- or chemical bleaching of the RET acceptor, RET efficiencies are calculated based on following equation (Bajar et al., 2016; Hoffmann et al., 2005; Van Munster et al., 2005):

$$E = 1 - D_{pre}/D_{post} \quad (3)$$

$D_{pre}$  and  $D_{post}$  describe the donor emission intensities before and after acceptor bleaching, respectively. The apRET approach offers a very straightforward way to quantify RET efficiencies but solely provides an endpoint study without observation of time-dependent RET efficiency variations.

Unlike siRET and apRET, FLIM enables a non-intensity-based technique to explore RET efficiency. Here, the speed of the fluorescence donor emission decay (also called the fluorescence lifetime) is recorded and correlated with the FRET efficiency. Due to the fact that RET accelerates the donor emission decay, RET efficiencies can be extracted from donor lifetime data in the presence and absence of the RET acceptor as follows (Bajar et al., 2016; Becker, 2012):

$$E = 1 - \tau_{DA}/\tau_D \quad (4)$$

$\tau_{DA}$  and  $\tau_D$  are the donor emission lifetimes in the presence and absence of the RET acceptor, respectively. FLIM provides many advantages over intensity-based methods such as the independence of donor and/or acceptor expression levels or spectral crosstalk. However, FLIM experiments necessitate expensive specialized instrumentation preventing its broad application in most research groups (Day and Davidson, 2012).

#### 1.10.3.2. Direct RET measurements

In contrast, direct quantification of RET can be obtained by correlating alterations in emission intensity (sensitized emission RET, seRET) and fluorescence polarization (polarization resolved RET, prRET) to changes in RET efficiency.

The term sensitized emission traces back to the fact that resonance energy transfer from a donor

fluorophore triggers RET acceptors to emit photons of their characteristic wavelength. In seRET methods, this acceptor emission intensity and other parameters are examined to detect changes in RET. The most common type of seRET methods is ratiometric RET. Here, donor and acceptor emission intensities upon optimal donor excitation (FRET) or enzymatic photon production (BRET) are monitored and usually expressed as acceptor emission over donor emission. In FRET setups, a clear change in FRET efficiency can directly be identified by the antiparallel signal of the individual emission channels (**Figure 1.15**). In BRET however, this is not always the case, especially when luciferases with a significant time-dependent emission decay (flash type luciferases, e.g. NanoLuciferase) are applied as donors.

The seRET method only requires the implementation of well-selected excitation (only for FRET) and emission filters but allows the investigation of highly dynamic RET changes over long time-scales (if photo-stable RET partners are applied). Therefore, seRET represents the most commonly used technique for RET studies (Bajar et al., 2016).

However, researchers should accurately determine the influence of spectral crosstalk between the RET fluorophores to correct for (i) donor-derived fluorescence emission in the acceptor channel (donor bleedthrough) and (ii) acceptor emission that is solely due to direct excitation through sample illumination (only in FRET; also known as false excitation) (Day and Davidson, 2012). Therefore, the specific correction factors have to be determined in separate experiments where only the donor (bleedthrough) or acceptor fluorophore (false excitation) are expressed without the respective RET partner.

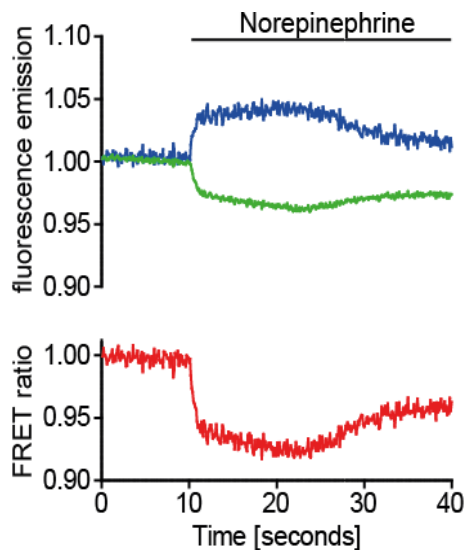


**Figure 1.15: Typical FRET traces.**  
*In ratiometric FRET experiments, both, donor (blue) and acceptor (green) emission intensities are recorded to calculate the resulting FRET ratio (red). Here, addition of norepinephrine induces a reduction in FRET efficiency of the FRET biosensor, detectable as antiparallel donor and acceptor emission intensities and decrease of the calculated FRET ratio.*

In comparison to all aforementioned RET techniques, prRET represents a unique way to detect changes in RET since neither emission wavelength, fluorescence intensity nor emission lifetime are monitored. Instead, samples are illuminated with polarized light so that only fluorophores with parallel dipole orientation are excited. Subsequently RET is measured as partially depolarized acceptor emission due to altering dipole orientation to the donor (Day and Davidson, 2012). The prRET methods is the single method that allows the study of homo-FRET pairs – a FRET pair consisting of two spectrally identical fluorophores (Bader et al., 2011). Analogous to the ratiometric seRET method, extra effort needs to be taken to correct for donor bleedthrough and acceptor false excitation to ensure reliable data interpretation (Mattheyses et al., 2004).

### 1.10.3.3. Time-resolved FRET measurements

The third frequently applied approach is Time-resolved FRET (TrFRET) that relies on the use of lanthanides (mostly cryptates of europium  $\text{Eu}^{3+}$  and terbium  $\text{Tb}^{3+}$ ) as energy donors. TrFRET offers the interesting feature that the donor emission commences with a significant time delay after excitation. Consequently, the lanthanide emission can be recorded after a specific delay window (typically between 10 – 100  $\mu\text{s}$ ) where the autofluorescence of the sample is substantially reduced to enable higher signal-to-noise ratios (Bazin et al., 2002). TrFRET is strictly spoken not a fluorescence-based principle since no singlet-to-singlet transition

occurs and is therefore often referred to as LRET – lanthanide-based resonance energy transfer (Selvin, 2002). However, TrFRET relies on the same fundamental mechanism with less dependency on donor-acceptor relative orientation and is often not differentiated from conventional FRET techniques (Lohse et al., 2012).

### 1.11. Relevance of FRET and BRET for life sciences

FRET and BRET biosensors act as “molecular rulers” detecting relative distance changes in the range of 1 – 10 nm with excellent temporal resolution. Owing to these features, RET has evolved into an inevitable technique to monitor highly dynamic and spatially constrained processes and complements well-established biophysical methods including conventional microscopy that is limited to a spatial resolution of  $\approx$  250 nm due to the way light diffracts (Abbe, 1873). The emergence of super-resolution microscopes has indeed pushed this limit to  $\approx$  10 nanometer but these techniques require long scanning times and thus, do not provide the optimal temporal resolution to study highly dynamic events (Sydor et al., 2015).

In general, FRET- and BRET-based biosensors are applied in an either *inter-* or *intramolecular* setup. In *intermolecular* RET studies, two distinct biomolecules are labeled with the interacting RET partners allowing for example the monitoring of protein-protein interaction or trafficking of biomolecules to subcellular compartments (Namkung et al., 2016). In contrast, *intramolecular* biosensors carry the RET partners within the same biomolecule. By this means, the conformational dynamics of a protein such as  $\beta$ -arrestin can be visualized (Nuber et al., 2016). Furthermore, flanking binding domains of, for instance, cAMP with RET partners allows for monitoring intracellular fluctuations of these second-messengers (Nikolaev et al., 2004). Following the first description by Theodor Förster (Forster, 1946) and subsequent verification of the FRET concept in model systems (Latt et al., 1965; Stryer and Haugland, 1967), first biochemical studies made use of the FRET technique focusing on proximity relationships in tRNA (Beardsley and Cantor, 1970) and the structures of apomyoglobin (Luk, 1971). Artificial BRET systems on the contrary, have been utilized almost three decades later for the study of protein-protein interactions involved in the regulation of the circadian rhythm (Xu et al., 1999) or dimerization of  $\beta_2$ AR (Angers et al., 2000). Since then, RET-based sensors have successfully been employed in various research fields. For instance, RET sensors helped monitoring structural dynamics of chemical entities (Xia et al., 2017), sensing intracellular ion concentrations (Aper et al., 2016; Mank et al., 2006; Zhang et al., 2008) or pH (Chan et al., 2011), study real-time drug release from nanomaterials in living cells (Chen et al., 2015) and *in vivo* (Cayre et al., 2018) or examine cellular compartments of enzymes like protein kinases (Ginefra et al., 2018; Zhou et al., 2015).

#### 1.11.1. GPCR studies with FRET and BRET biosensors

Various laboratories worldwide have successfully applied RET assays to address specific GPCR-related questions. Literally, every event within the GPCR signaling cascade can theoretically be monitored using a RET-based system in single-cell or even microtiter format. For example, FRET- and BRET-based assays are established to monitor the binding process of fluorescently labeled GPCR ligands to their cognate receptors in microtiter plate format (Emami-Nemini et al., 2013; Leyris et al., 2011; Stoddart et al., 2015a). The development of these methods represents a significant progress in receptor research because they provide both, temporal and spatial information on the binding properties of GPCR ligands, which could not be achieved with traditional binding assays.

Furthermore, RET-based biosensors capturing specific GPCR-mediated signaling events have been developed and shown to be valuable, complementary tools for the characterization of potential GPCR ligands.

To monitor GPCR activation on the G protein level, the first generation of FRET- and BRET-based sensors has been developed in the early 2000s for the two most abundant G protein subtypes  $G_i$  and  $G_s$  (Bunemann et al., 2003; Gales et al., 2005). Subsequently, these biosensors have been refined for better performance and practicability (Semack et al., 2016; van Unen et al., 2016). Biosensors for  $G_q$  and less common G protein subtypes have been reported several years later (Adjobo-Hermans et al., 2011; Mastop et al., 2018; Yano et al., 2017). Of note is the inspiring trend towards subtype-independent G protein sensors by introducing RET-partners into the  $G\beta\gamma$  subunit (Candelario and Chachisvilis, 2013). One can use these sensors as universal tools to acquire the activation of various GPCRs that couple to different G proteins.

Walking down the G protein-dependent signaling cascade, numerous RET-based sensors are validated to detect the activation of adenylyl cyclases (Ritt and Sivaramakrishnan, 2016) or fluctuations of intracellular second-messenger levels like cAMP (Klarenbeek et al., 2015; Nikolaev et al., 2004), IP<sub>1</sub> (Trinquet et al., 2011) and calcium (Evanko and Haydon, 2005; Mank et al., 2006). Furthermore, RET sensors of more distal effector proteins like extracellular-signal regulated kinase (ERK) enable monitoring their regulation in real-time in living cells (Harvey et al., 2008; Vandame et al., 2014).

On the side of the different GPCR-related signaling pathways, many RET systems have been developed to monitor G protein-independent events as for instance receptor oligomerization (Cottet et al., 2011) and internalization (Namkung et al., 2016). With the development of inter- and intramolecular sensors by the intelligent selection of favorable donor-acceptor labeling sites,  $\beta$ -arrestin recruitment (Bertrand et al., 2002) and activation (Charest et al., 2005; Nuber et al., 2016) can be visualized.

Especially worth mentioning is the essential role that RET biosensors play in the exploration of GPCR signaling compartments. These micro- or nanodomains display distinct, spatially confined levels of GPCR-controlled effector proteins and second-messengers (especially cAMP) and represent the basis for the regulation of many different physiological processes (Lefkimmatis and Zaccolo, 2014; Schleicher and Zaccolo, 2018; Wright et al., 2015).

In summary, RET-based biosensors are available for a plethora of receptor related events. The combination of all these RET-based assays may support the investigation of GPCRs' physiological roles, understanding structure-activity relationship of tested ligands to e.g. identify biased compounds and ultimately, design superior drug candidates.

#### 1.11.2. RET-based studies of GPCR conformational dynamics

The first report describing a conformational GPCR sensor in 2003 ushered a new era of RET-based GPCR studies (Vilardaga et al., 2003). By carefully selecting two conformationally sensitive insertion sites for the RET fluorophore partners (**Figure 1.16**), these biosensors facilitate the observation of GPCR conformational changes upon receptor stimulation in living cells with high temporal resolution (Lohse et al., 2012). The majority of intramolecular GPCR RET sensors are labeled with one RET partner in the third intracellular loop because TM5 and TM6 are expected to undergo the most pronounced movement during receptor activation. The other chromophore is often placed within the truncated or full-length C-terminus because the average distance between the third intracellular loop and this portion of the receptor (e.g. 6.2 nm for  $\beta_2$ AR (Granier et al., 2007)) is within the range allowing FRET (2.4 – 7.2 nm) to occur (Dacres et al., 2010).

Different GPCR ligands induce distinct FRET signals allowing these sensors to distinguish between GPCR ligands with varying potencies and efficacies. For example, weak partial GPCR agonists induce intermediate FRET signals that are higher than the values recorded for antagonist on the one hand but lower than strong partial or full agonist induced signals on the other hand (Nikolaev et al., 2006; Schihada et al., 2018; Zurn et al., 2009).

Besides the characterization of orthosteric ligands, RET-based GPCR sensors further allow to investigate the effects of GPCR allosteric modulators on the affinity and efficacy of orthosteric ligands (Maier-Peuschel et al., 2010). Pretreatment with positive allosteric modulators is expected to increase the extent, affinity and / or kinetics of the FRET signal emerging from agonist addition (Messerer et al., 2017).

Furthermore, the effects of stimuli other than binding of an extracellular compound can be examined with the use of these conformational GPCR sensors. For instance, conformational GPCR sensors unraveled the mechano- and voltage-dependent stimulation of the B<sub>2</sub>-bradykinin (B<sub>2</sub>R) and  $\alpha_2$ AAR, respectively (Chachisvilis et al., 2006; Rinne et al., 2013).

Besides their significance for classification of different stimuli, temporal information on receptor conformation transition gained with this type of assay complements the knowledge arisen from the static snapshots of GPCR crystallographic structures (Kauk and Hoffmann, 2018). These optical tools lay the basis for the study of fast GPCR activation kinetics – thus far extensively investigated only for the in many aspects exceptional GPCR rhodopsin due to a lack of appropriate techniques (Funatogawa et al., 2016; Monger et al., 1979; Vilardaga et al., 2003).



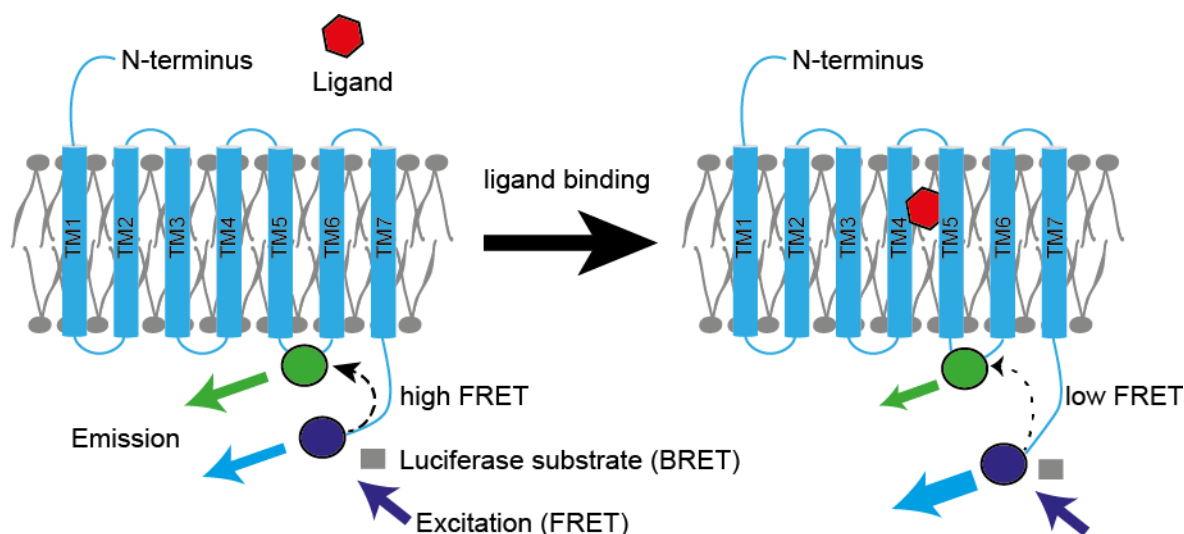


**Figure 1.16: Principle of intramolecular RET-based GPCR sensors.**

RET donor (dark blue) and acceptor fluorophores (green) are inserted in suitable positions within intracellular loops (here: intracellular loop 3) and the cytosolic C-terminus. In the basal state of the receptor sensor (left), RET partners are in close proximity enabling high resonance energy transfer from donor to acceptor. The receptor activation process upon ligand (red) binding encompasses prominent rearrangement of the transmembrane helices resulting in increased inter-fluorophore distance and subsequent loss in RET (right). The loss in RET is quantified as concurrent increase in donor emission intensity and decreasing acceptor emission intensity.

### 1.11.3. Limitations and challenges of conformational GPCR biosensors

Although powerful in many aspects, RET-based conformational GPCR sensors still face substantive limitations and downsides to be considered for assay selection and data interpretation.

For example, multi- and single-cell FRET studies reflect the averaged conformational dynamics of huge receptor ensembles (tens of thousands of sensors per cell) but not of single GPCRs. Thus, distinguishing between intermediate receptor conformations or altered equilibria of either fully active or inactive receptors is impossible in this experimental setup. However, combining FRET GPCR sensors with total internal reflection microscopy (TIRF) allows for investigation of single-molecule conformational dynamics to gain deeper understanding of GPCR activation mechanism (Gregorio et al., 2017). This elegant approach proves the existence of subpopulations of receptor intermediate states between the fully active and inactive conformation presenting another great upside of FRET-based GPCR biosensors.

All applications of FRET sensors described above require laborious and time-consuming sample preparation and visualization in a microscopic environment. No generalizable FRET-based GPCR sensor design that would enable to conduct conformational GPCR studies in microtiter plates is currently established. This is mainly due to the required external illumination of the FRET sample causing background fluorescence and acceptor false excitation thus reducing the signal-to-background ratio. To circumvent this downside of FRET-based biosensors, BRET versions of intramolecular GPCR sensors reporting agonist-specific signals in the low single-digit percent range have been developed and validated for use in microtiter plate format (Bourque et al., 2017; Devost et al., 2017; Sleno et al., 2017; Sleno et al., 2016; Szalai et al., 2012). However, still none of the reported RET-sensors achieves sufficient assay sensitivity and robustness to justify HTS suitability.

Other challenges regarding intramolecular GPCR sensors deal with the sensor design itself. For instance, the distance dependency of RET is an important factor when it comes to selecting the appropriate insertion sites for the RET donor-acceptor fluorophores (Hoffmann 2015). As mentioned above, a RET pair achieves the highest dynamic range when the inter-fluorophore distance approximates the Förster distance  $R_0$  of this specific RET pair and both fluorophores are in parallel orientation. For instance, fluorophores located at half  $R_0$  distance give rise to 98.5 % energy transfer whereas a double  $R_0$  distance results in only 1.5 % of energy transfer (Norskov-Lauritsen et al., 2014). Structural information (e.g. gained from crystallographic studies) on the receptor of interest can be a precious starting point for the distance calculation between potential insertion sites. However, a precise estimation of inter-fluorophore distances

is almost impossible without knowing how the insertion or truncation of amino acids affects the overall protein constitution. Thus, spotting proper insertion sites remains mostly a trial-and-error procedure that might involve large GPCR modifications such as truncation of certain amino acid sequences to yield suitable sensors (Reiner et al., 2010; Vilardaga et al., 2003; Ziegler et al., 2011).

Linked to the identification of proper fluorophore insertion sites is the question of how the introduction of fluorophores disrupts the overall receptor functionality including receptor expression, localization, and ligand binding properties and signaling. For example, the prominent insertion sites within the third intracellular loop and the C-terminus are essential for GPCR-G protein and GPCR- $\beta$ -arrestin interaction (Cahill et al., 2017; Rasmussen et al., 2011). Consequently, the introduction of bulky fluorophores (e.g. fluorescent proteins) but not small fluorescent dyes within these sensitive segments significantly hampers GPCR-mediated signaling for some receptor sensors (Hoffmann et al., 2005; Vilardaga et al., 2003). Therefore, rigorous sensor characterization is mandatory to exclude any impairment of vital receptor processes like ligand recognition and initiation of downstream signaling.

Besides described aspects involved in sensor design, several corrective actions are required while conducting and analyzing the experiment to minimize the impact of donor emission bleedthrough into the acceptor emission channel and increase acceptor emission resulting from false excitation. Another significant challenge that traditional GPCR RET-based biosensors face originates from the fact that most currently available GPCR sensors are comprised of fluorophores that emit in the blue-green part of the visible spectrum. RET GPCR biosensors emitting in the red part of the spectrum would in contrast present several upsides for GPCR studies. Since cellular autofluorescence is highest in the blue part of the visible spectrum, red-shifted RET sensors are less exposed to background fluorescence facilitating higher signal-to-noise ratios. Furthermore, the deeper tissue penetration of red light could ultimately result in the application of RET-based biosensors in tissue- or even animal model systems. Additionally, traditional blue-yellow RET sensors exhibit unacceptable crosstalk with other sophisticated research tools like photo-switchable (Agnetta et al., 2017; Hauwert et al., 2018; Levitz et al., 2017; Rovira et al., 2016) or caged GPCR ligands (Meyer zu Heringdorf et al., 2003; Palma-Cerda et al., 2012; Tadevosyan et al., 2016) and biosensors that monitor GPCR signaling events (Aubin, 1979; Avci et al., 2013; Tewson et al., 2013). In contrast, experimenters can simultaneously employ red-shifted GPCR and aforementioned techniques in a multiplex system.

In summary, if intramolecular GPCR sensors are verified for receptor function and experiments are performed under well controlled conditions, this type of biosensors presents a valuable tool to study various aspects of GPCR biology and pharmacology (Lohse and Hofmann, 2015). This is demonstrated by the validation of about 50 distinct conformational RET sensors for more than 20 different GPCRs (**Annex Table 7.3**) (Kauk and Hoffmann, 2018).

## 1.12. Techniques for intracellular GPCR labeling

As mentioned before, suitable RET donor-acceptor pairs need to be attached to conformationally sensitive sites of the receptor in order to sense the ligand-induced structural rearrangement of GPCRs. The following section introduces the labeling technologies available to stain intracellularly located protein sites and describes their class-specific up- and downsides when applied for the creation of intramolecular GPCR sensors.

### 1.12.1. Fluorescent proteins

Fluorescent proteins (FPs) represent the major tags employed for the visualization of GPCRs. The three-dimensional structure of the 28 kDa sized FPs is characterized by the class-typical  $\beta$ -barrel below the two protein termini encompassing the fluorescent chromophore in its center (**Figure 1.18**) (Tsien, 1998).

Since the cloning of the green fluorescent protein (GFP) from the jellyfish *Aequorea victoria*, numerous variants of fluorescent proteins covering all parts of the visible spectrum have been developed and partially applied in RET studies (Prasher et al., 1992). Cyan (CFP) and yellow (YFP) fluorescent proteins were the first applied fluorophores for the creation of intramolecular FRET GPCR sensors for  $\alpha_{2A}$ -adrenergic receptor ( $\alpha_{2A}$ AR) and PTHR1 (Vilardaga et al., 2003).

Optimization of the biophysical properties of fluorescent proteins have led to superior variants displaying

improved optical properties (e.g. quantum yield, extinction coefficient), photostability and pH-insensitivity that could be employed for the design of refined intracellular RET sensors (Klarenbeek et al., 2015; van Unen et al., 2016). For instance, the blue light-emitting protein mTurquoise2 (mTq2) shows higher quantum yield (about 93%), higher photostability and reduced dimerization tendency than first-generation fluorescent proteins qualifying mTq2 as one of the best FRET donors available so far (Cranfill et al., 2016; Goedhart et al., 2012). Additionally, many laboratories set out to improve the frequently used FRET acceptor YFP and to identify the optimal FRET acceptor for mTq2 among the optimized YFP variants (Griesbeck et al., 2001; Kremers et al., 2006; Mastop et al., 2017; Nagai et al., 2002; Nguyen and Daugherty, 2005).

Another great advancement in the field of fluorescent proteins has been realized with the generation of red-shifted fluorescent proteins laying the base for the design of advantageous red-shifted GPCR RET-based biosensors (Miyawaki et al., 2012).

The main reason why FPs represent the most frequently applied labeling technique in living cells is that these proteins offer the most direct way to introduce fluorophores to any biomolecule of interest. With the use of common cloning techniques, cDNA encoding the fluorescent construct can easily be inserted at the desired location of the target sequence yielding a fluorescent fusion protein of the protein of interest. FPs are fluorescent by itself and do not require any additional labeling or activation procedure once protein synthesis and maturation is completed. Thus, fluorescent proteins provide a fixed donor-to-acceptor stoichiometry when inserted into the same protein of interest to create a conformational FRET sensor. On the other hand, the tendency of some fluorescent proteins to associate into dimers and higher order oligomers represents a considerable disadvantage of FPs when used in RET studies. The dimerization tendency can artificially drive increases in RET – especially in intermolecular RET assays - and lead to misinterpretation of the experimental data (Verkhusha and Lukyanov, 2004). For this reason, FP variants with reduced dimerization, such as monomeric YFP (mYFP), should be preferred for this kind of assays. Additionally, the high molecular weight and bulky structure of all fluorescent proteins represents the most important downside of using FPs in intramolecular conformational GPCR sensors. Although no impairment of the ligand binding process has been reported for any conformational GPCR sensor so far, FP insertion at intracellular GPCR sites essential for interaction with signaling partners can sterically block these effector partners and perturb GPCR signaling.

#### 1.12.2. Bioluminescent enzymes – luciferases

Luciferases are extremely valuable enzymes for biomedical research. They emit light of a characteristic wavelength upon catalytic reaction with its substrate and, similarly to fluorescent proteins, can easily be attached to the target structure through genetic fusion.

The first luminescent enzyme cloned was firefly luciferase (Fluc) from *Photinus pyralis* in 1985 (Kricka and Leach, 1989). This was the starting point for a new era of biomedical research in which light emitting enzymes are employed to monitor gene expression, protein stability and protein-protein or protein-ligand interactions (Bertrand et al., 2002; Branchini et al., 2018; Stoddart et al., 2015a). Fluc is the 62 kDa protein responsible for the emission of 550-570 nm light of fireflies and click beetles upon ATP-dependent reaction with its substrate D-luciferin (Thorne et al., 2010). Fluc-based assays have been established to monitor GPCR-mediated cAMP production (DiRaddo et al., 2014), receptor internalization (Lu et al., 2016) and GPCR- $\beta$ -arrestin interaction in cellular model systems and organs of living animals (Takakura et al., 2012) owing to its red-shifted emission featuring deep tissue penetration. However to date, no intramolecular GPCR sensor employing Fluc as a BRET-donor is available probably due to its relatively large and bulky structure.

In contrast, *Renilla reniformis* luciferase (Rluc) presents a suitable energy donor in conformational GPCR biosensors (Bourque et al., 2017; Devost et al., 2017; Sleno et al., 2017; Sleno et al., 2016; Szalai et al., 2012). This 36 kDa luciferase was purified in the 1970s from the sea pansy and initially confirmed its significance for GPCR research as a donor in intermolecular BRET assays for the quantification of receptor- $\beta$ -arrestin interaction, G protein activation (Gales et al., 2005) and GPCR internalization (Namkung et al., 2016).

Gaussia luciferase (Gluc), naturally occurring in the mesopelagic copepod *Gaussia princeps*, covers another field of research application (Verhaegent and Christopoulos, 2002). Gluc presents significant protein stability and the ATP-independent nature of the catalytic reaction facilitates Gluc's functionality in extracellular medium. For this reason, Gluc's activity can be quantified in blood samples of living animals to correlate the luminescence intensity with different biological processes (Wurdinger et al., 2008). Furthermore, Gluc

reliably reports peptide ligand binding to GPCRs. Thanks to its relatively small size of 20 kDa, inactive Gluc fragments can be attached to the CXCR4 chemokine receptor (CXCR4) and its endogenous agonist CXCL12 without deleting their mutual affinities. Enzyme complementation upon CXCL12-CXCR4 interaction results in fragment complementation and a subsequent bioluminescent signal that allows for monitoring the ligand binding process in living mice (Luker and Luker, 2014).

The discovery of *Oplophorus* luciferase (Oluc) in the deep-sea shrimp *Oplophorus gracilirostris* led to the development of the most advanced luciferase available so far, named NanoLuciferase (Nluc) (Shimomura et al., 1978). Oluc is a 54-kDa protein that originally catalyzes the degradation of coelenterazine and is composed of two heterodimeric sub-units: a 35-kDa region and a smaller, 19-kDa subunit (Oluc-19) responsible for the catalytic activity of Oluc. Extensive mutagenetic modifications of Oluc-19 result in improved protein stability and, in combination with its novel luciferase substrate furimazine, an excellent bioluminescent system (Hall et al., 2012). Several characteristics of Nluc underlie its superiority over traditional bioluminescent enzymes such as Fluc and Rluc. First, Nluc exhibits the greatest brightness among all luciferases currently applied for biomedical research with an about 100-fold increased luminescence output compared to Rluc and Fluc. In addition, Nluc's reduced pH- and temperature-dependency allow for developing more robust and reliable assays and, ultimately, the relatively narrow emission peak at around 450 nm reduces spectral crosstalk when combined to other luminescent or fluorescent reporters. Several studies highlight the significant relevance of NanoLuciferase for GPCR research. For instance, tagging GPCR's extracellular N-termini with Nluc facilitates measuring the binding process of fluorescently tagged receptor ligands. This non-radioactive and less expensive approach, that moreover provides direct information on temporal aspects of ligand-receptor association/dissociation kinetics, has the power to substitute traditional binding assays in the future (Soave et al., 2016; Stoddart et al., 2015a; Stoddart et al., 2018; Wang et al., 2017). In addition to monitoring the ligand binding process of GPCRs, BRET-based assays utilizing Nluc as the energy donor for different kinds of acceptor fluorophores have been established for real-time studies of protein-protein interactions substantiating the universal appropriability of Nluc for BRET measurements (Machleidt et al., 2015; Mo and Fu, 2016). Owing to Nluc's bright luminescence, the dynamic process of  $\beta$ -arrestin recruitment to the vasopressin receptor 2 (VPR2) can be visualized even in single cells (Machleidt et al., 2015). To date, no conformational GPCR biosensors based on Nluc have been reported despite its favorable physicochemical properties and advantageous comparatively small size (**Figure 1.18**).

### 1.12.3. Fluorescence-Arsenical-Hairpin-binder

This type of labeling technique is based on the high affinity of  $As^{III}$  species to vicinal dithiols allowing the covalent binding of biarsenical molecules to an engineered peptide/protein sequence (Kalef and Gitler, 1994). The bis- $As^{III}$ -moiety has successfully been fused to different chemicals such as biotin for study of the cell surface (Pomorski and Krezel, 2011) but with respect to conformational GPCR sensors, Fluorescence-Arsenical-Hairpin-binder (FIAsH) and its red analog ReAsH (Resorufin-Arsenical-Hairpin-binder) are the most prominent representatives.

FIAsH is a small (700 Da), cell permeable fluorescent molecule that emits yellow light with an emission peak ( $\lambda_{Em}$ ) around 530 nm upon exposure to blue-green light (excitation peak  $\lambda_{Ex} = 490$  nm). The fluorescent dye comprises two Arsen atoms that are essential for FIAsH's characteristic feature to form a covalent bond with the peptide sequence Cystein-Cystein-Xaa-Xaa-Cystein-Cystein (CCXXCC, where Xaa denotes any amino acid) that shapes a hairpin structure in the protein of interest (Griffin et al., 1998).

The first report of a FIAsH-based FRET GPCR sensor, confirm that the small-size acceptor tag FIAsH remains the wild-type receptor functionality quantified as its potency to activate downstream G proteins. Moreover, replacing the traditional FRET acceptor YFP by FIAsH in  $\alpha_{2A}AR$  and  $A_{2A}R$  biosensors, substantially increased the sensor's dynamic range giving rise to the development of numerous FIAsH-based conformational GPCR sensors (Alvarez-Curto et al., 2011; Bourque et al., 2017; Devost et al., 2017; Hoffmann et al., 2005; Maier-Peuschel et al., 2010; Sleno et al., 2017; Sleno et al., 2016; Xu et al., 2012; Ziegler et al., 2011; Zurn et al., 2009). Of note, insertion of distinct peptide sequences into independent intracellular proteins allows the orthogonal labeling with the FRET partners FIAsH and ReAsH to monitor  $\beta$ -arrestin recruitment to PTHR1 (Zurn et al., 2010).

Like all labeling techniques that require staining of a target structure with small fluorescent dyes, also FIAsH labeling results in unspecific background fluorescence of the sample even if a more specific peptide sequence is employed for receptor tagging (Martin et al., 2005). To replace unspecifically bound FIAsH

molecules, a one-hour incubation with cell-toxic ethanedithiol (EDT) is required that might interfere with essential cellular processes and even induce cell death (Held and Biaglow, 1994; Hoffmann et al., 2010). Furthermore, FIAsh's low brightness and photostability limit its use to highly sensitive instrumentation and experimental setups with short illumination times (Spagnuolo et al., 2006).

#### 1.12.4. Self-labeling protein tags

Another possibility to introduce fluorescent molecules into GPCRs is based on the use of self-labeling protein tags like SNAP/CLIP-tag and HaloTag. These genetically modified enzymes catalyze the covalent attachment of an exogenously added synthetic ligand. They have initially been developed to achieve versatile tools for various experimental requirements (e.g. labeling with distinct fluorophores for optics-based studies or affinity tags for protein purification) with only one genetic fusion construct.

Although these tags might differ in some labeling properties, they share the main underlying concept. Mutations of specific amino acids involved in the catalytic reaction of an enzyme with its substrate disable the enzyme to release the substrate once they formed an intermediate, covalent conjugate. These modifications ultimately result in an irreversible binding of the substrate to the enzyme mutant. By chemically coupling bright organic dyes to the reactive linker moiety recognized by the enzyme, virtually any fluorophore can specifically be fused to the tag that, in turn, is incorporated into the protein of interest. In order to label intracellularly located protein sites, synthesized fluorophore-linker molecules have to be capable of crossing the membrane which limits the use of these techniques to rather hydrophobic fluorescent dyes.

SNAP/CLIP and HaloTag represent the major technologies relevant for GPCR studies and are therefore described in more detail in the following section.

##### 1.12.4.1. SNAP- and CLIP-tag technology

SNAP-tag® is the brand name of the 20 kDa human DNA repair protein O<sup>6</sup>-alkylguanine-DNA alkyltransferase (AGT; **Figure 1.18**) that catalyzes the attachment of O<sup>6</sup>-alkylguanine or O<sup>6</sup>-benzylguanine (BG) derivatives to a cysteine residue on the enzyme (**Figure 1.17A**) (Juillerat et al., 2003). In contrast, CLIP-tag™ represents a modified version of AGT that exhibits higher affinity to O<sup>2</sup>-benzylcytosine (BC) than to BG-derivatives. Combining SNAP- and CLIP technologies enables orthogonal and simultaneous labeling of cells expressing fusion proteins of these tags (Gautier et al., 2008).

Several BG- and BC-fluorophores are marketed by New England Biolabs® GmbH facilitating specific labeling of fusion proteins with fluorescent dyes that cover different parts of the visible spectrum. In fact, intermolecular LRET sensors that carry SNAP-tag at extracellular protein sites reflect the activation of multiple GPCRs and other membrane proteins in HTS format emphasizing the importance of SNAP-tag technology for GPCR research (Scholler et al., 2017). However, most available BG- and BC-derivatives are highly hydrophilic limiting the application of SNAP/CLIP mainly to the extracellular space. Another major downside of SNAP/CLIP technology is the intense background labeling of endogenously expressed AGT, present in most mammalian cell lines (Keppler et al., 2004). To overcome this limitation, experimenters should use AGT-deficient cell lines such as CHO-9 neo C5 and HeLa MR as model systems when employing these labeling techniques (Kaina et al., 1991).

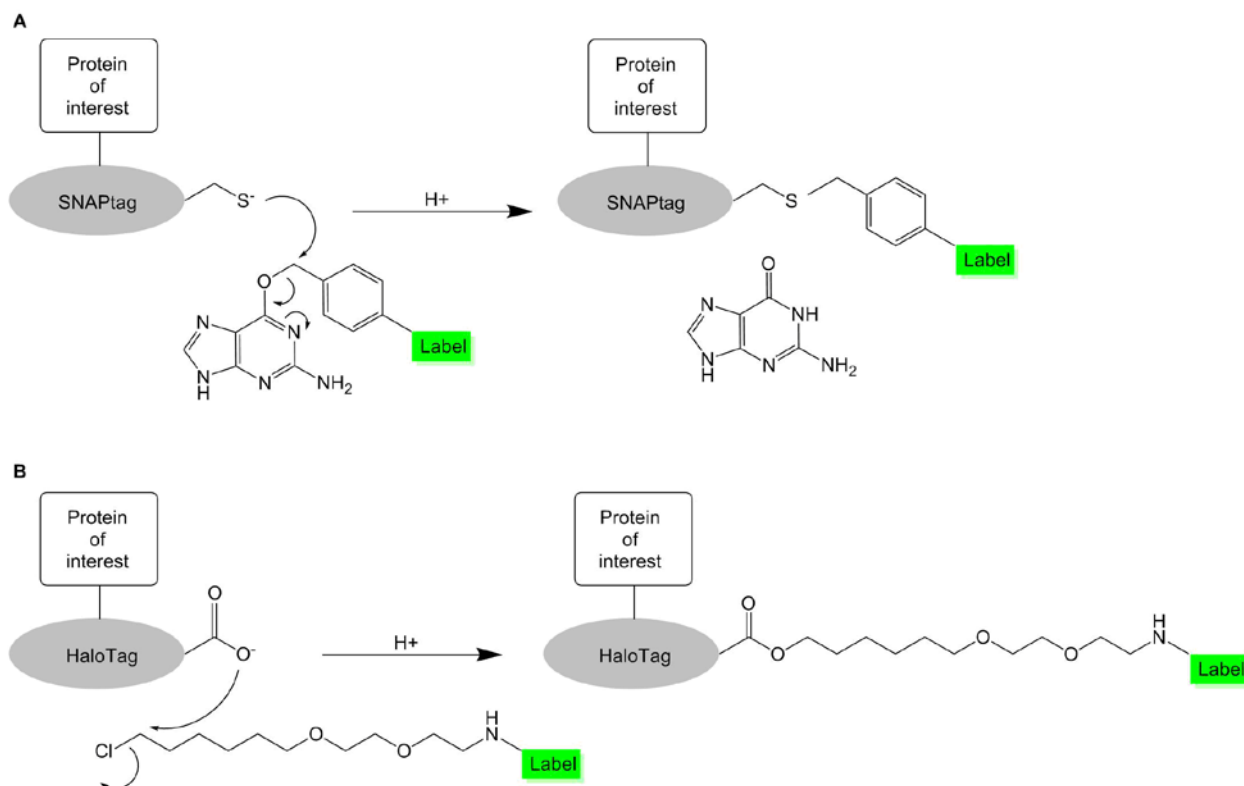


**Figure 1.17: Mechanism of self-labeling protein tags.**

A) SNAP-tag fusion protein undergoes a chemical reaction with a BG-derivative of the fluorescent chromophore. B) HaloTag fusion protein reacts with a fluorescently labeled haloalkane derivative.

#### 1.12.4.2. HaloTag technology

The bacterial enzyme haloalkane dehalogenase (DhaA) from *Rhodococcus* served as the point of origin for the engineering of the 33 kDa HaloTag self-labeling protein tag (Los et al., 2008). Essential for the original reaction of DhaA with its substrate is a Histidine (His<sup>272</sup>) residue hydrolyzing the intermediate covalent bond between a closely located nucleophilic aspartate and the substrate. Mutation of this substantial basic amino acid to phenylalanine combined with three further optimizing mutations result in the versatile HaloTag protein that covalently binds haloalkane derivatives with fast reaction kinetics inside living cells (**Figure 1.17B**) (Los et al., 2008).

With respect to GPCR research, HaloTag technology has been proven a valuable tool to purify GPCR fusion proteins from *Escherichia coli* (Locatelli-Hoops et al., 2013) and investigate GPCR internalization processes (Kumagai et al., 2015). Furthermore, the combination of a red HaloTag fluorescent ligand to the bright BRET donor Nluc yields an outstanding platform for protein-protein-interaction studies and has been employed to visualize  $\beta$ -arrestin recruitment to a G-protein-coupled receptor in a single-cell, microscopic format (Machleidt et al., 2015). To date, the suitability of HaloTag for the creation of intramolecular FRET and BRET biosensors to measure protein conformational dynamics remains unexploited although this technology offers highly specific labeling and several membrane-permeable fluorescent dyes. This might be due to the relatively high molecular mass and bulky tertiary structure of HaloTag (**Figure 1.18**) raising concerns on how it could impair protein expression and functionality.

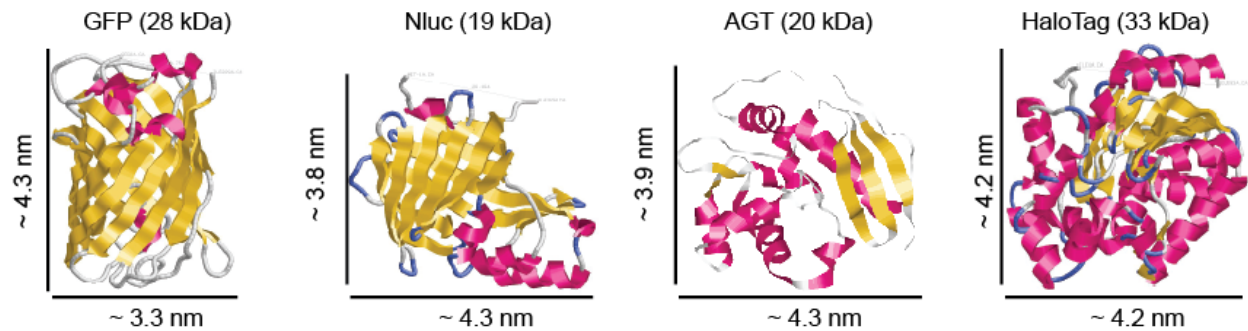


**Figure 1.18: Dimensions of protein tags.**

Crystal structures of the fluorescent protein GFP (1EMB), the luciferase Nluc (5IBO), *O*<sup>6</sup>-alkylguanine-DNA alkyltransferase (AGT) (1EH6) representing SNAP- and CLIP-tag and HaloTag (5UY1) accessed from [www.rcsb.org](http://www.rcsb.org). Partial structures in yellow and purple represent tertiary protein organization in  $\beta$ -strands and  $\alpha$ -helices, respectively.

#### 1.12.5. Labeling with unnatural amino acids

Labeling with unnatural amino acids (uAAs) currently represents the most exciting development in the field of site-specific protein labeling. This technology facilitates the incorporation of unnatural amino acids to a protein of interest and subsequent attachment of specific chemical entities including small organic fluorophores for its visualization in living cells (Italia et al., 2017).

In a first step, one of the three stop codons TAG (amber), TAA (ochre) or TGA (opal) need to be cloned into the desired position of the protein of interest. Subsequently, an engineered tRNA suppresses the termination of mRNA translation mediated by the stop codon and loads the (fluorescent) uAA to the nascent peptide chain. In order to do this, the unique codon-tRNA pair requires prior charging with the uAA by a corresponding, co-expressed aminoacyl-synthetase (Zhang et al., 2013a).

This labeling technique requires the least manipulation of the entire protein sequence since only one amino acid of the original protein sequence is mutated or inserted. Thus, labeling with uAAs offers the least invasive way for the incorporation of bright organic fluorescent labels in living cells available to date.

Unnatural amino acid labeling found its first important field of application in structural biology. Different laboratories successfully combined uAA labeling with nuclear magnetic resonance (Lampe et al., 2008), infrared and electron paramagnetic resonance (Fleissner et al., 2009; Schmidt et al., 2014) spectroscopy to elaborate the structures of various proteins – among them the prototypical GPCR rhodopsin (Ye et al., 2010). Furthermore, single-molecule experiments have validated its suitability for FRET studies *in vitro* (Tyagi and Lemke, 2015).

Yet, unnatural amino acid labeling is still in its infancy and several challenges need to be mastered to make this technology accessible to more experimenters and research methods such as RET inside living cells (Lin et al., 2017). For instance, identification of favorable amino acid transporter modifications will pave the way for increased cellular uptake of unnatural amino acids from growth media and ultimately result in higher labeling efficiencies (Lin et al., 2017).

### 1.13. Objective of the study

G-protein-coupled receptors play fundamental roles in virtually any cellular function. For this reason, these membrane-embedded proteins represent prime targets for therapeutic interventions in biomedical research. Although already 30% of currently approved drugs address GPCRs, their potential as therapeutic targets is not fully exploited since these therapeutics modulate only 100 – 140 receptors ( $\approx$  30%) within the entire druggable GPCR space comprising about 400 non-olfactory GPCRs. Despite tremendous efforts from both, academic and industrial research institutions on GPCR drug discovery, the community still lacks a simple and direct way to determine ligand effects on GPCRs that is amenable to high-throughput formats. Existing GPCR high-throughput assays either report the binding event without providing any information on intrinsic compound efficacies or monitor rather distal signaling outcomes that bear a great potential of false negative and false positive results and are influenced by receptor functional selectivity.

The most direct approach to evaluate the effect of a compound on a receptor is to assess the receptor's structural reorganization upon ligand binding. This gives information on the ligand's ability to engage the receptor and allows to determine its efficacy and affinity. Resonance energy transfer technology has successfully been used to monitor GPCR conformational dynamics and thereby, determine ligand efficacies and potencies in a living-cell and real-time assay format. For this reason, these biosensors have proven irreplaceable tools for GPCR research. Unfortunately, none of the existing conformational sensors facilitates the study of receptor conformational dynamics in HTS format slowing down the discovery of novel GPCR-directed therapeutics.

The goal of this project is to address this urgent necessity and develop a generalizable GPCR RET sensor design that yields sufficient sensitivity and robustness for performance in high-throughput screening campaigns. We set out to achieve this target through five main research objectives:

- 1) Employ the latest generation of fluorescent proteins and labeling techniques for the creation of a panel of FRET and BRET-based GPCR sensors. Subsequently, evaluate these different sensor designs for their capacity to report GPCR conformational changes in a microtiter plate format.
- 2) Characterize the most promising biosensor design by analyzing its capability to (i) discriminate between different ligands with distinct intrinsic efficacies and potencies and (ii) promote intracellular signaling.
- 3) Demonstrate the universal applicability of the new sensor design by applying this technology to different GPCR classes.
- 4) Evaluate the HTS-suitability of the biosensor design by assessing (i) their so-called Z-factors (Zhang et al., 1999), (ii) the assay throughput and (iii) rate of false positive screening hits.
- 5) Demonstrate the suitability of these sensors to investigate modulatory effects on GPCR dynamics through other endogenous membrane proteins.



## 2. Material and Methods

### 2.1. Materials

#### 2.1.1. Cell lines

Human Embryonic Kidney (HEK)-293 cells (ATCC)

HEK-TSA cells (ATCC)

Clonal line stably expressing  $\alpha_2AAR^{Nluc/Halo}$  generated from HEK-293 cells (this work)

Clonal line stably expressing  $\beta_2AR^{Nluc/Halo}$  generated from HEK-293 cells (this work)

Clonal line stably expressing  $PTHR1^{Nluc/Halo}$  generated from HEK-293 cells (this work)

#### 2.1.2. Cell culture media and supplements

Dulbecco's modified Eagle's medium (DMEM) (#21969-035 Gibco)

Dulbecco's phosphate buffered saline (DPBS) (#14190-094 Gibco)

Fetal bovine serum (FBS) (#S0115 Biochrom AG)

Penicillin/Streptomycin (#P4333 Sigma-Aldrich)

Trypsin / EDTA solution (P10-023100 PAN Biotech)

G-418 disulfate salt (#A1720 Sigma-Aldrich)

### 2.1.3. Plasmids

Plasmid	Source
murine $\alpha_2A$ AR <sub>CFP/YFP</sub> in pcDNA3	Institute of Pharmacology and Toxicology
murine $\alpha_2A$ AR in pcDNA3	Institute of Pharmacology and Toxicology
human $\beta_2$ AR <sub>CFP/YFP</sub> in pcDNA3	Institute of Pharmacology and Toxicology
human $\beta_2$ AR in pcDNA3	Institute of Pharmacology and Toxicology
human PTHR1 <sub>CFP/YFP</sub> in pIRES	Institute of Pharmacology and Toxicology
human PTHR1 in pcDNA3	Institute of Pharmacology and Toxicology
human CXCR4 in pcDNA3	Institute of Pharmacology and Toxicology
human AT1R in pcDNA3	Institute of Pharmacology and Toxicology
human S1PR1 in pcDNA3.1	Institute of Pharmacology and Toxicology
mCherry in pcDNA3	Institute of Pharmacology and Toxicology
pTagRFP-C vector	Evrogen (#FP141)
pFC14K HaloTag® CMV Flexi® Vector	Promega (#G966A)
pFC32K Nluc CMV229 neo Flexi® Vector	Promega (#N1331)
H187 EPAC FRET sensor (pcDNA3) (mTurq2Del-EPAC(dDEPCD)Q270E-tdcp173Venus(d) EPAC-S <sup>H187</sup> ) (Klarenbeek et al., 2015)	K. Jalink (The Netherlands Cancer Institute, Amsterdam, The Netherlands)
G $\alpha_{i2}$ FRET sensor in pIRES (van Unen et al., 2016) (pG $\beta$ -2A-cp173Venus-Gy <sub>2</sub> -IRES-G $\alpha_{i2}$ -mTurquoise2- $\Delta$ 9)	J. Goedhart (University of Amsterdam, Amsterdam, The Netherlands)
SNAP-GABA <sub>B1</sub> (Maurel et al., 2008)	J.P. Pin (Institut de Génomique Fonctionnelle, Montpellier, France)
RAMP2 in pViro2 (Schonauer et al., 2015)	A.G. Beck-Sickinger (University of Leipzig, Leipzig, Germany)
RAMP2 in pcDNA3	this work; Zabel U.
murine $\alpha_2A$ AR <sub>CFP/cpVenus173</sub> in pcDNA3	this work; Zabel U.
murine $\alpha_2A$ AR <sub>CFP/Halo</sub> in pcDNA3	this work; Zabel U.
murine $\alpha_2A$ AR <sub>CFP/SNAP</sub> in pcDNA3	this work; Zabel U.
murine $\alpha_2A$ AR <sub>Nluc/cpVenus173</sub> in pcDNA3	this work; Zabel U.
murine $\alpha_2A$ AR <sub>Nluc/TagRFP</sub> in pcDNA3	this work; Zabel U.
murine $\alpha_2A$ AR <sub>Nluc/mCherry</sub> in pcDNA3	this work; Zabel U.
murine $\alpha_2A$ AR <sub>Nluc/Halo</sub> in pcDNA3	this work; Zabel U.
murine $\alpha_2A$ AR <sub>Nluc/Halo(inverted version)</sub> in pcDNA3	this work; Zabel U.
murine $\alpha_2A$ AR <sub>Nluc/SNAP</sub> in pcDNA3	this work; Zabel U.
human $\beta_2$ AR <sub>Nluc/Halo</sub> in pcDNA3	this work; Zabel U.
human PTHR1 <sub>Nluc/Halo</sub> in pcDNA3	this work; Zabel U.
human AT1R <sub>Nluc/Halo</sub> in pcDNA3	this work; Zabel U.
human CXCR4 <sub>Nluc/Halo</sub> in pcDNA3	this work; Isbilir A.
human S1PR1 <sub>Nluc(K354)/Halo(N240)</sub>	this work; Schihada H.
human S1PR1 <sub>Nluc(K354)/Halo(K243)</sub>	this work; Schihada H.
human S1PR1 <sub>Nluc(S382)/Halo(N240)</sub>	this work; Schihada H.
human S1PR1 <sub>Nluc(S382)/Halo(K243)</sub>	this work; Schihada H.

**Table 2.1: Plasmids used in the course of this study.**

### 2.1.4. Primers

All primers used for generation and amplification of cDNA were synthesized and validated by Eurofins Genomics.

### 2.1.5. Cloning enzymes

All restriction enzymes, polymerases ligases and nucleotides employed for the generation of new plasmid DNA were purchased from New England Biolabs.

### 2.1.6. Fluorescent antibodies

HA-tag monoclonal antibody (16B12) Alexa Fluor 488 (#A-21287 Thermo Fisher Scientific)  
Monoclonal ANTI-FLAG® M2-Cy3™ antibody (#A9594 Sigma Aldrich)

### 2.1.7. Fluorescent SNAP-tag and HaloTag dyes and luciferase substrate

SNAP-Cell® 505-star (#S9103S NEB)  
SNAP-Cell® TMR-star (#S9105S NEB)  
SNAP-Cell® 647-SiR (#S9102S NEB)  
HaloTag® diAcFAM (#G8272 Promega)  
HaloTag® Oregon Green® (#G2801 Promega)  
HaloTag® R110Direct™ (#G3221 Promega)  
HaloTag® TMRDirect™ (#G2991 Promega)  
HaloTag® NanoBRET™ 618 Ligand (#G980A Promega)  
NanoBRET™ Nano-Glo® Substrate (furimazine) (#N157A Promega)

### 2.1.8. GPCR ligands

Norepinephrine (#A9512), epinephrine (#E4375), UK 14,304 (#U104), dopamine (#H8502), octopamine (#O0250), clonidine (#C7897), tyramine (#T2879), phentolamine (#P-7547), yohimbine (#Y3125), isoprenaline (#I5627), formoterol (#F9552), salbutamol (#S5013), salmeterol (#S5068), terbutaline (#T2528), labetalol (#L1011), carvedilol (#C3993), metoprolol (#PHR1076), propranolol (#P0884), ICI 118,551 (#I127), AMD3100 (#A5602), AMD3465 (#SML1433) were from Sigma-Aldrich. Oxymetazoline (#1142), IT1t (#4596), TC14012 (#4300), sphingosine-1-phosphate (#1370) were purchased from Tocris. PTH(1-34) (#H-4835), PTH(7-34) (#N-1110), (dw)-PTH(7-34) (#H-9115), PTHrP(1-34) (#H-6630), PTH(1-31) (#H-3408), PTH(3-34) (#H-3088) were from Bachem. Human SDF-1 $\alpha$  (CXCL12) (#300-28A) was purchased from Peprotech. The radioactive ligand [<sup>3</sup>H]RX821002 (#ART1751) was from Hartmann analytics. Angiotensin-II and losartan were kindly provided by V. Jahns (Institute of Pharmacology and Toxicology).

### 2.1.9. Commercially available kits

QIAGEN MIDI plus DNA extraction kit (#12945 QIAGEN)  
Effectene Transfection Reagent (#301425 QIAGEN)

### 2.1.10. Other consumables

Black-wall and black-bottomed 96-well plates (#781968 Brand GMBH)  
White-wall and white-bottomed 96-well plates (#781965 Brand GMBH)  
MultiScreen® Filter plates (#MAFCN0B50 Millipore)  
Millipore® glass-fiber filters (#F7036 Sigma-Aldrich)  
Poly-D-Lysine (#P6407 Sigma-Aldrich)  
Further chemicals applied for false positive testing (Institute of Pharmacology and Toxicology)

### 2.1.11. Plate readers

Synergy Neo2 (BioTek Instruments) equipped with filter optics and two independent injector modules  
GloMax® Discover Multimode Microplate Reader (Promega) equipped with filter optics  
CLARIOstar (BMG Labtech) equipped with monochromator optics

## 2.2. Methods

### 2.2.1. Molecular Biology

#### 2.2.1.1. Preparation of competent *Escherichia coli*

Competence of bacteria describes the ability of a specific strain to incorporate DNA. Since *Escherichia coli* (*E. coli*) are not competent by nature, an artificial competence was created via the following procedure: DH5 $\alpha$  *E. coli* were distributed on a LB agar plate and incubated over night at 37°C. The following day, a single colony was picked for inoculation of 50 ml Lysogeny broth (LB) medium and grown over night at 37°C in a circulatory shaker (180 rpm). The next morning, 250 ml of LB medium were inoculated with 4.5 ml of this pre-culture and incubated at 37°C in the circulatory shaker (180 rpm) to an optical density of 0.5 – 0.6. Subsequently, the suspension was centrifuged for 10 minutes with 3500 rpm (4°C) and the pellet was re-suspended in 25 ml Tris-buffered saline (TBS). After 90 minutes on ice the suspension was aliquoted, frozen in liquid nitrogen and stored at -80°C.

LB medium (autoclaved):            1% (w/v) Trypton  
   0.5% (w/v) yeast extract  
   1% (w/v) NaCl  
   H<sub>2</sub>O  
   (antibiotic if necessary)

LB agar plates:                        1% (W/V) agar in LB-medium  
   (selection antibiotic if necessary e.g. 100  $\mu$ g/ml Ampicillin)

TBS:                                        10% PEG3000  
   5% DMSO  
   20 mM MgCl<sub>2</sub>  
   LB medium

#### 2.2.1.2. Transformation of competent *Escherichia coli*

By definition, transformation implies the DNA uptake by competent bacteria and is used for the amplification of plasmid DNA. Competent cells of the *E. coli* strain DH5 $\alpha$  were used for transformation. Therefore, 100  $\mu$ l of bacteria suspension were slowly defrosted on ice and subsequently mixed with 100  $\mu$ l KCM-buffer and 1  $\mu$ g plasmid DNA or 20  $\mu$ l ligation product, respectively. After 20 minutes incubation on ice, the mix was kept at room temperature for another 10 minutes. After the incubation, 900  $\mu$ l of LB medium was added and bacteria were transferred to a rotational shaker for 90 minutes to regenerate (37°C, 300 rpm). To isolate successfully transformed bacteria, either the whole sample (ligation product) or an aliquot of 50  $\mu$ l was plated on agar plates containing the required selection antibiotic (e.g. 100  $\mu$ g/ml Ampicillin) and cultured over night at 37°C.

KCM-buffer:                            100 mM KCl  
   30 mM CaCl<sub>2</sub>  
   50 mM MgCl<sub>2</sub>  
   H<sub>2</sub>O

#### 2.2.1.3. Mini-plasmid preparation

To purify plasmid DNA, 5 ml of selection medium (e.g. LB 100 µg/ml Ampicillin) were inoculated with single colonies from overnight-cultured agar plates and incubated in a rotational shaker overnight at 37°C. The next day, an aliquot of 1.5 ml was centrifuged for 5 minutes at 5000 rpm. After resuspending the pellet in 50 – 100 µl supernatant, 300 µl of resuspension buffer and lysis buffer were added each subsequently to the sample. The mix was incubated for 2 minutes at room temperature before adding 300 µl neutralization buffer. During lysis, bacterial RNA degraded due to supplemented ribonuclease (RNase A). Then, 300 µl of neutralization buffer were added, the sample was mixed thoroughly and centrifuged for 20 minutes at 14,000 rpm (4°C). The supernatant was transferred to a new reaction tube and centrifuged again at 14,000 rpm (4°C). A new tube was preloaded with 750 µl of isopropanol and mixed with the supernatant for an additional centrifugation step (20 minutes, 14,000 rpm, 4°C). The supernatant was removed to wash the DNA-precipitate with 300 µl of 70% Ethanol. The consequent DNA pellet was dried at room temperature and subsequently diluted in 20 – 30 µl bi-distilled water. Part of this solution was used for the analysis via enzyme restriction.

Resuspension buffer P1:	50 mM Tris 10 mM EDTA 100 µg/ml RNase A, H <sub>2</sub> O, pH 8.0
Lysis buffer P2:	200 mM NaOH 1 % (w/v) SDS
Neutralization buffer P3:	3.0 M potassium acetate, pH 5.0

#### 2.2.1.4. Midi-plasmid preparation

To amplify plasmid DNA, a colony grown on an antibiotic agar plate was transferred to 20 – 25 ml LB medium and incubated over night at 37°C on a circulatory shaker. The DNA was isolated and purified using the Plasmid Midi Kit of Qiagen according to the manufacturer's instructions. Quiagen's protocol relies on alkaline lysis of bacteria followed by chromatographical purification of DNA via anion exchange.

#### 2.2.1.5. Adjustment of DNA preparation

After DNA purification, its concentration was photometrically measured at 260nm using the NanoDrop 2000/2000c Spectrophotometer and set to one µg/ml. The purity of the DNA preparation was evaluated via absorption measurement at 280 nm. The absorption ratio at 260 nm over 280 nm was confirmed to be  $\geq 1.8$  to exclude contamination by proteins.

#### 2.2.1.6. Polymerase-chain-reaction

Polymerase-chain-reaction (PCR) was employed to amplify specific DNA-fragments of a template plasmid. Oligonucleotides (primers) were used to set the starting and endpoint of the fragment amplification while the DNA-polymerase elongates the forward- and reverse-primers by fusing deoxyribonucleosids (dNTPs) to the last 3' nucleotide.

Standard-PCR was performed in a Mastercycler (Eppendorf AG, Hamburg) starting with the thermal denaturation of the DNA for 3 minutes at 94°C followed by 30 cycles of denaturation (30 seconds, 94°C), annealing of primers (1 minute, 55°C) and elongation of the DNA single-strand at the 5' end (2 minutes, 72°C). The final elongation was run at 72°C for 5 minutes.

PCR-assay:                    100 ng DNA template  
                                   2 µl 10 mM dNTP mix (dATP, dCTP, dGTP, dTTP)  
                                   0.5 pM forward-primer  
                                   0.5 pM reverse-primer  
                                   1 µl Pfu polymerase  
                                   10 µl polymerase buffer (10x)  
                                   ad 100 µl H<sub>2</sub>O

#### 2.2.1.7. Isolation and purification of PCR products and DNA fragments

Separation of different DNA strands relies on the size-dependent migratory speed of negatively charged DNA fragments in the electric field. The fluorophore ethidiumbromid stains the DNA in the agarose gel due to its distinctive increase in fluorescence intensity upon excitation with UV light after intercalation between DNA bases.

Verification and isolation of plasmid DNA was performed in 1 % (w/v) agarose gels. Agarose powder was mixed with Tris acetate buffer (TAE) and boiled till complete solubilization. Once, the solution was cooled down to ≈ 50°C, 7 µl of 1% ethidiumbromid solution were added and this mix was poured into a chamber for solidification. The gel was then transferred to the electrophoresis chamber and covered with TAE. Samples were admixed with 5 x DNA-loading buffer and transferred into the wells alongside 1 kb and 100 bp size standard. Electrophoresis was performed with 100 V for 40 – 50 minutes.

The separated DNA bands were identified and cut out under UV excitation. Qiagen QIAquick Gel Extraction Kit was used to extract and purify the DNA from the gel slice according to the manufacturer's instructions.

TAE buffer (50 x):            10 mM EDTA  
                                   50 mM sodium acetate  
                                   400 mM Tris-HCl, pH 8.0  
                                   H<sub>2</sub>O

DNA loading buffer (10 x): 0.25 % (m/w) bromophenol blue  
                                   50 % Glycerin  
                                   100 mM EDTA  
                                   H<sub>2</sub>O

#### 2.2.1.8. Cloning of plasmid DNA

Integration of a specific DNA fragment into a vector is essential to create plasmid DNA encoding a new protein derivative. Due to its good suitability for expression in mammalian cell lines, the plasmid pcDNA3 was used as a vector for the cloning of new DNA constructs. For the creation of the different RET sensors, the previously described FRET CFP/YFP sensors of the murine α<sub>2A</sub>AR (Vilardaga et al., 2003), the human β<sub>2</sub>AR (Reiner et al., 2010) and the human PTH1R (Vilardaga et al., 2003) or human wildtype AT1R, human wildtype CXCR4 and human wildtype S1PR1 were chosen as starting points of the cloning procedure. The cloning of all constructs was run according to the following protocol: First, the required DNA fragment was amplified from a DNA template via PCR. Thereby, the applied oligonucleotides allowed the attachment of specific restriction sites to the DNA sequence. Second, both, the PCR product and the vector were digested with restriction enzymes to yield complementary ends. Temperature and buffer composition were adjusted to applied enzymes to guarantee optimal reaction conditions. After isolation and purification of the DNA fragments, insert and vector DNA were fused in a ligation step. Therefore, both fragments were mixed in an optimal ratio according to equation 5 and ligated over night at 16°C.

$$\text{ng(Insert)} = \frac{\text{ng(Vector)} \cdot \text{kb(Insert)} \cdot 3}{\text{kb(Vector)}} \quad (5)$$

The ligase catalyzes the formation of a phosphodiester-bond between a 3'-hydroxygroup and the 5'-

phosphateresidue of complementary DNA sequences. As a result, the linear plasmid was cyclized and transformed into competent *E.coli*. Isolated colonies were picked and the plasmid DNA was purified via Mini-plasmid preparation. Each clone was tested by control digestion and positive clones were further verified via DNA sequencing performed by Eurofins Genomics (Ebersberg).

Restriction:                   3 µg DNA  
                                  2 µl per restriction enzyme  
                                  5 µl buffer  
                                  5 µl BSA (1 µg/µl)  
                                  ad 50 µl H<sub>2</sub>O

Ligation:                     DNA fragment  
                                  1 µl T4 ligase  
                                  1.5 µl ligase buffer  
                                  ad 15 µl H<sub>2</sub>O

## 2.2.2. Cell Biology

### 2.2.2.1. Cultivation and storage of cell lines

HEK-293 and HEK-TSA cells were grown in cell culture medium at 37°C and 5% CO<sub>2</sub>. Cells were passaged every 2-3 days after a confluency of 80 – 100% was reached. Therefore, old medium was aspirated and cells were washed carefully with DPBS. Subsequently, cells were incubated with 1 ml Trypsin-EDTA solution for one minute and suspended in 6 - 10 ml medium. An aliquot of this suspension was transferred to a new dish with fresh medium. Cells were used for approximately up to 40 passages for transient transfection. For long-term storage in -80°C or liquid nitrogen, cells were harvested according to the above described procedure but suspended in FCS- and DMSO-enriched medium and aliquoted into cryo-vials. These vials were initially stored -20°C for 2 hours and subsequently transferred to -80°C or liquid nitrogen. When cells were thawed, the freezing medium was replaced for fresh cell culture medium (without DMSO) as soon as cells were attached to the dish's surface.

Cell culture medium:           DMEM 4.5 g/l Glucose  
                                  10% (V/V) FCS  
                                  1% (V/V) L-Glutamine (200mM)  
                                  1% (V/V) Penicillin/Streptomycin  
                                  (100 U/ml Penicillin; 0.1 mg/ml Streptomycin)

Freezing medium:             80% (V/V) complete medium  
                                  10% (V/V) FCS  
                                  10% (V/V) DMSO

### 2.2.2.2. Transient transfection and plating

Exogenous DNA is introduced to eukaryotic cells through transient transfection. For experiments under transient expression, 1.5 x 10<sup>6</sup> HEK-TSA cells were seeded onto a 5.5 cm dishes and transfected the next day with 2 µg of plasmid DNA using Effectene transfection reagent (Quiagen) according to the manufacturer's protocol. In case two different plasmids were co-transfected, 4 µg total amount of DNA were mixed in a 1:1 ratio. Transient transfection of RAMP2 plasmids was conducted using Lipofectamine (ThermoFisher) according to the manufacturer's protocol. 24 hours after transfection, cells were transferred to poly-D-lysine (0.1 mg/ml in DPBS) pre-coated black-wall, black-bottomed (FRET experiments) or white-wall, white bottomed (BRET experiments) 96-well plates at a density of 50,000 (FRET) or 20,000 (BRET) cells per well and grown overnight at 37°C, 5% CO<sub>2</sub>.





Binding buffer:                    50 mM TRIS  
   100 mM NaCl  
   3 mM MgCl<sub>2</sub>  
   H<sub>2</sub>O (pH 7.4)

### 2.2.3. Radioligand binding

To assess total radioligand binding, 5 µg of membrane protein were incubated with different concentrations (0.04 – 12 nM) of α<sub>2A</sub>AR antagonist radioligand [<sup>3</sup>H]RX821002. 20 µM phentolamine was added in a separate test series to define unspecific binding. Competition binding was performed by incubating 2 µg membrane protein with 0.3 – 2.0 nM [<sup>3</sup>H]RX821002 and increasing concentrations of the different α<sub>2A</sub>AR ligands in the presence (= low affinity state for agonists) or absence (= high affinity state for agonists) of 10 µM GTP. Following incubation for 1 hour at room temperature, membranes were transferred to Millipore glass-fiber filters via vacuum filtration. These filters were incubated with scintillation cocktail (Roth) and membrane-bound radioactivity was measured with a scintillation counter.

### 2.2.4. Biophysical methods

#### 2.2.4.1. Measurement of fluorescence / bioluminescence spectra

HEK-TSA cells were transiently transfected with the different α<sub>2A</sub>AR BRET sensors and labeled as described above to read only the emission and excitation spectra of the different acceptor fluorophores. Nluc, CFP and YFP spectra were collected using unlabeled HEK-TSA cells expressing α<sub>2A</sub>AR<sub>Nluc/Halo</sub> (upon addition of Nluc substrate), α<sub>2A</sub>AR<sub>CFP/Halo</sub> or α<sub>2A</sub>AR<sub>YFP/Halo</sub>. All spectra were measured in RET buffer with 2 nm resolution from 400 to 700 nm using a CLARIOstar plate reader (BMG) in 96-well plates. Spectra are expressed as a percentage of the respective maximal excitation or emission peak.

RET buffer:                        2 mM HEPES  
   28 mM NaCl  
   1.08 mM KCl  
   0.2 mM MgCl<sub>2</sub>  
   0.4 mM CaCl<sub>2</sub>  
   H<sub>2</sub>O (pH 7.3)

#### 2.2.4.2. Measurement of FRET and BRET emission spectra

FRET and BRET emission spectra of (labeled) HEK-TSA cells expressing the different biosensors were recorded in RET buffer with 2 nm resolution from 400 to 700 nm upon donor excitation at 420 nm (FRET sensors) or addition of 1:1000 furimazine dilution (BRET) with a CLARIOstar plate reader (BMG) in 96-well plates. Spectra are expressed as a percentage of the maximal donor emission peak.

#### 2.2.4.3. Assessment of total cellular PTHR1<sub>Nluc/Halo</sub> expression levels

Total cellular expression levels of PTHR1<sub>Nluc/Halo</sub> was quantified through the absolute Nluc emission intensity of the unlabeled control using the Synergy Neo2 plate reader equipped with a 460/40 nm filter.

#### 2.2.4.4. Assessment of receptor surface expression

Surface localization of the different receptor constructs was quantified reading the emission intensities of fluorescently-tagged Anti-HA- or Anti-FLAG-tag antibodies using the Synergy Neo2 plate reader in 96-well plates. HEK cells incubated with Anti-Flag® M2 Cy3 ( $\beta_2AR^{Nluc/Halo}$  or  $\beta_2AR$ ) were excited using a 540/20 excitation and the emission intensity was recorded using 590/35 emission filter after automatic gain adjustment. Following automatic gain adjustment of the plate reader, fluorescence intensities of HEK-TSA cells stained with Anti-HA-AlexaFluor594 were measured using a 590/20 (excitation) – 620/15 (emission) filter combination.

#### 2.2.4.5. Assessment of $G\alpha_{i2}$ -FRET and H187-EPAC-FRET sensor expression levels

The Synergy Neo2 plate reader was employed to assess the cellular levels of the downstream  $G\alpha_{i2}$ - and H187-EPAC-FRET sensors expressed in HEK cells plated in 96-well plates. Therefore, following automatic gain adjustment of the plate reader, the FRET acceptors (cpVenus173 and tandem cpVenus173) were directly excited using a 500/20 nm excitation filter and resulting emission intensities were detected with a 540/20 filter.

#### 2.2.4.6. FRET measurements

Cells in 96-well plates expressing the different FRET sensors were washed once and covered with RET buffer. Basal FRET ratio was measured in 90  $\mu$ l RET buffer. Subsequently, 10  $\mu$ l of 10-fold ligand solution or buffer (negative control) was applied to each well and the stimulated FRET ratio was recorded. All FRET experiments were conducted at 37 °C with a Synergy Neo2 plate reader (BioTEK) equipped with 420/50 nm excitation and 485/20 nm emission filters for CFP. Acceptor emission of YFP, HaloTag® R110, HaloTag® diAcFAM, HaloTag® Oregon Green® and SNAP-cell 505-Star were detected with a 540/25 nm filter. To measure the emission of HaloTag® TMR-Direct and SNAP-cell TMR-Star a 590/35 nm filter was used. Emission of HaloTag® NanoBRET 618 and SNAP-cell 647SiR were detected with a 620/15 nm and 680/20 nm filter, respectively. 50 excitation flashes were applied per data point.

#### 2.2.4.7. BRET measurements

Cells transiently or stably expressing the BRET biosensors were washed once and incubated with substrate (90  $\mu$ l of 1:1000 in RET buffer for  $\beta_2AR^{Nluc/Halo(618)}$ ,  $PTHR1^{Nluc/Halo(618)}$ ,  $AT1R^{Nluc/Halo(618)}$ ,  $CXCR4^{Nluc/Halo(618)}$ ,  $S1PR1^{Nluc/Halo(618)}$ ; 90  $\mu$ l 1:4000 or as indicated for  $\alpha_2AAR^{Nluc/acceptor}$  in 96-well plates; 45  $\mu$ l dilution as indicated for  $\alpha_2AAR^{Nluc/acceptor}$  in 384-well plates) for 2-5 minutes at 37°C to allow for substrate diffusion and the basal BRET ratio was measured. Following this, 10  $\mu$ l (96-well plates) or 5  $\mu$ l (384-well plates) of 10-fold ligand solution or buffer was applied to each well and the stimulated BRET ratio was recorded. To reduce the fluctuation of the BRET ratio in Z-factor experiments, 7 individual BRET ratios within 5 minutes were measured and averaged before and after ligand addition. BRET experiments were performed at 37 °C with a GloMAX Discover (Promega) or Synergy Neo2 (BioTEK) plate reader equipped with a 460/40 nm filter to select the NanoLuc emission. For cpVenus173, HaloTag® R110, HaloTag® diAcFAM, HaloTag® Oregon Green® and SNAP-cell 505-Star a 520/20 nm filter was used to select the acceptor emission peaks. TagRFP, HaloTag® TMR-Direct and SNAP-cell TMR-Star emissions were detected with a 530 nm long pass filter. For HaloTag® NanoBRET 618 a 620/20 nm filter was used and a 600 nm long pass filter was applied for the BRET acceptors mCherry and SNAP-cell 647SiR. The integration time per data point was set to 0.3 seconds.

Experiments with higher temporal resolution were performed employing the Synergy Neo2 (BioTEK) plate reader, which is equipped with injectors and allows faster acquisition time. Data were recorded in well-mode, the acquisition interval was set to 1 second and the integration time to 0.3 seconds. After acquisition of baseline for 180 seconds, 10  $\mu$ l of solution with or without ligand (buffer control) were injected with a speed of 225  $\mu$ l per second (delivery time = 44 milliseconds) and the signal was recorded for 180 to 360 seconds.

## 2.2.5. Data analysis and statistics

FRET and BRET ratios before ( $\text{Ratio}_{\text{basal}}$ ) and after ligand or buffer addition ( $\text{Ratio}_{\text{stim}}$ ) were calculated as acceptor emission over donor emission. To correct for donor bleedthrough into the acceptor channel, the averaged ratio of the unlabeled control (UC) was subtracted from each ratio of labeled wells. For cells expressing biosensors with a fluorescent protein as acceptor, the mean UC ratio of the analogous unlabeled HaloTag construct was considered for bleedthrough correction. To quantify ligand induced conformational changes,  $\Delta\text{FRET}$  or  $\Delta\text{BRET}$  was calculated for each well as a percent over basal ( $((\text{Ratio}_{\text{stim}} - \text{Ratio}_{\text{basal}})/\text{Ratio}_{\text{basal}})*100$ ) and subtracted by the averaged  $\Delta\text{FRET}$  or  $\Delta\text{BRET}$  of buffer. Z-factors expressing the assay quality were calculated with the following equation:

$$Z = 1 - \frac{(3x\sigma_S + 3x\sigma_C)}{\mu_S - \mu_C} \quad (6)$$

where  $\sigma_S$  and  $\sigma_C$  are the standard deviations of  $\Delta\text{FRET}$  or  $\Delta\text{BRET}$  of positive and negative control, respectively and  $\mu_S$  and  $\mu_C$  express the mean of  $\Delta\text{FRET}$  or  $\Delta\text{BRET}$  values. If the positive control induced a decrease in the energy transfer (negative  $\Delta\text{RET}$  as for  $\alpha_2\text{AAR}_{\text{CFP/YFP}}$ ,  $\beta_2\text{AR}_{\text{Nluc/Halo(618)}}$ ,  $\text{PTHR1}_{\text{Nluc/Halo(618)}}$ ,  $\text{PTHR1}_{\text{CFP/YFP}}$ ) the denominator in equation is inverted ( $\mu_C - \mu_S$ ). As a positive control, we defined 100  $\mu\text{M}$  epinephrine for the  $\alpha_2\text{AAR}$  and  $\beta_2\text{AR}$  sensors and 10  $\mu\text{M}$  PTH(1-34) for PTHR1 sensors. Buffer was used as a negative control in all Z-factor experiments. For consistency, all agonist-induced RET changes were plotted as ascending curves or bars. Therefore, y-axes in all figures were inverted if agonists for the respective biosensor induced a reduction of the ratio. Data were analyzed using Prism 5.0 software (GraphPad) and expressed as mean  $\pm$  standard error mean (s.e.m.) Data from concentration-response experiments was fitted using a mono-exponential curve four-parameter fit. Kinetic BRET ratios were fitted to one-phase association or one-phase decay curves for norepinephrine or yohimbine and phentolamine, respectively. Radioactivity values from binding experiments were analyzed using a one-site fitting model if GTP was added prior the experiment. Data from competition binding experiments without exogenously added GTP was first analyzed for the statistically preferred fitting model applying extra-sum-of squares F-test comparing a one-component versus two-component fit. Superiority of the two-component model was confirmed for all agonists (partial or full) tested. The two-component fit was then conducted with the fraction of the high-affinity component (RH) fixed to 0.58, which is the mean RH of all data where this model was applied. Statistical differences were evaluated using one-way ANOVA test followed by Bonferroni multiple comparison, Student's t-test or extra-sum-of squares F-test. Differences were considered significant for values of  $p < 0.05$ .

### 3. Results

#### 3.1. Designing an $\alpha_{2A}$ AR biosensor suitable for microtiter plate experiments

We permuted the well-characterized model GPCR  $\alpha_{2A}$ AR to obtain a biosensor that reliably reports changes in receptor conformation in a microtiter plate format. It has been shown that combining CFP at the receptor C-terminus to YFP or FIAsH within icl3 yielded excellent intramolecular  $\alpha_{2A}$ AR FRET sensors for single-cell experiments (Hoffmann et al., 2005; Vilardaga et al., 2003). In both biosensors, the donor was fused to Val461 at the shortened C-terminus and the acceptor was inserted between Ala250 and Ser371 within the truncated icl3 (**Figure 3.1**). We maintained these insertion positions and the HA-tag at the receptor N-terminus and set out to employ both types of resonance energy transfer, FRET and BRET, to generate  $\alpha_{2A}$ AR conformational biosensors. In FRET sensors, we kept CFP as a fluorescent donor while Nluc was utilized for the creation of BRET-based biosensors. Both donors were combined with a set of different acceptor fluorophores to ultimately generate novel conformational biosensors for experimental examination in a microtiter plate format.

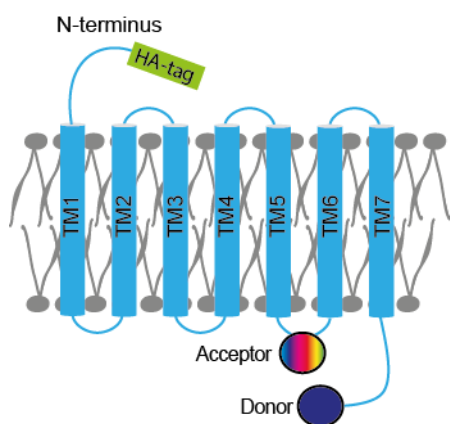


**Figure 3.1: Design of conformational  $\alpha_{2A}$ AR RET sensors.**

All  $\alpha_{2A}$ AR RET sensors explored in this study share the same insertion sites. Donor chromophores are fused to the C-terminus and acceptors are incorporated within icl3 or vice versa for the inverted version of  $\alpha_{2A}$ AR<sub>Nluc/Halo</sub>. An HA-tag is fused to the extracellular receptor N-terminus.

##### 3.1.1. Selected labeling techniques and chromophores

Overall, we generated 10 different FRET- and 11 BRET-based  $\alpha_{2A}$ AR conformational biosensors. All FRET sensors rely on the donor fluorophore CFP ( $\lambda_{Em} = 478$  nm) whereas the BRET analogues take advantage of the small and bright luciferase Nluc ( $\lambda_{Em} = 450$  nm) (**Figure 3.2A and B**).

To capitalize on the significant advancements in the field of fluorescent proteins, we initially combined these RET donors to suitable fluorescent protein acceptors. Specifically, we substituted the original FRET acceptor YFP for its refined circular-permuted analogue cpVenus173 ( $\lambda_{Em} = 530$  nm) and the orange and red fluorescent proteins TagRFP ( $\lambda_{Em} = 580$  nm) and mCherry ( $\lambda_{Em} = 610$  nm), respectively (**Figure 3.2A**). As an alternative to fluorescent proteins, we applied the latest generation of self-labeling protein techniques by tagging icl3 of  $\alpha_{2A}$ AR with HaloTag or SNAP-tag. This strategy allows to examine eight bright organic fluorophores (five membrane-permeable HaloTag and three membrane-permeable SNAP-tag dyes) covering a wide range of the visible spectrum as energy acceptors for both, CFP and Nluc (**Figure 3.2C and D**).

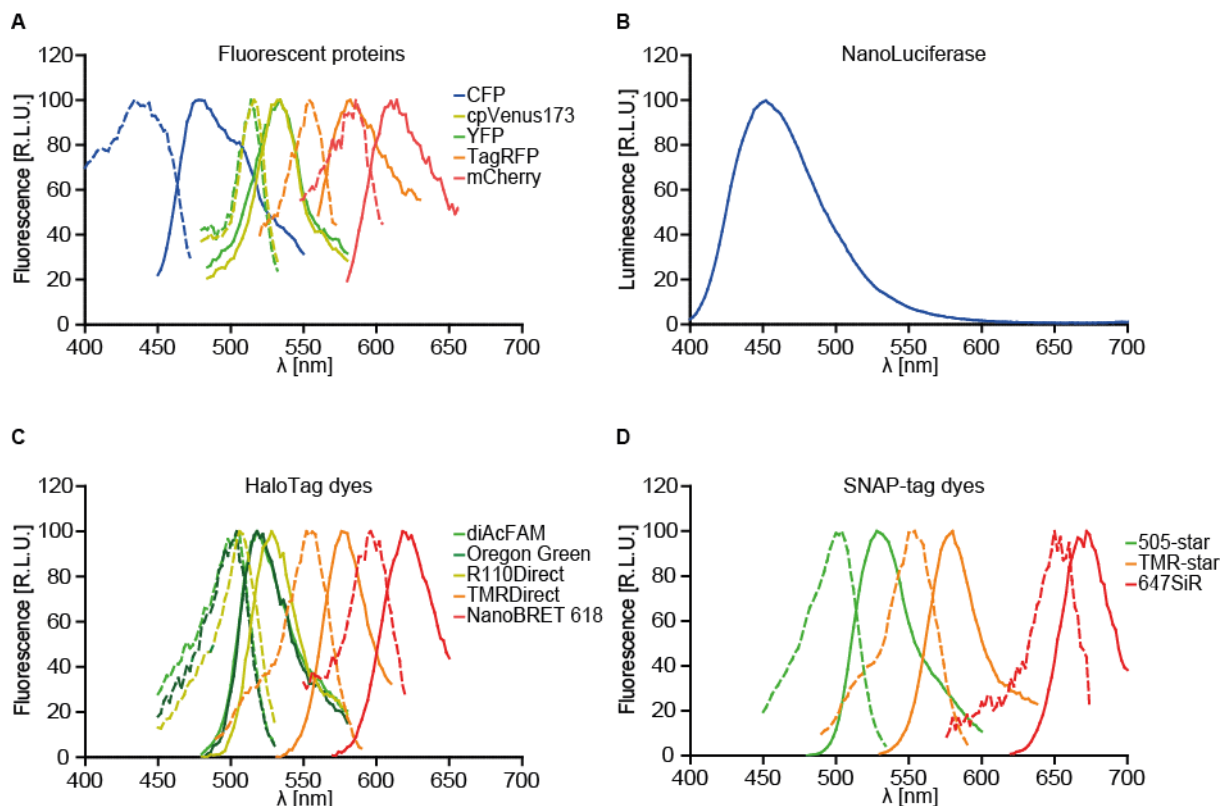


**Figure 3.2: Spectra of applied RET partners.**

Normalized excitation (dotted lines) and emission (filled lines) spectra of all chromophores employed for the creation of conformational  $\alpha_{2A}AR$  sensors are displayed. HEK-TSA cells were transiently transfected with  $\alpha_{2A}AR$  constructs bearing fluorescent proteins (A), NanoLuciferase (B) or the labeled protein tags HaloTag (C) and SNAP-tag (D). Data show mean of three replicates.

### 3.1.2. Basal energy transfer of $\alpha_{2A}AR$ sensors

The applied set of donor and acceptor fluorophores exhibits (i) diverse excitation and emission spectra (**Figure 3.2**), (ii) varying degrees of spectral overlap between donor emission and acceptor excitation and (iii) distinct photophysical properties (e.g. acceptor extinction coefficients). These parameters, altogether, affect the overall sensor performance.

In order to confirm resonance energy transfer in the basal state of  $\alpha_{2A}AR_{donor/acceptor}$  sensors, we recorded the emission spectra of the different conformational biosensors upon donor excitation (FRET) or furimazine addition (BRET), respectively, and compared these data to the spectra of the only-donor controls ( $\alpha_{2A}AR_{CFP/Halo(unlabeled)}$  for FRET sensors,  $\alpha_{2A}AR_{Nluc/Halo(unlabeled)}$  for BRET sensors). Transiently transfected (and labeled) HEK-TSA cells were grown overnight in 96-well plates to allow for cell adhesion to the well bottoms. Upon CFP excitation or Nluc substrate addition, the emission spectra were recorded using a CLARIOstar microtiter plate reader (**Figure 3.3**). Compared to the only-donor controls, all biosensors showed elevated emission intensities at the acceptor-characteristic wavelengths (e.g.  $\approx 530$  nm for YFP). This indicates the occurrence of donor-to-acceptor energy transfer in the ligand-free, basal state of the different  $\alpha_{2A}AR_{donor/acceptor}$  sensors, however, direct acceptor excitation can also contribute to the increased emission intensities at the acceptor-characteristic wavelengths in FRET  $\alpha_{2A}AR_{CFP/acceptor}$  sensors.

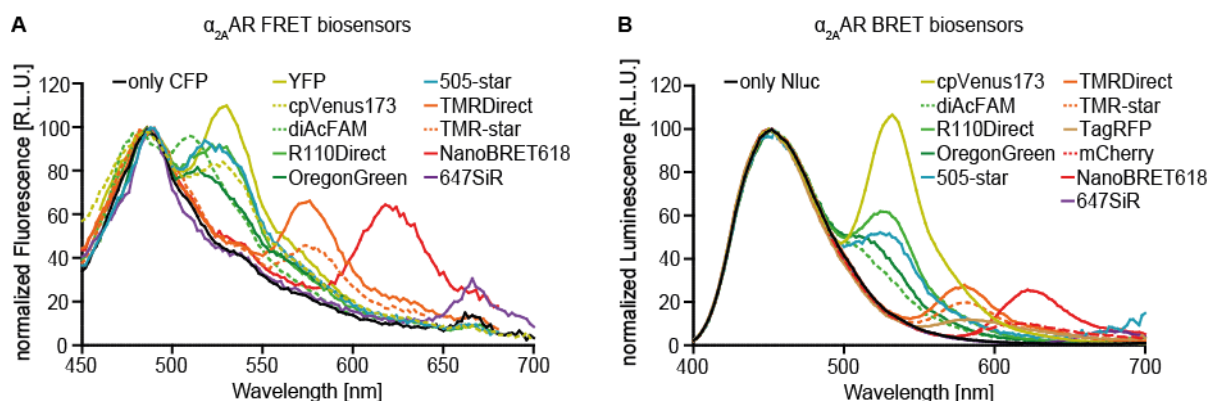


**Figure 3.3: Basal energy transfer in conformational  $\alpha_{2A}$ AR biosensors.**

FRET (A) and BRET (B) spectra of HEK-TSA cells transiently expressing the different  $\alpha_{2A}$ AR conformational biosensors were recorded upon CFP excitation (FRET) or luciferase substrate addition (BRET) and normalized for the donor emission peak. As an only-donor control, spectra of unlabeled HEK-TSA cells expressing  $\alpha_{2A}$ AR<sub>CFP/Halo</sub> or  $\alpha_{2A}$ AR<sub>Nluc/Halo</sub> were recorded following the same procedure (black). Data show mean of at least three replicates.

### 3.1.3. Sensitivity of $\alpha_{2A}$ AR sensors to agonist stimulation

The ability to transfer energy through dipole-dipole interaction in one specific (basal) protein conformation is an important but not sufficient requirement for conformational GPCR sensors. On top of that, valuable GPCR sensors must be capable of translating the ligand-induced conformational rearrangement of the receptor to a recordable change of the RET efficiency.

To evaluate whether the novel  $\alpha_{2A}$ AR FRET and BRET biosensors are capable of reporting ligand-induced receptor rearrangements, we performed ratiometric RET experiments with cells transiently expressing the different biosensors in 96-well plates. To induce a conformational reorganization of the  $\alpha_{2A}$ AR sensors, we exposed the cells to 100  $\mu$ M of the endogenous full  $\alpha_{2A}$ AR agonist norepinephrine and calculated the ligand-induced RET changes (%  $\Delta$ FRET or %  $\Delta$ BRET) (Figure 3.4).

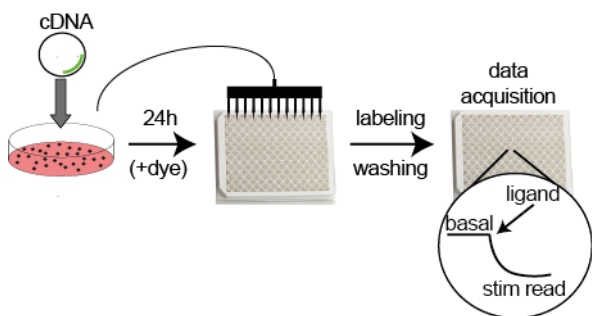


**Figure 3.4: Workflow of ratiometric RET experiments in 96-well plates.**

HEK-TSA cells were transiently transfected with the different  $\alpha_{2A}$ AR sensors, transferred to 96-well plates, labeled if necessary and tested for ligand-induced changes of the RET ratio.

To correct for technical artifacts due to the addition of norepinephrine-containing solution (e.g. resulting from altering refractive indices or absorbance properties of the cell-covering liquid), we stimulated the cells with buffer and used this negative control to discriminate between RET signals arising from changes in volume (= technical artifact) vs. agonist-induced GPCR conformational changes.

Five of ten tested  $\alpha_{2A}$ AR FRET sensors reported statistically significant FRET changes for norepinephrine compared to negative control:  $\alpha_{2A}$ AR<sub>CFP/YFP</sub>,  $\alpha_{2A}$ AR<sub>CFP/cpVenus173</sub>,  $\alpha_{2A}$ AR<sub>CFP/Halo(OregonGreen)</sub>,  $\alpha_{2A}$ AR<sub>CFP/Halo(R110Direct)</sub> and  $\alpha_{2A}$ AR<sub>CFP/SNAP(505-star)</sub> (Figure 3.5A). The combination of CFP to the green light emitting HaloTag dye R110Direct™ yielded the highest  $\Delta$ FRET but still showed considerable signal variation (mean  $\pm$  s.e.m.  $\Delta$ FRET(norepinephrine) = 4.89  $\pm$  1.34 %; Student's t-test norepinephrine vs. buffer: p = 0.0014).

Furthermore, norepinephrine-induced receptor conformational changes were detectable in seven of eleven generated  $\alpha_{2A}$ AR BRET sensors:  $\alpha_{2A}$ AR<sub>Nluc/cpVenus173</sub>,  $\alpha_{2A}$ AR<sub>Nluc/mCherry</sub>,  $\alpha_{2A}$ AR<sub>Nluc/Halo(diAcFAM)</sub>,  $\alpha_{2A}$ AR<sub>Nluc/Halo(OregonGreen)</sub>,  $\alpha_{2A}$ AR<sub>Nluc/Halo(R110Direct)</sub>,  $\alpha_{2A}$ AR<sub>Nluc/Halo(TMRDirect)</sub> and  $\alpha_{2A}$ AR<sub>Nluc/Halo(618)</sub> (Figure 3.5B).

Among all biosensors tested,  $\alpha_2AAR_{Nluc/Halo(618)}$  displayed the highest  $\Delta RET$  amplitude (mean  $\pm$  s.e.m.  $\Delta BRET(norepinephrine) = 8.15 \pm 0.72 \%$ ; Student's t-test norepinephrine vs. buffer:  $p < 0.0001$ ) – at least twofold higher than any other conformational  $\alpha_2AAR$  RET sensor design examined in this study.

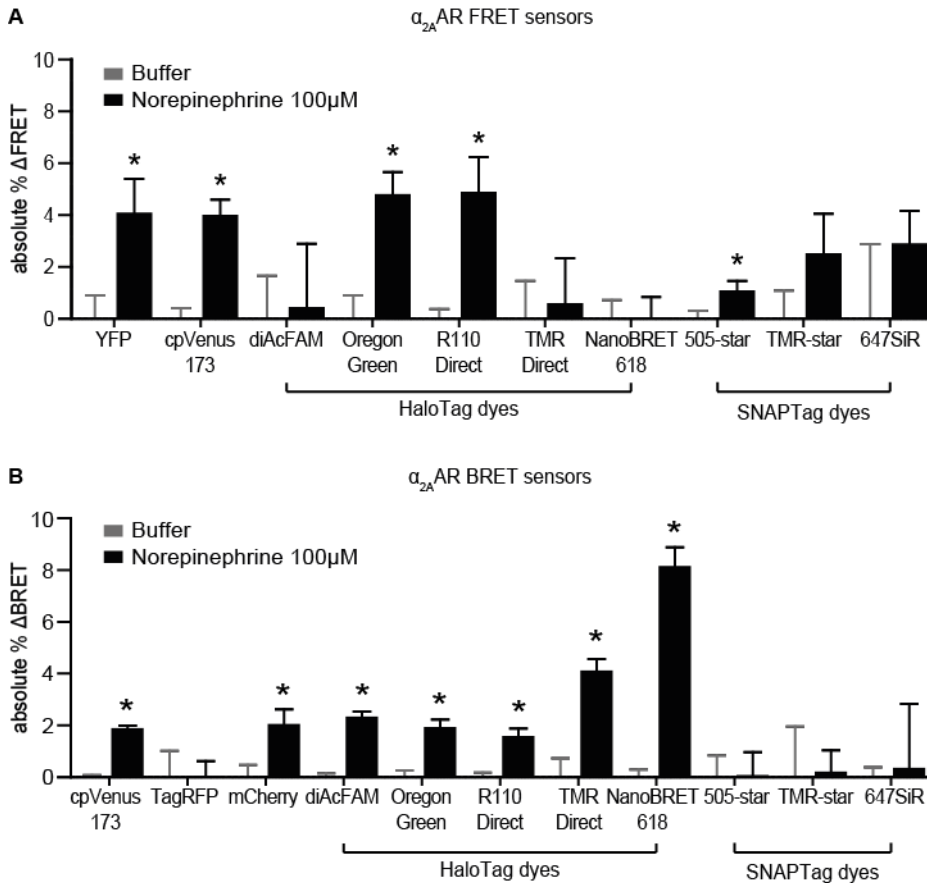


**Figure 3.5: Sensitivity of  $\alpha_2AAR$  sensors to agonist stimulation.**

HEK-TSA cells transiently expressing the ten different FRET (A) and eleven BRET (B) sensors were stimulated with 100  $\mu M$  of the full endogenous agonist norepinephrine or buffer to calculate  $\Delta FRET$  and  $\Delta BRET$  based on RET ratios before and after stimulation. Bar graphs show mean  $\pm$  s.e.m. of at least three independent experiments performed in quadruplicates or octuplicates. Statistical difference of norepinephrine-induced  $\Delta FRET$  or BRET versus buffer was analyzed conducting Student's t-test; \* $p \leq 0.05$ .

For some RET-based biosensors, inverting the donor and acceptor insertion sites has led to unexpected alterations of sensor performance (Ohta et al., 2016). With the goal of further improving the  $\alpha_2AAR_{Nluc/Halo(618)}$  biosensor's sensitivity, we followed this strategy and inverted the order of the BRET partners. Thereby, we created a version of  $\alpha_2AAR_{Nluc/Halo(618)}$  bearing Nluc within icl3 and HaloTag at the C-terminus and examined norepinephrine-induced BRET signals (Figure 3.6).

Also the swapped  $\alpha_2AAR_{Nluc/Halo(618)}$  biosensor was able to detect agonist-induced receptor conformational changes in microtiter plate format. However, a lower  $\Delta BRET$  amplitude was evident as compared to the original  $\alpha_2AAR_{Nluc/Halo(618)}$  version (mean  $\pm$  s.e.m.  $\Delta BRET(norepinephrine) = 5.05 \pm 0.35 \%$ ; Student's t-test norepinephrine vs. buffer:  $p < 0.0001$ ).

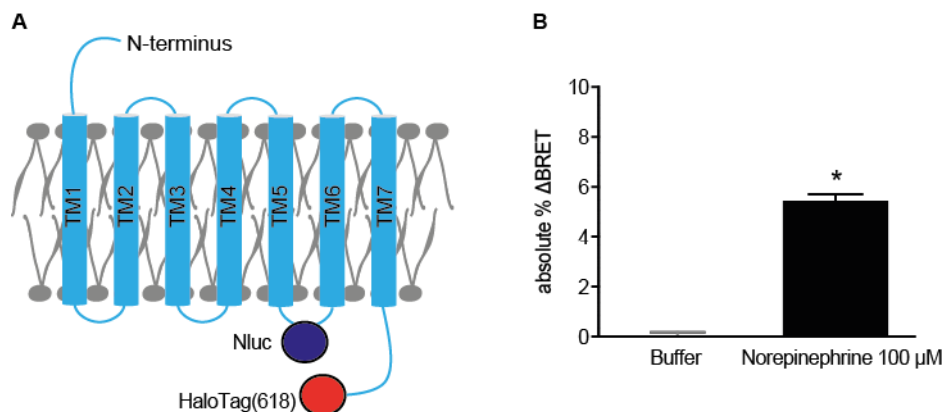


**Figure 3.6: Effect of inverting donor/acceptor positions within the  $\alpha_{2A}AR_{Nluc/Halo(618)}$  biosensor.**

**A)** Schematic of the inverted  $\alpha_{2A}AR_{Nluc/Halo(618)}$  sensor bearing Nluc within icl3 and labeled HaloTag fused to the C-terminus. **B)** HEK-TSA cells were transiently transfected with the inverted sensor version and treated with negative control buffer or 100  $\mu M$  of the full agonist norepinephrine to calculate ligand-induced  $\Delta BRET$  signals. Data show mean  $\pm$  s.e.m. of four independent experiments conducted in quadruplicates. Statistical significance of buffer- vs. norepinephrine-induced  $\Delta BRET$  was assessed applying Student's *t*-test. \* $p \leq 0.05$ .

### 3.2. Validation of the $\alpha_{2A}AR_{Nluc/Halo(618)}$ assay

Since  $\alpha_{2A}AR_{Nluc/Halo(618)}$  displayed the highest dynamic range among the sensors created, this BRET design was considered the most promising to develop HTS-compatible conformational GPCR sensors. Nevertheless, the capability to transform the conformational change induced by one endogenous agonist into a specific RET signal represents only one vital competence of a valuable intramolecular GPCR sensor. Discriminating receptor ligands with differing intrinsic activities and promoting intracellular signaling, as well as wildtype-like ligand binding affinities constitute further important characteristics of valuable conformational GPCR sensors.

To evaluate these characteristics and improve the assay reproducibility, we created a HEK-293 cell line stably expressing  $\alpha_{2A}AR_{Nluc/Halo(618)}$  and set out to examine several pharmacological aspects of this novel conformational biosensor. The individual cells within such stable cell lines display homogenous sensor expression levels increasing the signal-to-background ratio (less non-transfected cells) and providing improved comparability of different datasets due to the stable sensor expression levels over up to 30 cell passages.

#### 3.2.1. Ligand binding properties of $\alpha_{2A}AR_{Nluc/Halo(618)}$

Optimal GPCR biosensors, as any biomedical tool designed to identify and characterize novel potential drug candidates, should display wildtype pharmacological properties despite the introduction of intracellular tags. This will allow to reliably interpret experimental datasets with respect to the pharmacological properties of test compounds and to predict implications for potential future treatments. Therefore, we verified that the novel GPCR<sub>Nluc/Halo(618)</sub> sensors exhibit similar ligand binding properties as the respective wildtype receptor. Radioligand binding assays still represent the method of choice for this purpose since they require the minimal manipulation of the GPCR-ligand system. Thus, we conducted radioligand binding studies of wildtype  $\alpha_{2A}AR$  and  $\alpha_{2A}AR_{Nluc/Halo(618)}$  after expressing these receptor variants in HEK cells and purifying receptor-containing membrane fractions. We applied the tritiated  $\alpha_{2A}AR$  antagonist [<sup>3</sup>H]RX821002 in the presence of 10  $\mu M$  GTP to uncouple the receptors from endogenous G proteins and determine the receptors' binding affinities to a set of different  $\alpha_{2A}AR$  ligands (**Figure 3.7**). With the exception of tyramine, all other nine  $\alpha_{2A}AR$  ligands employed did not show any statistical difference in binding to wildtype  $\alpha_{2A}AR$  versus  $\alpha_{2A}AR_{Nluc/Halo}$  suggesting that this biosensors exhibits wildtype-like ligand binding affinities.



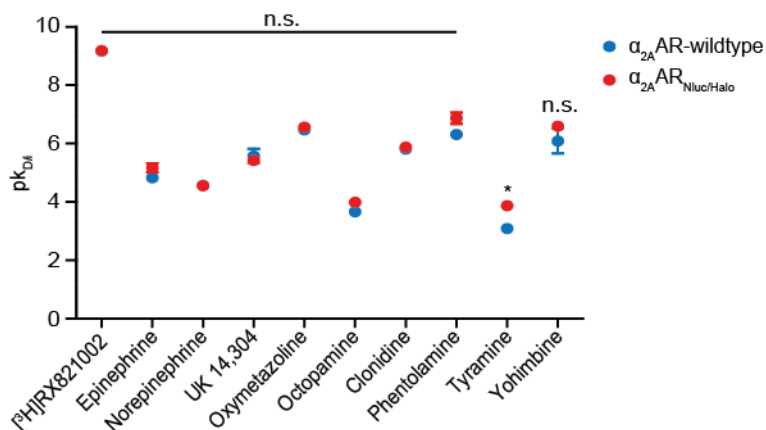


**Figure 3.7: Ligand binding properties of  $\alpha_{2A}AR^{Nluc/Halo}$  in the presence of GTP.**

Statistical difference of wildtype versus sensor binding values was analyzed applying Student's *t*-test. Data show mean  $\pm$  s.e.m. of at least three independent experiments.  $p \leq 0.05$ . n.s.: not significant

### 3.2.2. Optimization of the $\alpha_{2A}AR^{Nluc/Halo(618)}$ assay

Having confirmed that  $\alpha_{2A}AR^{Nluc/Halo(618)}$  features wildtype binding properties, we proceeded optimizing the BRET assay sensitivity in 96-well microtiter plates. We performed a set of experiments in which the BRET amplitude upon agonist stimulation was measured as a function of different assay parameters to identify the optimal experimental settings. Three major controllable assay parameters were tested: (a) cell density, (b) concentration of the Nluc substrate (furimazine) and (c) labeling concentration of the BRET acceptor dye. Additionally, the impact of stable vs. transient sensor expression was evaluated. **Cell density:** Initially, 20,000, 40,000 and 80,000 transiently transfected cells were seeded into 96-well plate, labeled with 100 nM acceptor dye, incubated with 1/4,000 furimazine stock dilution and stimulated with 100  $\mu$ M norepinephrine or buffer. The highest  $\Delta$ BRET was obtained with a density of 20,000 cells per well ( $7.97 \pm 0.58\%$  vs.  $5.05 \pm 0.54\%$  and  $5.58 \pm 0.51\%$  with 40,000 and 80,000 cells per well, respectively) (**Figure 3.8A**).

**Furimazine concentration:** Based on the results with altering cell densities, 20,000 transiently transfected and labeled (100 nM) sensor cells were incubated with 1/20,000, 1/4,000, 1/2,000 or 1/1,000 furimazine stock dilution to measure agonist-induced BRET signals as a function of Nluc-substrate concentration. No statistically relevant BRET change was obtained with 1/20,000 substrate dilution. In contrast, all higher furimazine concentrations yielded significant indiscernible  $\Delta$ BRET values (**Figure 3.8B**).

**BRET acceptor labeling concentration:** 20,000 stably expressing sensor cells were plated and labeled with varying concentrations of the BRET acceptor HaloTag(618) overnight. An improvement of the norepinephrine-induced BRET signal from  $\approx 10\%$  to  $\approx 15\%$  was recorded when a labeling concentration of HaloTag(618) less than 500 nM (300 nM, 100nM or 50 nM) was used (**Figure 3.8C**).

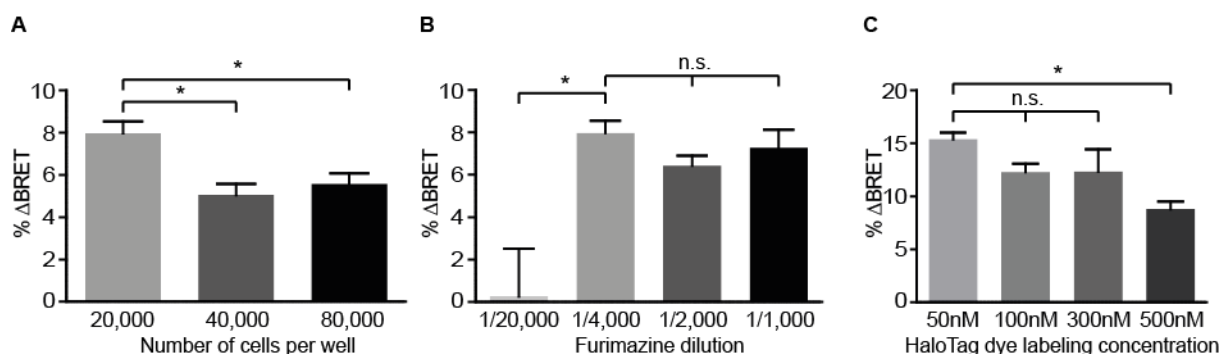


**Figure 3.8:  $\alpha_{2A}AR_{Nluc/Halo(618)}$  assay optimization.**

The optimal values of three assay parameters were identified in a 96-well plate format. (A) Increasing number of transiently transfected cells were seeded to measure the 100  $\mu$ M norepinephrine-induced BRET changes (transient sensor expression; dilution of substrate: 1/4,000; labeling concentration of HaloTag dye: 100 nM). (B) Norepinephrine-induced BRET changes were assessed as a function of the substrate dilution (furimazine) (transient sensor expression; cell density: 20,000 per well; labeling concentration of HaloTag dye: 100 nM). (C) Norepinephrine-induced BRET changes were assessed as a function of the BRET acceptor labeling concentration (stable sensor expression; cell density: 20,000 per well; substrate dilution: 1/4,000). Data represent mean  $\pm$  s.e.m. of at least three independent experiments conducted in quadruplicates. Difference was analyzed by one-way ANOVA followed by Bonferroni post hoc test. \* $p \leq 0.05$  versus 20,000 cells (A); 1/4,000 furimazine dilution (B); 50 nM NanoBRET618 (C).

Based on the results described above, the following assay settings were considered optimal and implemented in all following  $\alpha_{2A}AR_{Nluc/Halo(618)}$  experiments: 20,000 cells per well, 1/4,000 furimazine dilution and 50 nM HaloTag 618 labeling concentration.

Additionally, these experiments allowed us to evaluate the effect of stable sensor expression on assay performance. The comparison of the norepinephrine-induced BRET amplitudes obtained under identical assay conditions (20,000 cells per well, 1/4,000 substrate dilution, 100 nM labeling concentration) but upon transient (Figure 3.8A, bar “20,000”) vs. stable sensor expression (Figure 3.8C, bar “100nM”) highlighted the improved sensor performance resulting from stable expression. Both expression systems yielded an increase in BRET upon agonist stimulation, however, the stable sensor cell line reported significantly higher  $\Delta$ BRET signals compared to transiently transfected cells ( $12.30 \pm 0.77\%$  vs.  $7.97 \pm 0.58\%$ ;  $p < 0.0001$ ).

### 3.2.3. Kinetics of $\alpha_{2A}AR_{Nluc/Halo(618)}$ BRET signals

Conformational GPCR sensors constitute unique tools for the investigation of GPCR (de-)activation kinetics and ligand-GPCR residence times (i.e. the lifetime of a ligand-target complex). Especially ligand-GPCR residence time has raised increasing interest in the scientific community as an important drug parameter and represents a promising leverage point for the optimization of therapeutic drugs (Hoffmann et al., 2015). To determine whether the novel sensor design provides insights into GPCR activation and deactivation kinetics, we monitored conformational dynamics of  $\alpha_{2A}AR_{Nluc/Halo(618)}$  with a high temporal resolution (one data point / second) in a 96-well plate. The labeled stable sensor cell line  $\alpha_{2A}AR_{Nluc/Halo(618)}$  was exposed to a first injection of saturating concentrations of the  $\alpha_{2A}AR$  endogenous full agonist norepinephrine or the inverse agonist yohimbine (Figure 3.9). Both ligands evoked a rapid change of the BRET ratio reaching a plateau within 120 seconds. The amplitudes of these BRET signals were comparable but opposite in their directions. Norepinephrine increased the BRET ratio (= activation of the receptor) (Figure 3.9 blue line) whereas yohimbine reduced the energy transfer (= inactivation of the receptor) (Figure 3.9 black line) mirroring the contrary effects of these compounds on  $\alpha_{2A}AR$ -mediated downstream signaling (Annex table 7.4). To test the reversibility of the signal, cells prestimulated with norepinephrine were sequentially treated with the competitive antagonist phentolamine (Figure 3.9 red line). Phentolamine is expected to displace the agonist from its binding site and therefore restore the receptor’s inactive conformation. Accordingly, phentolamine reverted the norepinephrine-induced BRET signal and caused a BRET ratio similar to the one recorded upon yohimbine addition.

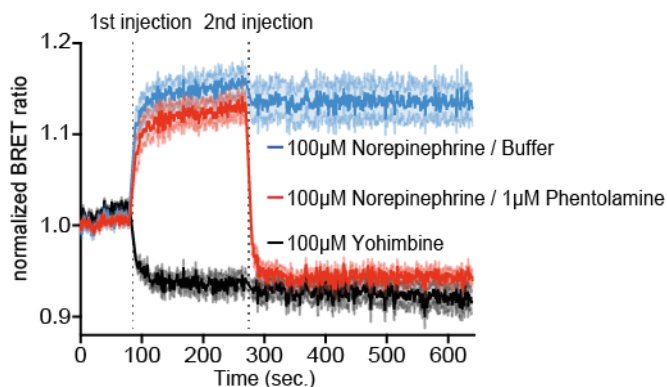


**Figure 3.9: Kinetics of  $\alpha_{2A}AR_{NLuc/Halo(618)}$  BRET signals.** The stable  $\alpha_{2A}AR_{NLuc/Halo(618)}$  cell line was exposed to a first injection of 100  $\mu M$  norepinephrine (blue and red) or yohimbine (black) and a second injection of buffer (blue) or 1  $\mu M$  phentolamine (red). Data show mean  $\pm$  s.e.m. of three independent experiments conducted in triplicates.

To examine whether  $\alpha_{2A}AR_{NLuc/Halo(618)}$  detects ligand-dependent activation/deactivation kinetics, we analyzed the BRET time-courses of the first injection of norepinephrine and yohimbine and the second injection of phentolamine (**Table 3.1**). The resulting  $\tau$ -values and corresponding 95% confidence intervals do not show statistically different kinetics of norepinephrine-induced increase versus yohimbine-induced decrease of the BRET ratio. However, the phentolamine-induced BRET decline following norepinephrine-prestimulation occurred significantly faster than the norepinephrine- and yohimbine-mediated changes of the BRET ratios.

$\alpha_{2A}AR$ ligand	Injection	$\tau$ (seconds)	95% CI
Norepinephrine	1 <sup>st</sup>	10.81	8.25 – 15.66
Yohimbine	1 <sup>st</sup>	9.99	8.09 – 13.05
Phentolamine	2 <sup>nd</sup>	6.42	5.65 – 7.43

**Table 3.1 Analysis of ligand-dependent  $\alpha_{2A}AR_{NLuc/Halo(618)}$  BRET kinetics.**

BRET time-courses from Figure 3.9 were fitted to mono-exponential association (norepinephrine) or decay (yohimbine and phentolamine) curves.

The similar kinetics for the norepinephrine- vs. yohimbine-induced BRET change are in contrast with previous kinetic studies with FRET-based  $\alpha_{2A}AR$  conformational biosensors that revealed  $\approx$  35-fold slower deactivation vs. activation kinetics (Vilardaga et al., 2005). This inconsistency may result from entirely different experimental settings. In the plate reader format, the BRET measurement is interrupted for  $\approx$  1.5 seconds to allow ligand delivery to the wells. Furthermore,  $\alpha_{2A}AR$  ligands are added on top of the basal assay volume that covers the sensor cells adherent to the well bottom. In contrast, the fluorescence-based single-cell experiments allow for simultaneous ligand-delivery and FRET acquisition. Moreover, the FRET-sensor expressing cell is directly superfused with the GPCR ligands minimizing the delay of the FRET response due to ligand diffusion. A more detailed comparison of the different experimental setups and their impact on kinetic receptor studies can be found in the discussion section of this thesis.

### 3.2.4. $\alpha_{2A}AR_{NLuc/Halo(618)}$ reports distinct ligand efficacies and potencies

Conformational GPCR biosensors have to faithfully report efficacies and potencies of varying test compounds and resemble the potencies of these ligands at the parent wildtype receptor to facilitate reliable conclusions for (patho-)physiological conditions. In order to ascertain that  $\alpha_{2A}AR_{NLuc/Halo(618)}$  features these characteristics, we selected a panel of well-characterized  $\alpha_{2A}AR$  ligands as reference compounds (**Annex Table 7.4**) and measured the BRET signals induced by saturating ligand concentrations and serial ligand dilutions.

Specifically, we measured the change in BRET induced by compound concentrations reported to saturate wildtype  $\alpha_{2A}AR$  to evaluate the sensor's capability to differentiate between ligands with distinct efficacies (**Figure 3.10A**). The  $\alpha_{2A}AR_{NLuc/Halo(618)}$  biosensor was able to report different receptor conformations ranging

from fully active (norepinephrine) to fully inactive (yohimbine). The inverse agonist yohimbine as well as the competitive antagonists phentolamine and tyramine drastically reduced the BRET ratio of  $\alpha_2AAR_{Nluc/Halo(618)}$  (yohimbine =  $-9.09 \pm 0.83\%$ ; phentolamine =  $-7.85 \pm 0.73\%$ ; tyramine =  $-9.03 \pm 0.59\%$ ). In contrast, the full agonists norepinephrine, epinephrine and UK 14,304 elevated the energy transfer (norepinephrine =  $+10.40 \pm 0.46\%$ ; epinephrine =  $+11.94 \pm 0.49\%$ ; UK 14,304 =  $+3.77 \pm 0.39\%$ ) and the weak partial agonists clonidine, oxymetazoline and octopamine evoked intermediate  $\Delta$ BRET responses (clonidine =  $-6.83 \pm 0.88\%$ ; oxymetazoline =  $-6.46 \pm 0.92\%$ ; octopamine =  $-5.78 \pm 1.00\%$ ). Only dopamine, reported to be a strong partial agonist (Zurn et al., 2009), did not significantly alter the biosensor's BRET ratio ( $0.55 \pm 1.04\%$ ). Overall, the conformational biosensor  $\alpha_2AAR_{Nluc/Halo(618)}$  resembled the reported ligand efficacies of various ligands with the only exception of dopamine, which failed to induce any significant BRET response. Subsequently, we examined the capability of  $\alpha_2AAR_{Nluc/Halo(618)}$  to reliably reflect  $\alpha_2AAR$  ligand potencies. Therefore, we stimulated with serial dilutions of all ten different  $\alpha_2AAR$  ligands to fit the concentration-dependent BRET responses of each ligand to a sigmoidal concentration-response curves (Figure 3.10B). Since the receptor's conformational change follows directly the ligand binding process, the resulting  $EC_{50}$ -values (i.e. the half maximal ligand concentration) were statistically compared to the corresponding binding affinities to  $\alpha_2AAR_{Nluc/Halo(618)}$  obtained from radioligand competition binding. The  $\alpha_2AAR$ , as well as other GPCRs, exhibits biphasic agonist binding curves in competition with radio- or fluorescently labeled antagonists in GTP-free membranes. It is well accepted that this biphasic nature is a consequence of distinct agonist affinities to G protein-free (low affinity;  $pk_L$ ) vs. G protein-associated GPCR states (high affinity;  $pk_H$ ). Both receptor populations coexist in membrane preparations (Bylund et al., 2001; Maguire et al., 1976). In intact cells however, which is the condition in which the BRET experiments were performed, this equilibrium might be shifted to the high-affinity agonist state if the receptor (sensor) shows high tendency to precouple to G proteins. Therefore, we conducted binding experiments in the presence or absence of externally added GTP, a treatment that uncouples receptors from G proteins (Figure 3.11). This analysis revealed that agonist (full or partial) potencies in the BRET assay significantly deviated from the ligand binding affinities in the presence of externally added GTP ( $pk_L$ ). However, no statistical difference was evident between  $pEC_{50}$ -values and  $pk_i$ -values obtained without externally added GTP ( $pk_H$ ). Potency data of antagonists and inverse agonist did not display any statistical difference to  $pk_L$ -values. For this reason, no further experiments without externally added GTP were performed for these  $\alpha_2AAR$  compounds. Overall, the BRET  $pEC_{50}$ -values of agonists correlate well with the high affinity binding values.

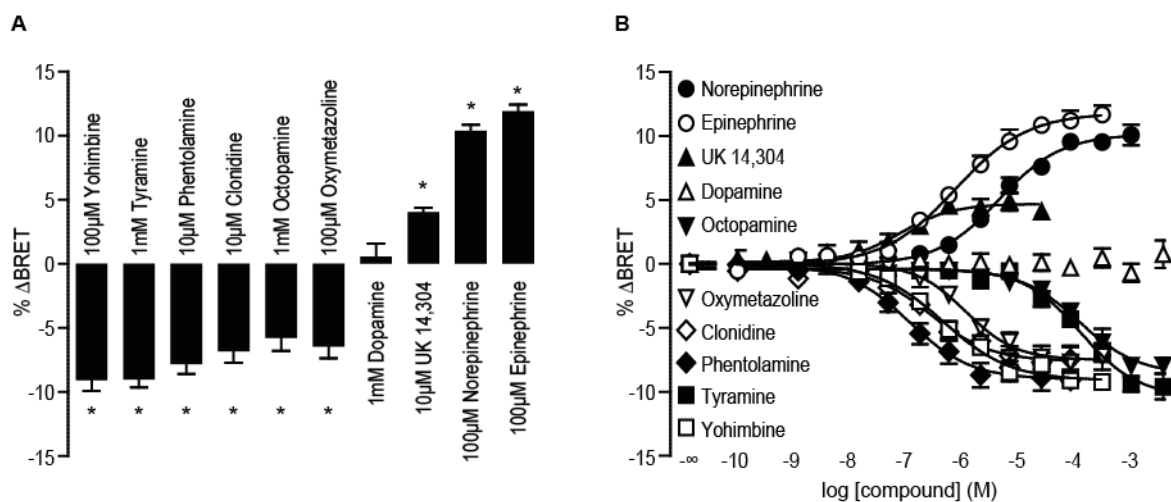


**Figure 3.10:  $\alpha_2AAR_{Nluc/Halo(618)}$  reports ligand- and concentration-dependent BRET signals.**

The stable  $\alpha_2AAR_{Nluc/Halo(618)}$  cell line was stimulated with saturating concentrations (A) or serial dilutions (B) of ten different  $\alpha_2AAR$  ligands. Data show mean  $\pm$  s.e.m. of at least three independent experiments conducted in quadruplicates. Statistical difference against negative control (buffer; not shown) was tested applying one-way ANOVA followed by Bonferroni post hoc test. \* $p \leq 0.05$ .

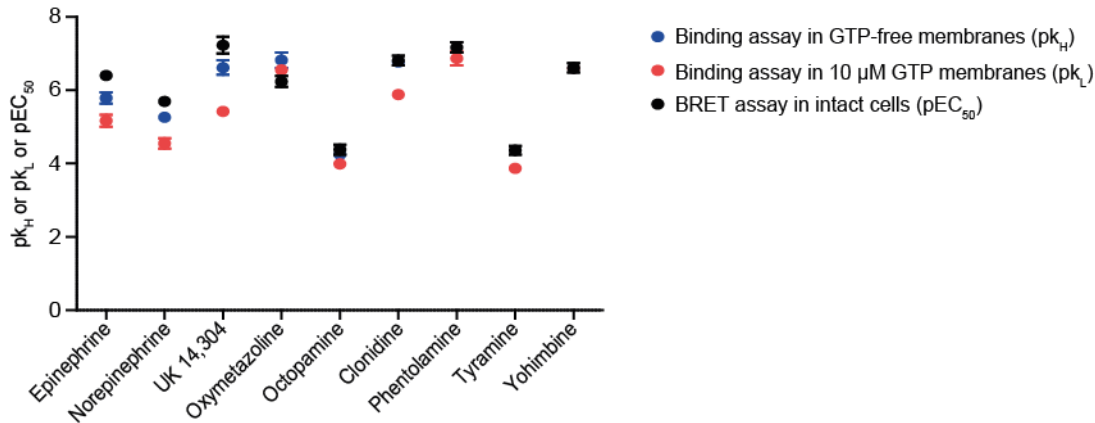


**Figure 3.11: Comparison of BRET EC<sub>50</sub> values with binding properties of  $\alpha_{2A}AR_{Nluc/Halo(618)}$ .** pEC<sub>50</sub>-values originating from  $\alpha_{2A}AR_{Nluc/Halo(618)}$  BRET experiments were tested for statistical difference to pK<sub>i</sub> binding parameters in the absence (pK<sub>H</sub>) or presence (pK<sub>L</sub>) of externally added GTP applying Student's t-test. \*p ≤ 0.05.

### 3.2.5. Signaling capacity of $\alpha_{2A}AR_{Nluc/Halo(618)}$

The biosensor  $\alpha_{2A}AR_{Nluc/Halo(618)}$  faithfully reports activation and deactivation kinetics of ligands with different pharmacological profiles. Next, we set out to evaluate the biosensor's capability to initiate the  $\alpha_{2A}AR$  associated signaling cascade. The  $\alpha_{2A}$ -adrenergic receptor naturally couples to inhibitory G proteins (G $\alpha_i$ ). Therefore, we chose the FRET-based G $\alpha_{i2}$  sensor to measure  $\alpha_{2A}AR_{Nluc/Halo(618)}$  mediated G protein activation (van Unen et al., 2016). Van Unen and co-workers refined the G $\alpha_{i2}$  FRET sensor initially developed by Bünemann et al. (Bunemann et al., 2003) by replacing the original FRET fluorophores for mTurquoise2 at the G $\alpha_{i2}$ -subunit and cpVenus<sup>173</sup> within the G $\gamma$ -subunit. Subsequently, they merged these two subunits with unmodified G $\beta$  on one plasmid to ensure expression of the subunits in a fixed ratio. We co-transfected HEK-TSA cells with  $\alpha_{2A}AR_{Nluc/Halo}$  and the FRET-based G $\alpha_{i2}$  sensor but did not label HaloTag or add the Nluc substrate to avoid spectral crosstalk during the FRET measurement. Upon GPCR stimulation with the endogenous agonist norepinephrine,  $\alpha_{2A}AR_{Nluc/Halo}$ -mediated G protein signaling was monitored through the reduction in G $\alpha_{i2}$  FRET ratio (**Figure 3.12**).

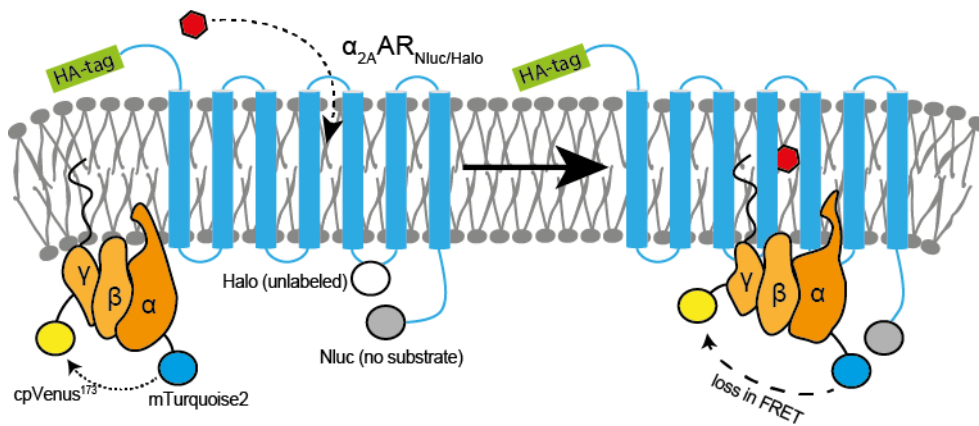


**Figure 3.12: Principle of FRET-based G $\alpha_i$ -sensor.** Cells co-expressing unlabeled  $\alpha_{2A}AR_{Nluc/Halo}$  along with the G $\alpha_{i2}$  FRET sensor (orange) are stimulated with a GPCR agonist (e.g. norepinephrine). GPCR activation induces receptor-G protein coupling and subsequent G protein activation, measured as a loss in FRET.

Before measuring agonist-induced G protein-activation, we examined whether cells co-expressing either wildtype  $\alpha_{2A}AR$  or  $\alpha_{2A}AR_{Nluc/Halo}$  along with G $\alpha_{i2}$  FRET sensor showed the same extent of GPCR and FRET

sensor expression since these two parameters might influence the sensitivity of the G protein activation assay.

We directly excited the G protein FRET acceptor cpVenus<sup>173</sup> and measured the resulting fluorescence emission intensity to quantify the FRET sensor expression. Thereby, we verified that the sensor was similarly expressed when co-expressed with wildtype  $\alpha_{2A}AR$  vs.  $\alpha_{2A}AR_{Nluc/Halo}$  (**Figure 3.13A**).

To determine the surface expression of wildtype  $\alpha_{2A}AR$  vs.  $\alpha_{2A}AR_{Nluc/Halo}$ , we utilized the N-terminal HA-tag on both GPCR constructs to stain the receptors localized in the plasma membrane with a fluorescent anti-HA-tag antibody. The subsequent fluorescent readout displayed comparable membrane expression of the two  $\alpha_{2A}AR$  variants (**Figure 3.13B**).

Additionally, cells were stimulated with serial dilution of norepinephrine to measure concentration-dependent FRET responses and obtain sigmoidal concentration-response curves. Interestingly, a significantly lower basal and norepinephrine-induced  $G_{\alpha_{i2}}$  FRET ratio was evident due to  $\alpha_{2A}AR_{Nluc/Halo}$  expression. Additionally, the agonist-induced  $G_{\alpha_{i2}}$  activation revealed a statistically significant right-shift by about two log-units when  $\alpha_{2A}AR_{Nluc/Halo(618)}$  was co-expressed in lieu of wildtype  $\alpha_{2A}AR$  ( $pEC_{50}$  with  $\alpha_{2A}AR_{Nluc/Halo} = 6.14 \pm 0.49$  vs.  $8.67 \pm 0.19$  with  $\alpha_{2A}AR$  wildtype) (**Figure 3.13C**).

These data suggest that  $\alpha_{2A}AR_{Nluc/Halo(618)}$  is capable of transmitting the extracellular stimulus and trigger G protein activation. However, the fusion of Nluc and HaloTag to  $\alpha_{2A}AR$  causes a substantial reduction of the receptor's potency to activate endogenous G proteins (right-shift of the  $EC_{50}$ ) and pushes the receptor in a conformation that allows for increased G protein activation in the ligand-free state (reduction of the basal  $G_{\alpha_{i2}}$  FRET ratio).

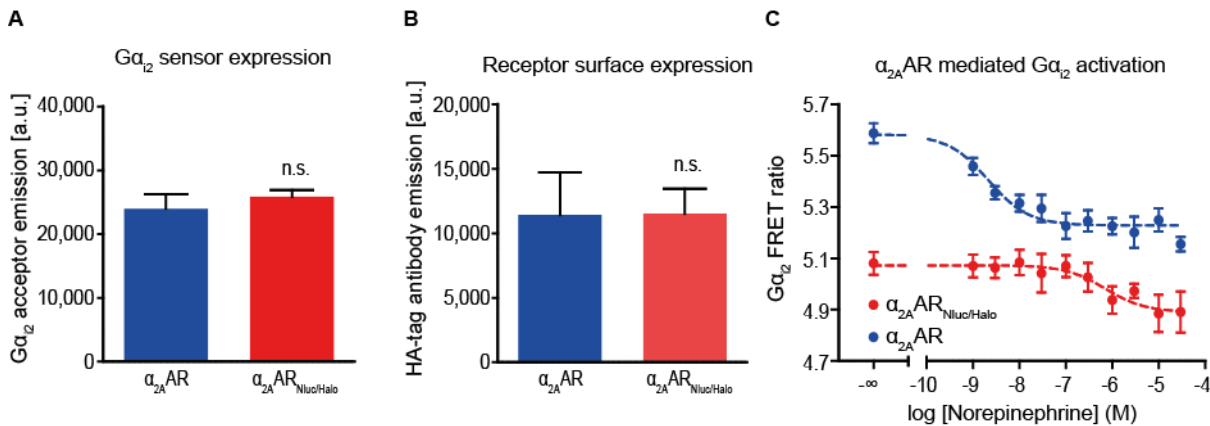


**Figure 3.13: Functionality of  $\alpha_{2A}AR_{Nluc/Halo(618)}$ .**

HEK cells co-expressing the  $G_{\alpha_{i2}}$  FRET sensor along with either N-terminally HA-tagged  $\alpha_{2A}AR_{Nluc/Halo}$  sensor (red) or  $\alpha_{2A}AR$  wildtype (blue) were seeded into 96-well plates to a density of 50,000 cells per well. **A)**  $G_{\alpha_{i2}}$  sensor expression was quantified through direct excitation of the FRET acceptor fluorophore and recording the resulting emission intensity. **B)** N-terminally HA-tagged  $\alpha_{2A}AR$  wildtype and  $\alpha_{2A}AR_{Nluc/Halo}$  were labeled with a fluorescent anti-HA-tag antibody to assess the surface localization of the receptors. **C)**  $G_{\alpha_{i2}}$  FRET ratios upon treatment with increasing concentrations of norepinephrine were fitted to sigmoidal concentration-response curves. Data represent mean  $\pm$  s.e.m. of three independent experiments performed in quadruplicates. In bar graphs, difference was analyzed by Student's *t*-test and extra-sum-of squares *F*-test was applied to test for statistical difference between the two  $EC_{50}$  values in (C). \* $p \leq 0.05$ .

### 3.3. Transferability of the novel sensor design

GPCR assay formats employed in biomedical research present generalizable sensor designs that are transferable to various GPCR families and receptor subtypes. To demonstrate that the novel BRET combination Nluc/Halo(618) constitutes such a universal sensor design for GPCR conformational studies, we used the same strategy (fusion of Nluc to C-terminus and HaloTag to icl3) to create a rhodopsin-like receptor ( $\beta_2AR$ ) and a secretin-like receptor biosensor (PTHR1).

### 3.3.1. Characterization of $\beta_2\text{AR}_{\text{Nluc/Halo}}$ conformational biosensor

We chose the  $\beta_2$ -adrenergic receptor as the first model GPCR to prove the transferability of the Nluc/Halo(618) sensor design since this rhodopsin-like receptor constitutes the best-characterized GPCR besides rhodopsin and shares several common features (e.g. binding of catecholamines) with previously validated  $\alpha_2\text{AR}$ .

To identify suitable positions for the two BRET partners, we capitalized on the insights gained by Reiner and colleagues who explored several donor / acceptor insertion sites for the design of FRET-based  $\beta_2\text{AR}$  conformational biosensors (Reiner et al., 2010). In accordance with the most sensitive FRET biosensor from Reiner et al., we fused Nluc to Glu369 at the truncated C-terminus and inserted HaloTag's sequence between Asp251 and Gly252 within icl3 of a N-terminally FLAG-tagged  $\beta_2\text{AR}$ .

#### 3.3.1.1. Competence of $\beta_2\text{AR}_{\text{Nluc/Halo}}$ to discriminate ligands with distinct efficacies and potencies

To analyze the capacity of  $\beta_2\text{AR}_{\text{Nluc/Halo}(618)}$  to faithfully report efficacies and potencies of highly diverse  $\beta_2\text{AR}$  targeting ligands, we generated a stable HEK sensor cell line and performed the established BRET assay in 96-well plates with a set of twelve  $\beta_2\text{AR}$  reference compounds that exhibit differing intrinsic activities and potencies (**Annex Table 7.4**).

Similarly to the validation of  $\alpha_2\text{AR}_{\text{Nluc/Halo}(618)}$ , we monitored the change in  $\beta_2\text{AR}_{\text{Nluc/Halo}(618)}$  conformation evoked by saturating concentrations of reference compounds to measure maximal ligand-dependent BRET changes (**Figure 3.14A**). The  $\beta_2\text{AR}_{\text{Nluc/Halo}(618)}$  biosensor reports receptor conformation-dependent BRET signals ranging from full activation obtained with the full endogenous agonist epinephrine (negative  $\Delta\text{BRET}$ ;  $-14.77 \pm 0.71\%$ ) to the fully inactive receptor state upon treatment with the inverse agonist ICI 118.551 (positive  $\Delta\text{BRET}$ ;  $+5.58 \pm 0.36\%$ ). All the other ligands displayed intermediate effects. Only the antagonists carvedilol and labetalol did not induce any significant  $\Delta\text{BRET}$  response. This outcome is in accordance with previous publications reporting partial agonistic effects of carvedilol and labetalol on some, but not all signaling cascades downstream  $\beta_2\text{AR}$  (van der Westhuizen et al., 2014). In contrast to  $\alpha_2\text{AR}_{\text{Nluc/Halo}(618)}$ , agonists reduced the BRET ratio of  $\beta_2\text{AR}_{\text{Nluc/Halo}(618)}$ . Similar deviations in the direction of the RET response have previously been reported for CFP/FIAsH- and CFP/YFP-tagged muscarinic acetylcholine and histamine receptors, respectively, and have been attributed to changes in the inter-fluorophore orientation rather than inter-fluorophore distance during the receptor activation process (Liu et al., 2018b; Ziegler et al., 2011)

Subsequently, we selected epinephrine and ICI 118.551 for concentration-response experiments (**Figure 3.14B**). Obtained  $\text{EC}_{50}$  values were in general agreement with affinity data to wildtype  $\beta_2\text{AR}$  as reported in literature (**Table 3.2**).

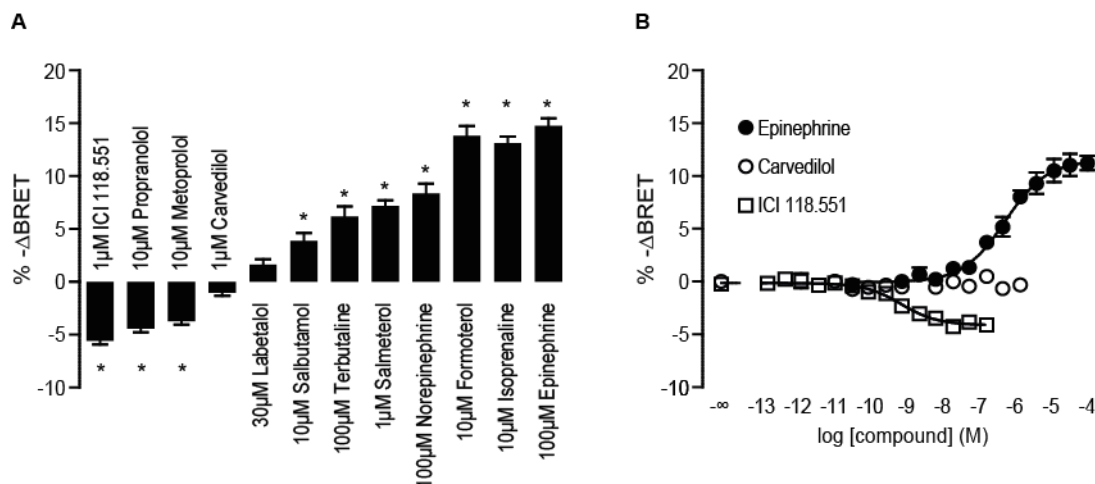


**Figure 3.14: Characterization of  $\beta_2AR_{NLuc/Halo(618)}$ .**

**A)** HEK cells stably expressing  $\beta_2AR_{NLuc/Halo(618)}$  were seeded into 96-well plate and treated with saturating concentrations of twelve  $\beta_2AR$  reference ligands. **B)** BRET changes of HEK cells stably expressing  $\beta_2AR_{NLuc/Halo(618)}$  and treated with serial dilutions of epinephrine, carvedilol and ICI 118,551 were plotted to sigmoidal concentration-response curves. Data are expressed as mean  $\pm$  s.e.m. from four independent experiments performed in quadruplicates. One-way ANOVA followed by Bonferroni post hoc test analyzed was applied in A to test for statistical difference against negative control (buffer; not shown). \* $p \leq 0.05$  versus buffer.

Ligand	$pEC_{50}$ (95% CI) BRET assay	$pk_i$ (95% CI) radioligand binding	Reference
Epinephrine	6.45 (6.18 – 6.73)	6.13 (5.98 – 6.29)	(Hoffmann et al., 2004)
ICI 118,551	9.57 (9.23 – 9.87)	9.15 (8.96 – 9.40)	

**Table 3.2: Comparison of BRET  $EC_{50}$  values with binding properties of  $\beta_2AR$  wildtype.**

### 3.3.1.2. Signaling capacity of $\beta_2AR_{NLuc/Halo(618)}$

The  $\beta_2$ -adrenergic receptor primarily couples to G proteins with stimulatory effects on adenylyl cyclases and thereby elevates intracellular cAMP levels. To quantify  $\beta_2AR_{NLuc/Halo(618)}$ -mediated downstream signaling, we took advantage of the excellent FRET-based cAMP sensor H187 developed by Klarenbeek and colleagues (Klarenbeek et al., 2015).

This FRET probe is based on EPAC labeled with the FRET partners mTurquoise2 and a tandem of two cpVenus<sup>173</sup> fluorophores. Binding of cAMP to this biosensor pushes the EPAC scaffold into a conformation that allows less energy transfer from mTurquoise2 to tandem cpVenus<sup>173</sup>. By this means, accumulation of intracellular cAMP in consequence of e.g. activation of  $G\alpha_s$ -coupled receptors can be monitored in real-time in living cells. We co-transfected HEK-TSA cells with  $\beta_2AR_{NLuc/Halo}$  and H187 sensor but did not label HaloTag or add the NLuc substrate to avoid spectral crosstalk during the FRET measurement. Upon GPCR stimulation with the endogenous agonist epinephrine,  $\beta_2AR_{NLuc/Halo}$ -mediated accumulation of intracellular cAMP was monitored through the reduction in H187 FRET ratio (**Figure 3.15**).



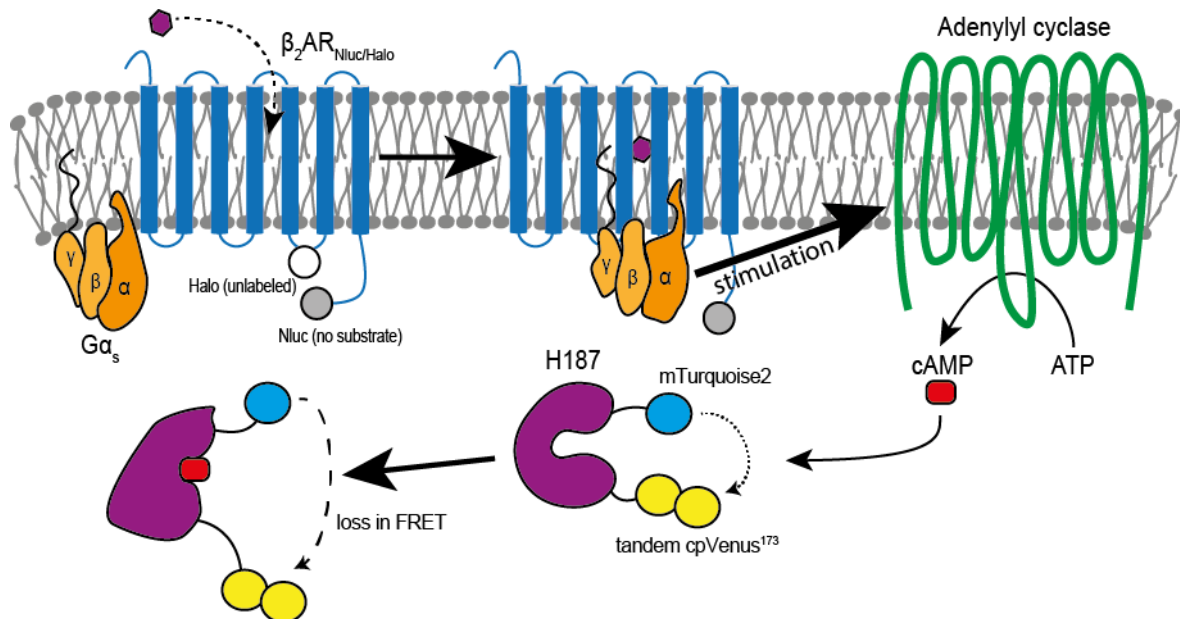


**Figure 3.15: Principle of EPAC-based H178 FRET sensor.**

Cells expressing unlabeled  $\beta_2AR_{Nluc/Halo}$  are stimulated with a GPCR agonist (e.g. isoprenaline). Receptor activation stimulates  $G\alpha_s$  (orange) that in turn activates endogenous adenylyl cyclases (green). Subsequently, adenylyl cyclases catalyze the production of intracellular cAMP (red) that binds to co-expressed EPAC-based H178 FRET cAMP sensor (purple). Binding of cAMP induces a conformational change of the FRET probe, detectable as a loss in FRET.

Before measuring GPCR-mediated cAMP production, we examined whether cells co-expressing either wildtype  $\beta_2AR$  or  $\beta_2AR_{Nluc/Halo(618)}$  along with H178 FRET sensor showed the same extent of GPCR and FRET sensor expression since these two parameters might influence the sensitivity of the cAMP assay. Therefore, we directly excited the H178 FRET acceptor tandem cpVenus<sup>173</sup> and verified similar sensor expression when co-expressed with wildtype  $\beta_2AR$  vs.  $\beta_2AR_{Nluc/Halo}$  through resulting fluorescence emission intensity (**Figure 3.16A**).

Subsequently, we determined the surface expression of wildtype  $\beta_2AR$  vs.  $\beta_2AR_{Nluc/Halo}$  by staining the N-terminal FLAG-tag on both GPCR constructs with a fluorescent anti-FLAG-tag antibody. The fluorescence emission readout displayed significantly reduced  $\beta_2AR_{Nluc/Halo}$  surface expression compared to the FLAG-tagged wildtype variant (**Figure 3.16B**).

Ultimately, cells were stimulated with serial dilution of isoprenaline to measure concentration-dependent FRET responses and obtain sigmoidal concentration-response curves. Here,  $\beta_2AR_{Nluc/Halo}$  expression resulted in significantly increased basal FRET ratio as compared to wildtype  $\beta_2AR$  indicating lower basal cAMP levels. This might be a consequence of the reduced GPCR surface expression levels or indicate decreased basal signaling activity of  $\beta_2AR_{Nluc/Halo}$  vs. wildtype  $\beta_2AR$ . Despite altered basal FRET ratio,  $\beta_2AR_{Nluc/Halo}$  stimulation resulted in wildtype-like FRET concentration-response curve with indiscernible EC<sub>50</sub>-values (pEC<sub>50</sub> with  $\beta_2AR_{Nluc/Halo}$  =  $8.99 \pm 0.24$  vs.  $9.09 \pm 0.23$  with  $\beta_2AR$  wildtype) (**Figure 3.16C**). These data indicate that the attachment of Nluc and HaloTag to  $\beta_2AR$  does not impair the receptor's capability to transmit extracellular stimuli and promote G protein-mediated downstream signaling cascades. However, control experiments argue for reduced  $\beta_2AR_{Nluc/Halo}$  surface expression and / or basal signaling activity. This could be a result of steric competition of Nluc and / or HaloTag with scaffolding proteins that target  $\beta_2AR$  to the plasma membrane and regulate its cellular distribution.

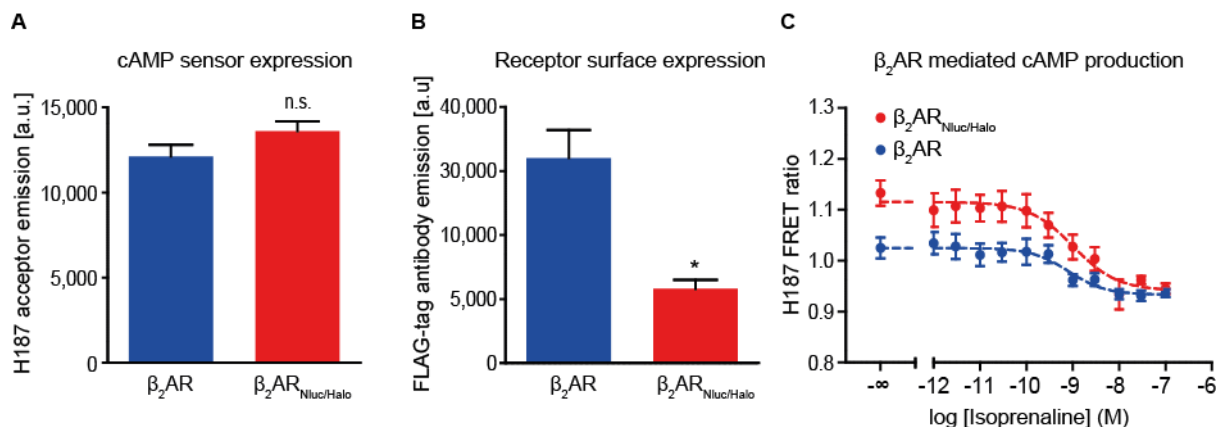


**Figure 3.16: Functionality of  $\beta_2AR_{Nluc/Halo(618)}$ .**

HEK cells co-expressing the cAMP FRET sensor H187 along with N-terminally FLAG-tagged  $\beta_2AR_{Nluc/Halo}$  sensor (red) or  $\beta_2AR$  wildtype (blue) were seeded into 96-well plates (50,000 cells per well). **A**) H187 sensor expression was quantified through direct excitation of the FRET acceptor fluorophores and recording the resulting emission intensity. **B**) N-terminally FLAG-tagged  $\beta_2AR$  wildtype and  $\beta_2AR_{Nluc/Halo}$  were labeled with a fluorescent anti-FLAG-tag antibody to assess their surface localization. **C**) H187 FRET ratios upon treatment with increasing concentrations of isoprenaline fitted to sigmoidal concentration-response curve. Data represent mean  $\pm$  s.e.m. of three independent experiments performed in quadruplicates. In bar graphs, difference was analyzed by Student's *t*-test and extra-sum-of squares *F*-test was applied to test for statistical difference between the two  $EC_{50}$  values in (C). \**p*  $\leq$  0.05.

### 3.3.2. Characterization of $PTHR1_{Nluc/Halo}$ conformational biosensor

Besides showing that the novel BRET combination of Nluc and HaloTag 618 represents a functional design for rhodopsin-like GPCR conformational biosensors, we aimed to demonstrate its suitability to investigate the conformational dynamics of another GPCR family. To this end, we applied the novel sensor design to the secretin-like PTHR1 and benefitted from the knowledge of tolerated tag insertion sites acquired by Vilardaga and co-workers (Vilardaga et al., 2003).

In accordance with previously described PTHR1 FRET biosensor, the BRET donor Nluc was fused to Gly497 and HaloTag was inserted between Gly395 and Arg396 in the third intracellular loop of a N-terminally HA-tagged PTHR1 receptor.

#### 3.3.2.1. Competence of $PTHR1_{Nluc/Halo}$ to discriminate ligands with distinct efficacies and potencies

We created a HEK cell line stably expressing  $PTHR1_{Nluc/Halo}$  and conducted experiments with saturating concentrations and serial dilutions of several PTHR1 peptide ligands in a 96-well microtiter format (**Annex 7.4**). Agonists of wildtype PTHR1 induced a statistically significant reduction of the BRET ratio versus negative control ( $\Delta$ BRET PTH(1-34) =  $-10.81 \pm 0.53$  %). However, no significant signal was detected for PTHR1 antagonists ( $\Delta$ BRET PTH(7-34) =  $-0.51 \pm 0.39$  %) (**Figure 3.17A**). Furthermore, addition of serial dilutions of three reference peptides covering the spectrum of available PTHR1 ligand efficacies revealed corresponding sigmoidal curves (**Figure 3.17B**). Obtained  $EC_{50}$  values were in general agreement with affinity data to wildtype PTHR1 as stated in literature (**Table 3.3**).

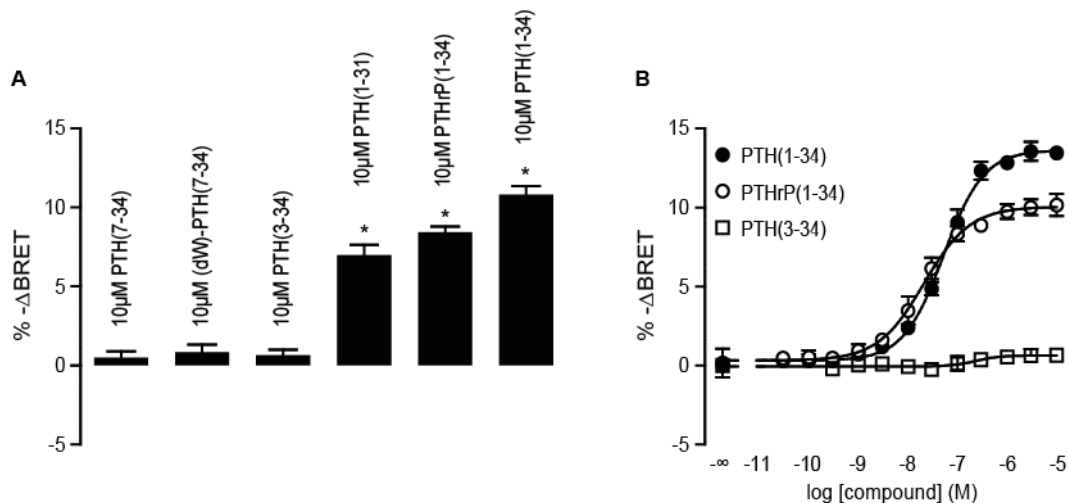


**Figure 3.17: Characterization of PTHR1<sup>Nluc/Halo(618)</sup>.**

**A)** HEK cells stably expressing PTHR1<sup>Nluc/Halo(618)</sup> were seeded into 96-well plate and treated with saturating concentrations of six PTHR1 reference peptide ligands. **B)** Concentration-response experiments were conducted with the full agonists PTH(1-34) and PTHrP(1-34) and the antagonist PTH(3-34) and BRET data were plotted to sigmoidal curves. Data are expressed as mean  $\pm$  s.e.m. from four independent experiments conducted in quadruplicates. Statistical difference against negative control (buffer; not shown) was analyzed by one-way ANOVA followed by Bonferroni post hoc test. \* $p \leq 0.05$ .

Ligand	pEC <sub>50</sub> $\pm$ s.e.m. BRET assay	pk <sub>i</sub> $\pm$ s.e.m. radioligand binding	Reference
PTH (1-34)	7.28 $\pm$ 0.04	7.41 $\pm$ 0.04	(Gardella et al., 1996)
PTHrP (1-34)	7.69 $\pm$ 0.08	7.82 $\pm$ 0.15 / 8.13 $\pm$ 0.33	(Gardella et al., 1995)
PTH (3-34)	6.63 $\pm$ 0.49	7.00 (s.e.m. not stated)	(Appleton et al., 2013)

**Table 3.3: Comparison of BRET EC<sub>50</sub> values with binding properties of PTHR1 wildtype.**

Subsequently, we conducted competition experiments to understand whether the lacking BRET response for PTHR1 antagonists (PTH(7-34), (dW)-PTH(7-34), PTH(3-34)) was caused by their inability to bind to PTHR1<sup>Nluc/Halo</sup> or whether they bind but do not alter sensor conformation. If the latter was true, these antagonists should compete with other PTHR1 ligands sharing the same binding site (e.g. the agonists PTH(1-34)) and significantly right-shift their concentration-response curves. In order to test this, we pre-incubated the stable sensor cell line with the antagonist (dW)-PTH(7-34) or buffer (negative control) and subsequently stimulated with serial dilutions of the PTHR1 agonist PTH(1-34) (**Figure 3.18**). We fitted the resulting BRET signals to sigmoidal concentration response curves and tested the resulting EC<sub>50</sub>-values for statistical difference using extra-sum-squares F-test. This analysis revealed a significant right-shift of PTH(1-34)-induced BRET signals due to pre-incubation with (dW)-PTH(7-34) supporting the concept that PTHR1 antagonists bind PTHR1<sup>Nluc/Halo</sup> but do not induce a GPCR conformational change (pEC<sub>50</sub> with buffer pre-incubation = 7.28  $\pm$  0.04 vs. 6.81  $\pm$  0.05 with 20nM (dW)-PTH(7-34) pre-incubation;  $p < 0.0001$ ).

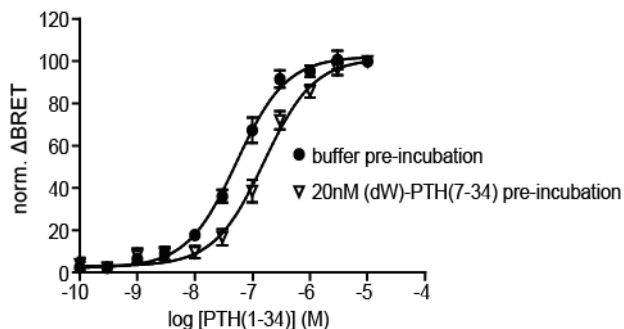


**Figure 3.18: Antagonistic effect of (dW)-PTH(7-34).**

Cells transiently expressing PTHR1<sup>Nluc/Halo</sup> were stimulated with serial dilutions of PTH(1-34) after 60 minutes pretreatment with the PTHR1 antagonist (20 nM) (dW)-PTH(7-34) or buffer. ΔBRET signals were fitted to sigmoidal concentration-response curves. Data are mean  $\pm$  s.e.m. of three independent experiments conducted in quadruplicates. Extra-sum-of squares F-test was applied to test for statistical difference between the two EC<sub>50</sub> values. \* $p \leq 0.05$ .

### 3.3.2.2. Signaling capacity of PTHR1<sub>Nluc/Halo(618)</sub>

PTHR1 has been reported to promote distinct signaling cascades through both, G<sub>q</sub> and G<sub>s</sub> proteins upon receptor activation. Thus, we could capitalize again on the excellent FRET-based cAMP H187 sensor to monitor PTHR1 mediated downstream responses (**Figure 3.19**).

Initially, we examined whether cells co-expressing either wildtype PTHR1 or PTHR1<sub>Nluc/Halo(618)</sub> along with H187 FRET sensor showed the same extent of GPCR and FRET sensor expression.

Direct excitation of the H187 FRET acceptor tandem cpVenus<sup>173</sup> displayed higher sensor expression in PTHR1<sub>Nluc/Halo</sub> vs. wildtype PTHR1 expressing cells (**Figure 3.19A**). Quantification of surface expression levels of wildtype PTHR1 vs. PTHR1<sub>Nluc/Halo</sub> by staining N-terminal HA-tags with a fluorescent anti-HA-tag antibody did not reveal any statistical difference (**Figure 3.19B**).

Subsequently, we stimulated with serial dilutions of agonist PTH(1-34) to measure concentration-dependent FRET responses and obtain sigmoidal concentration-response curves. PTHR1<sub>Nluc/Halo</sub> co-expression resulted in significantly increased basal FRET ratio as compared to wildtype PTHR1. This indicates lower basal cAMP levels because of reduced basal signaling activity of PTHR1<sub>Nluc/Halo</sub> compared to wildtype. Despite altered basal FRET ratio, PTHR1<sub>Nluc/Halo</sub> stimulation evoked negative, concentration-dependent FRET responses confirming the signaling capability of this conformational GPCR sensor (**Figure 3.19C**). However, this curve was significantly right-shifted compared to wildtype PTHR1 indicating reduced potency of PTHR1<sub>Nluc/Halo</sub> to initiate this downstream signaling cascade (pEC<sub>50</sub> with PTHR1<sub>Nluc/Halo</sub> = 7.57 ± 0.11 vs. 9.52 ± 0.11 with PTHR1 wildtype).

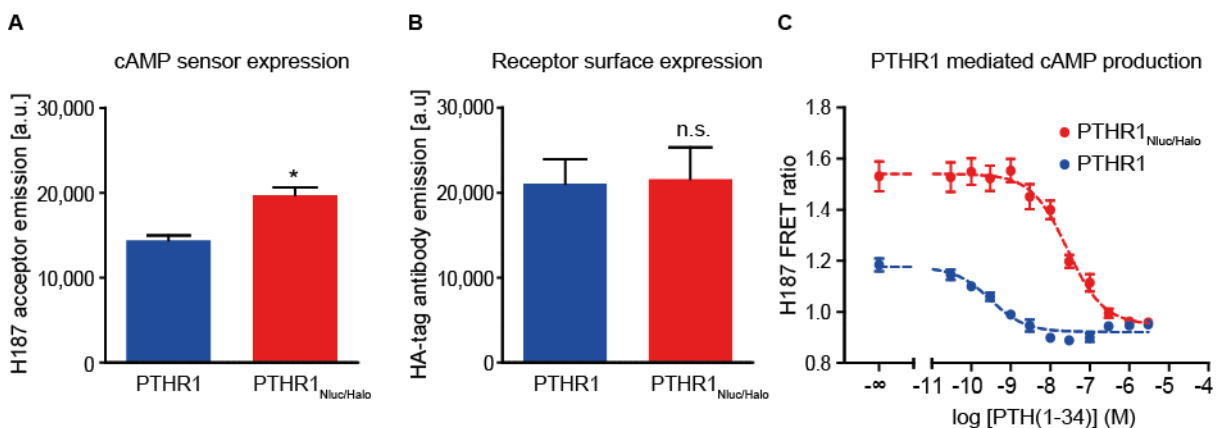


**Figure 3.19: Functionality of PTHR1<sub>Nluc/Halo(618)</sub>**

HEK cells co-expressing the cAMP FRET sensor H187 along with N-terminally HA-tagged PTHR1<sub>Nluc/Halo</sub> sensor (red) or PTHR1 wildtype (blue) were seeded into 96-well plates to a density of 50,000 cells per well. **A)** H187 sensor expression was quantified through direct excitation of the FRET acceptor fluorophore and recording the resulting emission intensity. **B)** N-terminally HA-tagged PTHR1 wildtype and PTHR1<sub>Nluc/Halo</sub> were labeled with a fluorescent anti-HA-tag antibody to assess the surface localization of the receptors. **C)** H187 FRET ratios upon treatment with increasing concentrations of PTH(1-34) fitted to sigmoidal concentration-response curve. Data represent mean ± s.e.m. of three independent experiments conducted in quadruplicates. In bar graphs, difference was analyzed by Student's *t*-test and extra-sum-of squares *F*-test was applied to test for statistical difference between the two EC<sub>50</sub> values in (C). \**p* ≤ 0.05.

## 3.4. Evaluation of High-throughput screening suitability of GPCR biosensors

We demonstrated that the novel Nluc/Halo(618) BRET sensor design reliably reports ligand-specific conformational changes in a concentration-dependent manner for three distinct GPCRs. These conformational changes are recorded as ΔBRET responses in 96-well microtiter format and allow for a fast and effective investigation of receptor pharmacology. However, such assays have to meet further essential requirements regarding the assay sensitivity, assay throughput and false positive/negative hit rates to be considered suitable for high-throughput screening.

### 3.4.1. Quality of GPCR conformational biosensor assays

One of the most crucial characteristics of an HTS-assay concerns its sensitivity (i.e. the lowest detectable signal significant versus negative control) to identify compounds acting through the target of interest. If this sensitivity is not sufficiently high, potential drug candidates might be classified as “non-active” after the first screening round and therefore excluded from further characterization and optimization. In 1999, the so-called Z-factor was introduced which represents an excellent parameter to determine the quality of an assay and allow for comparison of technically diverse methods (Zhang et al., 1999). This statistical parameter takes into account the signal amplitude and variability of reference positive and negative controls and is often referred to as the screening window coefficient. The ideal assay without signal variation would yield the maximum Z-factor of 1. Assays with Z-factors  $\geq 0.5$  represent excellent tools for screening purposes whereas assays with  $0 \leq Z < 0.5$  require more replicates to be tested to allow for reliable interpretation of screening data.  $Z < 0$  defines methods without any value for HTS. To assess the Z-factor of a new assay, half of the wells of a microtiter plate (96-wells or more) are treated with either positive (e.g. agonist) or negative control (vehicle), respectively, to obtain the signals' mean and standard deviations under both conditions.

In order to quantify the screening window coefficients of the novel GPCR conformational biosensors and thereby evaluate their HTS-compatibility, we performed Z-factor analyses of the  $\alpha_2\text{AAR}$ ,  $\beta_2\text{AR}$  and PTHR1 Nluc/Halo(618) sensors and compared them to the previous generation of FRET-based biosensors ( $\alpha_2\text{AAR}_{\text{CFP/YFP}}$ ,  $\beta_2\text{AR}_{\text{CFP/YFP}}$  and  $\text{PTHR1}_{\text{CFP/YFP}}$ ) which served as starting points for the creation of this novel set of conformational biosensors (**Figure 3.20**). To evaluate the reproducibility and robustness of the assays, these experiments were conducted on four independent days with sensor cells in different passages. To reduce the signal variation, these FRET and BRET experiments were conducted with a slightly modified protocol: Instead of capturing solely one FRET / BRET data point before and after ligand / buffer addition, five consecutive reads were measured and averaged before and after stimulation. This modification enhanced the epinephrine-induced BRET response of the  $\alpha_2\text{AAR}_{\text{Nluc/Halo(618)}}$  biosensor. In accordance with previous studies applying  $\alpha_2\text{AAR}_{\text{CFP/YFP}}$  and  $\text{PTHR1}_{\text{CFP/YFP}}$  in single-cell experiments, both sensors displayed decreases of the FRET ratio upon agonist treatment (Villardaga et al., 2003). However, the loss in FRET upon agonist treatment observed in single cells expressing  $\beta_2\text{AR}_{\text{CFP/YFP}}$  could not be reproduced in the 96-well plate format.

Taken together, all FRET variants displayed Z-factors below zero, making them practically useless for HTS ( $\alpha_2\text{AAR}_{\text{CFP/YFP}} = -1.60 \pm 0.97$ ;  $\beta_2\text{AR}_{\text{CFP/YFP}} = -1.66 \pm 0.89$ ;  $\text{PTHR1}_{\text{CFP/YFP}} = -10.97 \pm 4.05$ ). In contrast, the Z-factors of all three BRET-based GPCR biosensors were above the threshold of 0.5 and therefore represent excellent HTS assays ( $\alpha_2\text{AAR}_{\text{Nluc/Halo(618)}} = 0.65 \pm 0.01$ ;  $\beta_2\text{AR}_{\text{Nluc/Halo(618)}} = 0.79 \pm 0.04$ ;  $\text{PTHR1}_{\text{Nluc/Halo(618)}} = 0.52 \pm 0.02$ ). Additionally, the Z inter-day variations were very low with a maximum standard error mean of 0.04 for  $\beta_2\text{AR}_{\text{Nluc/Halo(618)}}$ , indicating a high robustness and reproducibility of the novel Nluc/Halo(618) GPCR assay.

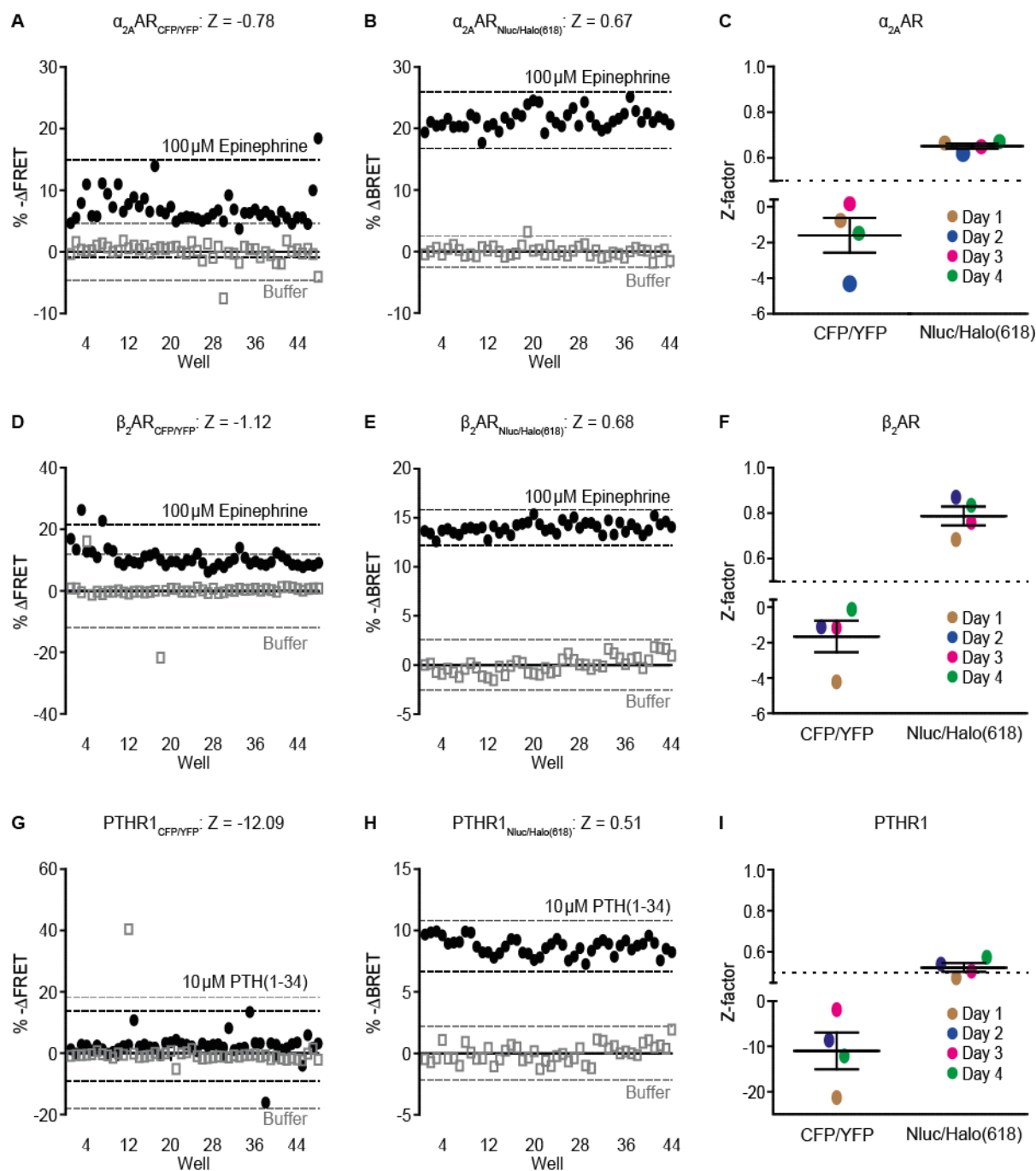


**Figure 3.20: Z-factors of GPCR conformational biosensor assays.**

HEK cells transiently (FRET) or stably (BRET) expressing the different conformational GPCR biosensors were stimulated with saturating concentrations of positive (epinephrine for  $\alpha_{2A}AR$  and  $\beta_2AR$ ; PTH(1-34) for PTHR1) or negative control (buffer). Shown are representative 96-well plate data of  $\alpha_{2A}AR_{CFP/YFP}$  (A),  $\alpha_{2A}AR_{Nluc/Halo}$  (B),  $\beta_2AR_{CFP/YFP}$  (D),  $\beta_2AR_{Nluc/Halo}$  (E), PTHR1<sub>CFP/YFP</sub> (G) and PTHR1<sub>Nluc/Halo</sub> (H) and the corresponding Z-factors (mean  $\pm$  s.e.m.) of four independent experiments with  $\alpha_{2A}AR$  (C),  $\beta_2AR$  (F) and PTHR1 (I) biosensors. The dotted lines in A, B, D, E, G and H illustrate the mean  $\pm$  3 x sd of positive and negative control.

### 3.4.2. Stability of BRET signals over time

High signal amplitude and low variation represent the primary requirements for an assay for its application in high-throughput screening but a successful HTS campaign further requires performance under automated

and high-speed conditions which greatly enhances the assay throughput (i.e. the number of data points per time). This throughput can be boosted significantly by stacking multiple plates in individual experimental steps. However, stacking is only possible if signals are stable over long time frames to achieve a broad reading window.

We recorded agonist (norepinephrine) and inverse agonist (yohimbine) induced BRET changes of  $\alpha_2\text{AAR}_{\text{Nluc}/\text{Halo}(618)}$  over a timeframe of 30 minutes after ligand addition and performed Z-factor experiments at the corresponding stimulation times to determine the time-stability of BRET signals and estimate the future automation potential of the conformational GPCR BRET assay (**Figure 3.21**). No reversal of norepinephrine- or yohimbine-induced BRET changes was evident over the whole observation period (**Figure 3.21A**) and the mean Z-factor of four independent plates was still above 0.5 30 minutes after stimulation ( $0.53 \pm 0.03$ ) (**Figure 3.21B**).

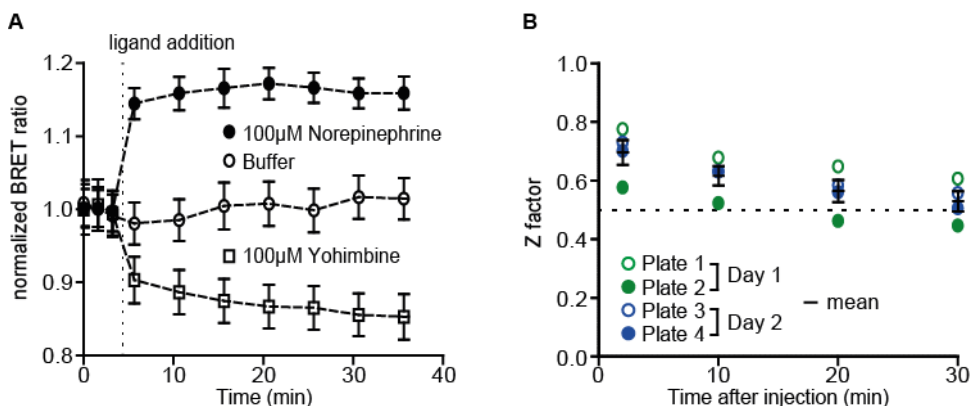


**Figure 3.21: Time-stability of  $\alpha_2\text{AAR}_{\text{Nluc}/\text{Halo}(618)}$  BRET changes.**

**A)** HEK cells stably expressing  $\alpha_2\text{AAR}_{\text{Nluc}/\text{Halo}(618)}$  were treated with the 100  $\mu\text{M}$  norepinephrine, buffer or 100  $\mu\text{M}$  yohimbine to record ligand-induced BRET signals over 30 minutes. **B)** Z-factors of the  $\alpha_2\text{AAR}_{\text{Nluc}/\text{Halo}(618)}$  assay were calculated after 2, 10, 20 and 30 minutes incubation with positive (epinephrine) or negative control (buffer). Data show mean  $\pm$  s.e.m. of four independent experiments performed in quadruplicates.

### 3.4.3. Miniaturization of the GPCR conformation assay

Apart from stacking multiple assay plates, downscaling the assay to smaller microtiter plates such as 384- and 1536-well plates represents another approach to enhance the assay throughput. Most HTS campaigns are usually conducted in 384- or 1536-well plates (Mayr and Bojanic, 2009) but assay miniaturization often requires de novo identification of optimal assay parameters.

To enable a future miniaturization of the GPCR BRET assay, we performed initial experiments to identify the optimal parameters to conduct the  $\alpha_2\text{AAR}_{\text{Nluc}/\text{Halo}(618)}$  BRET assay in 384-well microtiter plates and measured 100  $\mu\text{M}$  norepinephrine-induced BRET responses under varying experimental conditions. First, we tested eight different cell densities ranging from 1,000 to 40,000 cells per well and detected the biggest  $\Delta\text{BRET}$  amplitude with the highest cell density of 40,000 cells per well (**Figure 3.22A**). However, it cannot be excluded that further increases of the cell number yield even higher  $\Delta\text{BRET}$  signals and ongoing experiments are required to determine the optimal cell density in 384-well plate experiments. Additionally, we explored the optimal Nluc substrate dilution for the cell density of 40,000 cells per well and achieved the highest response with a 1/1,000 dilution (**Figure 3.22B**). These two experimental parameters (40,000 cells per well; 1/1,000 substrate dilution) were then combined to assess the quality of the  $\alpha_2\text{AAR}_{\text{Nluc}/\text{Halo}(618)}$  assay in 384-well plates. This analysis yielded a screening-sufficient, however not yet excellent Z-factor of 0.45 (**Figure 3.22C**).

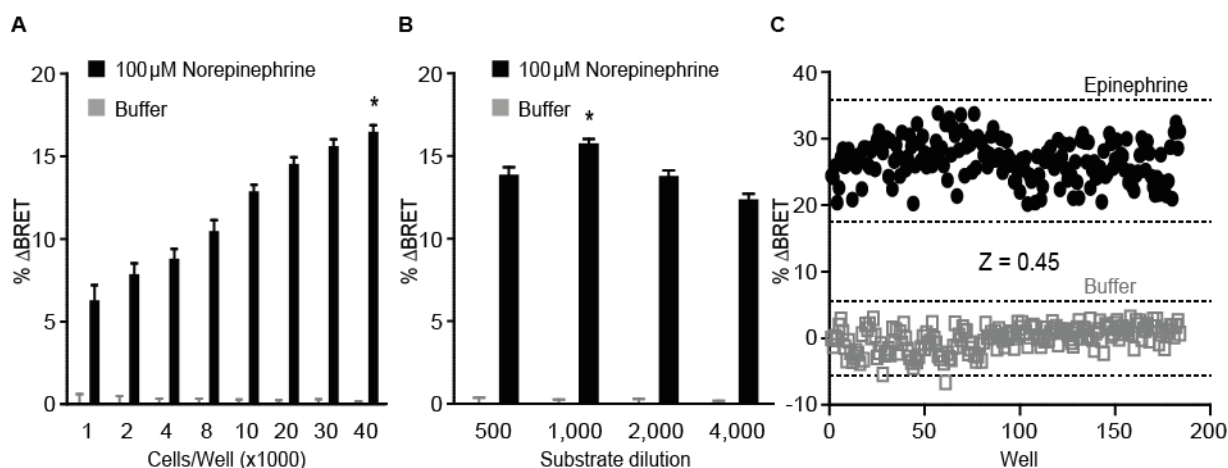


**Figure 3.22: Downscaling the  $\alpha_{2A}AR_{Nluc/Halo(618)}$  assay to 384-well plates.**

HEK cells stably expressing the  $\alpha_{2A}AR_{Nluc/Halo}$  biosensor were labeled with 50 nM HaloTag dye 618 and seeded into 384-well plates to measure agonist-induced BRET changes as a function of **A**) cell density (1/1,000 Nluc substrate dilution) or **B**) substrate dilution (40,000 cells seeded per well). **C**) 40,000 HEK cells stably expressing  $\alpha_{2A}AR_{Nluc/Halo}$  were plated per well to a 384-well plate, labeled with 50 nM HaloTag dye 618, incubated with 1,1000 dilution of luciferase substrate and stimulated with 100  $\mu$ M epinephrine or buffer to calculate the corresponding Z-factor. Data show mean  $\pm$  s.e.m. of 20 (A and B) or 184 (C) replicates. One-way ANOVA followed by Bonferroni post hoc test was applied to test for statistical difference against all other samples in A and B. \* $p \leq 0.05$ .

#### 3.4.4. False positive screening hit rate

All experimental procedures carry a certain risk to generate false positive hits (compounds that are considered as hits but not truly active) (Malo et al., 2006). It is essential to be aware of the assay-specific probability to produce such erroneous results when interpreting the experimental data and excellent screening assays applied in drug discovery feature low false positive hit rates.

To estimate the rate of false positive hits generated by the conformational GPCR BRET assay, we conducted the  $\alpha_{2A}AR_{Nluc/Halo(618)}$  assay with a panel of 54 compounds. We selected only compounds that are not reported to bind  $\alpha_{2A}AR$  and should therefore not induce a significant BRET response. This set of chemical entities covers different groups of pharmacologically active ligands and can be divided into six major classes:  $\beta_2AR$  ligands, endogenous ligands of GPCRs other than  $\alpha_{2A}AR$ , synthetic ligands of GPCRs other than  $\alpha_{2A}AR$ , ligands for ion channels, nucleotides and compounds that could not be grouped into one of these classes. The concentrations applied in this false positive screen were 10 – 100 times the  $pK_i$  or  $pEC_{50}$  (according to the IUPHAR database) of the compounds to their primary target. Among this set of compounds, the  $\beta_2AR$  ligand formoterol ( $-4.08 \pm 0.35$  %), the calcium channel blocker diltiazem ( $-3.04 \pm 0.55$  %), the activator of adenylyl cyclases forskolin ( $14.40 \pm 1.07$  %) and the natural detergent digitonin ( $54.48 \pm 0.61$  %) induced BRET responses exceeding the negative control (buffer)  $\pm 3x$  standard deviation window which is normally considered as background noise in high-throughput screens (Malo et al., 2006) (**Figure 3.23**). It is possible that some (or all) of these four compounds do indeed alter the receptor conformation but via different mechanisms than classic orthosteric ligands and could therefore be considered as true hits in an  $\alpha_{2A}AR$  ligand screening. For instance, digitonin is a well-established detergent which can be used to solubilize GPCRs and might therefore alter the original receptor conformation (Milic and Veprintsev, 2015). Yet, considering formoterol, diltiazem, forskolin and digitonin as false positive hits, these results implicate a false positive hit rate of 7.4%. This is well below the false positive rate of for example an optimized  $\beta$ -lactamase-based reporter assay used for the identification of 5-hydroxytryptamine 5-HT<sub>1A</sub> receptor antagonists (7728 compounds screened, 40% false positive rate) (Hallis et al., 2007).



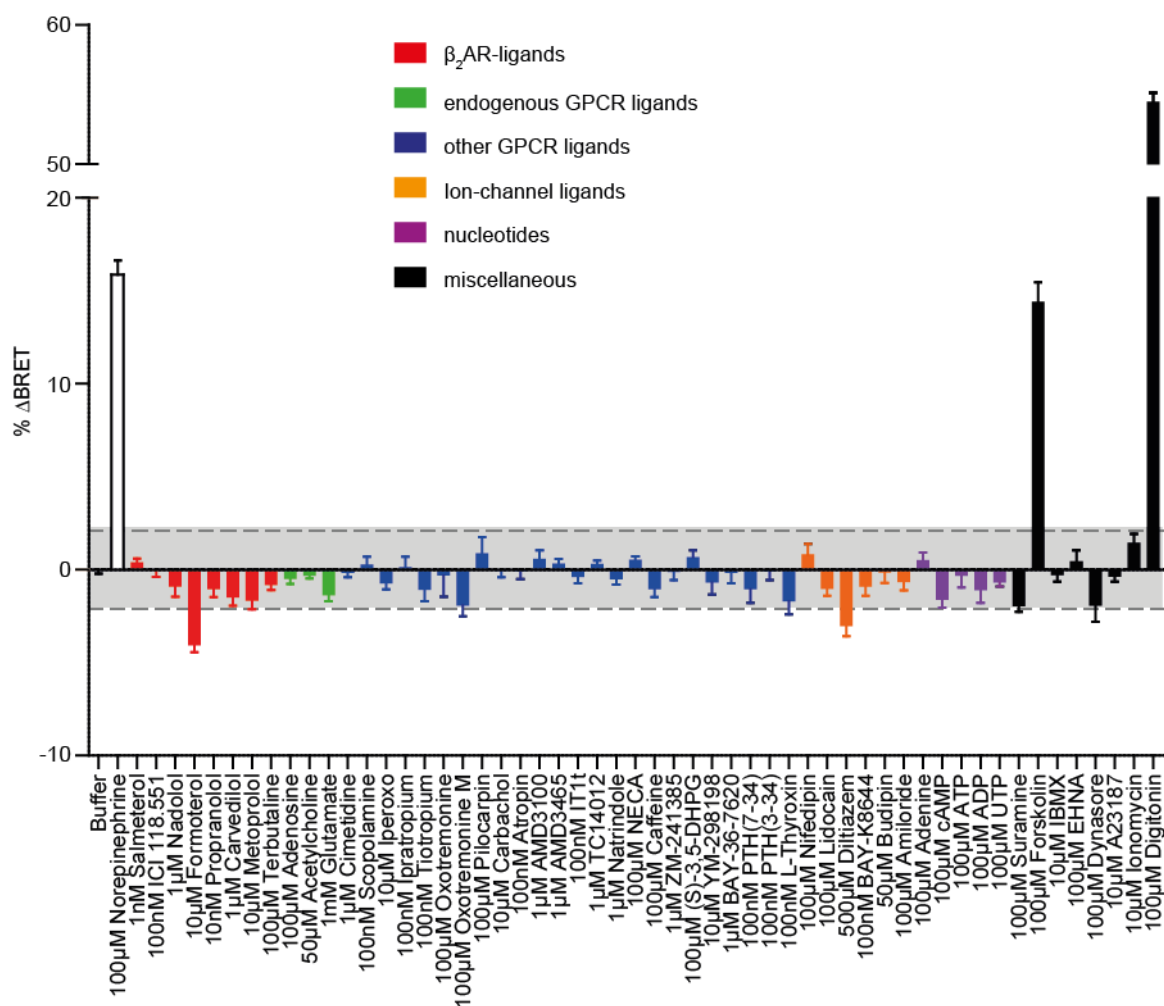


**Figure 3.23: False positive screening hits generated by  $\alpha_2\text{AR}_{\text{Nluc}/\text{Halo}}^{(618)}$ .** HEK cells stably expressing the  $\alpha_2\text{AR}_{\text{Nluc}/\text{Halo}}$  biosensor were treated with positive control (100  $\mu\text{M}$  norepinephrine), negative control (buffer) and a set of 54 compounds that should not bind to  $\alpha_2\text{AR}_{\text{Nluc}/\text{Halo}}$  to record the ligand-induced BRET changes. Data show mean  $\pm$  s.e.m. of four replicates. Test compounds were considered as hits if respective BRET signals exceeded the mean negative control (buffer)  $\pm$  3x sd window (grey area).

### 3.5. Extending the toolbox of GPCR conformational biosensors

Whenever new GPCRs are focused in a novel drug discovery program, a functional and highly sensitive biosensor has to be developed to allow the performance of such conformational studies in living cells and real time. In order to be ahead of such a possible future trend, we started to extend the toolbox of Nluc/Halo(618)-based conformational GPCR sensors and selected AT1R, CXCR4 and S1PR1 as target structures. These three receptors are of high interest in modern GPCR-targeted drug discovery campaigns. For instance, a wide group of FDA-approved AT1R blockers for the treatment of hypertension and cardiac hypertrophy already targets the AT1R but basic research as well as clinical studies keep reporting novel insights into agonist-independent receptor activation through disease-associated autoantibodies, mechanical stress or receptor mutations (Takezako et al., 2017).

CXCR4 and S1PR1 in contrast, are currently addressed by only one approved drug each. The S1PR1 modulator fingolimod (FTY-720, Gilenya®) is approved for the treatment of multiple sclerosis and plerixafor (AMD3100, Mozobil®) inhibits the entry of human immunodeficiency virus-1 (HIV-1) into human T-lymphocytes through antagonizing CXCR4. However, our perception of these GPCRs changes rapidly with a deeper understanding of their involvement in other pathophysiological processes and future treatment

optimization could help to preempt the development of drug resistance (HIV-1) (Park and Im, 2017; Zhang et al., 2016).

Following the cloning of biosensors for these three GPCRs, all sensors were evaluated for their capability to (i) allow donor-acceptor energy transfer in the ligand-free conformation by recording basal BRET spectra and (ii) report ligand-dependent conformational changes under transient expression levels.

### 3.5.1. Generation of the angiotensin-II-type 1 receptor biosensor

To generate the AT1R biosensors, the insertion sites for HaloTag and Nluc were selected based on previous studies with AT1R conformational biosensors (Devost et al., 2017). In detail, the BRET donor Nluc was fused to the last amino acid (E359) of the full-length C-terminus and HaloTag was inserted between I228 and Q229 within intracellular loop 3 (**Figure 3.24**).

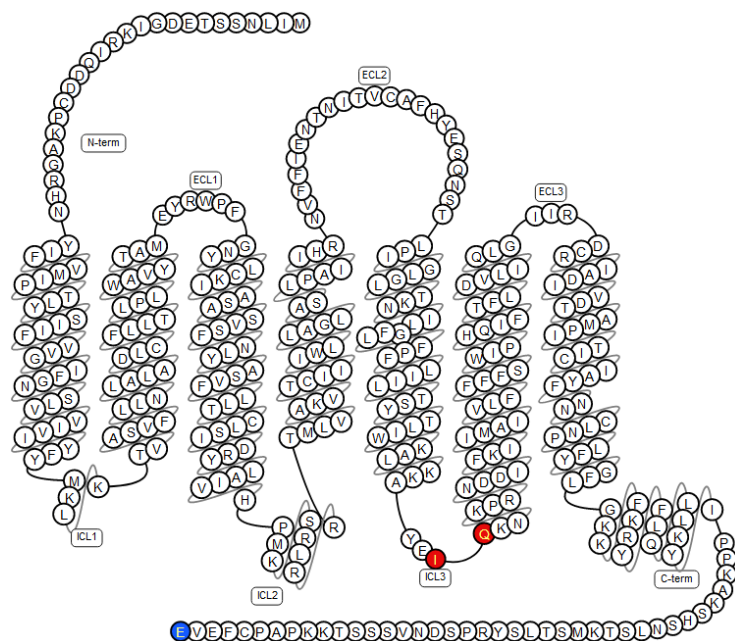


**Figure 3.24: Two-dimensional illustration of wildtype AT1R.**

The insertion sites for HaloTag and Nluc for the creation of AT1R<sub>Nluc/Halo</sub> are highlighted in red and blue, respectively. The illustration was downloaded from <http://gpcrdb.org/>

The BRET spectra of transiently transfected and HaloTag 618-labeled HEK-TSA cells revealed the characteristic Nluc-derived emission maximum at 450 nm and an additional emission peak at  $\approx 620$  nm that was not apparent in the only-donor control indicating occurrence of energy transfer (**Figure 3.25A**). Furthermore, stimulation of these cells with serial dilutions of the endogenous AT1R agonist angiotensin-II and the AT1R antagonist losartan (**Annex Table 7.4**) induced ligand-specific, concentration-dependent BRET signals of opposite directions, mirroring their contrary pharmacological actions through wildtype AT1R (**Figure 3.25B**). The EC<sub>50</sub> values derived from these concentration-response curves were in the same order of magnitude like affinity data of wildtype AT1R as stated in literature (**Table 3.4**). These data indicate that the AT1R<sub>Nluc/Halo(618)</sub> biosensor can be used to explore efficacies and potencies of AT1R-addressing compounds.

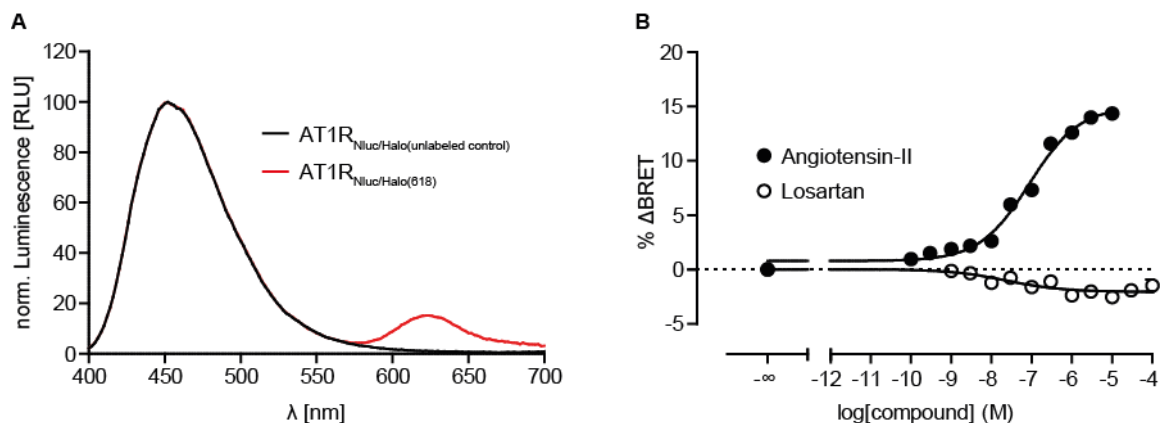


**Figure 3.25: Validation of the AT1R<sup>Nluc/Halo(618)</sup> biosensor.**

**A)** BRET emission spectra of labeled (red) and unlabeled (black) HEK cells transiently expressing the conformational biosensor AT1R<sup>Nluc/Halo</sup>. **B)** HEK cells transiently expressing AT1R<sup>Nluc/Halo(618)</sup> were stimulated with serial dilutions of angiotensin-II and losartan. Resulting BRET changes were fitted to sigmoidal concentration-response curves.

Ligand	Maximum ΔBRET ± s.e.m.	pEC <sub>50</sub> ± s.e.m. BRET assay	pk <sub>i</sub> ± s.e.m. binding to AT1R	Reference
Angiotensin-II	14.36 ± 0.69	7.06 ± 0.08	7.61 ± 0.23	(Bhuiyan MA, 2013)
Losartan	-2.54 ± 0.42	7.62 ± 0.50	7.17 ± 0.07	

**Table 3.4: Maximum BRET changes reported by AT1R<sup>Nluc/Halo(618)</sup> and comparison of ligand potencies reported by AT1R<sup>Nluc/Halo(618)</sup> with ligand binding affinities to wildtype AT1R.**

### 3.5.2. Generation of the chemokine CXCR4 receptor biosensor

No previous CXCR4 FRET or BRET biosensor has been generated. Therefore, we used the available crystal structure of this receptor to identify suitable insertion sites for the BRET labels (Wu et al., 2010). In this study, Wu et al. incorporated the T4-lysozyme (19 kDa; a classical approach to increase the receptor's crystallization tendency) within the remarkably short intracellular loop 3, between S229 and K230. We used the same strategy to introduce the HaloTag sequence and fused the BRET donor Nluc to S352 of the full-length, 50 amino acid C-terminus (**Figure 3.26**).

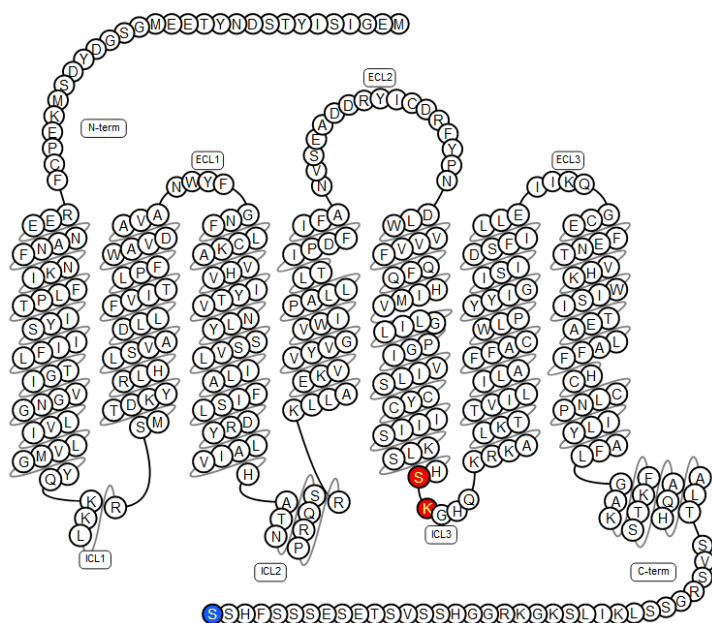


**Figure 3.26: Two-dimensional illustration of wildtype CXCR4.**

The insertion sites for HaloTag and Nluc for the creation of CXCR4<sup>Nluc/Halo</sup> are highlighted in red and blue, respectively. The illustration was downloaded from <http://qpcrdb.org/>

We applied the previously described protocol to evaluate the ability of CXCR4<sup>Nluc/Halo(618)</sup> to report the ligand-induced receptor conformational change. We measured the emission spectra of labeled and unlabeled HEK-TSA cells transiently expressing CXCR4<sup>Nluc/Halo</sup> and detected, besides the donor emission at 450 nm, a significant peak at  $\approx$  620 nm only in the labeled wells demonstrating occurring energy transfer from Nluc to HaloTag 618 (**Figure 3.27A**). Furthermore, we stimulated these cells with serial dilutions of five CXCR4 ligands of different pharmacological profiles (**Annex Table 7.4**). All of them evoked a concentration-dependent change in BRET (**Figure 3.27B**). In particular, the full (CXCL12) and partial agonists (AMD3100, AMD3465) increased the BRET ratio, whereas the antagonists TC14012 and IT1t induced a negative BRET response – in line with their inherent efficacies at wildtype CXCR4. Furthermore, we compared obtained EC<sub>50</sub> values with the affinity / potency data of these compounds to wildtype CXCR4 as stated in the literature (**Table 3.5**). With the exception of the endogenous agonist CXCL12, all compound EC<sub>50</sub>s are in general agreement with these data suggesting that CXCR4<sup>Nluc/Halo(618)</sup> presents a reliable tool to study efficacies and potencies of CXCR4 ligands. However, further experiments are required to understand the nature of the unexpectedly low potency of CXCL12 at inducing CXCR4<sup>Nluc/Halo(618)</sup> conformational changes.

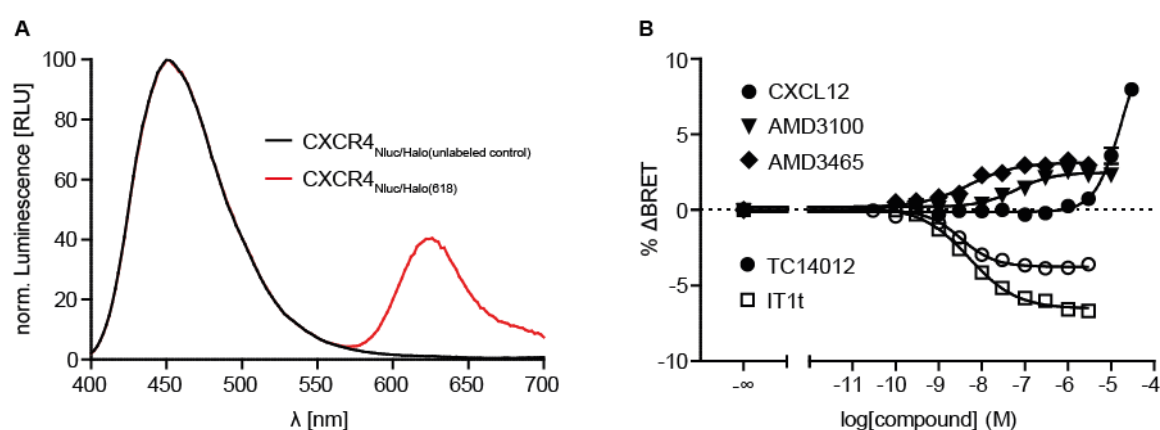


**Figure 3.27: Validation of the CXCR4<sup>Nluc/Halo(618)</sup> biosensor.**

**A)** BRET emission spectra of labeled (red) and unlabeled (black) HEK cells transiently expressing the biosensor CXCR4<sup>Nluc/Halo</sup>. **B)** HEK cells transiently expressing CXCR4<sup>Nluc/Halo(618)</sup> biosensor were stimulated with serial dilutions of CXCL12, AMD3100, AMD3465, vMIP-II, AT12341, TC14012 and IT1t. Resulting BRET changes were fitted to sigmoidal concentration-response curves.

Ligand	Maximum $\Delta$ BRET $\pm$ s.e.m.	pEC <sub>50</sub> $\pm$ s.e.m. BRET assay	Affinity / potency at wildtype CXCR4	Reference
CXCL12	7.97 $\pm$ 0.36	4.75 $\pm$ 0.18	pK <sub>i</sub> $\pm$ s.d. = 8.05 $\pm$ 0.17	(Loetscher et al., 1998)
AMD3100	2.34 $\pm$ 0.22	7.20 $\pm$ 0.11	pIC <sub>50</sub> = 7.48	(Hatse et al., 2005)
AMD3465	3.27 $\pm$ 0.30	8.29 $\pm$ 0.14	pIC <sub>50</sub> = 7.74	(Hatse et al., 2005)
TC14012	-3.86 $\pm$ 0.20	8.48 $\pm$ 0.07	pK <sub>i</sub> = 8.40	(Tamamura et al., 2003)
IT1t	-6.68 $\pm$ 0.17	8.29 $\pm$ 0.05	pIC <sub>50</sub> = 8.10 $\pm$ 0.10	(Thoma et al., 2008)

**Table 3.5: Maximum BRET changes reported by CXCR4<sup>Nluc/Halo(618)</sup> and comparison of ligand potencies reported by CXCR4<sup>Nluc/Halo(618)</sup> with ligand binding affinities to wildtype CXCR4.**

### 3.5.3. Generation of the sphingosine-1-phosphate receptor 1 biosensor

Also for the sphingosine-1-phosphate receptor 1, no previous conformational biosensors have been reported. Additionally, in the crystal structure of a human wildtype S1PR1, the T4 lysozyme replaced a series of 13 amino acids within icl3 and could therefore not aid the identification of tolerated BRET-label insertion sites. For these reasons, we cloned four distinct versions of S1PR1<sup>Nluc/Halo</sup> by combining two different HaloTag insertion sites to two Nluc positions (**Figure 3.28, Table 3.6**).

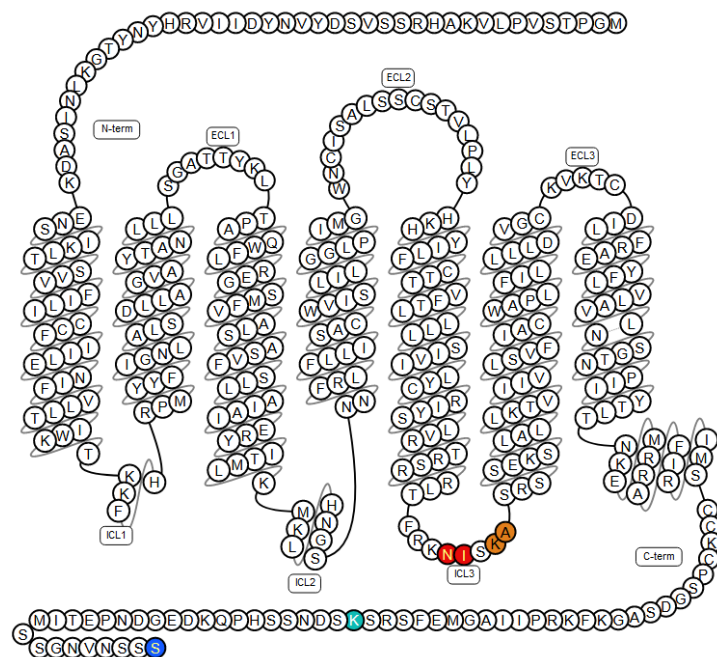


**Figure 3.28: Two-dimensional illustration of wildtype S1PR1.**

The insertion sites for HaloTag (red and orange) and Nluc (cyan and blue) for the creation of four S1PR1<sub>Nluc/Halo</sub> are highlighted. The illustration was downloaded from <http://gpcrdb.org/>

To verify energy transfer in the ligand-free, basal conformation of all four S1PR1<sub>Nluc/Halo</sub> biosensors, we recorded the BRET emission spectra of HaloTag 618-labeled HEK-TSA cells transiently expressing the different sensor versions and unlabeled cells transfected with S1PR1<sub>Nluc(K)/Halo(N)</sub> as a negative control (**Figure 3.29A**). All samples exhibited the Nluc-specific emission peak at 450 nm. Furthermore, a significant emission peak  $\approx$  620 nm was apparent for all four labeled sensor constructs demonstrating basal energy transfer in all four fusion proteins. The emission at 620 nm reached  $\approx$  20% of the maximum at 450 nm in S1PR1<sub>Nluc(S)/Halo(N)</sub> and S1PR1<sub>Nluc(S)/Halo(K)</sub> and about 40% for the sensors S1PR1<sub>Nluc(K)/Halo(N)</sub> and S1PR1<sub>Nluc(K)/Halo(K)</sub> indicating greater BRET efficiencies in constructs where Nluc is fused to K354 of a shortened C-terminus.

Subsequently, we evaluated the sensitivity of these four S1PR1 sensors to report ligand-induced conformational changes by stimulating transiently transfected cells with buffer (negative control) or the S1PR1 endogenous agonist sphingosin-1-phosphate (S1P) (**Figure 3.29B**). All four different sensors showed significant BRET signals upon agonist stimulation with the highest signal measured with S1PR1<sub>Nluc(S)/Halo(K)</sub> suggesting superior sensitivity of this sensor variant (**Table 3.6**). However, further sensor validation with pharmacologically distinct S1PR1 ligands and concentration-response experiments is required to verify the reliability of these biosensors for S1PR1 conformational studies.

Biosensor	Nluc fusion site	HaloTag fusion site	% $\Delta$ BRET(1 $\mu$ M S1P) mean $\pm$ s.e.m.
S1PR1 <sub>Nluc(K)/Halo(N)</sub>	K354	N240	1.28 $\pm$ 0.22
S1PR1 <sub>Nluc(K)/Halo(K)</sub>	K354	K243	2.85 $\pm$ 0.32
S1PR1 <sub>Nluc(S)/Halo(N)</sub>	S382	N240	1.01 $\pm$ 0.41
S1PR1 <sub>Nluc(S)/Halo(K)</sub>	S382	K243	3.17 $\pm$ 0.27

**Table 3.6: HaloTag and Nluc insertion sites in S1PR1 conformational BRET sensors.**

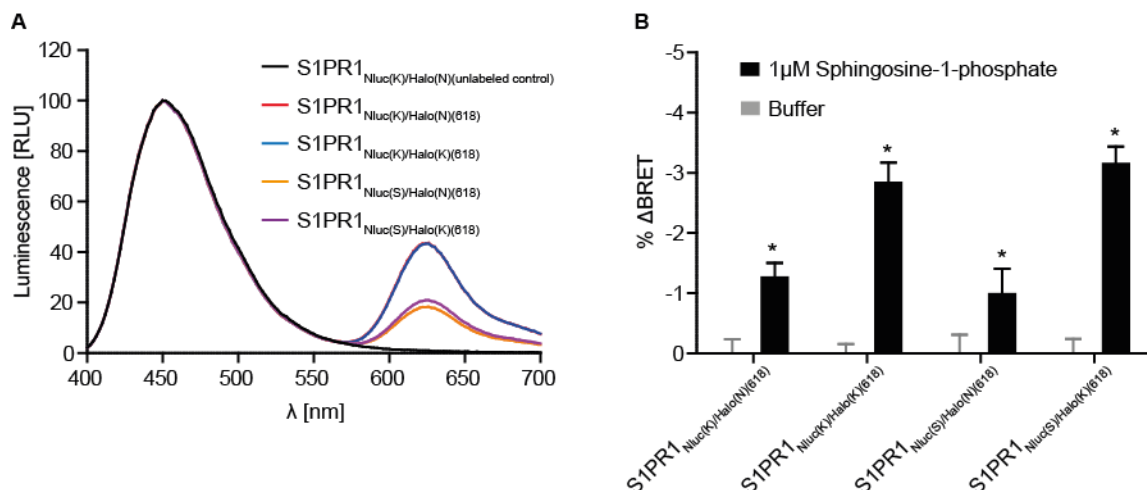


**Figure 3.29: Comparison of  $S1PR1_{N618/K618}$  biosensors.**

**A)** BRET emission spectra of labeled and unlabeled HEK cells transiently expressing the four  $S1PR1_{N618/K618}$  constructs. **B)** HEK cells transiently expressing four different  $S1PR1_{N618/K618}$  biosensors were stimulated with 1  $\mu$ M of the endogenous  $S1PR1$  agonist sphingosine-1-phosphate or buffer to record ligand-induced BRET changes. Statistical difference of sphingosine-1-phosphate-induced BRET changes against buffer was analyzed applying Student's *t*-test for each individual  $S1PR1_{N618/K618}$  sensor. \* $p \leq 0.05$

### 3.6. Application of GPCR biosensors to study modulatory effects of receptor activity-modifying proteins

The capability of our biosensors to report conformational dynamics of the receptors has so far only been validated upon stimulation with endogenous and synthetic ligands. However, different players including other membrane-embedded proteins, G proteins or lipids can also evoke receptor conformational changes. In theory, intramolecular GPCR biosensors should translate any change in receptor conformation that affects the inter-fluorophore distance and / or relative orientation into measurable  $\Delta$ RET signals, independent of the nature of the trigger.

We sought to explore whether the novel  $GPCR_{N618/K618}$  probes are able to report the effects of modulatory proteins on GPCR activation and thus, constitute optical tools to investigate the mechanisms and consequences of GPCR interaction with endogenous biomolecules. To this end, we examined the postulated modulatory action of receptor activity-modifying protein 2 (RAMP2) on PTHR1 using the  $PTH1R_{N618/K618}$  conformational biosensor (Christopoulos et al., 2003). RAMP2 displays increased total cellular expression and translocates to the plasma membrane upon co-expression of wildtype PTHR1. However, the mechanism and consequences for PTHR1 activation have thus far not been described. We co-transfected HEK cells stably expressing the  $PTH1R_{N618/K618}$  biosensor with RAMP2 or control plasmid (empty pcDNA3 vector) and recorded concentration-dependent, agonist-mediated BRET signals (**Figure 3.30**). The concentration-response curve of PTH(1-34) was significantly shifted to higher concentrations when RAMP2 was expressed alongside the PTHR1 biosensor supporting the proposed modulatory role of RAMP2 on PTHR1 conformational dynamics ( $pEC_{50} \pm$  s.e.m. (Control) =  $8.05 \pm 0.08$  vs.  $pEC_{50} \pm$  s.e.m. (RAMP2) =  $7.60 \pm 0.05$ ;  $p = 0.001$ ).

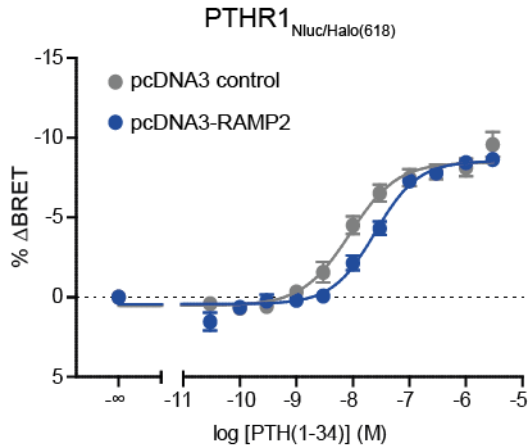


**Figure 3.30: Modulatory effect of RAMP2 on PTHR1<sub>Nluc/Halo(618)</sub> dynamics.** HEK cells stably expressing PTHR1<sub>Nluc/Halo(618)</sub> were transfected with either pcDNA3 vector (grey) or pcDNA3-RAMP2 (blue) and stimulated with serial dilutions of PTH(1-34) to measure agonist-induced BRET changes. Data show mean  $\pm$  s.e.m. of four independent experiments. Extra-sum-of-squares F-test was applied to test for statistical difference of EC<sub>50</sub>-values. \* $p \leq 0.05$ .

We aimed to understand whether the observed right-shift in the agonist concentration-response curve presents a PTHR1-RAMP2-specific outcome or can be found also with other GPCRs. Therefore, we performed an analogous set of experiments and stimulated cells stably expressing  $\beta_2$ AR<sub>Nluc/Halo(618)</sub> with the endogenous agonist epinephrine in the presence or absence of overexpressed RAMP2 (**Figure 3.31**). Here, we did not observe any significant shift of the agonist concentration-response curve as a function of RAMP2 co-expression (pEC<sub>50</sub>  $\pm$  s.e.m. (Control) = 7.28  $\pm$  0.13 vs. pEC<sub>50</sub>  $\pm$  s.e.m. (RAMP2) = 7.18  $\pm$  0.08;  $p = 0.48$ ) indicating that the modulatory effect of RAMP2 on PTHR1<sub>Nluc/Halo(618)</sub> is specific and not driven by an unspecific steric interplay between these two membrane proteins.

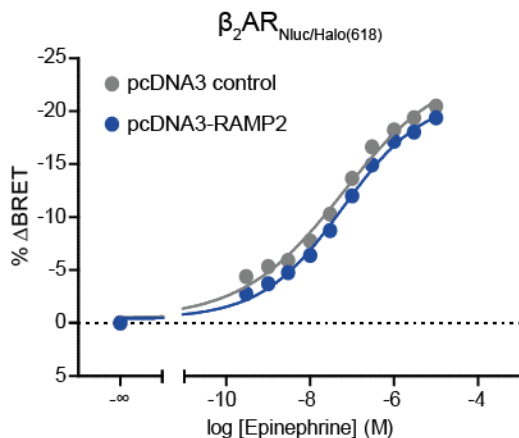


**Figure 3.31: Modulatory effect of RAMP2 on  $\beta_2$ AR<sub>Nluc/Halo(618)</sub> dynamics.** HEK cells stably expressing  $\beta_2$ AR<sub>Nluc/Halo(618)</sub> were transfected with either pcDNA3 vector (grey) or pcDNA3-RAMP2 (blue) and stimulated with serial dilutions of epinephrine to measure agonist-induced BRET changes. Data show mean  $\pm$  s.e.m. of four independent experiments. Extra-sum-of-squares F-test was applied to test for statistical difference of EC<sub>50</sub>-values. \* $p \leq 0.05$ .

To exclude that the shift in the concentration-response curve was a consequence of altered total expression levels of PTHR1<sub>Nluc/Halo</sub> but not of a direct GPCR-RAMP interaction, we compared the absolute donor emission intensities of the unlabeled control wells (no BRET acceptor) which correlate directly to the biosensor's expression levels (**Figure 3.32A**). RAMP2-expressing cells and control showed no statistically different Nluc emission intensities demonstrating similar expression levels of PTHR1<sub>Nluc/Halo</sub> (Control: 100.00  $\pm$  3.53 vs. RAMP2: 99.03  $\pm$  3.35;  $p = 0.84$ ). Additionally, we utilized the HA-tag epitope attached to the extracellular N-terminus of PTHR1<sub>Nluc/Halo</sub> to label with a fluorescently-tagged, membrane impermeable anti-HA-tag antibody and compare the sensor surface expression levels under both experimental conditions (**Figure 3.32B**). Again, statistical analysis did not reveal significant difference between HEK cells co-transfected with RAMP2 vs. control providing evidence for equal receptor surface levels (Control: 100.00  $\pm$  7.09 vs. RAMP2: 123.90  $\pm$  22.65;  $p = 0.33$ ). These data suggest that RAMP2 modulates the agonist-induced structural reorganization of PTHR1.

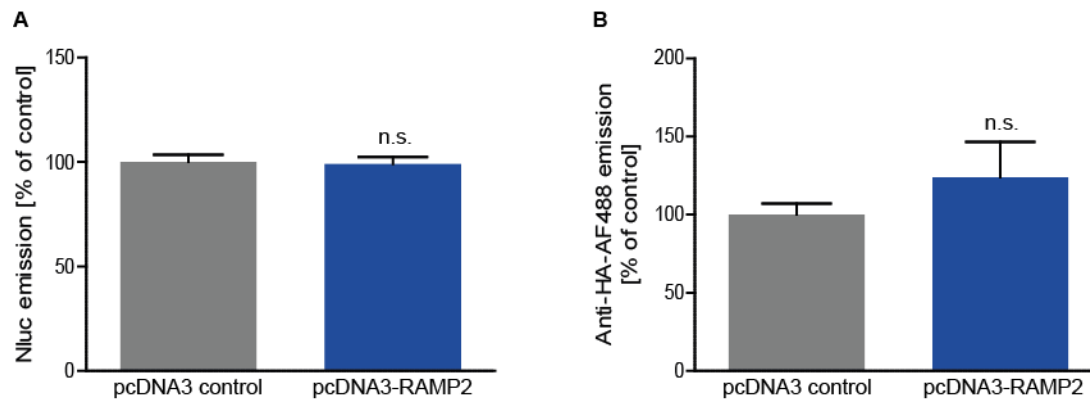


**Figure 3.32: Control of PTHR1<sup>Nluc/Halo(618)</sup> expression and localization.**

HEK cells stably expressing N-terminally HA-tagged PTHR1<sup>Nluc/Halo</sup> biosensor were transfected with pcDNA3 control or pcDNA3-RAMP2. **A)** Total cellular PTHR1<sup>Nluc/Halo</sup> expression was measured through absolute Nluc emission intensities in the unlabeled wells. **B)** The fraction of N-terminally HA-tagged PTHR1<sup>Nluc/Halo</sup> localized at the cell membrane was assessed through labeling with a fluorescently-tagged anti-HA-tag antibody and recording the absolute fluorescence emission intensity. Data show mean ± s.e.m. of three (B) or four (A) independent experiments. Statistical difference was tested through Student's t-test. \* $p \leq 0.05$ .



## 4. Discussion

### 4.1. GPCR<sub>Nluc/Halo(618)</sub> constitutes the optimal sensor design among currently available conformational GPCR sensors

In this work, we describe the most sensitive  $\alpha_2\text{AR}_{\text{donor/acceptor}}$  RET sensor design among 21 distinct biosensors tested to monitor ligand-induced structural receptor rearrangements. The biggest  $\Delta\text{RET}$  signals were measured with the BRET pair Nluc/Halo(618) yielding +8%  $\Delta\text{BRET}$  under transient  $\alpha_2\text{AR}_{\text{Nluc/Halo}}$  expression and more than +12%  $\Delta\text{BRET}$  with a stable sensor cell line upon endogenous agonist (norepinephrine) stimulation. Nluc/Halo(618) has never been applied to create conformational GPCR biosensors in any previous study. However, its superiority over other Nluc/Halo-dye combinations has been demonstrated in a study comparing several intermolecular BRET Nluc/Halo(X) sensors in a protein-protein interaction assay – a finding that is in accordance with the results of this work (Machleidt et al., 2015). To understand whether Nluc/Halo(618) generally constitutes the optimal RET pair for conformational GPCR studies, we compared the signal amplitudes of our sensors with previously reported GPCR biosensors that were likewise employed in microtiter plate experiments.

Since 2016, a new BRET/FIAsH design has been applied in four independent studies to construct  $\beta_2\text{AR}$ , AT1R, Prostaglandin F<sub>2</sub> $\alpha$  receptor (PGFR) and 5-hydroxytryptamine 2A receptor (5-HT<sub>2A</sub>) biosensors and investigate agonist-mediated receptor dynamics (Bourque et al., 2017; Devost et al., 2017; Powlowski, 2018; Sleno et al., 2016). Additionally, Nluc has been used for the creation of  $\beta_2\text{AR}_{\text{Nluc/GFP10}}$  and  $\beta_2\text{AR}_{\text{Nluc/YFP}}$  biosensors (Picard et al., 2018).

The PGFR and 5-HT<sub>2A</sub> Rluc/FIAsH-based biosensors showed poor BRET signals below -2% (upon PGF<sub>2</sub> $\alpha$  or serotonin stimulation, respectively). However, since these probes represent the first conformational biosensors for those GPCRs, it remains to be investigated whether the low amplitude is a GPCR-specific issue or can be enhanced with other donor/acceptor combinations (Powlowski, 2018; Sleno et al., 2016).

In another study, eight different  $\beta_2\text{AR}_{\text{Rluc/FIAsH}}$  versions have been evaluated for their ability to detect isoprenaline-induced receptor activation in microtiter plates. The best variant of  $\beta_2\text{AR}$  measured  $\approx$  +2% BRET response, about six times lower than the signal obtained with  $\beta_2\text{AR}_{\text{Nluc/Halo(618)}}$ . These results already indicate that Nluc/Halo(618) represents the optimal design also for  $\beta_2\text{AR}$ , but it is of note that the tag insertion sites were not identical in these biosensors (Bourque et al., 2017). In contrast, identical insertion sites (compared to  $\beta_2\text{AR}_{\text{Nluc/Halo(618)}}$ ) and donor / acceptor ordering have been targeted for the creation of two  $\beta_2\text{AR}$  biosensors that likewise employ the small and bright luciferase Nluc but couple this donor to either GFP10 or YFP in lieu of Halo(618) (Picard et al., 2018). The better version  $\beta_2\text{AR}_{\text{Nluc/YFP}}$  reports a maximal BRET change of less than -5% upon full stimulation with isoprenaline, about 2.5-times lower than the same stimulus measured with  $\beta_2\text{AR}_{\text{Nluc/Halo(618)}}$  ( $-13.14 \pm 0.59$  %).

In 2017, Devost et al. introduced an AT1R<sub>Rluc/FIAsH</sub> biosensor version tagged with both, Rluc and FIAsH within the receptor's C-terminus, which reported the highest amplitude measured with a conformational GPCR sensor in microtiter plates so far ( $\approx$  -7%  $\Delta\text{BRET}$  with angiotensin-II). However, whether the relative movement within AT1R's C-terminus causing this response is indeed an agonist-specific event and conserved through many GPCRs has not been elaborated. The more established positioning of the BRET acceptor FIAsH within icl3 caused a reduction of the signal amplitude to  $\approx$  -3%  $\Delta\text{BRET}$ . This biosensor represents the ideal benchmark to demonstrate the greatly enhanced sensitivity of the Nluc/Halo(618) design compared to Rluc/FIAsH for GPCR conformational biosensors. Both sensors share exactly the same tag insertion sites and donor/acceptor ordering (donor at C-terminus, acceptor within icl3) but AT1R<sub>Nluc/Halo(618)</sub> shows an almost five-fold higher  $\Delta\text{BRET}$  amplitude upon agonist stimulation ( $+14.36 \pm 0.69$  % for 10  $\mu\text{M}$  angiotensin-II).

The number of GPCR sensors that allows for direct comparison of the signal amplitude with GPCR<sub>Nluc/Halo(618)</sub> is very limited and further suffers from often varying insertion sites or different truncations of the original receptor sequences. However, in all comparisons ( $\alpha_2\text{AR}_{\text{Nluc/Halo(618)}}$  vs. 20  $\alpha_2\text{AR}_{\text{donor/acceptor}}$  sensors;  $\beta_2\text{AR}_{\text{Nluc/Halo(618)}}$  vs.  $\beta_2\text{AR}_{\text{CFP/YFP}}$  /  $\beta_2\text{AR}_{\text{Rluc/FIAsH}}$  /  $\beta_2\text{AR}_{\text{Nluc/YFP}}$ ; PTHR1<sub>Nluc/Halo(618)}</sub> vs. PTHR1<sub>CFP/YFP}</sub>; AT1R<sub>Nluc/Halo(618)}</sub> vs. AT1R<sub>Rluc/FIAsH}</sub>) Nluc/Halo(618) displayed the highest  $\Delta\text{RET}$  amplitude in microtiter plate experiments for four GPCRs indicating that this sensor design represents the most sensitive reporter system for GPCR dynamics. The superior sensitivity of Nluc/Halo(618) can arise from different underlying characteristics.

1) Nluc/Halo(618) relies on luminescent light output sidestepping the need for external sample illumination as required for all FRET-based biosensors and attenuating the interference from cell autofluorescence and RET acceptor direct excitation. In contrast, direct excitation of acceptors in FRET biosensors raises the

background signal and thereby reduces signal strength. The independence of Nluc/Halo(618), and all other BRET pairs, from exogenous sample excitation represents a key advantage of  $\alpha_2\text{AAR}_{\text{Nluc/Halo(618)}}$  and might contribute to its increased sensitivity.

2) The significant spectral separation of  $\approx 170$  nm between donor and acceptor emission maxima represents another important factor contributing to the high amplitude of  $\alpha_2\text{AAR}_{\text{Nluc/Halo(618)}}$ . Substantial spectral separation decreases the impact of donor bleedthrough into the acceptor emission channel, which in turn reduces background signal and improves assay sensitivity.

3) The sensitivity of an intramolecular RET sensors to conformational changes is highest when the inter-fluorophore distance approximates the specific Förster radius  $R_0$ , assuming constrained relative orientation. The fact that  $\alpha_2\text{AAR}_{\text{Nluc/Halo(618)}}$  shows the highest dynamic range upon agonist stimulation indicates that its Förster radius is closer to the real inter-fluorophore distance compared to all other tested donor/acceptor combinations.

With the rapid progress in protein labelling, it remains an unrealizable task to test all possible RET donor/acceptor combinations to further refine this class of biosensors. Therefore, researchers have to carefully select the most promising labelling techniques for the design of conformational GPCR reporters. Two current developments in the field of intracellular protein labelling in living cells appear very promising to lead to excellent FRET and BRET GPCR biosensors.

#### Large-Stokes-Shift fluorescent proteins:

In the early 2000s, Zapata-Hommer and Griesbeck created T-Sapphire, the first fluorescent protein exhibiting a Stokes-Shift (difference between excitation  $\lambda_{\text{Ex}}$  and emission maximum  $\lambda_{\text{Em}}$ ) greater than 100 nm ( $\lambda_{\text{Ex}} = 399$  nm;  $\lambda_{\text{Em}} = 511$  nm) (Zapata-Hommer and Griesbeck, 2003). T-Sapphire represents the first member of the fascinating class of so-called Large-Stokes-Shift fluorescent proteins (LSSFPs) and spurred the evolution of further, especially red-shifted fluorescent proteins like LSSmOrange ( $\lambda_{\text{Ex}} = 437$  nm;  $\lambda_{\text{Em}} = 572$  nm) and CyOFP1 ( $\lambda_{\text{Ex}} = 497$  nm and 523 nm;  $\lambda_{\text{Em}} = 589$  nm) (Chu et al., 2016; Shcherbakova et al., 2012).

When LSSmOrange is employed as RET-acceptor for instance, the significant spectral separation of  $\lambda_{\text{Ex}}$  and  $\lambda_{\text{Em}}$  facilitates substantial overlap of acceptor excitation and donor emission (and thus RET efficiency) despite coupling with far blue-shifted RET donors (e.g. CFP or Nluc). Moreover, the substantially red-shifted  $\lambda_{\text{Em}}$  of these fluorescent proteins (e.g. 450 nm of Nluc vs. 572 of LSSmOrange) results in significant spectral separation and relatively low donor bleedthrough into the RET acceptor channel. CyOFP1 has already proven to be a suitable BRET acceptor for Nluc in binding studies with a peptide-binding class A GPCR and it would be exciting to see how LSSFPs perform as RET-partners in intramolecular GPCR biosensors (Wang et al., 2017).

Novel Nluc substrates: Nluc's emission peak at  $\approx 450$  nm is determined through its distinct catalytic reaction with the substrate furimazine. However, recent chemical modifications of furimazine have shown to shift this emission maximum to the orange-red part of the visible spectrum (e.g. furimazine-derivative F30:  $\lambda_{\text{Em}} = 598$  nm) (Shakhmin et al., 2017).

In theory, these substrates allow for the generation of red/far-red or even red/near-infrared Nluc-based BRET sensors, which would be well within the optimal spectral range for *in vivo* imaging. Such conformational GPCR sensors could be used for instance, to validate ligand-induced receptor activation in living animals in the course of preclinical drug discovery efforts. However, this class of Nluc substrates is still in their infancy and many derivatives suffer from relatively low light output ( $< 1\%$  of Nluc/furimazine). Further chemical substrate modifications or engineering of progressed Nluc variants are required to advance towards *in vivo* application of BRET-based GPCR conformational biosensors.

#### 4.1.1. Impact of tag positioning on results of $\alpha_2\text{AAR}_{\text{donor/acceptor}}$ sensor comparison

Strictly speaking, the outcome that Nluc/Halo(618) represents the optimal BRET pair among tested  $\alpha_2\text{AAR}_{\text{donor/acceptor}}$  sensors applies only to the  $\alpha_2\text{AAR}$  with these specific insertion sites. The tag positions dictate the inter-fluorophore distance  $R$  and their relative orientation. However, different donor/acceptor pairs exhibit diverging Förster radii  $R_0$  affecting the sensor's dynamic range (highest  $\Delta\text{RET}$  amplitude when  $R$  approximates  $R_0$  assuming steady relative orientation).

Unless the structure of a RET GPCR sensor is resolved, it remains impossible to accurately predict the impact of changing the tag positions for a specific GPCR. However, crystal structures of the parent GPCRs allow for indicative estimations of tag relocation effects on sensor performance as exemplified with the nanobody-stabilized active state structure of  $\beta_2\text{AR}$  (PDB code: 3P0G).

The distance between Arg344 at the  $\beta_2$ AR C-terminus (last C-terminal amino acid resolved in this structure) and Lys227 at the cytoplasmic end of TM5 (N-terminal start of icl3) is 4.12 nm vs. 3.45 nm between Arg344 and Lys267 at the cytoplasmic end of TM6 (C-terminal end of icl3). Since the Förster radii of most applied FRET and BRET pairs are well above these distances (e.g. 4.9 nm for CFP/YFP; 4.4 nm for Rluc/YFP), a shift of the chromophore from Lys227 to Lys267 is expected to have a consistent effect (increase or decrease) on the sensors' signal amplitudes (Bajar et al., 2016; Dacres et al., 2010). In a study supporting this hypothesis, three distinct  $\alpha_2$ AR<sub>CFP/FIAsH</sub> sensors were tested for their FRET signals upon agonist stimulation. These constructs shared a consistent placement of CFP at the receptor C-terminus but were labelled with the FRET acceptor FIAsH in three distinct positions within the relatively long icl3 (157 amino acids): N-terminally close to TM5, in the middle of the loop or C-terminally close to TM6. Although the inter-fluorophore distance should differ among these constructs by at least several Angstrom, all sensors showed quite similar  $\Delta$ FRET amplitudes upon norepinephrine stimulation (Zurn et al., 2009).

The tag-specific steric surrounding of a label within a GPCR fusion protein represents another important factor that determines its exact position. Rigid GPCR sections (e.g. short intracellular loops) might influence the location of a bulky structure such as HaloTag more than of a smaller tag like Nluc and thereby superimpose effects caused by shifting the insertion sites by a few amino acids. The results with the inverted version of  $\alpha_2$ AR<sub>Nluc/Halo(618)</sub> support this idea. Although the same BRET partners and insertion sites are used in these constructs, the version with Nluc within icl3 exhibits a significantly lower  $\Delta$ BRET amplitude upon agonist stimulation. This must be due to distinct inter-fluorophore distances and/or relative orientations of the BRET labels between the original and inverted version of  $\alpha_2$ AR<sub>Nluc/Halo(618)</sub>.

In summary, it cannot be excluded that the selection of different tag insertion sites within  $\alpha_2$ AR<sub>donor/acceptor</sub> sensors might result in a different pattern of  $\Delta$ RET amplitudes. However, it is very likely that this would not change the overall outcome, that Nluc/Halo(618) represents the optimal RET pair for conformational GPCR sensors.

## 4.2. BRET-based GPCR<sub>Nluc/Halo(618)</sub> biosensors constitute functional GPCR variants

We demonstrate that the insertion of Nluc and HaloTag maintains wildtype-like receptor functionality since the ligand binding properties of  $\alpha_2$ AR<sub>Nluc/Halo</sub> and the capabilities of  $\alpha_2$ AR<sub>Nluc/Halo</sub>,  $\beta_2$ AR<sub>Nluc/Halo</sub> and PTHR1<sub>Nluc/Halo</sub> to promote their cognate downstream signaling cascades are similar to the respective wildtype receptors. Therefore, the novel conformational GPCR biosensors developed in this work can be used to study various features of receptor-ligand interactions in living cells and to interpret these results with respect to physiological and pathophysiological conditions.

### 4.2.1. $\alpha_2$ AR<sub>Nluc/Halo</sub> shows wildtype-like ligand binding characteristics

We performed radioligand binding experiments with the tritiated  $\alpha_2$ AR antagonist [<sup>3</sup>H]RX821002 to measure and compare the intrinsic affinities of a set of ten ligands towards  $\alpha_2$ AR<sub>Nluc/Halo</sub> and its parent wildtype receptor. To allow for direct comparison of these binding parameters, we prevented the formation of differing receptor populations by external addition of GTP that uncouples GPCRs from co-expressed G proteins (**Figure 3.7**).

Nine compounds display statistically identical affinities towards  $\alpha_2$ AR<sub>Nluc/Halo</sub> and wildtype  $\alpha_2$ AR. These include pharmacologically diverse ligands like the full and partial agonists norepinephrine and octopamine, respectively, the antagonist phentolamine and the inverse agonist yohimbine, as well as structurally distinct catecholamines, the monoterpene indole alkaloid yohimbine or synthetic 2-imidazolines (**Figure 4.1**).

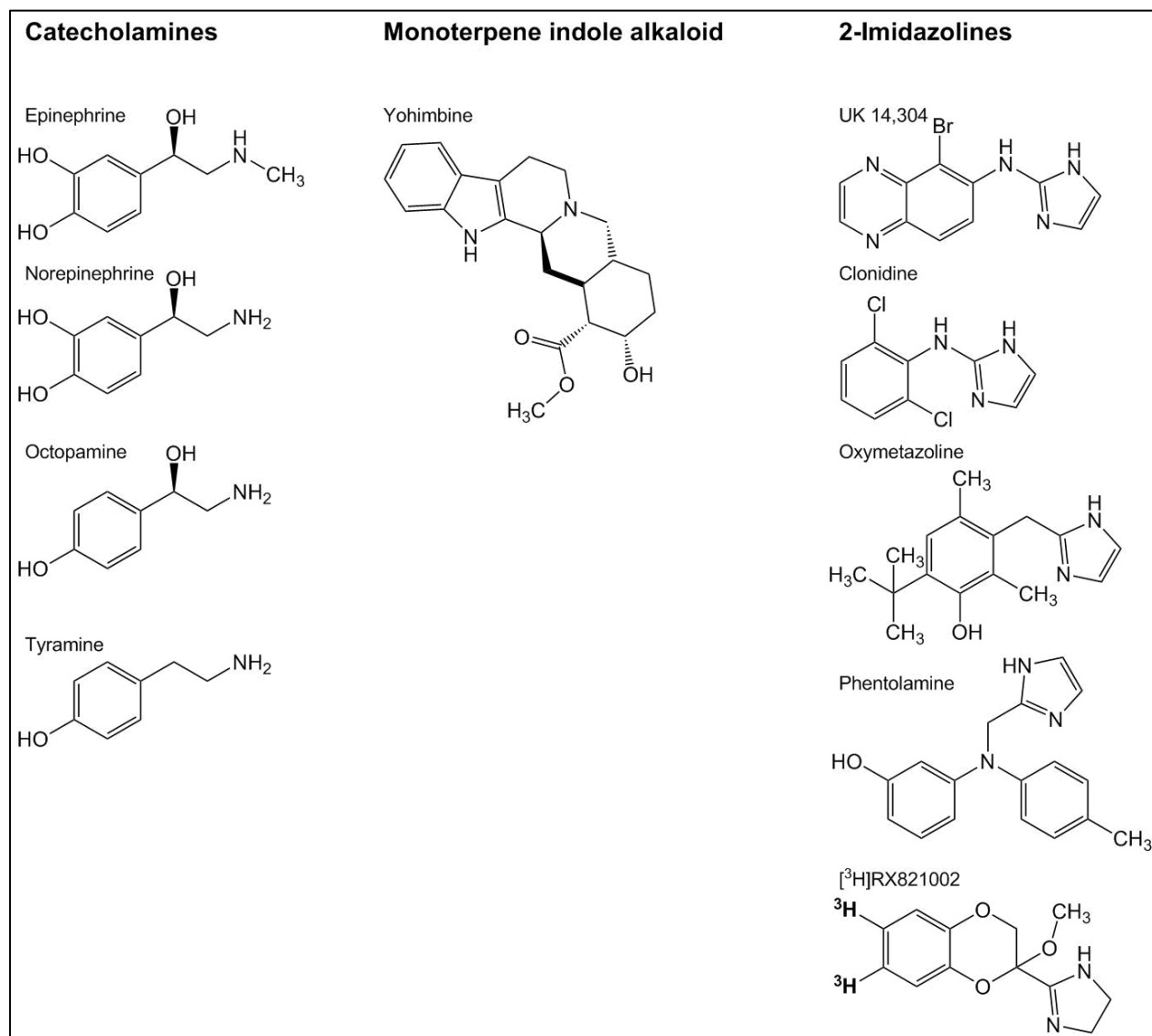


**Figure 4.1:** Structures of  $\alpha_{2A}AR$  ligands tested in radioligand binding experiments.

The fact that this panel of ligands presents the same affinities towards wildtype  $\alpha_{2A}AR$  and  $\alpha_{2A}AR_{Nluc/Halo}$  leads to two main conclusions. The attachment of Nluc and HaloTag to intracellular receptor domains does neither affect (i) the overall arrangement of the binding pocket nor (ii) impair essential physicochemical interactions between these ligands' functional groups and specific amino acid residues within this receptor cavity (e.g. between Ser204  $\alpha_{2A}AR$  and the *para*-hydroxyl group of catecholamines) (Peltonen et al., 2003). This hypothesis is in accordance with the observations from other RET-based conformational GPCR sensors that showed wildtype-identical (Hoffmann et al., 2005; Maier-Peuschel et al., 2010; Nikolaev et al., 2006; Reiner et al., 2010) or somewhat reduced (Villardaga et al., 2003) ligand binding affinities.

In contrast, the antagonist tyramine was the only compound exhibiting distinct  $pK_i$  values indicating higher affinity towards  $\alpha_{2A}AR_{Nluc/Halo}$  vs.  $\alpha_{2A}AR$ . Tyramine's structure forms the backbone of other catecholamines that displayed unaltered affinities (**Figure 4.1**) making it very unlikely that tyramine exhibits a unique way of interaction with the receptor's binding pocket which is impaired in the  $\alpha_{2A}AR_{Nluc/Halo(618)}$  construct. This supports the hypothesis that the increased affinity of tyramine towards  $\alpha_{2A}AR_{Nluc/Halo}$  rather represents an experimental artifact caused by, for instance, differing receptor levels (e.g. due to varying transfection efficiencies) or agglomerates in the  $\alpha_{2A}AR_{Nluc/Halo}$  vs.  $\alpha_{2A}AR$  membrane preparations (Hein P., 2005).

Overall, these binding data provide strong evidence that the capability of  $\alpha_{2A}AR_{Nluc/Halo}$  in binding diverse

receptor ligands is not affected by the attachment of Nluc and HaloTag to intracellular receptor sites. We further suppose that this applies also to other GPCR<sup>Nluc/Halo</sup> sensors that rely on analogous insertion sites.

#### 4.2.2. BRET-based GPCR<sup>Nluc/Halo</sup> biosensors retain signaling capacity

To determine the signaling capability of GPCR<sup>Nluc/Halo</sup> biosensors, we monitored downstream signaling events of these receptors. For  $\alpha_2$ AR biosensor, a preferential coupler to  $G_i$ , we employed the refined  $G\alpha_{i2}$  FRET sensor (van Unen et al., 2016) while for  $\beta_2$ AR and PTHR1, that preferentially couple to  $G_s$ , we employed the cAMP FRET-based sensor H187 (Klarenbeek et al., 2015) since no comparable FRET assay currently exists for  $G\alpha_s$ -coupled receptors. Assessing the signaling capacity of a receptor at the level of G protein activation provides some advantages over capturing receptor-mediated cAMP accumulation. G protein activation follows immediately on GPCR stimulation while cAMP accumulation happens several steps later and usually reports the equilibrium between cAMP production and degradation. Analysis of these experiments revealed that all three GPCR<sup>Nluc/Halo</sup> fusion proteins are capable of downstream signaling, however, with distinct characteristics compared to their parent wildtype receptors. These differences are discussed in the following paragraphs.

##### 4.2.2.1. $\alpha_2$ AR<sup>Nluc/Halo</sup> displays reduced potency to mediate G protein activation

Norepinephrine-stimulation of both,  $\alpha_2$ AR wildtype and  $\alpha_2$ AR<sup>Nluc/Halo</sup> evoked  $G\alpha_{i2}$  activation as demonstrated by a significant decrease of the  $G\alpha_{i2}$  FRET ratio confirming the capability of the novel GPCR sensor to promote its native downstream cascade (**Figure 3.13C**). However, the prominent right-shift of the  $\alpha_2$ AR<sup>Nluc/Halo</sup>-mediated FRET response by more than two log-units indicates a substantial impairment of its signaling competence. There are three factors that might contribute to this prominent deviation.

1) The attachment of two bulky and high-molecular weight tags (**Figure 1.18**; HaloTag 33 kDa, 19 kDa Nluc) to intracellular receptor domains could sterically block the formation of a stable GPCR-G protein complex. This concept is supported by a similar or even greater signaling attenuation observed with other GPCR RET biosensors composed of two bulky protein tags (Hoffmann et al., 2005; Vilardaga et al., 2003).

2) Additionally, the drastic truncation of  $\alpha_2$ AR<sup>Nluc/Halo</sup>'s third intracellular loop by 120 amino acids represents another factor that might alter the receptor's tertiary structure (in particular the organization of transmembrane helices TM5 and TM6) and diminish its tendency to activate G proteins. The previously described FRET analogue  $\alpha_2$ AR<sup>CFP/YFP</sup> lacks the same strain of amino acids within icl3 and displayed a likewise reduced downstream signaling capacity (in this study assessed through GIRK opening) (Vilardaga et al., 2003).

3) The third and probably most unexpected option that could contribute to the significant right-shift of  $\alpha_2$ AR<sup>Nluc/Halo</sup>-mediated G protein activation bases on another striking difference between the wildtype  $\alpha_2$ AR vs.  $\alpha_2$ AR<sup>Nluc/Halo</sup>-mediated  $G\alpha_{i2}$  FRET responses. Even without norepinephrine-stimulation, a remarkably reduced basal  $G\alpha_{i2}$  FRET ratio can be detected in cells expressing this sensor along with  $\alpha_2$ AR<sup>Nluc/Halo</sup>. Such a decrease in FRET is generally considered as G protein activation and therefore indicates pre-coupled and constitutively active populations of  $\alpha_2$ AR<sup>Nluc/Halo</sup> in living cells. This concept of constitutive activity of  $\alpha_2$ AR<sup>Nluc/Halo</sup> is further supported by the facts that weak partial agonists (clonidine, octopamine, oxmetazoline) induce antagonist-like responses at the receptor level (negative  $\Delta$ BRET; **Figure 3.10**) and the results from radioligand binding experiments indicating precoupling of  $\alpha_2$ AR<sup>Nluc/Halo</sup> with endogenous G proteins in living cells (**Figure 3.11**).

Such precoupling and basal signaling of  $\alpha_2$ AR<sup>Nluc/Halo</sup> could contribute to its significantly right-shifted G protein FRET response since substantially higher agonist concentrations are required to saturate yet uncoupled receptor populations and trigger further activation of prior inactive G proteins. The underlying reasons for the constitutive activity of  $\alpha_2$ AR<sup>Nluc/Halo</sup> remain unclear since a comparable GPCR sensor has so far not been reported, not even for the FRET analogue  $\alpha_2$ AR<sup>CFP/YFP</sup>. Comparing the assumed spatial integration of HaloTag/Nluc vs. CFP/YFP into the  $\alpha_2$ AR scaffold in a two-dimensional model shows that especially the bulky HaloTag requires more space than e.g. YFP and might therefore "open" the cytosolic surface of this biosensor (**Figure 4.2**). Furthermore, the substantially larger N-to-C-terminal distance in HaloTag (28.09 Å; PDB code: 5UY1) compared to fluorescent proteins (18.75 Å; PDB code: 1EMB) might introduce steric tension between TM5 and TM6 and alter the receptor's overall conformation. These

conformational manipulations could, for instance, create a cavity enabling the coupling of G proteins and lead to the postulated increased basal activity of  $\alpha_{2A}AR_{Nluc/Halo}$ . However, this presumed altered basal conformation of  $\alpha_{2A}AR_{Nluc/Halo}$  and its tendency to precouple G proteins does not interfere with its great utility as a tool to study GPCR conformational dynamics by pharmacological ligands or other kinds of stimuli.

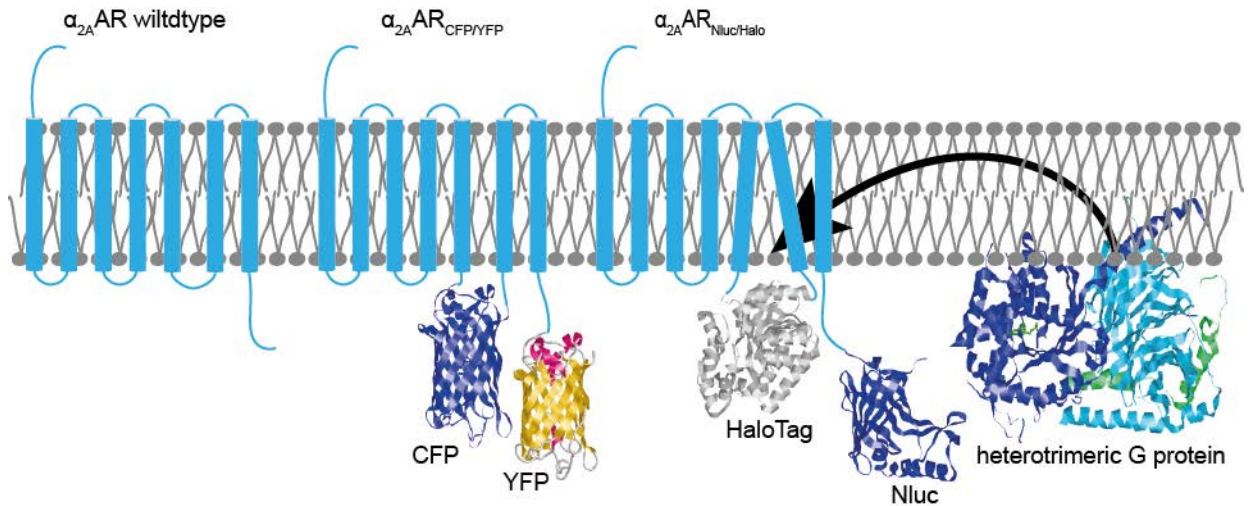


**Figure 4.2: Model for steric effects of BRET tags on  $\alpha_{2A}AR$  conformation.**

The three exemplary structures of wildtype  $\alpha_{2A}AR$  (left) and two equivalently designed FRET ( $\alpha_{2A}AR_{CFP/YFP}$ ) and BRET ( $\alpha_{2A}AR_{Nluc/Halo}$ ) biosensors illustrate a possible mechanism for an increased basal signaling activity of  $\alpha_{2A}AR_{Nluc/Halo}$ . The bulkier structure and bigger N-to-C-terminal distance of HaloTag vs. fluorescent proteins within  $\alpha_{2A}AR$ 's ic13 could relocate adhered helices TM5 and TM6 and simultaneously open a cavity for G protein association (PDB codes: 1EMB, 5IBO, 5UY1, 1GG2).

#### 4.2.2.2. $\beta_2AR_{Nluc/Halo}$ mediates cAMP production but displays decreased surface expression

Stimulation of cells expressing the FRET-based cAMP sensor along with either wildtype  $\beta_2AR$  or  $\beta_2AR_{Nluc/Halo}$  resulted in very similar concentration-response curves with indistinguishable  $EC_{50}$  values and maximal FRET response (**Figure 3.16C**). These findings indicate that  $\beta_2AR_{Nluc/Halo}$  constitutes wildtype-like signaling capacity. The only deviation between  $\beta_2AR_{Nluc/Halo}$  and  $\beta_2AR$  wildtype with respect to the cAMP production is given by the fact that the basal cAMP level appears to be lower in  $\beta_2AR_{Nluc/Halo}$ -expressing cells. This is most likely due to the reduced surface expression of  $\beta_2AR_{Nluc/Halo}$  (**Figure 3.16B**). If a smaller number of receptors is exposed to the cell surface, less functional receptor-G protein complexes are built leading to a decreased production of cAMP.

Overall, these data demonstrate that the BRET-based  $\beta_2AR$  biosensor is able to signal through  $G_s$  and promote cAMP production with wildtype-like characteristics despite decreased surface expression. The equivalent  $\beta_2AR_{CFP/YFP}$  FRET sensor has not been evaluated with regards to its surface expression and signaling capacity. However, pharmacological characterization of several full-length  $\beta_2AR_{Rluc/FAsH}$  sensors showed unaltered surface expression and basal, as well as agonist-induced cAMP production suggesting a role for HaloTag and the truncated C-terminus of  $\beta_2AR_{Nluc/Halo}$  in the reduced surface expression and basal cAMP production (Bourque et al., 2017). Especially the truncated C-terminus  $\beta_2AR_{Nluc/Halo}$  (44 distal amino acids cut off; Gln370 – Leu413) lacks important signal sequences that have been attributed vital roles in regulating receptor internalization, degradation and recycling (Hanyaloglu and von Zastrow, 2007; Lauffer et al., 2010).

#### 4.2.2.3. PTHR1<sub>Nluc/Halo</sub>-mediated cAMP production

Maximal stimulation with the full agonist PTH(1-34) triggered a comparable elevation of intracellular cAMP in PTHR1<sub>Nluc/Halo</sub> and wildtype receptor expressing cells (**Figure 3.19C**). Similar to  $\alpha_2$ AR<sub>Nluc/Halo</sub> however, a greatly right-shifted EC<sub>50</sub> value ( $\approx 2$  log units) indicates reduced potency of this fusion protein to promote downstream signaling. Contrary to the  $\alpha_2$ AR BRET biosensor, no icl3 truncation was required for the generation of PTHR1<sub>Nluc/Halo</sub> but the C-terminus was shortened by 96 distal amino acids (Nluc fusion to Gly497; Pro498 – Met593 lacking) to yield a functional biosensor. Intriguingly, the equivalent FRET probe PTHR1<sub>CFP/YFP</sub> displayed a similarly right-shifted concentration-response curve of receptor-mediated cAMP production (Villardaga et al., 2003). This suggests that either those 96 C-terminal amino acids are involved in G protein activation or that the overall structure of PTHR1 is more vulnerable to the incorporation of bulky tags. The observed higher FRET ratio of the cAMP sensor when co-expressed with PTHR1<sub>Nluc/Halo</sub> vs. wildtype PTHR1 can be due to differential cAMP sensor expression levels or reduced basal signaling activity of PTHR1<sub>Nluc/Halo</sub>. In contrast to  $\beta_2$ AR<sub>Nluc/Halo</sub>, this is not due to a diminished surface expression, since labeling of wildtype PTHR1 and PTHR1<sub>Nluc/Halo</sub> with a cell-impermeable, fluorescent antibody demonstrated equal receptor surface expression levels (**Figure 3.19B**). Instead, the lacking response of PTHR1 antagonists in the conformational BRET assays rather points to substantially reduced constitutive activity of PTHR1<sub>Nluc/Halo</sub>. Overall, these data demonstrate that the PTHR1 BRET sensor promotes cAMP production upon receptor stimulation, although, with reduced potency. Furthermore, PTHR1<sub>Nluc/Halo</sub> displays wildtype-like surface expression levels but might feature a reduced constitutive activity compared to wildtype PTHR1.

### 4.3. GPCR<sub>Nluc/Halo(618)</sub> biosensors reliably report ligand efficacy and potency

In this work, we demonstrate that the different conformational GPCR<sub>Nluc/Halo(618)</sub> biosensors reliably report both, efficacy and potency of applied receptor ligands. Specifically, we tested 36 distinct ligands in concentrations reported to saturate their cognate receptor with six different GPCR<sub>Nluc/Halo(618)</sub> biosensors:  $\alpha_2$ AR<sub>Nluc/Halo(618)</sub> (ten compounds) (**Figure 3.10**),  $\beta_2$ AR<sub>Nluc/Halo(618)</sub> (twelve compounds) (**Figure 3.14**), PTHR1<sub>Nluc/Halo(618)</sub> (six compounds) (**Figure 3.17**), AT1R<sub>Nluc/Halo(618)</sub> (two compounds) (**Figure 3.25**), CXCR4<sub>Nluc/Halo(618)</sub> (five compounds) (**Figure 3.27**) and S1PR1<sub>Nluc/Halo(618)</sub> (one compound) (**Figure 3.29**). Furthermore, 23 of these compounds were studied in concentration-response experiments using five of these GPCR<sub>Nluc/Halo(618)</sub> sensors. The resulting potency values mimicked the ligands' affinities / potencies to the cognate wildtype receptors confirming the capacity of this sensor design to discriminate compounds with distinct efficacies and affinities / potencies. Therefore, Nluc/Halo(618)-based GPCR sensors present a reliable novel system to determine the pharmacological profiles of diverse GPCR ligands.

#### 4.3.1. GPCR<sub>Nluc/Halo(618)</sub> faithfully reveal ligand efficacies

##### 4.3.1.1. BRET responses of agonists

All GPCR biosensors reported BRET responses for their endogenous, as well as synthetic full agonists that were significantly different from 1) the negative control (buffer) and 2) all other types of ligands including partial agonists and antagonists. The capability of GPCR sensors to detect their cognate full (endogenous) agonists represents the prime requirement for future applications.

##### 4.3.1.2. BRET responses of antagonists

Additionally,  $\alpha_2$ AR<sub>Nluc/Halo(618)</sub>,  $\beta_2$ AR<sub>Nluc/Halo(618)</sub>, AT1R<sub>Nluc/Halo(618)</sub> and CXCR4<sub>Nluc/Halo(618)</sub> revealed opposite BRET changes promoted by antagonists and inverse agonists mirroring their contrary pharmacological effects.

The feature to directly (i.e. without agonist pre-incubation) detect GPCR antagonists and inverse agonists constitutes a key advantage of the novel Nluc/Halo(618) sensor design since it allows for direct screening of inactivating GPCR ligands, a compound type that accounts for more than 40% of all GPCR-directed drugs

in current clinical trials (Hauser et al., 2017). Among the numerous (> 50) RET-based conformational GPCR sensors reported today (**Annex Table 7.3**), only few have been shown to directly (i.e. without receptor preactivation) identify inverse agonists (Fernandez-Duenas et al., 2014; Vilardaga et al., 2005) or antagonist (Rochais et al., 2007) through agonist opposed FRET signals. Intriguingly, the original CFP/YFP FRET sensor of  $\alpha_{2A}$ AR was incapable of recording any significant FRET response upon addition of the neutral antagonist phentolamine, highlighting the key role of the novel BRET partners Nluc/Halo(618) for the enhanced sensitivity towards detection of GPCR antagonists (Vilardaga et al., 2003).

#### 4.3.1.3. BRET responses of partial and biased agonists

In addition to discriminating agonists and antagonists, the different GPCR biosensors have further shown to report statistically lower BRET signals for partial agonists compared to full agonist responses. Furthermore, previously postulated biased  $\beta_2$ AR ligands (salmeterol and formoterol) evoked intermediate BRET responses substantially smaller than that of the balanced full agonist isoprenaline (Rajagopal et al., 2011; van der Westhuizen et al., 2014). This observation is in accordance with a conformational AT1R-based FIAsH/Rluc biosensor that detected significantly different BRET responses for balanced vs. biased agonists (Devost et al., 2017)

#### 4.3.1.4. GPCR ligands that lacked significant BRET responses

Some compounds did not evoke any statistically different BRET response compared to negative control.

i) Dopamine is described as a  $\alpha_{2A}$ AR strong partial agonist (Zurn et al., 2009). As such, it can bind and stabilize the receptor in a conformation that is distinct from its basal state. In our hands however, dopamine was not able to induce any significant BRET change of  $\alpha_{2A}$ AR<sub>Nluc/Halo(618)</sub>. This lack of response is in line with our hypothesis that  $\alpha_{2A}$ AR<sub>Nluc/Halo</sub> adopts a constitutively active conformation that is stabilized but not altered upon dopamine binding.

ii) Carvedilol and labetalol are generally considered neutral antagonists of  $\beta_2$ AR (IUPHAR database (Harding et al., 2018)) but lately these compounds have been attributed partial agonistic activities (van der Westhuizen et al., 2014). In our hands, carvedilol and labetalol were incapable of inducing any significant BRET signals in the  $\beta_2$ AR<sub>Nluc/Halo(618)</sub> assay while other neutral antagonists like metoprolol and propranolol evoked significant negative responses. These data support the notion that carvedilol and labetalol represent partial agonists of  $\beta_2$ AR and stabilize the basal, partially active conformation of  $\beta_2$ AR<sub>Nluc/Halo(618)</sub>.

iii) All three employed PTHR1 antagonists (PTH(7-34), (dW)-PTH(7-34) and PTH(3-34)) did not display any significant BRET change in the PTHR1<sub>Nluc/Halo(618)</sub> assay although we confirmed that at least one of them ((dW)-PTH(7-34)) is competing with the agonist PTH(1-34) for binding to PTHR1<sub>Nluc/Halo(618)</sub> (**Figure 3.18**). The antagonist PTH(7-34) has also shown this lack of response in the previous FRET version of this biosensor, arguing against a specific Nluc- or HaloTag induced issue (Vilardaga et al., 2003). The lack of a significant BRET signal despite sufficient ligand-receptor interaction indicates that the different PTHR1 antagonists do not promote the transition of the receptor into a new structural organization but stabilize the basal PTHR1 conformation. Therefore, PTHR1<sub>Nluc/Halo</sub> is further assumed to show very low extent of basal activity which is supported by the data from receptor-mediated basal cAMP production.

#### 4.3.1.5. GPCR ligands that evoked unexpected BRET signals

In contrast to ligands that lacked significant BRET responses, four compounds were able to provoke significant BRET signals, however, the amplitude and implied efficacy of these BRET changes were somewhat unexpected.

i) UK 14,304 at  $\alpha_{2A}$ AR<sub>Nluc/Halo(618)</sub> was expected to promote full agonist-like BRET changes based on its pharmacological characterization in radiolabeled GTP $\gamma$ S assays (90  $\pm$  8% response of norepinephrine) (Jasper et al., 1998). In the conformational GPCR readout however, UK 14,304 induced significantly lower BRET signals than the corresponding full agonist norepinephrine indicating that this ligand favors the engagement of a distinct receptor conformation.



Previous studies employing CFP/YFP and CFP/FIAsH  $\alpha_{2A}$ AR FRET conformational biosensors have exclusively reported indistinguishable responses for UK 14,304 and norepinephrine (Nikolaev et al., 2006; Vilardaga et al., 2005). However, a recent single-molecule study found distinct norepinephrine vs. UK 14,304-triggered association and dissociation rates of  $\alpha_{2A}$ AR-G<sub>ai</sub> complexes, which provides evidence for different underlying principles of UK 14,304- $\alpha_{2A}$ AR vs. norepinephrine- $\alpha_{2A}$ AR interaction (Sungkaworn et al., 2017).

ii) Similar to UK 14,304 at  $\alpha_{2A}$ AR, norepinephrine has been considered a full agonist of  $\beta_2$ AR based on downstream signaling responses. The  $\beta_2$ AR<sup>Nluc/Halo(618)</sup> assay however, revealed an intermediate BRET change compared to the full agonists epinephrine and isoprenaline. In accordance with our results, earlier  $\beta_2$ AR conformational studies employing NMR spectroscopy of a [<sup>19</sup>F]-labeled receptor (Liu et al., 2012) or a FRET-based biosensor (Reiner et al., 2010) demonstrated that norepinephrine indeed provokes a partial conformational change compared to the full agonists isoprenaline and epinephrine, respectively.

Taken together, these lines of evidence suggest that UK 14,304 at  $\alpha_{2A}$ AR and Norepinephrine at  $\beta_2$ AR stabilize partially active receptor conformations. These slight conformational differences are blurred with continual signal amplification along the downstream signaling pathway and can therefore only be detected with techniques providing high-resolution insights into GPCR conformation.

iii) The CXCR4 ligands AMD3465 and AMD3100 have been subjected to contrary classifications by different research groups:

Based on its inhibitory effects on CXCL12 mediated G protein activation, Ca<sup>2+</sup> flux and cell chemotaxis, AMD3465 was considered an antagonist of CXCR4 (Bodart et al., 2009). However, also partial agonist can reduce the downstream response triggered by stronger partial or full agonists and intriguingly, AMD3465 was further attributed partial agonistic activity owing to its ability to mediate ERK phosphorylation (Yang et al., 2007). Similarly, AMD3100 potently inhibited CXCL12-induced Ca<sup>2+</sup> flux, chemotaxis and CXCR4 endocytosis (Hatse et al., 2002) but has been shown in an independent study to induce G protein activation through CXCR4 and trigger partial (in comparison to CXCL12) responses in Ca<sup>2+</sup> mobilization assays when administered alone (Zhang et al., 2002).

Exposure of CXCR4<sup>Nluc/Halo(618)</sup> expressing cells to AMD3465 and AMD3100 evoked significant increases of the BRET ratio that were lower than the maximal BRET response of the full endogenous agonist CXCL12. These data support the postulations of Yang et al. and Zhang et al. that AMD3465 and AMD3100 present partial agonistic activities at CXCR4.

In summary, the cases of UK 14,304, Norepinephrine ( $\beta_2$ AR) and the two AMD ligands highlight two outstanding features of intramolecular GPCR biosensors. First, these biosensors elucidate the pharmacologic profiles of GPCR ligands with highest precision (absent impact of signal amplification) allowing to detect even slight differences in ligand efficacies (e.g. norepinephrine vs. epinephrine at  $\beta_2$ AR). Second, exploring compound effects on receptor conformation enables their pharmacological characterization independent of different receptor downstream pathways and provides a more representative picture of the ligand's overall action.

#### 4.3.2. GPCR<sup>Nluc/Halo(618)</sup> faithfully reveal ligand potencies

Altogether, we tested 23 distinct compounds in BRET concentration-response experiments with five GPCR<sup>Nluc/Halo(618)</sup> biosensors:  $\alpha_{2A}$ AR<sup>Nluc/Halo(618)</sup> (ten compounds) (**Figure 3.10**),  $\beta_2$ AR<sup>Nluc/Halo(618)</sup> (three compounds) (**Figure 3.14**), PTHR1<sup>Nluc/Halo(618)</sup> (three compounds) (**Figure 3.17**), AT1R<sup>Nluc/Halo(618)</sup> (two compounds) (**Figure 3.25**) and CXCR4<sup>Nluc/Halo(618)</sup> (five compounds) (**Figure 3.27**).

Among the tested compounds, only for dopamine and carvedilol no EC<sub>50</sub> values could be calculated because they failed to elicit BRET signals through  $\alpha_{2A}$ AR<sup>Nluc/Halo(618)</sup> and  $\beta_2$ AR<sup>Nluc/Halo(618)</sup>, respectively, that could be fitted to sigmoidal concentration-response curves. To compare the resulting EC<sub>50</sub> values with the true affinities of these compounds, we performed radioligand binding experiment with  $\alpha_{2A}$ AR<sup>Nluc/Halo</sup> membranes and screened the literature for reported affinities or potencies of applied  $\beta_2$ AR, PTHR1, AT1R and CXCR4 ligands to the corresponding wildtype receptors. Whenever possible, binding affinities (pK<sub>D</sub> or pK<sub>i</sub>) were preferred since the conformational BRET readout should in theory not be subject to any signal amplification but resemble the ligand-GPCR association process. If such data was not available, we selected the most proximal (e.g. GTPγS is more proximal than cAMP or Ca<sup>2+</sup>) downstream potency value we found (EC<sub>50</sub> or IC<sub>50</sub>; half maximal inhibitory ligand concentration) to reduce the risk of misinterpretation due to signal amplification.

All five conformational BRET biosensors accurately resembled the ligands' intrinsic affinities / potencies,

demonstrated by a maximum discrepancy of  $\approx 0.6$  log units (epinephrine and UK 14,304 at  $\alpha_2\text{AR}_{\text{Nluc/Halo}(618)}$ ). Only the CXCR4 endogenous agonist CXCL12 displayed a significantly  $\approx 3$  log lower potency in the conformational assay compared to its reported binding affinity ( $\text{pEC}_{50} = 4.75 \pm 0.18$  vs.  $\text{pK}_i = 8.05 \pm 0.17$  as reported by (Loetscher et al., 1998)). This prominent discrepancy is quite unexpected. Other tested CXCR4 ligands engaging the same orthosteric site of CXCR4 (e.g. AMD3100 and AMD3465) did not show any comparable shift in the  $\text{CXCR4}_{\text{Nluc/Halo}(618)}$  assay indicating that the properties of this binding pocket are not affected by the attachment of Nluc and HaloTag. Thus, it remains to be elucidated whether the low potency of CXCL12 in triggering a conformational change of  $\text{CXCR4}_{\text{Nluc/Halo}(618)}$  has a true physiological meaning or represents a technical artifact due to interference with CXCR4's geometry. The first crucial step in solving this issue is to assess the binding affinity of CXCL12 to the biosensor  $\text{CXCR4}_{\text{Nluc/Halo}(618)}$ . If the attachment of BRET donor and acceptor indeed reduces the affinity of the endogenous agonist, one would expect a  $\text{pK}_i$  value similar to the BRET  $\text{EC}_{50}$  value of 4.75.

Overall, the concentration-response experiments with numerous ligands demonstrated that the novel GPCR sensor design  $\text{Nluc/Halo}(618)$  reliably reveals the intrinsic ligand potencies to manipulate receptor conformation. Thus, these biosensors can be employed in lieu of ligand binding and GPCR downstream assays to obtain quantitative information on ligand-receptor interactions.

#### 4.4. Studying GPCR (de-) activation kinetics with $\text{GPCR}_{\text{Nluc/Halo}(618)}$ biosensors

Since their first description in 2003, GPCRs have been used as optical tools to study receptor activation and deactivation kinetics (Ahles et al., 2011; Ahles et al., 2015; Ambrosio and Lohse, 2012; Hlavackova et al., 2012; Nikolaev et al., 2006; Vilardaga et al., 2003; Xu et al., 2012; Ziegler et al., 2011). To evaluate whether the  $\text{GPCR}_{\text{Nluc/Halo}(618)}$  biosensors can be applied for such investigations, we employed the injector module of the Synergy Neo2 plate reader for automated delivery of norepinephrine and yohimbine to basal-state  $\alpha_2\text{AR}_{\text{Nluc/Halo}(618)}$  and phentolamine to norepinephrine-prestimulated cells and calculated the resulting rate constants ( $\tau$ ) (**Figure 3.9**).

##### 4.4.1. Stimulation of basal-state $\alpha_2\text{AR}_{\text{Nluc/Halo}(618)}$

With the conformational BRET assay, we did not detect any differences between activation (triggered by norepinephrine) and deactivation kinetics (yohimbine) starting from basal receptor conformation. This finding is in contradiction to previous observations, that switching receptors from basal to the yohimbine-stabilized inactive conformation represents a  $\approx 35$  times slower process ( $\tau > 1$  s) than the transition from basal to active with norepinephrine ( $\tau \approx 40$  ms) (Vilardaga et al., 2005). This discrepancy can either derive from the different sensor designs (in particular the novel RET donor / acceptor pair  $\text{Nluc/Halo}(618)$ ) or from the discrete experimental setups.

Thus far, we cannot exclude the impact of Nluc and HaloTag on the speed of receptor dynamics. Both components constitute bulkier tags compared to fluorescent proteins and FIAsH and might therefore slow down the receptor switch from one conformation to the other. Performing such kinetic studies with  $\text{Nluc/Halo}(618)$ - and e.g. CFP/YFP- or CFP/FIAsH-based sensors under the same experimental setups could provide further information on the effect of HaloTag and Nluc on receptor activation kinetics.

Kinetic FRET studies are commonly conducted in single-cell experiments where a syringe is placed in close proximity ( $< 100 \mu\text{m}$ ) of the cell under observation enabling rapid solution exchange in less than 10 ms and simultaneous fluorescence recoding (**Figure 4.3A**).

In contrast,  $\text{GPCR}_{\text{Nluc/Halo}(618)}$  experiments are conducted in microtiter plates which drastically alters the overall experimental setup in view of kinetic analysis (**Figure 4.3B**). The two major deviations from the FRET system are discussed hereafter.

Ligand delivery process: The ligand solution is added to the cell-covering liquid and needs to diffuse through the buffer column (in our experiments  $90 \mu\text{l}$  basal assay volume,  $\approx 2.5$  mm height) to reach the cells. This represents one important factor that slows down the entire process from ligand delivery to BRET response and might blur the differences in activation vs. deactivation kinetics. Additionally, the longer diffusion path in the BRET system and the fact that thousands of cells (instead of a single cell) constitute the sample hampers a synchronous stimulation of the sample. Thus, some cells are reached by the ligand earlier than others which distorts the time-course of the BRET response and overlays kinetic differences. Thus, further

technical refinement of the ligand delivery process, e.g. a FRET-like system where the injector dips into the sample and delivers the ligand in close proximity of the cells, are required to enhance the accuracy of kinetic BRET measurements.

Consecutive luminescence read and ligand injection: Another major technical limitation of the BRET system is that all currently commercially available plate readers do not allow for simultaneous dual-wavelength recording and liquid injection but require a switch from the optical module to the injector module for the ligand delivery step. Before we performed the kinetic experiments, we compared four different BRET plate readers (Synergy Neo2 from BioTek, Mithras LB940 from Berthold Technologies, CLARIOstar from BMG Labtech and GloMax® Discover from Promega) for this switching speed. The Synergy Neo2 showed to be the fastest among these four, however, the module change still causes a “blind window” of about 1.5 seconds between the last data point before and the first data point after injection. Thus, we miss the most crucial data points for an accurate calculation of the rate constant  $\tau$ . Future plate readers that simultaneously record the luminescence emission and inject ligand solutions would allow a big step towards accurate measurements of BRET kinetics. This could be achieved for example by a combination of top-injection and bottom-read through transparent bottom wells of the microtiter plate.

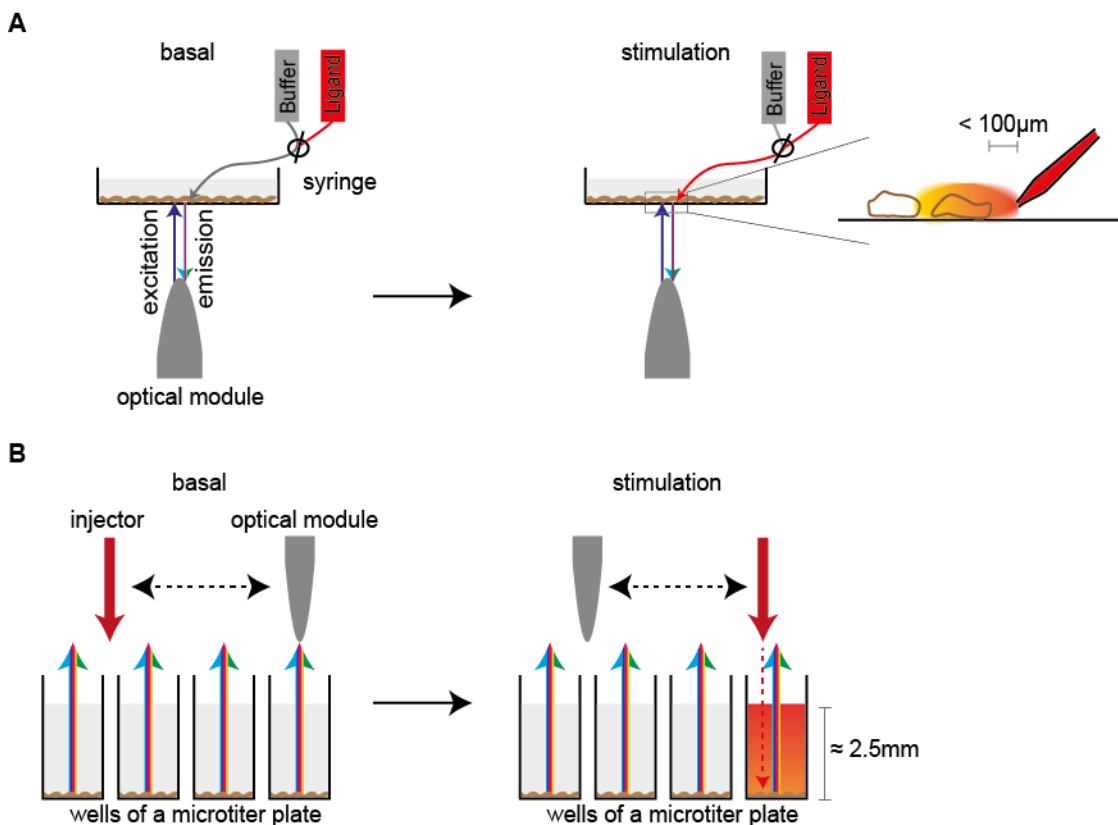


**Figure 4.3: Technical setup for kinetic measurement with RET-based GPCR biosensors.**

A) Fluorescence-based kinetic measurements are performed combining fluorescence microscopy with a specialized perfusion system that enables continuous superfusion of the cells with differing solutions and rapid solution exchange. B) In contrast, luminescence-based measurements are mostly performed in microtiter plates requiring a luminescence plate reader equipped with an injector module. For agent injection, the injector and optical module exchange positions and switch back after delivery of the sample.

#### 4.4.2. Deactivation of active-state $\alpha_2AAR_{Nluc/Halo(618)}$

Despite the technical limitations of kinetic BRET measurements described above, we found that the addition of phentolamine to active-state GPCRs (cells prestimulated with norepinephrine) provoked a conformational change that was substantially faster than the structural switches starting from the sensor's basal

conformation. The original CFP/YFP FRET pendant  $\alpha_2\text{AR}_{\text{Nluc/Halo}(618)}$  also reported a rapid reversion of norepinephrine's FRET response upon phentolamine addition, however, no statistical analysis was performed to compare the rate constants of norepinephrine- vs. phentolamine-induced conformational switches (Vilardaga et al., 2003). It remains to be elucidated whether phentolamine also evokes these fast deactivation switches when applied to basal-state  $\alpha_2\text{AR}$  sensors or if these fast transitions are constrained to preactivated receptors. The latter case could demonstrate an increased sensitivity of GPCRs to fall back to the inactive state once they were stimulated by agonists and might represent a novel mechanism of cells to protect themselves from excessive stimulation.

#### 4.5. High-throughput screening suitability of $\text{GPCR}_{\text{Nluc/Halo}(618)}$ biosensors

In this study, we report the first high-throughput screening-compatible GPCR biosensor design composed of Nluc and Halo(618). These biosensors provide excellent assay quality (in terms of Z-factor), allow for sufficient data throughput due to high signal stability over time and feature low rates of false positive screening hits.

##### 4.5.1. $\text{GPCR}_{\text{Nluc/Halo}(618)}$ biosensors provide excellent screening windows

Despite sufficient signal amplitude, any HTS method should further display low background and signal variation to allow for reliable signal vs. noise distinction within a big screening window (the range in which a signal can clearly be distinguished from background). Concerning high-throughput screening, the Z-factor represents the commonly accepted parameter to determine the assay specific screening window.

Analysis of these Z-factors for  $\alpha_2\text{AR}_{\text{Nluc/Halo}(618)}$ ,  $\beta_2\text{AR}_{\text{Nluc/Halo}(618)}$  and  $\text{PTHR1}_{\text{Nluc/Halo}(618)}$  revealed that all three biosensors present excellent screening windows ( $Z > 0.5$ ) for their application in HTS (**Figure 3.20**). Furthermore, analogous Z-factor assessment their FRET pendants  $\alpha_2\text{AR}_{\text{CFP/YFP}}$ ,  $\beta_2\text{AR}_{\text{CFP/YFP}}$  and  $\text{PTHR1}_{\text{Nluc/Halo}(618)}$ , which were all below 0, highlights the significant improvement in signal vs. noise distinction achieved by the novel sensor design Nluc/Halo(618).

##### 4.5.2. $\text{GPCR}_{\text{Nluc/Halo}(618)}$ facilitate high data throughput

Besides the quality of an assay, the number of data points that can be generated within a specific time window (e.g. per day) represents another crucial property to employ a new method in a screening program. This parameter is termed the assay throughput and highly depends on the stability of the signal, which in turn limits the potential of assay automation and stacking of multiple plates.

Assessment of the time-stability of the BRET signal displays a time window of at least 30 minutes after ligand addition where the method still provides excellent quality for compound screening ( $Z\text{-factor} > 0.5$ ) (**Figure 3.21**).

Given this reading window of 30 minutes after compound addition, the throughput of this assay essentially depends on the equipment available for pipetting and plate reading. Under optimal conditions, it depends only on the time required to read the plate before and after addition of compounds, while under the most basic conditions, the time needed to read a single plate would encompass the times required for the basal read, addition of compounds, and a second read.

We performed the experiments with a plate reader (Synergy Neo2) that successively reads the wells of the microtiter plate and therefore requires about 40 seconds per 96-well plate. Using this setting with optimized automation and plate stacking,  $\approx 40$  assay plates can be read within the window guaranteeing excellent assay quality resulting in a throughput of  $\approx 7,200$  data points / hour or  $\approx 170,000$  data points / day. Thus, a library of one million compounds could be tested within six days. However, customized plate readers used in the pharmaceutical industry allow for simultaneous read of all wells of a microtiter plate. Performing the  $\text{GPCR}_{\text{Nluc/Halo}(618)}$  assay with these readers drastically reduces the read time per plate to the integration time (= time that photons are captured by photomultipliers) per well, which is 0.3 seconds in our experiments. Estimating an overall window of two seconds per plate (0.3 seconds read +  $\approx 1.7$  seconds to switch to next plate), 1800 96-well plates can be read per hour giving rise to  $\approx 170,000$  data points / hour and  $\approx 4$  million data points / day.

Overall, these data show that conformational biosensors already provide high data throughput under automated conditions in 96-well format. Further increase of the throughput and reduction of expenditure (especially for microtiter plates, Nluc substrate, HaloTag dye) can be achieved through optimization of the promising 384-well plate protocol (**Figure 3.22**) and subsequent assay miniaturization to 1536-well format.

#### 4.5.3. GPCR<sub>Nluc/Halo(618)</sub> biosensors display low false positive rates

Another important characteristic of HTS assays concerns their reliability in detecting compounds acting through the target of interest. In an ideal GPCR conformation assay, all hits generated in the screen are truly targeting the GPCR of interest (zero false positives) and no compound of the tested library engaging the receptor is missed in the hit list (zero false negatives).

A large number of false positive screening hits poses a serious problem in HTS programs because these erroneous results demand on subsequent secondary assays to verify the hits from the primary screen. The more false positives are reported in the first screen, the more compounds need to be counter-screened causing high expenditures, as well as time exposure.

To estimate the false positive rate of the conformational GPCR<sub>Nluc/Halo(618)</sub> assay, we tested a set of 54 structurally and pharmacologically diverse compounds that have not been reported to bind to wildtype  $\alpha_2AAR$  in the  $\alpha_2AAR_{Nluc/Halo(618)}$  assay (**Figure 3.23**). Four ligands (formoterol, diltiazem, forskolin, digitonin) induced a BRET response outside the mean buffer  $\pm 3 \times$  standard deviation window which is usually considered as a cutoff for hit identification in HTS (Malo et al., 2006) giving rise to a false positive rate of  $\approx 7 \%$  (**Figure 4.4**). This is well below the range of a TrFRET based assay for nuclear receptor recruitment (21 – 32 %) (Zhang et al., 2005).

Formoterol is an agonist at  $\beta_2AR$  and constitutes the same chemical scaffold like norepinephrine (phenol,  $\beta$ -hydroxy group, basic amine; **Figure 4.4**). Although we could not find any reports for formoterol affinity towards  $\alpha_2AAR$ , it is likely that its  $\Delta$ BRET response at  $\alpha_2AAR_{Nluc/Halo(618)}$  presents true partial agonism ( $-4.08 \pm 0.35 \%$ , for comparison true weak  $\alpha_2AAR$  partial agonist octopamine:  $-5.78 \pm 0.10 \%$ ). Similarly, the calcium-channel blocker Diltiazem shares some structural similarities with typical adrenergic compounds (basic amine,  $\beta$ -hydroxyl group after ester-bond cleavage) that could trigger affinity towards  $\alpha_2AAR$  (**Figure 4.4**).

Interestingly, forskolin and digitonin evoked very prominent BRET signals similar (forskolin) or even more than three-fold higher (digitonin) than the  $\alpha_2AAR$  full agonist norepinephrine. Both compounds are reported to integrate in the plasma membrane where they can create holes or interact with other membrane components. Additionally, digitonin is a well-established detergent used to solubilize purified GPCRs. Thus, digitonin might also solubilize  $\alpha_2AAR_{Nluc/Halo(618)}$  leading to micelles in which the biosensors folds in distinct conformations. In more general terms, there is a variety of different biochemical and biophysical (e.g. quenching of the donor and / or acceptor emission) mechanisms that could cause the observed  $\Delta$ BRET response induced by non-orthosteric GPCR ligands like digitonin or forskolin, for instance.

We are aware of the limited validity of the small compound library tested for false positive assessment. However, many of the chemicals tested are known to engage GPCRs other than  $\alpha_2AAR$  and might therefore constitute a representative subset of a GPCR compound library. The false positive rate of less than 10 % presents an excellent property of GPCR<sub>Nluc/Halo(618)</sub> biosensors. We hypothesize that the low rate of false positives relies on the proximal nature of this readout solely capturing the effects at the receptor level. In contrast, cAMP and other downstream assays also detect intracellular responses that are independent from the GPCR of interest and originate from the activation of other cellular receptors.

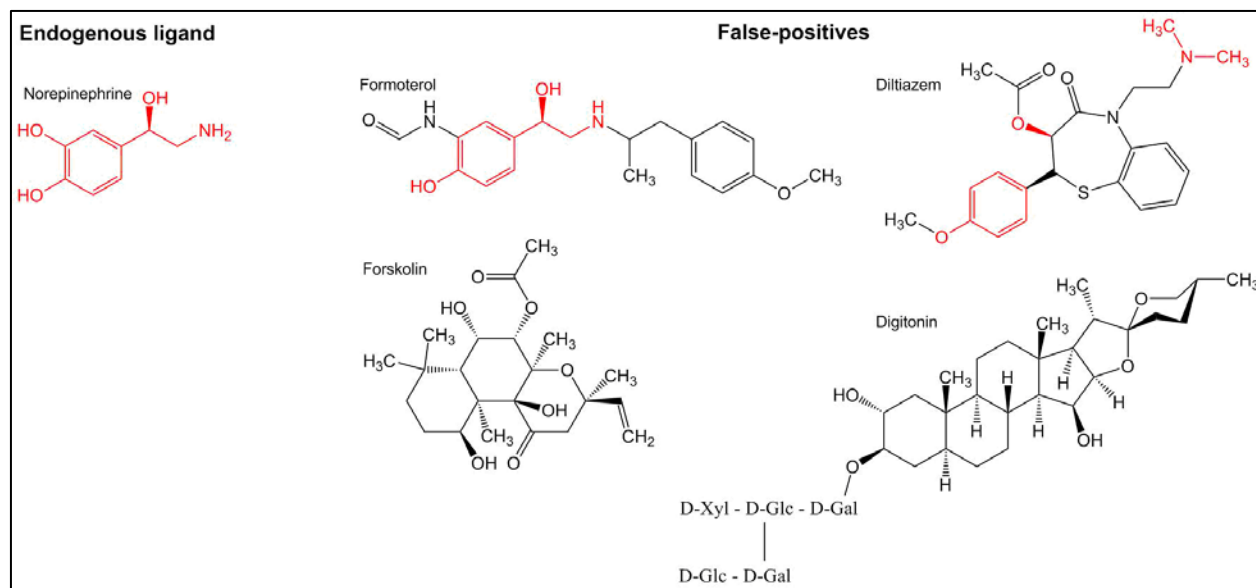


**Figure 4.4: Chemical structures of false positive hits in  $\alpha_2AAR_{Nluc/Halo(618)}$  assay.**

The structures of the endogenous  $\alpha_2AAR$  ligand norepinephrine and the four false positives formoterol, diltiazem, forskolin and digitonin are depicted. Important structural characteristics of norepinephrine for binding to  $\alpha_2AAR$  are highlighted in red: Catechol hydroxyl group,  $\beta$ -hydroxyl group, basic amine. D-Xyl denotes for D-xylose, D-Glc for D-glucose and D-Gal for D-galactose.

#### 4.5.4. False negative hits of $GPCR_{Nluc/Halo(618)}$ biosensors

As described previously, false negatives are the compounds that are indistinguishable from the negative control although they truly act through the target of interest. Six of 36 GPCR ligands tested in the course of this study did not directly (i.e. when applied to basal-state receptor sensors) evoke significant BRET responses although they are reported to bind the cognate wildtype GPCR (dopamine at  $\alpha_2AAR_{Nluc/Halo(618)}$ , carvedilol and labetalol at  $\beta_2AR_{Nluc/Halo(618)}$  and three PTHR1 antagonists at  $PTHR1_{Nluc/Halo(618)}$ ). We explain this lack of signal with the stabilization of the basal GPCR sensor conformation and this number gives rise to a false negative rate of  $\approx 17\%$ , well within the range of obtained with other RET-based assays (Zhang et al., 2005). However, to classify these six compounds as false negatives, data showing that these compounds do neither induce BRET responses when the biosensors start from a different conformation (e.g. after prestimulation with agonists) are required. We have conducted such experiments only for the PTHR1 ligand (dW)-PTH(7-34) (**Figure 3.18**) and these data showed that (dW)-PTH(7-34) can be classified as an PTHR1 ligand using the  $PTHR1_{Nluc/Halo(618)}$  biosensor. Thus, the rate of 6/36 (17%) mentioned above is most likely overestimating the false negative rate of the conformational BRET assay and underestimating the power of these  $GPCR_{Nluc/Halo(618)}$  biosensors to identify true ligands of the parent GPCRs.

Keeping the false negative rate as low as possible is a major goal in assay development since every false negative compound might represent a potential drug candidate that could fetch billions of USD for the company but is not entering subsequent phases of drug discovery and thus, never entering the healthcare market. In general, proximal readouts like the receptor conformation assay presented here should display significantly less false negative hits compared to downstream assays like cAMP or  $Ca^{2+}$  because these methods are prone to miss biased ligands. For future screening campaigns utilizing  $GPCR_{Nluc/Halo(618)}$  biosensors however, we would strongly recommend to determine the constitutive activity of the sensor and estimate the sensors basal conformation. This information would aid the estimation of possible false negative results: if the sensor's constitutive activity is high, it very likely adopts a preactive basal conformation. Thus, the risk to falsely consider ligands full or strong partial agonists as negative compounds is high but in turn, the probability of false negative antagonists are significantly decreased. Depending on the desired pharmacological profile of targeted compounds, the constitutive activity of the GPCR sensor can be manipulated by introduction of activating or inactivating mutations (e.g. mutation of the highly conserved DRY-motif in GPCRs confers constitutive activity) to reduce the false negative rate of the assay (Rovati et al., 2007).

#### 4.6. GPCR<sub>Nluc/Halo(618)</sub> represent reliable tools to study receptor modulators

With the example of RAMP-GPCR interaction, we demonstrate that herein developed BRET-based conformational GPCR sensors can be applied to investigate the role of modulatory proteins on structural dynamics of G-protein-coupled receptors.

In detail, GPCR sensors provided insights into receptor modulation through (i) mechanical stress (Chachisvilis et al., 2006), (ii) synthetic allosteric / dualsteric ligands (Bock et al., 2012; Maier-Peuschel et al., 2010), (iii) altering membrane potential (Rinne et al., 2013) or association with (iv) other GPCRs (Szalai et al., 2012; Vilaradaga et al., 2008), (v) G proteins, (vi)  $\beta$ -arrestins (Picard et al., 2018; Tateyama and Kubo, 2013a; Tateyama and Kubo, 2013b) or (vii) enzymes like carboxypeptidase M (Zhang et al., 2011a; Zhang et al., 2013b). We aimed to explore whether such modulatory processes can be investigated in microtiter plate format using the herein developed GPCR<sub>Nluc/Halo(618)</sub> sensor design. Therefore, we selected the proposed interaction of PTHR1 with receptor activity-modifying protein 2 (RAMP2) which relies on the finding that PTHR1 co-expression translocates fluorescently labeled RAMP2 to the plasma membrane and elevates total RAMP2 levels (Christopoulos et al., 2003).

We found that co-expression of RAMP2 desensitizes the class B GPCR to respond to agonist PTH(1-34) stimulation (**Figure 3.30**). Since control of total and surface PTHR1 sensor expression displayed no dependence on RAMP co-expression, we suppose a specific RAMP2-PTH1 interaction as a plausible mechanism to explain the right-shift of the EC<sub>50</sub>. To elucidate such mechanisms, subsequent deeper investigations are required. Yet, we hypothesize two different scenarios that may work independently or converge to evoke observed receptor desensitization:

1) RAMP2 could interact with PTHR1 in a way that favors a specific receptor conformation displaying decreased affinity towards agonist binding. The fact that both complexes, RAMP2-GPCR and PTH(1-34)-PTH1 are postulated to rely on interfaces involving extracellular regions argues for this concept (Archbold et al., 2011; Castro et al., 2005). Ligand binding experiments in the presence and absence of RAMP2 combined to site-directed mutagenesis of RAMP's and PTHR1's extracellular domains could help to challenge this hypothesis.

2) Secondly, RAMP2 could act as a connector between two or more PTHR1 entities. The desensitization effect could then result from agonist-binding to one protomer and subsequent inactivation of the other(s) mediated by RAMP2 (**Figure 4.5**). A similar process, although with the opposite outcome, has been reported for the metabotropic  $\gamma$ -amino-n-butyric acid type B receptor (GABA<sub>B</sub>). This receptor presents a constitutive heterodimer composed of the heptahelical subunits GB1 and GB2. Only GB1 is capable of ligand engagement and displays increased affinity towards agonist binding when coupled to GB2. On the other hand, solely GB2 is able to promote downstream signaling upon transactivation by agonist-bound GB1 (Galvez et al., 2001). The relevance of this concept for the PTHR1-RAMP2 complex could be tested by co-expression of binding-deficient PTHR1<sub>Nluc/Halo(618)</sub> along with wildtype PTHR1 (without BRET components) and RAMP2.

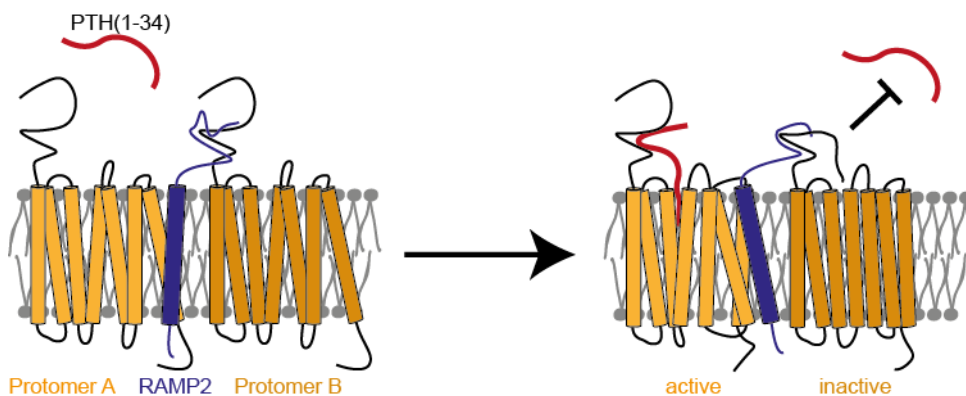


**Figure 4.5: Concept of RAMP-mediated GPCR trans-inactivation.**

Two PTHR1 protomers connected via RAMP2 constitute a functional entity. Upon agonist binding to one protomer, RAMP2 mediates inactivation of the second protomer.

Taken together, we show that the readout of GPCR<sub>Nluc/Halo(618)</sub> conformational dynamics provides an excellent approach to study the effects and mechanisms of GPCR partnering biomolecules. Such studies can aid future identification of new drug targets and fasten the development of novel classes of therapeutics. The investigation of PTHR1 interaction with RAMP2 elicits decreased sensitivity of the class B receptor to undergo agonist-induced conformational reorganization. However, further experiments are necessary to understand the mechanism and (patho-)physiological consequences of this cooperation of two distinct membrane proteins.

#### 4.7. Conclusion

This work describes the first validation of a universal BRET-based conformational GPCR sensor design to study ligand efficacy and potency in real-time and living cells in a high-throughput screening-compatible assay format. We demonstrate the universal applicability of this BRET pair by developing Nluc/Halo(618)-based biosensors for six distinct GPCRs and monitor ligand-induced structural reorganization of these receptors upon ligand binding. Thus far, no attempt to create a novel GPCR sensor based on Nluc/Halo(618) has failed and among the six biosensors developed in the course of this study, CXCR4<sub>Nluc/Halo(618)</sub> and S1PR1<sub>Nluc/Halo(618)</sub> represent the first RET conformational biosensors for these GPCRs. GPCR<sub>Nluc/Halo(618)</sub> biosensors simultaneously report ligand efficacies and potencies, provide excellent signal quality and data throughput for application in HTS and present low false positive and false negative rates. With next-generation plate readers that allow for simultaneous luminescence readout and ligand injection, these biosensors have the potential to further provide kinetic information on GPCR activation and deactivation kinetics. Ultimately, we illustrate that GPCR<sub>Nluc/Halo(618)</sub> biosensors can be used to study the mechanism of GPCR interaction with endogenous modulators such as receptor-activity modifying proteins.

#### 4.8. Outlook

The key development presented in this work is the refinement of the previously established principle of RET-based conformational GPCR sensors to allow for application in high-throughput programs. This feature lifts the GPCR-RET technique on a higher, drug discovery-tailored level.

Capturing ligand effects at the receptor level constitutes the most direct way to detect novel GPCR targeting compounds. Thus, employment of conformational GPCR sensors in drug discovery campaigns should provide a more reliable readout and lead to the identification of new, previously missed, active chemicals and boost their transition from fundamental studies to clinical trials. Moreover, if future plate reader generations allow for simultaneous BRET readout and ligand injection, these biosensors can additionally be used for kinetic GPCR activation / deactivation studies and therefore facilitate high-content, rather than solely high-throughput screening. This temporal information will deepen our understanding of differential ligand-GPCR interactions and give rise to novel types of GPCR therapeutics.

It is very compelling to apply this technique to GPCRs whose activation mechanisms are less understood or show unique features as for instance the fascinating class of adhesion and frizzled GPCRs. Thus far, no conformational biosensors exist for any of these GPCRs and studying their structural dynamics in a HTS-manner could help understanding their unique roles as cellular receptors and open new avenues for the treatment of diverse pathological conditions.

Furthermore, quantifying ligand effects directly at the receptor level represents a great progress for future GPCR de-orphanization programs. The downstream signaling cascades of many orphan GPCRs are yet unknown representing a significant obstacle for the selection of appropriate assays to identify their endogenous ligands. Establishing conformational biosensors of these receptors for use in high-throughput formats will remedy this issue and fasten the identification of endogenous and synthetic ligands for orphan GPCRs.

Ultimately, high-throughput investigation of GPCR dynamics and their modulation through endogenous biomolecules like membrane proteins or lipids can aid the establishment of novel targets for therapeutic interventions. RAMPs represent such potential drug targets. For instance, pharmacological stabilization or disruption of the desensitized RAMP2-PTHR1 complex could open the avenue for new osteo-anabolic compounds for the treatment of bone disorders.



## 5. Summary

G-protein-coupled receptors (GPCRs) comprise the largest family of membrane-embedded proteins and regulate a diverse array of physiological processes in eukaryotic cells to control various cell functions in the human body. They represent the cellular surface receptors for different kinds of extracellular stimuli including photons, small chemical entities, peptides and lipids. Binding of these different ligands to their cognate receptor stabilizes distinct GPCR conformations that in turn initiate intracellular signalling cascades, most prominently through their canonical effector partners the membrane-anchored G proteins. While endogenous agonists initiate receptor downstream signalling, other endogenous biomolecules including lipids, ions or further membrane-embedded proteins can modulate the function of GPCRs and, in consequence, their downstream effects.

Owing to their immense significance for numerous physiological and pathophysiological processes, GPCRs have always been a major target class for the treatment of various diseases. Today, about 30% of all approved pharmaceuticals exert their action through GPCRs. However, their great potential as targets for medical interventions is not fully exploited. In fact, more than 200 of all non-olfactory GPCRs are not yet addressed by therapeutic drugs since very sparse information is available about their pharmacology and physiological implications. Another factor slowing down GPCR drug discovery refers to the methods employed to identify novel GPCR-targeting compounds. All these approaches either capture the ligand-binding event without providing any information on the ligands' efficacies or monitor rather downstream signalling events such as fluctuating concentrations of second-messengers (mainly cAMP and Ca<sup>2+</sup>) or reporter gene expression. However, also downstream assays suffer from considerable downsides such as increased risk of false negative screening results due to biased signalling profiles of tested compounds.

Conformational GPCR biosensors based on fluorescence resonance energy transfer (FRET) have been used since the early 2000s to study ligand-induced receptor dynamics. This technology offers the most direct way to quantify both, ligand efficacy and potency. However, all FRET and BRET (bioluminescence resonance energy transfer) biosensors so far have failed to display sufficient signal quality to be implemented in high-throughput screening (HTS) campaigns.

This work presents the first GPCR biosensor design that achieves excellent signal amplitude qualifying this approach for HTS. We evaluated 21 different FRET and BRET  $\alpha_{2A}$ -adrenergic receptor ( $\alpha_{2A}$ AR) biosensors and identified the combination of the small and bright luciferase NanoLuciferase (Nluc) with the red-fluorescent HaloTag dye 618 as the most sensitive reporter system. The  $\alpha_{2A}$ AR<sub>Nluc/Halo(618)</sub> biosensor reliably reports ligand efficacy and potency in a microtiter plate format. To confirm the universal applicability of this design, we validated five analogous Nluc/Halo(618)-based biosensors for different GPCR classes and show that these GPCR-fusion proteins are capable of promoting their cognate signalling pathways. We further demonstrate that GPCR<sub>Nluc/Halo(618)</sub> biosensors represent excellent tools to monitor ligand-induced receptor conformational dynamics in a high-throughput format and can be used to study interaction mechanisms of GPCRs with endogenous receptor modulators.

Taken together, we developed the first HTS-compatible assay for the study of GPCR dynamics. These biosensors reveal the ligands' pharmacological profiles directly at the receptor level and are therefore independent from signal amplification, biased signalling or crosstalk between different signalling cascades – factors compromising other GPCR screening tools. This technique can aid future GPCR-targeted drug discovery programs, deepen our understanding of yet untargeted receptors including orphan GPCRs and contribute to the characterization of GPCR modulators as potential drug targets.

## 6. Zusammenfassung

Die Klasse der G-protein-gekoppelten Rezeptoren (GPCRs) stellt die größte Familie membranständiger Proteine dar. GPCRs regulieren eine Vielzahl diverser physiologischer Prozesse in eukaryotischen Zellen und kontrollieren so unterschiedliche Zellfunktionen im menschlichen Organismus. Sie stellen die Zelloberflächenrezeptoren für verschiedenartige extrazelluläre Stimuli, wie zum Beispiel Photonen, niedermolekulare chemische Verbindungen, Peptide und Lipide dar. Die Wechselwirkung mit diesen sogenannten Liganden stabilisiert spezifische GPCR-Konformationen. Diese dienen wiederum als Ausgangspunkt für nachgeschaltete intrazelluläre Signalkaskaden, die beispielweise über membranverankerte G-Proteine vermittelt werden können. Während endogene GPCR-Agonisten diese Signalweiterleitung verstärken, können andere Biomoleküle wie Lipide, Ionen oder andersartige Membranproteine die Funktion, und damit die Signalweiterleitung der GPCRs modulieren.

Aufgrund ihrer Einbindung in eine Vielzahl physiologischer und pathophysiologischer Prozesse, wurden GPCRs schon früh als Angriffspunkte („Targets“) zur Behandlung verschiedener Erkrankungen erforscht und genutzt. Heutzutage vermitteln etwa 30% aller zugelassenen Arzneistoffe ihre Wirkung über G-protein-gekoppelte Rezeptoren. Dennoch wird das große Potential dieser Rezeptorfamilie als Targets für medikamentöse Behandlungen noch nicht in vollem Umfang ausgeschöpft. Tatsächlich gibt es für mehr als 200 GPCRs, die nicht der olfaktorischen Wahrnehmung dienen, noch keine Arzneistoffe, da wenig über deren Pharmakologie und physiologische Bedeutung bekannt ist. Zudem wird die Entwicklung neuartiger GPCR-Liganden erheblich durch das eingeschränkte Methodenrepertoire beeinträchtigt. Alle derzeit etablierten Techniken zur Identifizierung neuer GPCR-Liganden erfassen entweder den Ligand-GPCR-Bindungsprozess, der keine Informationen über die tatsächliche Aktivität der Verbindung liefert, oder messen weit-nachgeschaltete Signale, wie Änderungen sogenannter „Second-Messenger“-Konzentrationen (meist cAMP oder Calcium) und Reporter-Gen-Expressionslevel. Aufgrund ihrer Entfernung vom eigentlichen Rezeptor-Aktivierungsprozess haben diese Methoden allerdings bedeutende Nachteile und produzieren so häufig Falsch-Positive und Falsch-Negative Ergebnisse.

Seit den frühen 2000er wurden GPCR-Konformationssensoren auf Basis von Fluoreszenz-Resonanz-Energie-Transfer (FRET) zur Messung der Ligand-induzierten Rezeptordynamik genutzt. Jedoch wies keiner der bisher entwickelten FRET- oder BRET- (Biolumineszenz-Resonanz-Energie-Transfer) Sensoren ausreichende Signalstärke auf, um im Hochdurchsatz-Screening (HTS) angewendet werden zu können.

Die vorliegende Studie beschreibt das erste GPCR-Sensordesign, das aufgrund seiner exzellenten Signalstärke im Hochdurchsatz-Verfahren verwendet werden kann. Wir haben 21 unterschiedliche FRET- und BRET-Sensoren des  $\alpha_{2A}$ -adrenergen Rezeptors ( $\alpha_{2A}$ AR) getestet und dabei die Kombination der kleinen und hellen Luziferase NanoLuciferase (Nluc) mit dem rot-fluoreszierenden HaloTag-Farbstoff 618 als sensitivstes RET-Paar identifiziert. Der  $\alpha_{2A}$ AR<sup>Nluc/Halo(618)</sup> Biosensor ermöglicht die Messung der Aktivität und Wirkstärke von  $\alpha_{2A}$ AR-Liganden im Mikrotiterplattenformat. Um die universelle Anwendbarkeit dieses Sensordesigns zu prüfen, wurden fünf weitere Nluc/Halo(618)-basierende Sensoren für GPCRs unterschiedlicher Unterfamilien entwickelt. Zudem konnten wir zeigen, dass diese GPCR<sup>Nluc/Halo(618)</sup>-Fusionsproteine weiterhin ihre natürlichen Signalkaskaden in Gang setzen können und damit die biologische Funktionalität dieser Rezeptoren erhalten ist. Außerdem belegt die vorliegende Arbeit, dass diese neue Sensor-Generation zur Messung Ligand-vermittelter Rezeptordynamiken im Hochdurchsatz-Format und zur Untersuchung der GPCR-Regulation durch endogene Modulatoren genutzt werden kann.

Zusammenfassend kann gesagt werden, dass wir den ersten HTS-kompatiblen Assay zur Messung der GPCR-Konformationsänderungen entwickelt haben. Diese Biosensoren erlauben die Charakterisierung neuartiger GPCR-Liganden direkt auf der Rezeptorebene und funktionieren damit unabhängig von nachgeschalteter Signalamplifikation oder Überlagerung verschiedener Signalwege, welche die Aussagekraft traditioneller GPCR-Screening-Verfahren häufig beeinträchtigen. Diese Technik kann zur Entdeckung neuartiger GPCR-Arzneistoffe genutzt werden, zu einem besseren Verständnis bisher kaum erforschter Rezeptoren beitragen und der Identifizierung und Charakterisierung potentieller GPCR-Modulatoren dienen.

## 7. Annex

**Table 7.1: Resolved structures of GPCRs.**

(as of April 4<sup>th</sup>, 2018) Taken from <http://gpcrdb.org/> (Pandy-Szekeres et al., 2018)

GPCR family	Receptor	Number of unique structures	PDB code
Class A	5-hydroxytryptamine 5-HT <sub>1B</sub> receptor	3	5V54, 4IAQ, 4IAR
	5-hydroxytryptamine 5-HT <sub>2B</sub> receptor	4	5TUD, 5TVN, 4NC3, 4IB4
	5-hydroxytryptamine 5-HT <sub>2C</sub> receptor	2	6BQG, 6BQH
	Adenosine A <sub>1</sub> receptor	2	5N2S, 5UEN
	Adenosine A <sub>2A</sub> receptor	44	5WF5, 5WF6, 5OM4, 5OLZ, 5OM1, 5OLG, 5OLV, 5OLO, 5OLH, 6AQF, 5VRA, 5NM2, 5NM4, 5NLX, 5N2R, 5MZP, 5MZJ, 5JTB, 5UUI, 5UIG, 5K2A, 5K2B, 5K2D, 5K2C, 5G53, 5IU4, 5IUB, 5IU7, 5IUA, 5IU8, 4UG2, 4UHR, 4EIY, 3UZA, 3UZC, 3VGA, 3VG9, 3PWH, 3RFM, 3REY, 2YDO, 2YDV, 3QAK, 3EML
	Apelin receptor	1	5VBL
	Angiotensin AT <sub>1</sub> receptor	2	4ZUD, 4YAY
	Angiotensin AT <sub>2</sub> receptor	3	5UNH, 5UNG, 5UNF
	Leukotriene BLT <sub>1</sub> receptor	1	5X33
	Complement peptide receptor C5a <sub>1</sub>	1	5O9H
	Cannabinoid CB <sub>1</sub> receptor	4	5XRA, 5XR8, 5U09, 5TGZ
	Chemokine CCR2 receptor	1	5T1A
	Chemokine CCR5 receptor	2	5UIW, 4MBS
	Chemokine CCR9 receptor	1	5LWE
	Chemokine CXCR4 receptor	6	4RWS, 3OE9, 3ODU, 3OE8, 3OE0, 3OE6
	Dopamine D <sub>2</sub> receptor	1	6CM4
	Dopamine D <sub>3</sub> receptor	1	3PBL
	Dopamine D <sub>4</sub> receptor	2	5WIU, 5WIV
	Endothelin ET <sub>B</sub> receptor	4	5XPR, 5X93, 5GLI, 5GLH
	Free Fatty acid FFA1 receptor	3	5TZR, 5TZY, 4PHU
	Histamine H <sub>1</sub> receptor	1	3RZE
	Lysophospholipid LPA <sub>1</sub> receptor	3	4Z34, 4Z35, 4Z36
	Lysophospholipid LPA <sub>6</sub> receptor	1	4XSZ
	Muscarinic Acetylcholine M <sub>1</sub> receptor	1	5CXV
	Muscarinic Acetylcholine M <sub>2</sub> receptor	3	4MQT, 4MQS, 3UON
	Muscarinic Acetylcholine M <sub>3</sub> receptor	4	4U14, 4U16, 4U15, 4DAJ
	Muscarinic Acetylcholine M <sub>4</sub> receptor	1	5DSG

GPCR family	Receptor	Number of unique structures	PDB code
	NOP opioid receptor	3	5DHG, 5DHH, 4EA3
	Neurotensin NTS <sub>1</sub> receptor	8	5TO4, 4XES, 4XEE, 4BUO, 4BVO, 3ZEV, 4BWB, 4GRV
	Orexin OX <sub>1</sub> receptor	2	4ZJC, 4ZJ8
	Orexin OX <sub>2</sub> receptor	3	5WS3, 5WQC, 4S0V
	P2Y <sub>1</sub> receptor	2	4XNW, 4XNV
	P2Y <sub>12</sub> receptor	3	4PY0, 4PXZ, 4NTJ
	Proteinase-activated PAR1 receptor	1	3VW7
	Proteinase-activated PAR2 receptor	2	5NDZ, 5NJ6, 5NDD
	Rhodopsin	46	6FK9, 6FK8, 6FKD, 6FKC, 6FK6, 6FKB, 6FKA, 5WKT, 5W0P, 5TE3, 5TE5, 5EN0, 5DYS, 5DGY, 4X1H, 4ZWJ, 4WW3, 4PXF, 4J4Q, 4BEY, 4BEZ, 4A4M, 3AYM, 3AYN, 2X72, 3PQR, 3PXO, 3OAX, 3DQB, 3C9M, 3C9L, 3CAP, 2T73, 2ZIY, 2PED, 2J4Y, 2I35, 2I36, 2I37, 2G87, 2HPY, 1U19, 1GZM, 1L9H, 1HZX, 1F88
	Lysophospholipid S1PR1 receptor	2	3V2W, 3V2Y
	US28	2	4XT3, 4XT1
	β <sub>1</sub> -adrenergic receptor	18	5F8U, 5A8E, 4BVN, 3ZPQ, 3ZPR, 4GPO, 4AMI, 4AMJ, 2YCY, 2YCX, 2Y CZ, 2YCW, 2Y01, 2Y03, 2Y00, 2Y02, 2Y04, 2VT4
	β <sub>1</sub> -adrenergic receptor	21	5X7D, 5D6L, 5JQH, 5D5B, 5D5A, 4QKX, 4LDO, 4LDL, 4LDE, 4GBR, 3SN6, 3P0G, 3PDS, 3NY8, 3NYA, 3NY9, 3KJ6, 3D4S, 2R4S, 2R4R, 2RH1
	δ-opioid receptor	4	4RWa, 4RWD, 4N6H, 4EJ4
κ-opioid receptor	2	6B73, 4DJH	
μ-opioid receptor	2	5C1M, 4DKL	
Class B	Corticotropin-releasing factor CRF <sub>1</sub> receptor	2	4Z9G, 4K5Y
	Calcitonin receptor	1	4UZ7
	Glucagon-like peptide GLP-1 receptor	5	6B3J, 5NX2, 5VEW, 5VAI, 5VEX
	Glucagon receptor	5	5YQZ, 5XF1, 5XEZ, 5EE7, 4L6R
Class C	Metabotropic glutamate mGlu <sub>1</sub> receptor	1	4OR2
	Metabotropic glutamate mGlu <sub>5</sub> receptor	5	6FFH, 6FFI, 5CGD, 5CGC, 4O09
Class F	SMO	9	5V56, 5V57, 5L7D, 5L7I, 4QIM, 4QIN, 4Q9R, 4N4W, 4JKV

**Table 7.2: GPCR-RAMP interactions.**  
Adapted from (Hay and Pioszak, 2016)

GPCR	Interacting RAMP	Reference(s)
GPR30	RAMP3	(Lenhart et al., 2013)
Calcitonin-like receptor	RAMP1-3	(Dackor et al., 2007; Gibbons et al., 2007; Poyner et al., 2002; Zhang et al., 2007)
Calcitonin receptor	RAMP1-3	(Poyner et al., 2002; Zhang et al., 2011b)
PTHr1	RAMP2	(Christopoulos et al., 2003)
PTHr2	RAMP3	(Christopoulos et al., 2003)
Vasoactive intestinal peptide/pituitary adenylate cyclase-activating peptide receptor 1 (VPAC <sub>1</sub> )	RAMP1-3	(Christopoulos et al., 2003)
Vasoactive intestinal peptide/pituitary adenylate cyclase-activating peptide receptor 2 (VPAC <sub>2</sub> )	RAMP1-3	(Wootten et al., 2013b)
CRF <sub>1</sub>	RAMP2	(Muller et al., 2007; Wootten et al., 2013a)
Glucagon receptor	RAMP2	(Christopoulos et al., 2003)
Secretin receptor	RAMP3	(Harikumar et al., 2009)
Calcium-sensing receptor	RAMP1, RAMP3	(Bouschet et al., 2005; Desai et al., 2014)

**Table 7.3: RET-based GPCR conformational biosensors.**

GPCR subtype	RET donor/acceptor pairs	Reference(s)
Parathyroid hormone receptor 1	CFP/YFP, Nluc/Halo(618)	(Schihada et al., 2018; Vilardaga et al., 2003)
$\alpha_2A$ -adrenergic receptor	CFP/YFP, CFP/FIAsH, CFP/cpVenus <sup>173</sup> , CFP/Halo(diAcFAM), CFP/Halo(Oregon Green), CFP/Halo(R110), CFP/Halo(TMRDirect), CFP/Halo(618), CFP/SNAP(505-star), CFP/SNAP(TMR-star), CFP/SNAP(647SiR), Nluc/cpVenus <sup>173</sup> , Nluc/TagRFP, Nluc/mCherry, Nluc/Halo(diAcFAM), Nluc/Halo(Oregon Green), Nluc/Halo(R110), Nluc/Halo(TMRDirect), Nluc/Halo(618), Nluc/SNAP(505-star), Nluc/SNAP(TMR-star), Nluc/SNAP(647SiR),	(Ambrosio and Lohse, 2012; Nikolaev et al., 2006; Rinne et al., 2013; Schihada et al., 2018; Vilardaga et al., 2003; Vilardaga et al., 2008; Vilardaga et al., 2005; Zurn et al., 2009)
Metabotropic glutamate mGlu <sub>1</sub> receptor	CFP/YFP	(Hlavackova et al., 2012; Tateyama et al., 2004)
Adenosine A <sub>2A</sub> receptor	CFP/YFP, CFP/FIAsH, FIAsH/ReAsH	(Fernandez-Duenas et al., 2014; Hoffmann et al., 2005; Zurn et al., 2010)
Bradykinin B <sub>2</sub> receptor	CFP/YFP	(Chachisvilis et al., 2006)
Bradykinin B <sub>1</sub> receptor	CFP/FIAsH	(Zhang et al., 2011a; Zhang et al., 2013b)
$\beta_2$ -adrenergic receptor	CFP/YFP, CFP/FIAsH, Rluc/FIAsH, Nluc/GFP10, Nluc/YFP, Nluc/Halo(618)	(Ahles et al., 2011; Bourque et al., 2017; Nakanishi et al., 2006; Picard et al., 2018; Reiner et al., 2010; Schihada et al., 2018)
$\beta_1$ -adrenergic receptor	CFP/YFP	(Ahles et al., 2015; Bornholz et al., 2013; Rochais et al., 2007)
Muscarinic Acetylcholine receptor M <sub>1</sub>	CFP/YFP, CFP/FIAsH, Cerulean/YFP	(Chang and Ross, 2012; Jensen et al., 2009; Markovic et al., 2012; Tateyama and Kubo, 2013b; Ziegler et al., 2011)
Muscarinic Acetylcholine receptor M <sub>2</sub>	CFP/FIAsH	(Bock et al., 2012; Maier-Peuschel et al., 2010)
Muscarinic Acetylcholine receptor M <sub>3</sub>	CFP/YFP, CFP/FIAsH	(Alvarez-Curto et al., 2011; Tateyama and Kubo, 2013a; Ziegler et al., 2011)
Muscarinic Acetylcholine receptor M <sub>5</sub>	CFP/FIAsH	(Ziegler et al., 2011)
GABA <sub>B</sub> receptor	Cerulean/YFP	(Matsushita et al., 2010)
5-hydroxytryptamine 5-HT <sub>1B</sub> receptor	Cerulean/Citrine	(Candelario, 2012)
5-hydroxytryptamine 5-HT <sub>2A</sub> receptor	Rluc/FIAsH	(Powlowski, 2018)
Histamine H <sub>3</sub> receptor	CFP/YFP	(Liu et al., 2018b)
Angiotensin-II-type 1 receptor	Rluc/YFP, Rluc/FIAsH	(Devost et al., 2017; Szalai et al., 2012)
Vasopressin V <sub>2</sub> receptor	Lumi-4 Tb/FIAsH	(Rahmeh et al., 2012)
Orexin OX <sub>1</sub> receptor	CFP/FIAsH	(Xu et al., 2012)
Orexin OX <sub>2</sub> receptor	CFP/FIAsH	(Xu et al., 2012)
P2Y <sub>1</sub> receptor	CFP/YFP	(Tateyama and Kubo, 2013a)
Ghrelin receptor	Lumi-4 Tb/AlexaFluor488 (through uAA)	(Damian et al., 2015)
Prostaglandin F <sub>2</sub> $\alpha$ receptor	Rluc/FIAsH	(Sleno et al., 2016)
Cannabinoid CB <sub>1</sub> receptor	CFP/YFP	(Liu et al., 2018a)

**Table 7.4: Pharmacological classification of GPCR ligands applied in this study.**

\*: IUPHAR ligand classification database: <http://www.guidetopharmacology.org/>

Harding SD, Sharman JL, Faccenda E, Southan C, Pawson AJ, Ireland S, Gray AJG, Bruce L, Alexander SPH, Anderton S, Bryant C, Davenport AP, Doerig C, Fabbro D, Levi-Schaffer F, Spedding M, Davies JA; NC-IUPHAR. (2018) **The IUPHAR/BPS Guide to PHARMACOLOGY in 2018: updates and expansion to encompass the new guide to IMMUNOPHARMACOLOGY.** *Nucl. Acids Res.* **46** (Issue D1): D1091-D1106. doi: 10.1093/nar/gkx1121.

Target	Ligand	Activity	Reference*
$\alpha_2$ AR	(-)-Epinephrine	Full agonist	IUPHAR
	(-)-Norepinephrine	Full agonist	IUPHAR
	UK 14,304	Full agonist / Partial agonist	IUPHAR / (Sungkaworn et al., 2017)
	Dopamine	Partial agonist	(Peltonen et al., 2003)
	Oxymetazoline	Partial agonist	IUPHAR
	Octopamine	Partial agonist	(Peltonen et al., 2003)
	Clonidine	Partial agonist	IUPHAR
	Phentolamine	Antagonist	IUPHAR
	Tyramine	Antagonist	(Nikolaev et al., 2006)
	Yohimbine	Antagonist / Inverse agonist	IUPHAR / (Wade et al., 2001)
$\beta_2$ AR	(-)-Epinephrine	Full agonist	IUPHAR
	Isoprenaline	Full agonist	IUPHAR
	Salmeterol	Full Agonist	IUPHAR
	Formoterol	Agonist	IUPHAR
	(-)-Norepinephrine	Agonist	IUPHAR
	Terbutaline	Partial agonist	IUPHAR
	Salbutamol	Partial agonist	IUPHAR
	Labetalol	Antagonist / Partial agonist	IUPHAR / (van der Westhuizen et al., 2014)
	Carvedilol	Antagonist / Partial agonist	IUPHAR / (van der Westhuizen et al., 2014)
	Metoprolol	Antagonist	IUPHAR
	Propranolol	Antagonist	IUPHAR
ICI 118,551	Inverse agonist	IUPHAR	
PTHr1	PTH(1-34)	Full agonist	(Gardella et al., 1996)
	PTHrP(1-34)	Full agonist	(Gardella et al., 1995)
	PTH(1-31)	Agonist	(Appleton et al., 2013)
	(dW)-PTH(7-34)	Antagonist	IUPHAR
	PTH(7-34)	Antagonist	(Appleton et al., 2013)
	PTH(3-34)	Antagonist	(Appleton et al., 2013)
AT1R	Angiotensin-II	Full agonist	IUPHAR
	Losartan	Antagonist	IUPHAR
CXCR4	CXCL12	Full agonist	IUPHAR
	AMD3100	Antagonist / partial agonist	(Hatse et al., 2002) / (Zhang et al., 2002)
	AMD3465	Antagonist / partial agonist	(Bodart et al., 2009) / (Yang et al., 2007)
	TC14012	Antagonist	(Burger et al., 2005)
	IT1t	Antagonist	IUPHAR
S1PR1	Sphingosin-1-phosphate	Full agonist	IUPHAR

## 8. Abbreviations

<b><math>\alpha_{2A}</math>AR:</b>	$\alpha_{2A}$ -adrenergic receptor
<b><math>\beta_1</math>AR:</b>	$\beta_1$ -adrenergic receptor
<b><math>\beta_2</math>AR:</b>	$\beta_2$ -adrenergic receptor
<b>A<sub>2A</sub>AR:</b>	Adenosine A <sub>2A</sub> receptor
<b>AC:</b>	Adenylyl cylcase
<b>AGT:</b>	O <sup>6</sup> -alkylguanine-DNA alkyltransferase
<b>AHK:</b>	$\alpha$ -helical domain
<b>AIDS:</b>	Acquired Immunodeficiency Syndrom
<b>AP2:</b>	Clathrin adaptor protein 2
<b>apRET:</b>	Acceptor photobleaching RET
<b>AT1R:</b>	Angiotensin-II-receptor subtype 1
<b>ATP:</b>	Adenosine triphosphate
<b>BC:</b>	O <sup>6</sup> -benzylcytosine
<b>BG:</b>	O <sup>6</sup> -benzylguanine
<b>BRET:</b>	Bioluminescence resonance energy transfer
<b>cAMP:</b>	Cyclic adenosine monophosphate
<b>CaSR:</b>	Calcium-sensing receptor
<b>CB1:</b>	Cannabinoid receptor 1
<b>CCR5:</b>	Chemokine CCR5 receptor
<b>CFP:</b>	Cyan fluorescent protein
<b>CLR:</b>	Calcitonin-like receptor
<b>CRE:</b>	cAMP response element
<b>CXCR4:</b>	Chemokine CXCR4 receptor
<b>CyOFP:</b>	Cyan-excitabile orange fluorescent protein
<b>DAG:</b>	Diacylglycerol
<b>DhaA:</b>	Haloalkane dehalogenase
<b>DMEM:</b>	Dulbecco's modified Eagle's medium
<b>DPBS:</b>	Dulbecco's phosphate buffered saline
<b>EC<sub>50</sub>:</b>	Half maximal effective concentration
<b>ecl:</b>	Extracellular loop
<b>EDT:</b>	Ethan-dithiol
<b>EGFP:</b>	Enhanced green fluorescent protein
<b>EMA:</b>	European Medicines Agency (European health agency)
<b>EPAC:</b>	Exchange protein directly activated by cAMP
<b>ER:</b>	Endoplasmic reticulum
<b>ERK:</b>	Extracellular-signal regulated kinase



<b>FCS:</b>	Fetal calf serum
<b>FDA:</b>	Food and Drug Administration (US health agency)
<b>FIAsH:</b>	Fluorescence-Arsenical-Hairpin-binder
<b>FLIM:</b>	Fluorescence lifetime imaging
<b>Fluc:</b>	Firefly luciferase
<b>FP:</b>	Fluorescent protein
<b>FRET:</b>	Fluorescence resonance energy transfer
<b>FZD:</b>	Frizzled/Taste2 receptor
<b>GABA<sub>B</sub>:</b>	$\gamma$ -aminobutyric acid receptor B
<b>GAIN-domain:</b>	GPCR autoproteolysis-inducing domain
<b>GAP:</b>	GTPase activating protein
<b>GDP:</b>	Guanosine diphosphate
<b>GFP:</b>	Green fluorescent protein
<b>GIRK:</b>	G-protein-coupled inwardly rectifying potassium channel
<b>Gluc:</b>	Gaussia luciferase
<b>GPCR:</b>	G-protein-coupled receptor
<b>GRK:</b>	G-protein-coupled receptor kinase
<b>HEK:</b>	Human embryonic kidney
<b>HOMO:</b>	Highest occupied molecular orbital
<b>HTS:</b>	High-throughput screening
<b>IC<sub>50</sub>:</b>	Half maximal inhibitory concentration
<b>icl:</b>	Intracellular loop
<b>k<sub>d</sub>:</b>	Dissociation constant
<b>k<sub>i</sub>:</b>	Inhibitory constant
<b>IP<sub>3</sub>:</b>	Inositol-1,4,5-trisphosphat
<b>LB:</b>	Lysogeny broth
<b>LSSmOrange:</b>	Large-Stokes-Shift monomeric orange fluorescent protein
<b>LUMO:</b>	Lowest unoccupied molecular orbital
<b>mAChR:</b>	Muscarinic acetylcholine receptor
<b>MCR2:</b>	Melanocortin receptor 2
<b>MD:</b>	Molecular dynamics
<b>MOR:</b>	$\mu$ -opioid receptor
<b>mTq2:</b>	mTurquoise2
<b>mYFP:</b>	Monomeric yellow fluorescent protein
<b>NAM:</b>	Negative allosteric modulator
<b>Nluc:</b>	Nanoluciferase
<b>NMR:</b>	Nuclear magnetic resonance
<b>Oluc:</b>	Oplophorus luciferase

<b>PAM:</b>	Positive allosteric modulator
<b>PAR<sub>1</sub>:</b>	Proteinase-activated receptor 1
<b>PCR:</b>	Polymerase-chain-reaction
<b>PGFR:</b>	Prostaglandin F <sub>2α</sub> receptor
<b>PIP<sub>2</sub>:</b>	Phosphatidylinositol-4,5-bisphosphate
<b>PLCβ:</b>	Phospholipase C
<b>PKA:</b>	Protein kinase A
<b>PKC:</b>	Protein kinase C
<b>PTH:</b>	Parathyroid hormone
<b>PTH<sub>R</sub>1:</b>	Parathyroid hormone receptor 1
<b>prRET:</b>	Polarization resolved RET
<b>QSAR:</b>	Quantitative structure activity relationship
<b>RAMP:</b>	Receptor activity-modifying protein
<b>ReAsH:</b>	Resorufin-Arsenical-Hairpin-binder
<b>RET:</b>	Resonance energy transfer
<b>RGS:</b>	Regulator of G protein signaling
<b>RhoGEF:</b>	Rho guanine nucleotide exchange factor
<b>Rluc:</b>	Renilla luciferase
<b>RWG:</b>	Resonant waveguide grating
<b>S1P:</b>	Sphingosine-1-phosphate
<b>S1P<sub>R</sub>1:</b>	Sphingosine-1-phosphate receptor 1
<b>seRET:</b>	Sensitized emission RET
<b>siRET:</b>	Spectral imaging RET
<b>TAE:</b>	Tris acetate buffer
<b>TBS:</b>	Tris buffered saline
<b>TEV:</b>	Tobacco etch virus
<b>TIRF:</b>	Total internal reflection fluorescence
<b>TrFRET:</b>	Time-resolved FRET
<b>TM:</b>	Transmembrane domain
<b>TSHR:</b>	Thyroid stimulating hormone receptor
<b>uAA:</b>	Unnatural amino acid
<b>YFP:</b>	Yellow fluorescent protein

## 9. References

- Abbe E (1873) Beitrage zur Theorie des Mikroskops und der mikroskopischen Wahrnehmung, in *Arch Mikroskop Anat* pp 413–420.
- Acharya C, Coop A, Polli JE and Mackerell AD, Jr. (2011) Recent advances in ligand-based drug design: relevance and utility of the conformationally sampled pharmacophore approach. *Curr Comput Aided Drug Des* **7**(1): 10-22.
- Adjobo-Hermans MJ, Goedhart J, van Weeren L, Nijmeijer S, Manders EM, Offermanns S and Gadella TW, Jr. (2011) Real-time visualization of heterotrimeric G protein Gq activation in living cells. *BMC Biol* **9**: 32.
- Agnati LF, Ferre S, Genedani S, Leo G, Guidolin D, Filaferro M, Carriba P, Casado V, Lluís C, Franco R, Woods AS and Fuxe K (2006) Allosteric modulation of dopamine D2 receptors by homocysteine. *J Proteome Res* **5**(11): 3077-3083.
- Agnetta L, Kauk M, Canizal MCA, Messerer R, Holzgrabe U, Hoffmann C and Decker M (2017) A Photoswitchable Dualsteric Ligand Controlling Receptor Efficacy. *Angew Chem Int Ed Engl* **56**(25): 7282-7287.
- Ahles A, Rochais F, Frambach T, Bunemann M and Engelhardt S (2011) A polymorphism-specific "memory" mechanism in the beta(2)-adrenergic receptor. *Sci Signal* **4**(185): ra53.
- Ahles A, Rodewald F, Rochais F, Bunemann M and Engelhardt S (2015) Interhelical interaction and receptor phosphorylation regulate the activation kinetics of different human beta1-adrenoceptor variants. *The Journal of biological chemistry* **290**(3): 1760-1769.
- Alvarez-Curto E, Prihandoko R, Tautermann CS, Zwier JM, Padiani JD, Lohse MJ, Hoffmann C, Tobin AB and Milligan G (2011) Developing chemical genetic approaches to explore G protein-coupled receptor function: validation of the use of a receptor activated solely by synthetic ligand (RASSL). *Molecular pharmacology* **80**(6): 1033-1046.
- Ambrosio M and Lohse MJ (2012) Nonequilibrium activation of a G-protein-coupled receptor. *Molecular pharmacology* **81**(6): 770-777.
- Andrisani OM (1999) CREB-mediated transcriptional control. *Crit Rev Eukaryot Gene Expr* **9**(1): 19-32.
- Angers S, Salahpour A, Joly E, Hilairat S, Chelsky D, Dennis M and Bouvier M (2000) Detection of beta 2-adrenergic receptor dimerization in living cells using bioluminescence resonance energy transfer (BRET). *Proceedings of the National Academy of Sciences of the United States of America* **97**(7): 3684-3689.
- Aparoy P, Reddy KK and Reddanna P (2012) Structure and ligand based drug design strategies in the development of novel 5- LOX inhibitors. *Curr Med Chem* **19**(22): 3763-3778.
- Aper SJA, Dierickx P and Merckx M (2016) Dual Readout BRET/FRET Sensors for Measuring Intracellular Zinc. *ACS chemical biology* **11**(10): 2854-2864.
- Appleton KM, Lee MH, Alele C, Alele C, Luttrell DK, Peterson YK, Morinelli TA and Luttrell LM (2013) Biasing the parathyroid hormone receptor: relating in vitro ligand efficacy to in vivo biological activity. *Methods Enzymol* **522**: 229-262.
- Arac D, Boucard AA, Bolliger MF, Nguyen J, Soltis SM, Sudhof TC and Brunger AT (2012) A novel evolutionarily conserved domain of cell-adhesion GPCRs mediates autoproteolysis. *EMBO J* **31**(6): 1364-1378.
- Archbold JK, Flanagan JU, Watkins HA, Gingell JJ and Hay DL (2011) Structural insights into RAMP modification of secretin family G protein-coupled receptors: implications for drug development. *Trends Pharmacol Sci* **32**(10): 591-600.
- Attramadal H, Arriza JL, Aoki C, Dawson TM, Codina J, Kwatra MM, Snyder SH, Caron MG and Lefkowitz RJ (1992) Beta-arrestin2, a novel member of the arrestin/beta-arrestin gene family. *The Journal of biological chemistry* **267**(25): 17882-17890.

- Attwood TK and Findlay JB (1994) Fingerprinting G-protein-coupled receptors. *Protein Eng* **7**(2): 195-203.
- Aubin JE (1979) Autofluorescence of viable cultured mammalian cells. *J Histochem Cytochem* **27**(1): 36-43.
- Aubry L, Guetta D and Klein G (2009) The arrestin fold: variations on a theme. *Curr Genomics* **10**(2): 133-142.
- Avci P, Gupta A, Sadasivam M, Vecchio D, Pam Z, Pam N and Hamblin MR (2013) Low-level laser (light) therapy (LLLT) in skin: stimulating, healing, restoring. *Semin Cutan Med Surg* **32**(1): 41-52.
- Avlani VA, Ma W, Mun HC, Leach K, Delbridge L, Christopoulos A and Conigrave AD (2013) Calcium-sensing receptor-dependent activation of CREB phosphorylation in HEK293 cells and human parathyroid cells. *Am J Physiol Endocrinol Metab* **304**(10): E1097-1104.
- Bader AN, Hoetzel S, Hofman EG, Voortman J, van Bergen en Henegouwen PM, van Meer G and Gerritsen HC (2011) Homo-FRET imaging as a tool to quantify protein and lipid clustering. *Chemphyschem* **12**(3): 475-483.
- Bajar BT, Wang ES, Zhang S, Lin MZ and Chu J (2016) A Guide to Fluorescent Protein FRET Pairs. *Sensors (Basel)* **16**(9).
- Ballesteros JA, Jensen AD, Liapakis G, Rasmussen SG, Shi L, Gether U and Javitch JA (2001) Activation of the beta 2-adrenergic receptor involves disruption of an ionic lock between the cytoplasmic ends of transmembrane segments 3 and 6. *The Journal of biological chemistry* **276**(31): 29171-29177.
- Barbash S, Lorenzen E, Persson T, Huber T and Sakmar TP (2017) GPCRs globally coevolved with receptor activity-modifying proteins, RAMPs. *Proceedings of the National Academy of Sciences of the United States of America* **114**(45): 12015-12020.
- Barnea G, Strapps W, Herrada G, Berman Y, Ong J, Kloss B, Axel R and Lee KJ (2008) The genetic design of signaling cascades to record receptor activation. *Proceedings of the National Academy of Sciences of the United States of America* **105**(1): 64-69.
- Baud V, Chisoe SL, Viegas-Pequignot E, Diriong S, N'Guyen VC, Roe BA and Lipinski M (1995) EMR1, an unusual member in the family of hormone receptors with seven transmembrane segments. *Genomics* **26**(2): 334-344.
- Bazin H, Trinquet E and Mathis G (2002) Time resolved amplification of cryptate emission: a versatile technology to trace biomolecular interactions. *J Biotechnol* **82**(3): 233-250.
- Beardsley K and Cantor CR (1970) Studies of transfer RNA tertiary structure by singlet-singlet energy transfer. *Proceedings of the National Academy of Sciences of the United States of America* **65**(1): 39-46.
- Becker W (2012) Fluorescence lifetime imaging--techniques and applications. *J Microsc* **247**(2): 119-136.
- Benovic JL, Kuhn H, Weyand I, Codina J, Caron MG and Lefkowitz RJ (1987) Functional desensitization of the isolated beta-adrenergic receptor by the beta-adrenergic receptor kinase: potential role of an analog of the retinal protein arrestin (48-kDa protein). *Proceedings of the National Academy of Sciences of the United States of America* **84**(24): 8879-8882.
- Berridge MJ (1993) Inositol trisphosphate and calcium signalling. *Nature* **361**(6410): 315-325.
- Berthouze M, Venkataramanan V, Li Y and Shenoy SK (2009) The deubiquitinases USP33 and USP20 coordinate beta2 adrenergic receptor recycling and resensitization. *EMBO J* **28**(12): 1684-1696.
- Bertrand L, Parent S, Caron M, Legault M, Joly E, Angers S, Bouvier M, Brown M, Houle B and Menard L (2002) The BRET2/arrestin assay in stable recombinant cells: a platform to screen for compounds that interact with G protein-coupled receptors (GPCRs). *J Recept Signal Transduct Res* **22**(1-4): 533-541.
- Bhuiyan MA SM, Nagatomo T (2013) Binding Affinity of Candesartan, Losartan, Telmisartan and Valsartan with Angiotensin II Receptor 1 Subtype, in *Bangladesh Pharmaceutical Journal* pp 10-14.

- Bock A, Merten N, Schrage R, Dallanocce C, Batz J, Klockner J, Schmitz J, Matera C, Simon K, Kebig A, Peters L, Muller A, Schrobang-Ley J, Trankle C, Hoffmann C, De Amici M, Holzgrabe U, Kostenis E and Mohr K (2012) The allosteric vestibule of a seven transmembrane helical receptor controls G-protein coupling. *Nature communications* **3**: 1044.
- Bock A, Schrage R and Mohr K (2017) Allosteric modulators targeting CNS muscarinic receptors. *Neuropharmacology*.
- Bodart V, Anastassov V, Darkes MC, Idzan SR, Labrecque J, Lau G, Mosi RM, Neff KS, Nelson KL, Ruzek MC, Patel K, Santucci Z, Scarborough R, Wong RS, Bridger GJ, Macfarland RT and Fricker SP (2009) Pharmacology of AMD3465: a small molecule antagonist of the chemokine receptor CXCR4. *Biochem Pharmacol* **78**(8): 993-1000.
- Bohn LM, Gainetdinov RR, Lin FT, Lefkowitz RJ and Caron MG (2000) Mu-opioid receptor desensitization by beta-arrestin-2 determines morphine tolerance but not dependence. *Nature* **408**(6813): 720-723.
- Bornholz B, Weidtkamp-Peters S, Schmitmeier S, Seidel CA, Herda LR, Felix SB, Lemoine H, Hescheler J, Nguemo F, Schafer C, Christensen MO, Mielke C and Boege F (2013) Impact of human autoantibodies on beta1-adrenergic receptor conformation, activity, and internalization. *Cardiovasc Res* **97**(3): 472-480.
- Bourque K, Petrin D, Sleno R, Devost D, Zhang A and Hebert TE (2017) Distinct Conformational Dynamics of Three G Protein-Coupled Receptors Measured Using FIAsh-BRET Biosensors. *Front Endocrinol (Lausanne)* **8**: 61.
- Bouschet T, Martin S and Henley JM (2005) Receptor-activity-modifying proteins are required for forward trafficking of the calcium-sensing receptor to the plasma membrane. *J Cell Sci* **118**(Pt 20): 4709-4720.
- Boute N, Jockers R and Issad T (2002) The use of resonance energy transfer in high-throughput screening: BRET versus FRET. *Trends Pharmacol Sci* **23**(8): 351-354.
- Bouvier M (2001) Oligomerization of G-protein-coupled transmitter receptors. *Nat Rev Neurosci* **2**(4): 274-286.
- Branchini BR, Southworth TL, Fontaine DM, Kohrt D, Florentine CM and Grossel MJ (2018) A Firefly Luciferase Dual Color Bioluminescence Reporter Assay Using Two Substrates To Simultaneously Monitor Two Gene Expression Events. *Sci Rep* **8**(1): 5990.
- Brandish PE, Hill LA, Zheng W and Scolnick EM (2003) Scintillation proximity assay of inositol phosphates in cell extracts: high-throughput measurement of G-protein-coupled receptor activation. *Analytical biochemistry* **313**(2): 311-318.
- Bunemann M, Frank M and Lohse MJ (2003) Gi protein activation in intact cells involves subunit rearrangement rather than dissociation. *Proceedings of the National Academy of Sciences of the United States of America* **100**(26): 16077-16082.
- Burd CG and Emr SD (1998) Phosphatidylinositol(3)-phosphate signaling mediated by specific binding to RING FYVE domains. *Mol Cell* **2**(1): 157-162.
- Burger M, Hartmann T, Krome M, Rawluk J, Tamamura H, Fujii N, Kipps TJ and Burger JA (2005) Small peptide inhibitors of the CXCR4 chemokine receptor (CD184) antagonize the activation, migration, and antiapoptotic responses of CXCL12 in chronic lymphocytic leukemia B cells. *Blood* **106**(5): 1824-1830.
- Butcher AJ, Prihandoko R, Kong KC, McWilliams P, Edwards JM, Bottrill A, Mistry S and Tobin AB (2011) Differential G-protein-coupled receptor phosphorylation provides evidence for a signaling bar code. *The Journal of biological chemistry* **286**(13): 11506-11518.
- Butcher RW, Ho RJ, Meng HC and Sutherland EW (1965) Adenosine 3',5'-monophosphate in biological materials. II. The measurement of adenosine 3',5'-monophosphate in tissues and the role of the cyclic nucleotide in the lipolytic response of fat to epinephrine. *The Journal of biological chemistry* **240**(11): 4515-4523.

- Bylund DB, Gerety ME, Happe HK and Murrin LC (2001) A robust GTP-induced shift in alpha(2)-adrenoceptor agonist affinity in tissue sections from rat brain. *J Neurosci Methods* **105**(2): 159-166.
- Cahill TJ, 3rd, Thomsen AR, Tarrasch JT, Plouffe B, Nguyen AH, Yang F, Huang LY, Kahsai AW, Bassoni DL, Gavino BJ, Lamerdin JE, Triest S, Shukla AK, Berger B, Little Jt, Antar A, Blanc A, Qu CX, Chen X, Kawakami K, Inoue A, Aoki J, Steyaert J, Sun JP, Bouvier M, Skiniotis G and Lefkowitz RJ (2017) Distinct conformations of GPCR-beta-arrestin complexes mediate desensitization, signaling, and endocytosis. *Proceedings of the National Academy of Sciences of the United States of America* **114**(10): 2562-2567.
- Calebiro D, Nikolaev VO, Gagliani MC, de Filippis T, Dees C, Tacchetti C, Persani L and Lohse MJ (2009) Persistent cAMP-signals triggered by internalized G-protein-coupled receptors. *PLoS Biol* **7**(8): e1000172.
- Candelario J and Chachisvilis M (2013) Real-time detection of G protein activation using monomolecular Ggamma FRET sensors. *J Recept Signal Transduct Res* **33**(1): 63-72.
- Candelario JC, M. (2012) Mechanical stress stimulates conformational changes in 5-hydroxytryptamine receptor 1B in bone cells. *Cell Mol Biol* **5**: 277-286.
- Carpenter B, Nehme R, Warne T, Leslie AG and Tate CG (2016) Structure of the adenosine A(2A) receptor bound to an engineered G protein. *Nature* **536**(7614): 104-107.
- Carpenter B and Tate CG (2017) Active state structures of G protein-coupled receptors highlight the similarities and differences in the G protein and arrestin coupling interfaces. *Curr Opin Struct Biol* **45**: 124-132.
- Castro M, Nikolaev VO, Palm D, Lohse MJ and Vilardaga JP (2005) Turn-on switch in parathyroid hormone receptor by a two-step parathyroid hormone binding mechanism. *Proceedings of the National Academy of Sciences of the United States of America* **102**(44): 16084-16089.
- Cayre F, Mura S, Andreiuk B, Sobot D, Gouazou S, Desmaele D, Klymchenko AS and Couvreur P (2018) In Vivo FRET Imaging to Predict the Risk Associated with Hepatic Accumulation of Squalene-Based Prodrug Nanoparticles. *Adv Healthc Mater* **7**(3).
- Chachisvilis M, Zhang YL and Frangos JA (2006) G protein-coupled receptors sense fluid shear stress in endothelial cells. *Proceedings of the National Academy of Sciences of the United States of America* **103**(42): 15463-15468.
- Chan YH, Wu C, Ye F, Jin Y, Smith PB and Chiu DT (2011) Development of ultrabright semiconducting polymer dots for ratiometric pH sensing. *Anal Chem* **83**(4): 1448-1455.
- Chang S and Ross EM (2012) Activation biosensor for G protein-coupled receptors: a FRET-based m1 muscarinic activation sensor that regulates G(q). *PLoS one* **7**(9): e45651.
- Charest PG, Terrillon S and Bouvier M (2005) Monitoring agonist-promoted conformational changes of beta-arrestin in living cells by intramolecular BRET. *EMBO Rep* **6**(4): 334-340.
- Chen H, Wang Z, Zong S, Chen P, Zhu D, Wu L and Cui Y (2015) A graphene quantum dot-based FRET system for nuclear-targeted and real-time monitoring of drug delivery. *Nanoscale* **7**(37): 15477-15486.
- Chen W, ten Berge D, Brown J, Ahn S, Hu LA, Miller WE, Caron MG, Barak LS, Nusse R and Lefkowitz RJ (2003) Dishevelled 2 recruits beta-arrestin 2 to mediate Wnt5A-stimulated endocytosis of Frizzled 4. *Science* **301**(5638): 1391-1394.
- Chen XT, Pitis P, Liu G, Yuan C, Gotchev D, Cowan CL, Rominger DH, Koblish M, Dewire SM, Crombie AL, Violin JD and Yamashita DS (2013) Structure-activity relationships and discovery of a G protein biased mu opioid receptor ligand, [(3-methoxythiophen-2-yl)methyl]({2-[(9R)-9-(pyridin-2-yl)-6-oxaspiro-[4.5]decan- 9-yl]ethyl})amine (TRV130), for the treatment of acute severe pain. *J Med Chem* **56**(20): 8019-8031.
- Cheng Z, Garvin D, Paguio A, Stecha P, Wood K and Fan F (2010) Luciferase Reporter Assay System for Deciphering GPCR Pathways. *Current chemical genomics* **4**: 84-91.

- Choe HW, Kim YJ, Park JH, Morizumi T, Pai EF, Krauss N, Hofmann KP, Scheerer P and Ernst OP (2011) Crystal structure of metarhodopsin II. *Nature* **471**(7340): 651-655.
- Christopoulos A, Christopoulos G, Morfis M, Udawela M, Laburthe M, Couvineau A, Kuwasako K, Tilakaratne N and Sexton PM (2003) Novel receptor partners and function of receptor activity-modifying proteins. *The Journal of biological chemistry* **278**(5): 3293-3297.
- Chu J, Oh Y, Sens A, Ataie N, Dana H, Macklin JJ, Laviv T, Welf ES, Dean KM, Zhang F, Kim BB, Tang CT, Hu M, Baird MA, Davidson MW, Kay MA, Fiolka R, Yasuda R, Kim DS, Ng HL and Lin MZ (2016) A bright cyan-excitable orange fluorescent protein facilitates dual-emission microscopy and enhances bioluminescence imaging in vivo. *Nature biotechnology* **34**(7): 760-767.
- Chun E, Thompson AA, Liu W, Roth CB, Griffith MT, Katritch V, Kunken J, Xu F, Cherezov V, Hanson MA and Stevens RC (2012) Fusion partner toolchest for the stabilization and crystallization of G protein-coupled receptors. *Structure* **20**(6): 967-976.
- Ciancetta A, Sabbadin D, Federico S, Spalluto G and Moro S (2015) Advances in Computational Techniques to Study GPCR-Ligand Recognition. *Trends Pharmacol Sci* **36**(12): 878-890.
- Clark AL and Mitchelson F (1976) The inhibitory effect of gallamine on muscarinic receptors. *Br J Pharmacol* **58**(3): 323-331.
- Clegg RM (1995) Fluorescence resonance energy transfer. *Curr Opin Biotechnol* **6**(1): 103-110.
- Conigrave AD, Quinn SJ and Brown EM (2000) L-amino acid sensing by the extracellular Ca<sup>2+</sup>-sensing receptor. *Proceedings of the National Academy of Sciences of the United States of America* **97**(9): 4814-4819.
- Conway BR and Demarest KT (2002) The use of biosensors to study GPCR function: applications for high-content screening. *Receptors Channels* **8**(5-6): 331-341.
- Cottet M, Albizu L, Comps-Agrar L, Trinquet E, Pin JP, Mouillac B and Durroux T (2011) Time resolved FRET strategy with fluorescent ligands to analyze receptor interactions in native tissues: application to GPCR oligomerization. *Methods Mol Biol* **746**: 373-387.
- Craft CM, Whitmore DH and Wiechmann AF (1994) Cone arrestin identified by targeting expression of a functional family. *The Journal of biological chemistry* **269**(6): 4613-4619.
- Cranfill PJ, Sell BR, Baird MA, Allen JR, Lavagnino Z, de Gruiter HM, Kremers GJ, Davidson MW, Ustione A and Piston DW (2016) Quantitative assessment of fluorescent proteins. *Nature methods* **13**(7): 557-562.
- Cunningham BT, Li P, Schulz S, Lin B, Baird C, Gerstenmaier J, Genick C, Wang F, Fine E and Laing L (2004) Label-free assays on the BIND system. *J Biomol Screen* **9**(6): 481-490.
- Dackor R, Fritz-Six K, Smithies O and Caron K (2007) Receptor activity-modifying proteins 2 and 3 have distinct physiological functions from embryogenesis to old age. *The Journal of biological chemistry* **282**(25): 18094-18099.
- Dacres H, Wang J, Dumancic MM and Trowell SC (2010) Experimental determination of the Forster distance for two commonly used bioluminescent resonance energy transfer pairs. *Anal Chem* **82**(1): 432-435.
- Damian M, Mary S, Maingot M, M'Kadmi C, Gagne D, Leyris JP, Denoyelle S, Gaibelet G, Gavara L, Garcia de Souza Costa M, Perahia D, Trinquet E, Mouillac B, Galandrin S, Gales C, Fehrentz JA, Floquet N, Martinez J, Marie J and Baneres JL (2015) Ghrelin receptor conformational dynamics regulate the transition from a preassembled to an active receptor:Gq complex. *Proceedings of the National Academy of Sciences of the United States of America* **112**(5): 1601-1606.
- Day RN and Davidson MW (2012) Fluorescent proteins for FRET microscopy: monitoring protein interactions in living cells. *Bioessays* **34**(5): 341-350.
- De Lean A, Stadel JM and Lefkowitz RJ (1980) A ternary complex model explains the agonist-specific binding properties of the adenylate cyclase-coupled beta-adrenergic receptor. *The Journal of biological chemistry* **255**(15): 7108-7117.

- Degorce F, Card A, Soh S, Trinquet E, Knapik GP and Xie B (2009) HTRF: A technology tailored for drug discovery - a review of theoretical aspects and recent applications. *Current chemical genomics* **3**: 22-32.
- DeGraff JL, Gurevich VV and Benovic JL (2002) The third intracellular loop of alpha 2-adrenergic receptors determines subtype specificity of arrestin interaction. *The Journal of biological chemistry* **277**(45): 43247-43252.
- Desai AJ, Roberts DJ, Richards GO and Skerry TM (2014) Role of receptor activity modifying protein 1 in function of the calcium sensing receptor in the human TT thyroid carcinoma cell line. *PLoS one* **9**(1): e85237.
- Devost D, Sleno R, Petrin D, Zhang A, Shinjo Y, Okde R, Aoki J, Inoue A and Hebert TE (2017) Conformational profiling of the AT1 angiotensin II receptor reflects biased agonism, G protein coupling and cellular context. *The Journal of biological chemistry*.
- DeVree BT, Mahoney JP, Velez-Ruiz GA, Rasmussen SG, Kuszak AJ, Edwald E, Fung JJ, Manglik A, Masureel M, Du Y, Matt RA, Pardon E, Steyaert J, Kobilka BK and Sunahara RK (2016) Allosteric coupling from G protein to the agonist-binding pocket in GPCRs. *Nature* **535**(7610): 182-186.
- DiRaddo JO, Miller EJ, Hathaway HA, Grajkowska E, Wroblewska B, Wolfe BB, Liotta DC and Wroblewski JT (2014) A real-time method for measuring cAMP production modulated by Galphai/o-coupled metabotropic glutamate receptors. *J Pharmacol Exp Ther* **349**(3): 373-382.
- Dorr P, Westby M, Dobbs S, Griffin P, Irvine B, Macartney M, Mori J, Rickett G, Smith-Burchnell C, Napier C, Webster R, Armour D, Price D, Stammen B, Wood A and Perros M (2005) Maraviroc (UK-427,857), a potent, orally bioavailable, and selective small-molecule inhibitor of chemokine receptor CCR5 with broad-spectrum anti-human immunodeficiency virus type 1 activity. *Antimicrob Agents Chemother* **49**(11): 4721-4732.
- Downes GB and Gautam N (1999) The G protein subunit gene families. *Genomics* **62**(3): 544-552.
- Eggeling C, Brand L, Ullmann D and Jager S (2003) Highly sensitive fluorescence detection technology currently available for HTS. *Drug Discov Today* **8**(14): 632-641.
- Eglen RM and Reisine T (2008) Photoproteins: important new tools in drug discovery. *Assay Drug Dev Technol* **6**(5): 659-671.
- Ellis J and Seidenberg M (1992) Two allosteric modulators interact at a common site on cardiac muscarinic receptors. *Molecular pharmacology* **42**(4): 638-641.
- Emami-Nemini A, Roux T, Leblay M, Bourrier E, Lamarque L, Trinquet E and Lohse MJ (2013) Time-resolved fluorescence ligand binding for G protein-coupled receptors. *Nature protocols* **8**(7): 1307-1320.
- Evanko DS and Haydon PG (2005) Elimination of environmental sensitivity in aameleon FRET-based calcium sensor via replacement of the acceptor with Venus. *Cell Calcium* **37**(4): 341-348.
- Evellin S, Mongillo M, Terrin A, Lissandron V and Zaccolo M (2004) Measuring dynamic changes in cAMP using fluorescence resonance energy transfer. *Methods Mol Biol* **284**: 259-270.
- Fan F and Wood KV (2007) Bioluminescent assays for high-throughput screening. *Assay Drug Dev Technol* **5**(1): 127-136.
- Fang Y, Li G and Ferrie AM (2007) Non-invasive optical biosensor for assaying endogenous G protein-coupled receptors in adherent cells. *J Pharmacol Toxicol Methods* **55**(3): 314-322.
- Ferguson SS, Zhang J, Barak LS and Caron MG (1998) Role of beta-arrestins in the intracellular trafficking of G-protein-coupled receptors. *Adv Pharmacol* **42**: 420-424.
- Fernandez-Duenas V, Gomez-Soler M, Lopez-Cano M, Taura JJ, Ledent C, Watanabe M, Jacobson KA, Vilardaga JP and Ciruela F (2014) Uncovering caffeine's adenosine A2A receptor inverse agonism in experimental parkinsonism. *ACS chemical biology* **9**(11): 2496-2501.



- Ferrandon S, Feinstein TN, Castro M, Wang B, Bouley R, Potts JT, Gardella TJ and Vilardaga JP (2009) Sustained cyclic AMP production by parathyroid hormone receptor endocytosis. *Nature chemical biology* **5**(10): 734-742.
- Ferrer M, Kolodin GD, Zuck P, Peltier R, Berry K, Mandala SM, Rosen H, Ota H, Ozaki S, Inglese J and Strulovici B (2003) A fully automated [<sup>35</sup>S]GTPγS scintillation proximity assay for the high-throughput screening of Gi-linked G protein-coupled receptors. *Assay Drug Dev Technol* **1**(2): 261-273.
- Fleissner MR, Brustad EM, Kalai T, Altenbach C, Cascio D, Peters FB, Hideg K, Peucker S, Schultz PG and Hubbell WL (2009) Site-directed spin labeling of a genetically encoded unnatural amino acid. *Proceedings of the National Academy of Sciences of the United States of America* **106**(51): 21637-21642.
- Flock T, Hauser AS, Lund N, Gloriam DE, Balaji S and Babu MM (2017) Selectivity determinants of GPCR-G-protein binding. *Nature* **545**(7654): 317-322.
- Forster T (1946) Energiewanderung Und Fluoreszenz. *Naturwissenschaften* **33**(6): 166-175.
- Foster DJ and Conn PJ (2017) Allosteric Modulation of GPCRs: New Insights and Potential Utility for Treatment of Schizophrenia and Other CNS Disorders. *Neuron* **94**(3): 431-446.
- Frang H, Mukkala VM, Syysto R, Ollikka P, Hurskainen P, Scheinin M and Hemmila I (2003) Nonradioactive GTP binding assay to monitor activation of g protein-coupled receptors. *Assay Drug Dev Technol* **1**(2): 275-280.
- Fredriksson R, Lagerstrom MC, Lundin LG and Schiöth HB (2003) The G-protein-coupled receptors in the human genome form five main families. Phylogenetic analysis, paralogon groups, and fingerprints. *Molecular pharmacology* **63**(6): 1256-1272.
- Fronik P, Gaiser BI and Sejer Pedersen D (2017) Bitopic Ligands and Metastable Binding Sites: Opportunities for G Protein-Coupled Receptor (GPCR) Medicinal Chemistry. *J Med Chem* **60**(10): 4126-4134.
- Funatogawa C, Szundi I and Kliger DS (2016) A Comparison between the Photoactivation Kinetics of Human and Bovine Rhodopsins. *Biochemistry* **55**(50): 7005-7013.
- Gales C, Rebois RV, Hogue M, Trieu P, Breit A, Hebert TE and Bouvier M (2005) Real-time monitoring of receptor and G-protein interactions in living cells. *Nature methods* **2**(3): 177-184.
- Gales C, Van Durm JJ, Schaak S, Pontier S, Percherancier Y, Audet M, Paris H and Bouvier M (2006) Probing the activation-promoted structural rearrangements in preassembled receptor-G protein complexes. *Nat Struct Mol Biol* **13**(9): 778-786.
- Galvez T, Duthey B, Kniazeff J, Blahos J, Rovelli G, Bettler B, Prezeau L and Pin JP (2001) Allosteric interactions between GB1 and GB2 subunits are required for optimal GABA(B) receptor function. *EMBO J* **20**(9): 2152-2159.
- Gao ZG and Jacobson KA (2013) Allosteric modulation and functional selectivity of G protein-coupled receptors. *Drug Discov Today Technol* **10**(2): e237-243.
- Gardella TJ, Luck MD, Jensen GS, Usdin TB and Juppner H (1996) Converting parathyroid hormone-related peptide (PTHrP) into a potent PTH-2 receptor agonist. *The Journal of biological chemistry* **271**(33): 19888-19893.
- Gardella TJ, Luck MD, Wilson AK, Keutmann HT, Nussbaum SR, Potts JT, Jr. and Kronenberg HM (1995) Parathyroid hormone (PTH)-PTH-related peptide hybrid peptides reveal functional interactions between the 1-14 and 15-34 domains of the ligand. *The Journal of biological chemistry* **270**(12): 6584-6588.
- Garippa RJ, Hoffman AF, Gradl G and Kirsch A (2006) High-throughput confocal microscopy for beta-arrestin-green fluorescent protein translocation G protein-coupled receptor assays using the Evotec Opera. *Methods Enzymol* **414**: 99-120.

- Gautier A, Juillerat A, Heinis C, Correa IR, Jr., Kindermann M, Beaufils F and Johnsson K (2008) An engineered protein tag for multiprotein labeling in living cells. *Chemistry & biology* **15**(2): 128-136.
- Giaever I and Keese CR (1984) Monitoring fibroblast behavior in tissue culture with an applied electric field. *Proceedings of the National Academy of Sciences of the United States of America* **81**(12): 3761-3764.
- Giaever I and Keese CR (1991) Micromotion of mammalian cells measured electrically. *Proceedings of the National Academy of Sciences of the United States of America* **88**(17): 7896-7900.
- Gibbons C, Dackor R, Dunworth W, Fritz-Six K and Caron KM (2007) Receptor activity-modifying proteins: RAMPing up adrenomedullin signaling. *Mol Endocrinol* **21**(4): 783-796.
- Gilman AG (1987) G proteins: transducers of receptor-generated signals. *Annu Rev Biochem* **56**: 615-649.
- Ginefra P, Filippi BGH, Donovan P, Bessonard S and Constam DB (2018) Compartment-Specific Biosensors Reveal a Complementary Subcellular Distribution of Bioactive Furin and PC7. *Cell Rep* **22**(8): 2176-2189.
- Glickman JF, Schmid A and Ferrand S (2008) Scintillation proximity assays in high-throughput screening. *Assay Drug Dev Technol* **6**(3): 433-455.
- Goedhart J, von Stetten D, Noirclerc-Savoye M, Lelimosin M, Joosen L, Hink MA, van Weeren L, Gadella TW, Jr. and Royant A (2012) Structure-guided evolution of cyan fluorescent proteins towards a quantum yield of 93%. *Nature communications* **3**: 751.
- Goodman OB, Jr., Krupnick JG, Santini F, Gurevich VV, Penn RB, Gagnon AW, Keen JH and Benovic JL (1996) Beta-arrestin acts as a clathrin adaptor in endocytosis of the beta2-adrenergic receptor. *Nature* **383**(6599): 447-450.
- Goodman OB, Jr., Krupnick JG, Santini F, Gurevich VV, Penn RB, Gagnon AW, Keen JH and Benovic JL (1998) Role of arrestins in G-protein-coupled receptor endocytosis. *Adv Pharmacol* **42**: 429-433.
- Goyet E, Bouquier N, Ollendorff V and Perroy J (2016) Fast and high resolution single-cell BRET imaging. *Sci Rep* **6**: 28231.
- Granier S, Kim S, Shafer AM, Ratnala VR, Fung JJ, Zare RN and Kobilka B (2007) Structure and conformational changes in the C-terminal domain of the beta2-adrenoceptor: insights from fluorescence resonance energy transfer studies. *The Journal of biological chemistry* **282**(18): 13895-13905.
- Gregorio GG, Masureel M, Hilger D, Terry DS, Juette M, Zhao H, Zhou Z, Perez-Aguilar JM, Hauge M, Mathiasen S, Javitch JA, Weinstein H, Kobilka BK and Blanchard SC (2017) Single-molecule analysis of ligand efficacy in beta2AR-G-protein activation. *Nature* **547**(7661): 68-73.
- Griesbeck O, Baird GS, Campbell RE, Zacharias DA and Tsien RY (2001) Reducing the environmental sensitivity of yellow fluorescent protein. Mechanism and applications. *The Journal of biological chemistry* **276**(31): 29188-29194.
- Griffin BA, Adams SR and Tsien RY (1998) Specific covalent labeling of recombinant protein molecules inside live cells. *Science* **281**(5374): 269-272.
- Groer CE, Tidgewell K, Moyer RA, Harding WW, Rothman RB, Prisinzano TE and Bohn LM (2007) An opioid agonist that does not induce mu-opioid receptor--arrestin interactions or receptor internalization. *Molecular pharmacology* **71**(2): 549-557.
- Haasen D, Schnapp A, Valler MJ and Heilker R (2006a) G protein-coupled receptor internalization assays in the high-content screening format. *Methods Enzymol* **414**: 121-139.
- Haasen D, Wolff M, Valler MJ and Heilker R (2006b) Comparison of G-protein coupled receptor desensitization-related beta-arrestin redistribution using confocal and non-confocal imaging. *Comb Chem High Throughput Screen* **9**(1): 37-47.
- Hall MP, Unch J, Binkowski BF, Valley MP, Butler BL, Wood MG, Otto P, Zimmerman K, Vidugiris G, Machleidt T, Robers MB, Benink HA, Eggers CT, Slater MR, Meisenheimer PL, Klaubert DH, Fan

- F, Encell LP and Wood KV (2012) Engineered Luciferase Reporter from a Deep Sea Shrimp Utilizing a Novel Imidazopyrazinone Substrate. *ACS chemical biology* **7**(11): 1848-1857.
- Hallis TM, Kopp AL, Gibson J, Lebakken CS, Hancock M, Van Den Heuvel-Kramer K and Turek-Etienne T (2007) An improved beta-lactamase reporter assay: multiplexing with a cytotoxicity readout for enhanced accuracy of hit identification. *J Biomol Screen* **12**(5): 635-644.
- Hamann J, Aust G, Arac D, Engel FB, Formstone C, Fredriksson R, Hall RA, Harty BL, Kirchhoff C, Knapp B, Krishnan A, Liebscher I, Lin HH, Martinelli DC, Monk KR, Peeters MC, Piao X, Promel S, Schoneberg T, Schwartz TW, Singer K, Stacey M, Ushkaryov YA, Vallon M, Wolfrum U, Wright MW, Xu L, Langenhan T and Schioth HB (2015) International Union of Basic and Clinical Pharmacology. XCIV. Adhesion G protein-coupled receptors. *Pharmacological reviews* **67**(2): 338-367.
- Hamann J, Eichler W, Hamann D, Kerstens HM, Poddighe PJ, Hoovers JM, Hartmann E, Strauss M and van Lier RA (1995) Expression cloning and chromosomal mapping of the leukocyte activation antigen CD97, a new seven-span transmembrane molecule of the secretion receptor superfamily with an unusual extracellular domain. *J Immunol* **155**(4): 1942-1950.
- Hammer MM, Wehrman TS and Blau HM (2007) A novel enzyme complementation-based assay for monitoring G-protein-coupled receptor internalization. *Faseb J* **21**(14): 3827-3834.
- Hanson BJ, Wetter J, Bercher MR, Kopp L, Fuerstenau-Sharp M, Vedvik KL, Zielinski T, Doucette C, Whitney PJ and Revankar C (2009) A homogeneous fluorescent live-cell assay for measuring 7-transmembrane receptor activity and agonist functional selectivity through beta-arrestin recruitment. *J Biomol Screen* **14**(7): 798-810.
- Hanyaloglu AC and von Zastrow M (2007) A novel sorting sequence in the beta2-adrenergic receptor switches recycling from default to the Hrs-dependent mechanism. *The Journal of biological chemistry* **282**(5): 3095-3104.
- Harding SD, Sharman JL, Faccenda E, Southan C, Pawson AJ, Ireland S, Gray AJG, Bruce L, Alexander SPH, Anderton S, Bryant C, Davenport AP, Doerig C, Fabbro D, Levi-Schaffer F, Spedding M, Davies JA and Nc I (2018) The IUPHAR/BPS Guide to PHARMACOLOGY in 2018: updates and expansion to encompass the new guide to IMMUNOPHARMACOLOGY. *Nucleic Acids Res* **46**(D1): D1091-D1106.
- Hargrave PA, McDowell JH, Curtis DR, Wang JK, Juszczak E, Fong SL, Rao JK and Argos P (1983) The structure of bovine rhodopsin. *Biophys Struct Mech* **9**(4): 235-244.
- Harikumar KG, Simms J, Christopoulos G, Sexton PM and Miller LJ (2009) Molecular basis of association of receptor activity-modifying protein 3 with the family B G protein-coupled secretin receptor. *Biochemistry* **48**(49): 11773-11785.
- Harvey CD, Ehrhardt AG, Cellurale C, Zhong H, Yasuda R, Davis RJ and Svoboda K (2008) A genetically encoded fluorescent sensor of ERK activity. *Proceedings of the National Academy of Sciences of the United States of America* **105**(49): 19264-19269.
- Hastings JW (1983) Biological diversity, chemical mechanisms, and the evolutionary origins of bioluminescent systems. *J Mol Evol* **19**(5): 309-321.
- Hatse S, Princen K, Bridger G, De Clercq E and Schols D (2002) Chemokine receptor inhibition by AMD3100 is strictly confined to CXCR4. *FEBS Lett* **527**(1-3): 255-262.
- Hatse S, Princen K, De Clercq E, Rosenkilde MM, Schwartz TW, Hernandez-Abad PE, Skerlj RT, Bridger GJ and Schols D (2005) AMD3465, a monomacrocyclic CXCR4 antagonist and potent HIV entry inhibitor. *Biochem Pharmacol* **70**(5): 752-761.
- Hauser AS, Attwood MM, Rask-Andersen M, Schioth HB and Gloriam DE (2017) Trends in GPCR drug discovery: new agents, targets and indications. *Nat Rev Drug Discov* **16**(12): 829-842.
- Hauwert NJ, Mocking TAM, Da Costa Pereira D, Kooistra AJ, Wijnen LM, Vreeker GCM, Verweij EWE, De Boer AH, Smit MJ, De Graaf C, Vischer HF, de Esch IJP, Wijtmans M and Leurs R (2018) Synthesis

- and Characterization of a Bidirectional Photoswitchable Antagonist Toolbox for Real-Time GPCR Photopharmacology. *Journal of the American Chemical Society* **140**(12): 4232-4243.
- Hay DL and Pioszak AA (2016) Receptor Activity-Modifying Proteins (RAMPs): New Insights and Roles. *Annu Rev Pharmacol Toxicol* **56**: 469-487.
- Heifetz A, James T, Morao I, Bodkin MJ and Biggin PC (2016) Guiding lead optimization with GPCR structure modeling and molecular dynamics. *Curr Opin Pharmacol* **30**: 14-21.
- Hein P, Frank M, Hoffmann C, Lohse MJ and Bunemann M (2005) Dynamics of receptor/G protein coupling in living cells. *EMBO J* **24**(23): 4106-4114.
- Hein P, Rochais F, Hoffmann C, Dorsch S, Nikolaev VO, Engelhardt S, Berlot CH, Lohse MJ and Bunemann M (2006) Gs activation is time-limiting in initiating receptor-mediated signaling. *The Journal of biological chemistry* **281**(44): 33345-33351.
- Hein P, MMC, Leineweber K., Wieland T., Wettschureck N., Offermanns S. (2005) Receptor and Binding Studies. *Springer, Berlin, Heidelberg*(Paractical Methods in Cardiovascular Research): 723-783.
- Held KD and Biaglow JE (1994) Mechanisms for the oxygen radical-mediated toxicity of various thiol-containing compounds in cultured mammalian cells. *Radiat Res* **139**(1): 15-23.
- Hicke L and Dunn R (2003) Regulation of membrane protein transport by ubiquitin and ubiquitin-binding proteins. *Annu Rev Cell Dev Biol* **19**: 141-172.
- Higashijima T, Ferguson KM, Sternweis PC, Smigel MD and Gilman AG (1987) Effects of Mg<sup>2+</sup> and the beta gamma-subunit complex on the interactions of guanine nucleotides with G proteins. *The Journal of biological chemistry* **262**(2): 762-766.
- Hilger D, Masureel M and Kobilka BK (2018) Structure and dynamics of GPCR signaling complexes. *Nat Struct Mol Biol* **25**(1): 4-12.
- Hill SJ, Williams C and May LT (2010) Insights into GPCR pharmacology from the measurement of changes in intracellular cyclic AMP; advantages and pitfalls of differing methodologies. *Br J Pharmacol* **161**(6): 1266-1275.
- Hirasawa A, Tsumaya K, Awaji T, Katsuma S, Adachi T, Yamada M, Sugimoto Y, Miyazaki S and Tsujimoto G (2005) Free fatty acids regulate gut incretin glucagon-like peptide-1 secretion through GPR120. *Nat Med* **11**(1): 90-94.
- Hislop JN and von Zastrow M (2011) Analysis of GPCR localization and trafficking. *Methods Mol Biol* **746**: 425-440.
- Hlavackova V, Zabel U, Frankova D, Batz J, Hoffmann C, Prezeau L, Pin JP, Blahos J and Lohse MJ (2012) Sequential inter- and intrasubunit rearrangements during activation of dimeric metabotropic glutamate receptor 1. *Sci Signal* **5**(237): ra59.
- Ho MK, Su Y, Yeung WW and Wong YH (2009) Regulation of transcription factors by heterotrimeric G proteins. *Curr Mol Pharmacol* **2**(1): 19-31.
- Hoffmann C, Castro M, Rinken A, Leurs R, Hill SJ and Vischer HF (2015) Ligand Residence Time at G-protein-Coupled Receptors-Why We Should Take Our Time To Study It. *Molecular pharmacology* **88**(3): 552-560.
- Hoffmann C, Gaietta G, Bunemann M, Adams SR, Oberdorff-Maass S, Behr B, Vilardaga JP, Tsien RY, Ellisman MH and Lohse MJ (2005) A FIAsh-based FRET approach to determine G protein-coupled receptor activation in living cells. *Nature methods* **2**(3): 171-176.
- Hoffmann C, Gaietta G, Zurn A, Adams SR, Terrillon S, Ellisman MH, Tsien RY and Lohse MJ (2010) Fluorescent labeling of tetracysteine-tagged proteins in intact cells. *Nature protocols* **5**(10): 1666-1677.
- Hoffmann C, Leitz MR, Oberdorf-Maass S, Lohse MJ and Klotz KN (2004) Comparative pharmacology of human beta-adrenergic receptor subtypes--characterization of stably transfected receptors in CHO cells. *Naunyn Schmiedebergs Arch Pharmacol* **369**(2): 151-159.

- Hofmann KP, Scheerer P, Hildebrand PW, Choe HW, Park JH, Heck M and Ernst OP (2009) A G protein-coupled receptor at work: the rhodopsin model. *Trends Biochem Sci* **34**(11): 540-552.
- Hollenstein K, de Graaf C, Bortolato A, Wang MW, Marshall FH and Stevens RC (2014) Insights into the structure of class B GPCRs. *Trends Pharmacol Sci* **35**(1): 12-22.
- Holloway AC, Qian H, Pipolo L, Ziogas J, Miura S, Karnik S, Southwell BR, Lew MJ and Thomas WG (2002) Side-chain substitutions within angiotensin II reveal different requirements for signaling, internalization, and phosphorylation of type 1A angiotensin receptors. *Molecular pharmacology* **61**(4): 768-777.
- Holzgrabe U and Decker M (2017) Bitopic muscarinic agonists and antagonists and uses thereof: a patent evaluation of US20160136145A1. *Expert Opin Ther Pat* **27**(2): 121-125.
- Huang G, Nimczick M and Decker M (2015a) Rational Modification of the Biological Profile of GPCR Ligands through Combination with Other Biologically Active Moieties. *Arch Pharm (Weinheim)* **348**(8): 531-540.
- Huang W, Manglik A, Venkatakrishnan AJ, Laeremans T, Feinberg EN, Sanborn AL, Kato HE, Livingston KE, Thorsen TS, Kling RC, Granier S, Gmeiner P, Husbands SM, Traynor JR, Weis WI, Steyaert J, Dror RO and Kobilka BK (2015b) Structural insights into micro-opioid receptor activation. *Nature* **524**(7565): 315-321.
- Ikeda Y, Kumagai H, Motozawa Y, Suzuki J and Komuro I (2015) Biased Agonism of the Angiotensin II Type I Receptor. *Int Heart J* **56**(5): 485-488.
- Irannejad R and von Zastrow M (2014) GPCR signaling along the endocytic pathway. *Curr Opin Cell Biol* **27**: 109-116.
- Isberg V, Mordalski S, Munk C, Rataj K, Harpsoe K, Hauser AS, Vroiling B, Bojarski AJ, Vriend G and Gloriam DE (2016) GPCRdb: an information system for G protein-coupled receptors. *Nucleic Acids Res* **44**(D1): D356-364.
- Italia JS, Zheng Y, Kelemen RE, Erickson SB, Addy PS and Chatterjee A (2017) Expanding the genetic code of mammalian cells. *Biochem Soc Trans* **45**(2): 555-562.
- Jaakola VP, Griffith MT, Hanson MA, Cherezov V, Chien EY, Lane JR, Ijzerman AP and Stevens RC (2008) The 2.6 angstrom crystal structure of a human A2A adenosine receptor bound to an antagonist. *Science* **322**(5905): 1211-1217.
- Jasper JR, Lesnick JD, Chang LK, Yamanishi SS, Chang TK, Hsu SA, Daunt DA, Bonhaus DW and Eglén RM (1998) Ligand efficacy and potency at recombinant alpha2 adrenergic receptors: agonist-mediated [<sup>35</sup>S]GTPgammaS binding. *Biochem Pharmacol* **55**(7): 1035-1043.
- Jensen JB, Lyssand JS, Hague C and Hille B (2009) Fluorescence changes reveal kinetic steps of muscarinic receptor-mediated modulation of phosphoinositides and Kv7.2/7.3 K<sup>+</sup> channels. *J Gen Physiol* **133**(4): 347-359.
- Johnson EN, Shi X, Cassaday J, Ferrer M, Strulovici B and Kunapuli P (2008) A 1,536-well [(35)S]GTPgammaS scintillation proximity binding assay for ultra-high-throughput screening of an orphan galphai-coupled GPCR. *Assay Drug Dev Technol* **6**(3): 327-337.
- Juillerat A, Gronemeyer T, Keppler A, Gendreizig S, Pick H, Vogel H and Johnsson K (2003) Directed evolution of O6-alkylguanine-DNA alkyltransferase for efficient labeling of fusion proteins with small molecules in vivo. *Chemistry & biology* **10**(4): 313-317.
- Kadmiel M, Matson BC, Espenschied ST, Lenhart PM and Caron KM (2017) Loss of receptor activity-modifying protein 2 in mice causes placental dysfunction and alters PTH1R regulation. *PLoS one* **12**(7): e0181597.
- Kaina B, Fritz G, Mitra S and Coquerelle T (1991) Transfection and expression of human O6-methylguanine-DNA methyltransferase (MGMT) cDNA in Chinese hamster cells: the role of MGMT in protection against the genotoxic effects of alkylating agents. *Carcinogenesis* **12**(10): 1857-1867.

- Kalef E and Gitler C (1994) Purification of vicinal dithiol-containing proteins by arsenical-based affinity chromatography. *Methods Enzymol* **233**: 395-403.
- Kang Y, Zhou XE, Gao X, He Y, Liu W, Ishchenko A, Barty A, White TA, Yefanov O, Han GW, Xu Q, de Waal PW, Ke J, Tan MH, Zhang C, Moeller A, West GM, Pascal BD, Van Eps N, Caro LN, Vishnivetskiy SA, Lee RJ, Suino-Powell KM, Gu X, Pal K, Ma J, Zhi X, Boutet S, Williams GJ, Messerschmidt M, Gati C, Zatsepin NA, Wang D, James D, Basu S, Roy-Chowdhury S, Conrad CE, Coe J, Liu H, Lisova S, Kupitz C, Grotjohann I, Fromme R, Jiang Y, Tan M, Yang H, Li J, Wang M, Zheng Z, Li D, Howe N, Zhao Y, Standfuss J, Diederichs K, Dong Y, Potter CS, Carragher B, Caffrey M, Jiang H, Chapman HN, Spence JC, Fromme P, Weierstall U, Ernst OP, Katritch V, Gurevich VV, Griffin PR, Hubbell WL, Stevens RC, Cherezov V, Melcher K and Xu HE (2015) Crystal structure of rhodopsin bound to arrestin by femtosecond X-ray laser. *Nature* **523**(7562): 561-567.
- Katanaev VL (2010) The Wnt/Frizzled GPCR signaling pathway. *Biochemistry (Mosc)* **75**(12): 1428-1434.
- Kauk M and Hoffmann C (2018) Intramolecular and Intermolecular FRET Sensors for GPCRs - Monitoring Conformational Changes and Beyond. *Trends Pharmacol Sci* **39**(2): 123-135.
- Keppler A, Kindermann M, Gendreizig S, Pick H, Vogel H and Johnsson K (2004) Labeling of fusion proteins of O6-alkylguanine-DNA alkyltransferase with small molecules in vivo and in vitro. *Methods* **32**(4): 437-444.
- Keseru GM and Makara GM (2006) Hit discovery and hit-to-lead approaches. *Drug Discov Today* **11**(15-16): 741-748.
- Khan SM, Sleno R, Gora S, Zylbergold P, Laverdure JP, Labbe JC, Miller GJ and Hebert TE (2013) The expanding roles of Gbetagamma subunits in G protein-coupled receptor signaling and drug action. *Pharmacological reviews* **65**(2): 545-577.
- Kimple AJ, Bosch DE, Giguere PM and Siderovski DP (2011) Regulators of G-protein signaling and their Galpha substrates: promises and challenges in their use as drug discovery targets. *Pharmacological reviews* **63**(3): 728-749.
- Klarenbeek J, Goedhart J, van Batenburg A, Groenewald D and Jalink K (2015) Fourth-generation epac-based FRET sensors for cAMP feature exceptional brightness, photostability and dynamic range: characterization of dedicated sensors for FLIM, for ratiometry and with high affinity. *PLoS one* **10**(4): e0122513.
- Knierim B, Hofmann KP, Ernst OP and Hubbell WL (2007) Sequence of late molecular events in the activation of rhodopsin. *Proceedings of the National Academy of Sciences of the United States of America* **104**(51): 20290-20295.
- Kolb P, Ferreira RS, Irwin JJ and Shoichet BK (2009) Docking and chemoinformatic screens for new ligands and targets. *Curr Opin Biotechnol* **20**(4): 429-436.
- Komolov KE and Benovic JL (2018) G protein-coupled receptor kinases: Past, present and future. *Cell Signal* **41**: 17-24.
- Kornienko O, Lacson R, Kunapuli P, Schneeweis J, Hoffman I, Smith T, Alberts M, Inglese J and Strulovici B (2004) Miniaturization of whole live cell-based GPCR assays using microdispensing and detection systems. *J Biomol Screen* **9**(3): 186-195.
- Kovacs JJ, Whalen EJ, Liu R, Xiao K, Kim J, Chen M, Wang J, Chen W and Lefkowitz RJ (2008) Beta-arrestin-mediated localization of smoothensin to the primary cilium. *Science* **320**(5884): 1777-1781.
- Koval A, Kopein D, Purvanov V and Katanaev VL (2010) Europium-labeled GTP as a general nonradioactive substitute for [(35)S]GTPgammaS in high-throughput G protein studies. *Analytical biochemistry* **397**(2): 202-207.
- Krasel C, Bunemann M, Lorenz K and Lohse MJ (2005) Beta-arrestin binding to the beta2-adrenergic receptor requires both receptor phosphorylation and receptor activation. *The Journal of biological chemistry* **280**(10): 9528-9535.

- Kratochwil NA, Gatti-McArthur S, Hoener MC, Lindemann L, Christ AD, Green LG, Guba W, Martin RE, Malherbe P, Porter RH, Slack JP, Winnig M, Dehmlow H, Grether U, Hertel C, Narquizian R, Panousis CG, Kolczewski S and Steward L (2011) G protein-coupled receptor transmembrane binding pockets and their applications in GPCR research and drug discovery: a survey. *Curr Top Med Chem* **11**(15): 1902-1924.
- Kremers GJ, Goedhart J, van Munster EB and Gadella TW, Jr. (2006) Cyan and yellow super fluorescent proteins with improved brightness, protein folding, and FRET Forster radius. *Biochemistry* **45**(21): 6570-6580.
- Kricka LJ and Leach FR (1989) In memoriam Dr Marlene DeLuca. 1987 O. M. Smith Lecture. Firefly luciferase: mechanism of action, cloning and expression of the active enzyme. *J Biolumin Chemilumin* **3**(1): 1-5.
- Kristiansen K (2004) Molecular mechanisms of ligand binding, signaling, and regulation within the superfamily of G-protein-coupled receptors: molecular modeling and mutagenesis approaches to receptor structure and function. *Pharmacol Ther* **103**(1): 21-80.
- Kuder K and Kiec-Kononowicz K (2008) Fluorescent GPCR ligands as new tools in pharmacology. *Curr Med Chem* **15**(21): 2132-2143.
- Kumagai H, Ikeda Y, Motozawa Y, Fujishiro M, Okamura T, Fujio K, Okazaki H, Nomura S, Takeda N, Harada M, Toko H, Takimoto E, Akazawa H, Morita H, Suzuki J, Yamazaki T, Yamamoto K, Komuro I and Yanagisawa M (2015) Quantitative Measurement of GPCR Endocytosis via Pulse-Chase Covalent Labeling. *PLoS one* **10**(5): e0129394.
- Kunapuli P, Ransom R, Murphy KL, Pettibone D, Kerby J, Grimwood S, Zuck P, Hodder P, Lacson R, Hoffman I, Inglese J and Strulovici B (2003) Development of an intact cell reporter gene beta-lactamase assay for G protein-coupled receptors for high-throughput screening. *Analytical biochemistry* **314**(1): 16-29.
- Lagasse HA, Alexaki A, Simhadri VL, Katagiri NH, Jankowski W, Sauna ZE and Kimchi-Sarfaty C (2017) Recent advances in (therapeutic protein) drug development. *F1000Res* **6**: 113.
- Lam AJ, St-Pierre F, Gong Y, Marshall JD, Cranfill PJ, Baird MA, McKeown MR, Wiedenmann J, Davidson MW, Schnitzer MJ, Tsien RY and Lin MZ (2012) Improving FRET dynamic range with bright green and red fluorescent proteins. *Nature methods* **9**(10): 1005-1012.
- Lampe JN, Floor SN, Gross JD, Nishida CR, Jiang Y, Trnka MJ and Ortiz de Montellano PR (2008) Ligand-induced conformational heterogeneity of cytochrome P450 CYP119 identified by 2D NMR spectroscopy with the unnatural amino acid (13)C-p-methoxyphenylalanine. *Journal of the American Chemical Society* **130**(48): 16168-16169.
- Laporte SA, Oakley RH, Zhang J, Holt JA, Ferguson SS, Caron MG and Barak LS (1999) The beta2-adrenergic receptor/betaarrestin complex recruits the clathrin adaptor AP-2 during endocytosis. *Proceedings of the National Academy of Sciences of the United States of America* **96**(7): 3712-3717.
- Latorraca NR, Venkatakrisnan AJ and Dror RO (2017) GPCR Dynamics: Structures in Motion. *Chem Rev* **117**(1): 139-155.
- Latt SA, Cheung HT and Blout ER (1965) Energy Transfer. A System with Relatively Fixed Donor-Acceptor Separation. *Journal of the American Chemical Society* **87**: 995-1003.
- Lauffer BE, Melero C, Temkin P, Lei C, Hong W, Kortemme T and von Zastrow M (2010) SNX27 mediates PDZ-directed sorting from endosomes to the plasma membrane. *J Cell Biol* **190**(4): 565-574.
- Lee MH, Appleton KM, Strungs EG, Kwon JY, Morinelli TA, Peterson YK, Laporte SA and Luttrell LM (2016) The conformational signature of beta-arrestin2 predicts its trafficking and signalling functions. *Nature* **531**(7596): 665-668.
- Lefkimmiatis K and Zaccolo M (2014) cAMP signaling in subcellular compartments. *Pharmacol Ther* **143**(3): 295-304.

- Lefkowitz RJ, Roth J and Pastan I (1970) Radioreceptor assay of adrenocorticotrophic hormone: new approach to assay of polypeptide hormones in plasma. *Science* **170**(3958): 633-635.
- Lefkowitz RJ and Shenoy SK (2005) Transduction of receptor signals by beta-arrestins. *Science* **308**(5721): 512-517.
- Lenhart PM, Broselid S, Barrick CJ, Leeb-Lundberg LM and Caron KM (2013) G-protein-coupled receptor 30 interacts with receptor activity-modifying protein 3 and confers sex-dependent cardioprotection. *J Mol Endocrinol* **51**(1): 191-202.
- Levitz J, Broichhagen J, Leippe P, Konrad D, Trauner D and Isacoff EY (2017) Dual optical control and mechanistic insights into photoswitchable group II and III metabotropic glutamate receptors. *Proceedings of the National Academy of Sciences of the United States of America* **114**(17): E3546-E3554.
- Leyris JP, Roux T, Trinquet E, Verdier P, Fehrentz JA, Oueslati N, Douzon S, Bourrier E, Lamarque L, Gagne D, Galleyrand JC, M'Kadmi C, Martinez J, Mary S, Baneres JL and Marie J (2011) Homogeneous time-resolved fluorescence-based assay to screen for ligands targeting the growth hormone secretagogue receptor type 1a. *Analytical biochemistry* **408**(2): 253-262.
- Liang YL, Khoshouei M, Radjainia M, Zhang Y, Glukhova A, Tarrasch J, Thal DM, Furness SGB, Christopoulos G, Coudrat T, Danev R, Baumeister W, Miller LJ, Christopoulos A, Kobilka BK, Wootten D, Skinotis G and Sexton PM (2017) Phase-plate cryo-EM structure of a class B GPCR-G-protein complex. *Nature* **546**(7656): 118-123.
- Liggett SB, Ostrowski J, Chesnut LC, Kurose H, Raymond JR, Caron MG and Lefkowitz RJ (1992) Sites in the third intracellular loop of the alpha 2A-adrenergic receptor confer short term agonist-promoted desensitization. Evidence for a receptor kinase-mediated mechanism. *The Journal of biological chemistry* **267**(7): 4740-4746.
- Lin X, Yu AC and Chan TF (2017) Efforts and Challenges in Engineering the Genetic Code. *Life (Basel)* **7**(1).
- Liu JJ, Horst R, Katritch V, Stevens RC and Wuthrich K (2012) Biased signaling pathways in beta2-adrenergic receptor characterized by 19F-NMR. *Science* **335**(6072): 1106-1110.
- Liu Y, Chen L-Y, Zeng H, Ward R, Wu N, Ma L, Mu X, Li Q-L, Yang Y, An S, Guo X-X, Hao Q and Xu T-R (2018a) Assessing the real-time activation of the cannabinoid CB1 receptor and the associated structural changes using a FRET biosensor. *The International Journal of Biochemistry & Cell Biology* **99**: 114-124.
- Liu Y, Zeng H, Pediani JD, Ward RJ, Chen LY, Wu N, Ma L, Tang M, Yang Y, An S, Guo XX, Hao Q and Xu TR (2018b) Visualization of the activation of the histamine H3 receptor (H3R) using novel fluorescence resonance energy transfer biosensors and their potential application to the study of H3R pharmacology. *FEBS J* **285**(12): 2319-2336.
- Locatelli-Hoops S, Sheen FC, Zoubak L, Gawrisch K and Yeliseev AA (2013) Application of HaloTag technology to expression and purification of cannabinoid receptor CB2. *Protein Expr Purif* **89**(1): 62-72.
- Loetscher P, Gong JH, Dewald B, Baggiolini M and Clark-Lewis I (1998) N-terminal peptides of stromal cell-derived factor-1 with CXC chemokine receptor 4 agonist and antagonist activities. *The Journal of biological chemistry* **273**(35): 22279-22283.
- Lohse MJ (1993) Molecular mechanisms of membrane receptor desensitization. *Biochim Biophys Acta* **1179**(2): 171-188.
- Lohse MJ, Benovic JL, Codina J, Caron MG and Lefkowitz RJ (1990) beta-Arrestin: a protein that regulates beta-adrenergic receptor function. *Science* **248**(4962): 1547-1550.
- Lohse MJ and Hofmann KP (2015) Spatial and Temporal Aspects of Signaling by G-Protein-Coupled Receptors. *Molecular pharmacology* **88**(3): 572-578.
- Lohse MJ, Maiellaro I and Calebiro D (2014) Kinetics and mechanism of G protein-coupled receptor activation. *Curr Opin Cell Biol* **27**: 87-93.



- Lohse MJ, Nuber S and Hoffmann C (2012) Fluorescence/bioluminescence resonance energy transfer techniques to study G-protein-coupled receptor activation and signaling. *Pharmacological reviews* **64**(2): 299-336.
- Lorenz WW, McCann RO, Longiaru M and Cormier MJ (1991) Isolation and expression of a cDNA encoding *Renilla reniformis* luciferase. *Proceedings of the National Academy of Sciences of the United States of America* **88**(10): 4438-4442.
- Los GV, Encell LP, McDougall MG, Hartzell DD, Karassina N, Zimprich C, Wood MG, Learish R, Ohana RF, Urh M, Simpson D, Mendez J, Zimmerman K, Otto P, Vidugiris G, Zhu J, Darzins A, Klaubert DH, Bulleit RF and Wood KV (2008) HaloTag: a novel protein labeling technology for cell imaging and protein analysis. *ACS chemical biology* **3**(6): 373-382.
- Lu B, Chen L, Zhang Y, Shi Y and Zhou N (2016) Quantitative analysis of G-protein-coupled receptor internalization using DnaE intein-based assay. *Methods Cell Biol* **132**: 293-318.
- Luk CK (1971) Energy transfer between tryptophans and aromatic ligands in apomyoglobin. *Biopolymers* **10**(8): 1317-1329.
- Luker KE and Luker GD (2014) Split Gaussia luciferase for imaging ligand-receptor binding. *Methods Mol Biol* **1098**: 59-69.
- Luttrell LM (2014) Minireview: More than just a hammer: ligand "bias" and pharmaceutical discovery. *Mol Endocrinol* **28**(3): 281-294.
- Luttrell LM and Lefkowitz RJ (2002) The role of beta-arrestins in the termination and transduction of G-protein-coupled receptor signals. *J Cell Sci* **115**(Pt 3): 455-465.
- Lyga S, Volpe S, Werthmann RC, Gotz K, Sungkaworn T, Lohse MJ and Calebiro D (2016) Persistent cAMP Signaling by Internalized LH Receptors in Ovarian Follicles. *Endocrinology* **157**(4): 1613-1621.
- Machleidt T, Woodroffe CC, Schwinn MK, Mendez J, Robers MB, Zimmerman K, Otto P, Daniels DL, Kirkland TA and Wood KV (2015) NanoBRET-A Novel BRET Platform for the Analysis of Protein-Protein Interactions. *ACS chemical biology* **10**(8): 1797-1804.
- Maguire ME, Van Arsdale PM and Gilman AG (1976) An agonist-specific effect of guanine nucleotides on binding to the beta adrenergic receptor. *Molecular pharmacology* **12**(2): 335-339.
- Maier-Peuschel M, Frolich N, Dees C, Hommers LG, Hoffmann C, Nikolaev VO and Lohse MJ (2010) A fluorescence resonance energy transfer-based M2 muscarinic receptor sensor reveals rapid kinetics of allosteric modulation. *The Journal of biological chemistry* **285**(12): 8793-8800.
- Malo N, Hanley JA, Cerquozzi S, Pelletier J and Nadon R (2006) Statistical practice in high-throughput screening data analysis. *Nature biotechnology* **24**(2): 167-175.
- Manglik A, Kim TH, Masureel M, Altenbach C, Yang Z, Hilger D, Lerch MT, Kobilka TS, Thian FS, Hubbell WL, Prosser RS and Kobilka BK (2015) Structural Insights into the Dynamic Process of beta2-Adrenergic Receptor Signaling. *Cell* **161**(5): 1101-1111.
- Manglik A and Kobilka B (2014) The role of protein dynamics in GPCR function: insights from the beta2AR and rhodopsin. *Curr Opin Cell Biol* **27**: 136-143.
- Mank M, Reiff DF, Heim N, Friedrich MW, Borst A and Griesbeck O (2006) A FRET-based calcium biosensor with fast signal kinetics and high fluorescence change. *Biophys J* **90**(5): 1790-1796.
- Marion S, Oakley RH, Kim KM, Caron MG and Barak LS (2006) A beta-arrestin binding determinant common to the second intracellular loops of rhodopsin family G protein-coupled receptors. *The Journal of biological chemistry* **281**(5): 2932-2938.
- Markovic D, Holdich J, Al-Sabah S, Mistry R, Krasel C, Mahaut-Smith MP and Challiss RA (2012) FRET-based detection of M1 muscarinic acetylcholine receptor activation by orthosteric and allosteric agonists. *PLoS one* **7**(1): e29946.
- Martin BR, Giepmans BN, Adams SR and Tsien RY (2005) Mammalian cell-based optimization of the biarsenical-binding tetracysteine motif for improved fluorescence and affinity. *Nature biotechnology* **23**(10): 1308-1314.

- Marullo S and Bouvier M (2007) Resonance energy transfer approaches in molecular pharmacology and beyond. *Trends Pharmacol Sci* **28**(8): 362-365.
- Mastop M, Bindels DS, Shaner NC, Postma M, Gadella TWJ, Jr. and Goedhart J (2017) Characterization of a spectrally diverse set of fluorescent proteins as FRET acceptors for mTurquoise2. *Sci Rep* **7**(1): 11999.
- Mastop M, Reinhard NR, Zuconelli CR, Terwey F, Gadella TWJ, Jr., van Unen J, Adjobo-Hermans MJW and Goedhart J (2018) A FRET-based biosensor for measuring Galpha13 activation in single cells. *PloS one* **13**(3): e0193705.
- Matsushita S, Nakata H, Kubo Y and Tateyama M (2010) Ligand-induced rearrangements of the GABA(B) receptor revealed by fluorescence resonance energy transfer. *The Journal of biological chemistry* **285**(14): 10291-10299.
- Mattheyses AL, Hoppe AD and Axelrod D (2004) Polarized fluorescence resonance energy transfer microscopy. *Biophys J* **87**(4): 2787-2797.
- Maurel D, Comps-Agrar L, Brock C, Rives ML, Bourrier E, Ayoub MA, Bazin H, Tinel N, Durroux T, Prezeau L, Trinquet E and Pin JP (2008) Cell-surface protein-protein interaction analysis with time-resolved FRET and snap-tag technologies: application to GPCR oligomerization. *Nature methods* **5**(6): 561-567.
- May LT, Leach K, Sexton PM and Christopoulos A (2007) Allosteric modulation of G protein-coupled receptors. *Annu Rev Pharmacol Toxicol* **47**: 1-51.
- Mayr LM and Bojanic D (2009) Novel trends in high-throughput screening. *Curr Opin Pharmacol* **9**(5): 580-588.
- McLatchie LM, Fraser NJ, Main MJ, Wise A, Brown J, Thompson N, Solari R, Lee MG and Foord SM (1998) RAMPs regulate the transport and ligand specificity of the calcitonin-receptor-like receptor. *Nature* **393**(6683): 333-339.
- McLaughlin JN, Shen LX, Holinstat M, Brooks JD, DiBenedetto E and Hamm HE (2005) Functional selectivity of G protein signaling by agonist peptides and thrombin for the protease-activated receptor-1. *Journal of Biological Chemistry* **280**(26): 25048-25059.
- Messerer R, Kauk M, Volpato D, Alonso Canizal MC, Klockner J, Zabel U, Nuber S, Hoffmann C and Holzgrabe U (2017) FRET Studies of Quinolone-Based Bitopic Ligands and Their Structural Analogues at the Muscarinic M1 Receptor. *ACS chemical biology* **12**(3): 833-843.
- Meyer zu Heringdorf D, Liliom K, Schaefer M, Danneberg K, Jaggar JH, Tigyi G and Jakobs KH (2003) Photolysis of intracellular caged sphingosine-1-phosphate causes Ca<sup>2+</sup> mobilization independently of G-protein-coupled receptors. *FEBS Lett* **554**(3): 443-449.
- Middleton RJ and Kellam B (2005) Fluorophore-tagged GPCR ligands. *Curr Opin Chem Biol* **9**(5): 517-525.
- Milic D and Veprintsev DB (2015) Large-scale production and protein engineering of G protein-coupled receptors for structural studies. *Frontiers in pharmacology* **6**: 66.
- Milligan G (2003) Principles: extending the utility of [<sup>35</sup>S]GTP gamma S binding assays. *Trends Pharmacol Sci* **24**(2): 87-90.
- Milligan G (2004) G protein-coupled receptor dimerization: function and ligand pharmacology. *Molecular pharmacology* **66**(1): 1-7.
- Milligan G and Kostenis E (2006) Heterotrimeric G-proteins: a short history. *Br J Pharmacol* **147** Suppl 1: S46-55.
- Miyawaki A, Shcherbakova DM and Verkhusha VV (2012) Red fluorescent proteins: chromophore formation and cellular applications. *Curr Opin Struct Biol* **22**(5): 679-688.
- Mo XL and Fu H (2016) BRET: NanoLuc-Based Bioluminescence Resonance Energy Transfer Platform to Monitor Protein-Protein Interactions in Live Cells. *Methods Mol Biol* **1439**: 263-271.

- Mohr K, Schmitz J, Schrage R, Trankle C and Holzgrabe U (2013) Molecular alliance-from orthosteric and allosteric ligands to dualsteric/bitopic agonists at G protein coupled receptors. *Angew Chem Int Ed Engl* **52**(2): 508-516.
- Mombaerts P (2004) Genes and ligands for odorant, vomeronasal and taste receptors. *Nat Rev Neurosci* **5**(4): 263-278.
- Monger TG, Alfano RR and Callender RH (1979) Photochemistry of rhodopsin and isorhodopsin investigated on a picosecond time scale. *Biophys J* **27**(1): 105-115.
- Morin JG and Hastings JW (1971) Energy transfer in a bioluminescent system. *J Cell Physiol* **77**(3): 313-318.
- Muller JM, Debaigt C, Goursaud S, Montoni A, Pineau N, Meunier AC and Janet T (2007) Unconventional binding sites and receptors for VIP and related peptides PACAP and PHI/PHM: an update. *Peptides* **28**(9): 1655-1666.
- Mullershausen F, Zecri F, Cetin C, Billich A, Guerini D and Seuwen K (2009) Persistent signaling induced by FTY720-phosphate is mediated by internalized S1P1 receptors. *Nature chemical biology* **5**(6): 428-434.
- Nagai T, Ibata K, Park ES, Kubota M, Mikoshiba K and Miyawaki A (2002) A variant of yellow fluorescent protein with fast and efficient maturation for cell-biological applications. *Nature biotechnology* **20**(1): 87-90.
- Nakanishi J, Takarada T, Yunoki S, Kikuchi Y and Maeda M (2006) FRET-based monitoring of conformational change of the beta2 adrenergic receptor in living cells. *Biochemical and biophysical research communications* **343**(4): 1191-1196.
- Namkung Y, Le Gouill C, Lukashova V, Kobayashi H, Hogue M, Khoury E, Song M, Bouvier M and Laporte SA (2016) Monitoring G protein-coupled receptor and beta-arrestin trafficking in live cells using enhanced bystander BRET. *Nature communications* **7**: 12178.
- Naor Z (2009) Signaling by G-protein-coupled receptor (GPCR): studies on the GnRH receptor. *Front Neuroendocrinol* **30**(1): 10-29.
- Nguyen AW and Daugherty PS (2005) Evolutionary optimization of fluorescent proteins for intracellular FRET. *Nature biotechnology* **23**(3): 355-360.
- Nikolaev VO, Bunemann M, Hein L, Hannawacker A and Lohse MJ (2004) Novel single chain cAMP sensors for receptor-induced signal propagation. *The Journal of biological chemistry* **279**(36): 37215-37218.
- Nikolaev VO, Hoffmann C, Bunemann M, Lohse MJ and Vilardaga JP (2006) Molecular basis of partial agonism at the neurotransmitter alpha2A-adrenergic receptor and Gi-protein heterotrimer. *The Journal of biological chemistry* **281**(34): 24506-24511.
- Noel JP, Hamm HE and Sigler PB (1993) The 2.2 Å crystal structure of transducin-alpha complexed with GTP gamma S. *Nature* **366**(6456): 654-663.
- Norskov-Lauritsen L, Thomsen AR and Brauner-Osborne H (2014) G protein-coupled receptor signaling analysis using homogenous time-resolved Forster resonance energy transfer (HTRF(R)) technology. *Int J Mol Sci* **15**(2): 2554-2572.
- Novoselova TV, Jackson D, Campbell DC, Clark AJ and Chan LF (2013) Melanocortin receptor accessory proteins in adrenal gland physiology and beyond. *J Endocrinol* **217**(1): R1-11.
- Nuber S, Zabel U, Lorenz K, Nuber A, Milligan G, Tobin AB, Lohse MJ and Hoffmann C (2016) beta-Arrestin biosensors reveal a rapid, receptor-dependent activation/deactivation cycle. *Nature* **531**(7596): 661-664.
- Oakley RH, Hudson CC, Cruickshank RD, Meyers DM, Payne RE, Jr., Rhem SM and Loomis CR (2002) The cellular distribution of fluorescently labeled arrestins provides a robust, sensitive, and universal assay for screening G protein-coupled receptors. *Assay Drug Dev Technol* **1**(1 Pt 1): 21-30.
- Ohguro H, Van Hooser JP, Milam AH and Palczewski K (1995) Rhodopsin phosphorylation and dephosphorylation in vivo. *The Journal of biological chemistry* **270**(24): 14259-14262.

- Ohta Y, Kamagata T, Mukai A, Takada S, Nagai T and Horikawa K (2016) Nontrivial Effect of the Color-Exchange of a Donor/Acceptor Pair in the Engineering of Förster Resonance Energy Transfer (FRET)-Based Indicators. *ACS chemical biology* **11**(7): 1816-1822.
- Okude J, Ueda T, Kofuku Y, Sato M, Nobuyama N, Kondo K, Shiraishi Y, Mizumura T, Onishi K, Natsume M, Maeda M, Tsujishita H, Kuranaga T, Inoue M and Shimada I (2015) Identification of a Conformational Equilibrium That Determines the Efficacy and Functional Selectivity of the  $\mu$ -Opioid Receptor. *Angew Chem Int Ed Engl* **54**(52): 15771-15776.
- Oldham WM and Hamm HE (2006) Structural basis of function in heterotrimeric G proteins. *Q Rev Biophys* **39**(2): 117-166.
- Palczewski K, Kumasaka T, Hori T, Behnke CA, Motoshima H, Fox BA, Le Trong I, Teller DC, Okada T, Stenkamp RE, Yamamoto M and Miyano M (2000) Crystal structure of rhodopsin: A G protein-coupled receptor. *Science* **289**(5480): 739-745.
- Palma-Cerda F, Auger C, Crawford DJ, Hodgson AC, Reynolds SJ, Cowell JK, Swift KA, Cais O, Vyklicky L, Corrie JE and Ogden D (2012) New caged neurotransmitter analogs selective for glutamate receptor sub-types based on methoxynitroindoline and nitrophenylethoxycarbonyl caging groups. *Neuropharmacology* **63**(4): 624-634.
- PalsRylaarsdam R and Hosey MM (1997) Two homologous phosphorylation domains differentially contribute to desensitization and internalization of the m2 muscarinic acetylcholine receptor. *Journal of Biological Chemistry* **272**(22): 14152-14158.
- Pandy-Szekeres G, Munk C, Tsonkov TM, Mordalski S, Harpsoe K, Hauser AS, Bojarski AJ and Gloriam DE (2018) GPCRdb in 2018: adding GPCR structure models and ligands. *Nucleic Acids Res* **46**(D1): D440-D446.
- Park SJ and Im DS (2017) Sphingosine 1-Phosphate Receptor Modulators and Drug Discovery. *Biomol Ther (Seoul)* **25**(1): 80-90.
- Patel TB, Du Z, Pierre S, Cartin L and Scholich K (2001) Molecular biological approaches to unravel adenylyl cyclase signaling and function. *Gene* **269**(1-2): 13-25.
- Peltonen JM, Nyronen T, Wurster S, Pihlavisto M, Hoffren AM, Marjamaki A, Xhaard H, Kanerva L, Savola JM, Johnson MS and Scheinin M (2003) Molecular mechanisms of ligand-receptor interactions in transmembrane domain V of the  $\alpha$ 2A-adrenoceptor. *Br J Pharmacol* **140**(2): 347-358.
- Peters MF, Vaillancourt F, Heroux M, Valiquette M and Scott CW (2010) Comparing label-free biosensors for pharmacological screening with cell-based functional assays. *Assay Drug Dev Technol* **8**(2): 219-227.
- Picard L-P, Schönegege AM, Lohse MJ and Bouvier M (2018) Bioluminescence resonance energy transfer-based biosensors allow monitoring of ligand- and transducer-mediated GPCR conformational changes. *Communications Biology* **1**(1): 106.
- Pomorski A and Krezel A (2011) Exploration of biarsenical chemistry--challenges in protein research. *ChemBiochem : a European journal of chemical biology* **12**(8): 1152-1167.
- Ponsioen B, Zhao J, Riedl J, Zwartkruis F, van der Krogt G, Zaccolo M, Moolenaar WH, Bos JL and Jalink K (2004) Detecting cAMP-induced Epac activation by fluorescence resonance energy transfer: Epac as a novel cAMP indicator. *EMBO Rep* **5**(12): 1176-1180.
- Powlowski PB, K.; Jones-Tabah, J.; Sleno R.; Devost D., Hébert, T.E. (2018) Conformational Profiling of the 5-HT<sub>2A</sub> Receptor Using FIAsH BRET *Springer Protocols*.
- Poyner DR, Sexton PM, Marshall I, Smith DM, Quirion R, Born W, Muff R, Fischer JA and Foord SM (2002) International Union of Pharmacology. XXXII. The mammalian calcitonin gene-related peptides, adrenomedullin, amylin, and calcitonin receptors. *Pharmacological reviews* **54**(2): 233-246.
- Prasher DC, Eckenrode VK, Ward WW, Prendergast FG and Cormier MJ (1992) Primary structure of the *Aequorea victoria* green-fluorescent protein. *Gene* **111**(2): 229-233.

- Premont RT and Gainetdinov RR (2007) Physiological roles of G protein-coupled receptor kinases and arrestins. *Annu Rev Physiol* **69**: 511-534.
- Prinster SC, Hague C and Hall RA (2005) Heterodimerization of g protein-coupled receptors: specificity and functional significance. *Pharmacological reviews* **57**(3): 289-298.
- Raehal KM, Walker JK and Bohn LM (2005) Morphine side effects in beta-arrestin 2 knockout mice. *J Pharmacol Exp Ther* **314**(3): 1195-1201.
- Rahmeh R, Damian M, Cottet M, Orcel H, Mendre C, Durroux T, Sharma KS, Durand G, Pucci B, Trinquet E, Zwier JM, Deupi X, Bron P, Baneres JL, Mouillac B and Granier S (2012) Structural insights into biased G protein-coupled receptor signaling revealed by fluorescence spectroscopy. *Proceedings of the National Academy of Sciences of the United States of America* **109**(17): 6733-6738.
- Rajagopal S, Ahn S, Rominger DH, Gowen-MacDonald W, Lam CM, Dewire SM, Violin JD and Lefkowitz RJ (2011) Quantifying ligand bias at seven-transmembrane receptors. *Molecular pharmacology* **80**(3): 367-377.
- Rasmussen SG, Choi HJ, Rosenbaum DM, Kobilka TS, Thian FS, Edwards PC, Burghammer M, Ratnala VR, Sanishvili R, Fischetti RF, Schertler GF, Weis WI and Kobilka BK (2007) Crystal structure of the human beta2 adrenergic G-protein-coupled receptor. *Nature* **450**(7168): 383-387.
- Rasmussen SG, DeVree BT, Zou Y, Kruse AC, Chung KY, Kobilka TS, Thian FS, Chae PS, Pardon E, Calinski D, Mathiesen JM, Shah ST, Lyons JA, Caffrey M, Gellman SH, Steyaert J, Skiniotis G, Weis WI, Sunahara RK and Kobilka BK (2011) Crystal structure of the beta2 adrenergic receptor-Gs protein complex. *Nature* **477**(7366): 549-555.
- Reiner S, Ambrosio M, Hoffmann C and Lohse MJ (2010) Differential Signaling of the Endogenous Agonists at the beta(2)-Adrenergic Receptor. *Journal of Biological Chemistry* **285**(46): 36188-36198.
- Rinne A, Birk A and Bunemann M (2013) Voltage regulates adrenergic receptor function. *Proceedings of the National Academy of Sciences of the United States of America* **110**(4): 1536-1541.
- Ritt M and Sivaramakrishnan S (2016) Correlation between Activity and Domain Complementation in Adenylyl Cyclase Demonstrated with a Novel Fluorescence Resonance Energy Transfer Sensor. *Molecular pharmacology* **89**(4): 407-412.
- Rochais F, Vilardaga JP, Nikolaev VO, Bunemann M, Lohse MJ and Engelhardt S (2007) Real-time optical recording of beta1-adrenergic receptor activation reveals supersensitivity of the Arg389 variant to carvedilol. *J Clin Invest* **117**(1): 229-235.
- Rondard P, Goudet C, Kniazeff J, Pin JP and Prezeau L (2011) The complexity of their activation mechanism opens new possibilities for the modulation of mGlu and GABAB class C G protein-coupled receptors. *Neuropharmacology* **60**(1): 82-92.
- Rosenbaum DM, Rasmussen SG and Kobilka BK (2009) The structure and function of G-protein-coupled receptors. *Nature* **459**(7245): 356-363.
- Roth BL and Chuang DM (1987) Multiple mechanisms of serotonergic signal transduction. *Life Sci* **41**(9): 1051-1064.
- Rovati GE, Capra V and Neubig RR (2007) The highly conserved DRY motif of class A G protein-coupled receptors: beyond the ground state. *Molecular pharmacology* **71**(4): 959-964.
- Rovira X, Trapero A, Pittolo S, Zussy C, Faucherre A, Jopling C, Giraldo J, Pin JP, Gorostiza P, Goudet C and Llebaria A (2016) OptoGluNAM4.1, a Photoswitchable Allosteric Antagonist for Real-Time Control of mGlu4 Receptor Activity. *Cell Chem Biol* **23**(8): 929-934.
- Rozenfeld R and Devi LA (2011) Exploring a role for heteromerization in GPCR signalling specificity. *Biochem J* **433**(1): 11-18.
- Rozenfeld R, Gupta A, Gagnidze K, Lim MP, Gomes I, Lee-Ramos D, Nieto N and Devi LA (2011) AT1R-CB(1)R heteromerization reveals a new mechanism for the pathogenic properties of angiotensin II. *EMBO J* **30**(12): 2350-2363.

- Santos R, Ursu O, Gaulton A, Bento AP, Donadi RS, Bologa CG, Karlsson A, Al-Lazikani B, Hersey A, Oprea TI and Overington JP (2017) A comprehensive map of molecular drug targets. *Nat Rev Drug Discov* **16**(1): 19-34.
- Sapsford KE, Berti L and Medintz IL (2006) Materials for fluorescence resonance energy transfer analysis: beyond traditional donor-acceptor combinations. *Angew Chem Int Ed Engl* **45**(28): 4562-4589.
- Scheerer P and Sommer ME (2017) Structural mechanism of arrestin activation. *Curr Opin Struct Biol* **45**: 160-169.
- Schetz JA and Sibley DR (1997) Zinc allosterically modulates antagonist binding to cloned D1 and D2 dopamine receptors. *J Neurochem* **68**(5): 1990-1997.
- Schihada H, Vandenberghe S, Zabel U, Frank M, Lohse MJ and Maiellaro I (2018) A universal bioluminescence resonance energy transfer sensor design enables high-sensitivity screening of GPCR activation dynamics. *Communications Biology* **1**(1): 105.
- Schleicher K and Zaccolo M (2018) Using cAMP Sensors to Study Cardiac Nanodomains. *J Cardiovasc Dev Dis* **5**(1).
- Schmidt MJ, Borbas J, Drescher M and Summerer D (2014) A genetically encoded spin label for electron paramagnetic resonance distance measurements. *Journal of the American Chemical Society* **136**(4): 1238-1241.
- Scholler P, Moreno-Delgado D, Lecat-Guillet N, Doumazane E, Monnier C, Charrier-Savournin F, Fabre L, Chouvet C, Soldevila S, Lamarque L, Donsimoni G, Roux T, Zwier JM, Trinquet E, Rondard P and Pin JP (2017) HTS-compatible FRET-based conformational sensors clarify membrane receptor activation. *Nature chemical biology* **13**(4): 372-380.
- Schonauer R, Kaiser A, Holze C, Babilon S, Kobberling J, Riedl B and Beck-Sickingher AG (2015) Fluorescently labeled adrenomedullin allows real-time monitoring of adrenomedullin receptor trafficking in living cells. *J Pept Sci* **21**(12): 905-912.
- Scott CW and Peters MF (2010) Label-free whole-cell assays: expanding the scope of GPCR screening. *Drug Discov Today* **15**(17-18): 704-716.
- Selvin PR (2002) Principles and biophysical applications of lanthanide-based probes. *Annu Rev Biophys Biomol Struct* **31**: 275-302.
- Semack A, Malik RU and Sivaramakrishnan S (2016) G Protein-selective GPCR Conformations Measured Using FRET Sensors in a Live Cell Suspension Fluorometer Assay. *Journal of visualized experiments : JoVE*(115).
- Serrano-Vega MJ, Magnani F, Shibata Y and Tate CG (2008) Conformational thermostabilization of the beta1-adrenergic receptor in a detergent-resistant form. *Proceedings of the National Academy of Sciences of the United States of America* **105**(3): 877-882.
- Sexton PM, Poyner DR, Simms J, Christopoulos A and Hay DL (2012) RAMPs as drug targets. *Adv Exp Med Biol* **744**: 61-74.
- Shakhmin A, Hall MP, Machleidt T, Walker JR, Wood KV and Kirkland TA (2017) Coelenterazine analogues emit red-shifted bioluminescence with NanoLuc. *Org Biomol Chem* **15**(40): 8559-8567.
- Shcherbakova DM, Hink MA, Joosen L, Gadella TW and Verkhusha VV (2012) An orange fluorescent protein with a large Stokes shift for single-excitation multicolor FCCS and FRET imaging. *Journal of the American Chemical Society* **134**(18): 7913-7923.
- Shen Q, Wang G, Li S, Liu X, Lu S, Chen Z, Song K, Yan J, Geng L, Huang Z, Huang W, Chen G and Zhang J (2016) ASD v3.0: unraveling allosteric regulation with structural mechanisms and biological networks. *Nucleic Acids Res* **44**(D1): D527-535.
- Shenoy SK and Lefkowitz RJ (2011) beta-Arrestin-mediated receptor trafficking and signal transduction. *Trends Pharmacol Sci* **32**(9): 521-533.
- Shenoy SK, McDonald PH, Kohout TA and Lefkowitz RJ (2001) Regulation of receptor fate by ubiquitination of activated beta 2-adrenergic receptor and beta-arrestin. *Science* **294**(5545): 1307-1313.

- Shimomura O, Masugi T, Johnson FH and Haneda Y (1978) Properties and reaction mechanism of the bioluminescence system of the deep-sea shrimp *Oplophorus gracilorostri*. *Biochemistry* **17**(6): 994-998.
- Shoback DM, Bilezikian JP, Turner SA, McCary LC, Guo MD and Peacock M (2003) The calcimimetic cinacalcet normalizes serum calcium in subjects with primary hyperparathyroidism. *J Clin Endocrinol Metab* **88**(12): 5644-5649.
- Shukla AK, Westfield GH, Xiao K, Reis RI, Huang LY, Tripathi-Shukla P, Qian J, Li S, Blanc A, Oleskie AN, Dosey AM, Su M, Liang CR, Gu LL, Shan JM, Chen X, Hanna R, Choi M, Yao XJ, Klink BU, Kahsai AW, Sidhu SS, Koide S, Penczek PA, Kossiakoff AA, Woods VL, Jr., Kobilka BK, Skiniotis G and Lefkowitz RJ (2014) Visualization of arrestin recruitment by a G-protein-coupled receptor. *Nature* **512**(7513): 218-222.
- Simon MI, Strathmann MP and Gautam N (1991) Diversity of G proteins in signal transduction. *Science* **252**(5007): 802-808.
- Sleno R, Devost D, Petrin D, Zhang A, Bourque K, Shinjo Y, Aoki J, Inoue A and Hebert TE (2017) Conformational biosensors reveal allosteric interactions between heterodimeric AT1 angiotensin and prostaglandin F2alpha receptors. *The Journal of biological chemistry* **292**(29): 12139-12152.
- Sleno R, Petrin D, Devost D, Goupil E, Zhang A and Hebert TE (2016) Designing BRET-based conformational biosensors for G protein-coupled receptors. *Methods* **92**: 11-18.
- Smith JS, Lefkowitz RJ and Rajagopal S (2018) Biased signalling: from simple switches to allosteric microprocessors. *Nat Rev Drug Discov*.
- Smrcka AV (2008) G protein betagamma subunits: central mediators of G protein-coupled receptor signaling. *Cell Mol Life Sci* **65**(14): 2191-2214.
- Soave M, Stoddart LA, Brown A, Woolard J and Hill SJ (2016) Use of a new proximity assay (NanoBRET) to investigate the ligand-binding characteristics of three fluorescent ligands to the human beta1-adrenoceptor expressed in HEK-293 cells. *Pharmacol Res Perspect* **4**(5): e00250.
- Southan C, Sharman JL, Benson HE, Faccenda E, Pawson AJ, Alexander SP, Buneman OP, Davenport AP, McGrath JC, Peters JA, Spedding M, Catterall WA, Fabbro D, Davies JA and Nc I (2016) The IUPHAR/BPS Guide to PHARMACOLOGY in 2016: towards curated quantitative interactions between 1300 protein targets and 6000 ligands. *Nucleic Acids Res* **44**(D1): D1054-1068.
- Spagnuolo CC, Vermeij RJ and Jares-Erijman EA (2006) Improved photostable FRET-competent biarsenical-tetracysteine probes based on fluorinated fluoresceins. *Journal of the American Chemical Society* **128**(37): 12040-12041.
- Sprang SR (1997) G protein mechanisms: insights from structural analysis. *Annu Rev Biochem* **66**: 639-678.
- Sriram K and Insel PA (2018) GPCRs as targets for approved drugs: How many targets and how many drugs? *Molecular pharmacology*.
- Stoddart LA, Johnstone EK, Wheal AJ, Goulding J, Robers MB, Machleidt T, Wood KV, Hill SJ and Pflieger KD (2015a) Application of BRET to monitor ligand binding to GPCRs. *Nature methods* **12**(7): 661-663.
- Stoddart LA, Johnstone EKM, Wheal AJ, Goulding J, Robers MB, Machleidt T, Wood KV, Hill SJ and Pflieger KDG (2015b) Application of BRET to monitor ligand binding to GPCRs. *Nature methods* **12**(7): 661-+.
- Stoddart LA, Kilpatrick LE and Hill SJ (2018) NanoBRET Approaches to Study Ligand Binding to GPCRs and RTKs. *Trends Pharmacol Sci* **39**(2): 136-147.
- Stryer L (1978) Fluorescence energy transfer as a spectroscopic ruler. *Annu Rev Biochem* **47**: 819-846.
- Stryer L and Haugland RP (1967) Energy transfer: a spectroscopic ruler. *Proceedings of the National Academy of Sciences of the United States of America* **58**(2): 719-726.

- Sungkaworn T, Jobin ML, Burnecki K, Weron A, Lohse MJ and Calebiro D (2017) Single-molecule imaging reveals receptor-G protein interactions at cell surface hot spots. *Nature* **550**(7677): 543-547.
- Suzuki N, Hajicek N and Kozasa T (2009) Regulation and physiological functions of G12/13-mediated signaling pathways. *Neurosignals* **17**(1): 55-70.
- Sydor AM, Czymmek KJ, Puchner EM and Mennella V (2015) Super-Resolution Microscopy: From Single Molecules to Supramolecular Assemblies. *Trends Cell Biol* **25**(12): 730-748.
- Szalai B, Barkai L, Turu G, Szidonya L, Varnai P and Hunyady L (2012) Allosteric interactions within the AT(1) angiotensin receptor homodimer: role of the conserved DRY motif. *Biochem Pharmacol* **84**(4): 477-485.
- Tadevosyan A, Villeneuve LR, Fournier A, Chatenet D, Nattel S and Allen BG (2016) Caged ligands to study the role of intracellular GPCRs. *Methods* **92**: 72-77.
- Takakura H, Hattori M, Takeuchi M and Ozawa T (2012) Visualization and quantitative analysis of G protein-coupled receptor-beta-arrestin interaction in single cells and specific organs of living mice using split luciferase complementation. *ACS chemical biology* **7**(5): 901-910.
- Takezako T, Unal H, Karnik SS and Node K (2017) Current topics in angiotensin II type 1 receptor research: Focus on inverse agonism, receptor dimerization and biased agonism. *Pharmacol Res* **123**: 40-50.
- Tamamura H, Hori A, Kanzaki N, Hiramatsu K, Mizumoto M, Nakashima H, Yamamoto N, Otaka A and Fujii N (2003) T140 analogs as CXCR4 antagonists identified as anti-metastatic agents in the treatment of breast cancer. *Febs Letters* **550**(1-3): 79-83.
- Tang XL, Wang Y, Li DL, Luo J and Liu MY (2012) Orphan G protein-coupled receptors (GPCRs): biological functions and potential drug targets. *Acta Pharmacologica Sinica* **33**(3): 363-371.
- Tateyama M, Abe H, Nakata H, Saito O and Kubo Y (2004) Ligand-induced rearrangement of the dimeric metabotropic glutamate receptor 1alpha. *Nat Struct Mol Biol* **11**(7): 637-642.
- Tateyama M and Kubo Y (2013a) Analyses of the effects of Gq protein on the activated states of the muscarinic M3 receptor and the purinergic P2Y1 receptor. *Physiol Rep* **1**(5): e00134.
- Tateyama M and Kubo Y (2013b) Binding of Gq protein stabilizes the activated state of the muscarinic receptor type 1. *Neuropharmacology* **65**: 173-181.
- Tewson PH, Quinn AM and Hughes TE (2013) A multiplexed fluorescent assay for independent second-messenger systems: decoding GPCR activation in living cells. *J Biomol Screen* **18**(7): 797-806.
- Thal DM, Vuckovic Z, Draper-Joyce CJ, Liang YL, Glukhova A, Christopoulos A and Sexton PM (2018) Recent advances in the determination of G protein-coupled receptor structures. *Curr Opin Struct Biol* **51**: 28-34.
- Thoma G, Streiff MB, Kovarik J, Glickman F, Wagner T, Beerli C and Zerwes HG (2008) Orally bioavailable isothiourreas block function of the chemokine receptor CXCR4 in vitro and in vivo. *J Med Chem* **51**(24): 7915-7920.
- Thorne N, Inglese J and Auld DS (2010) Illuminating insights into firefly luciferase and other bioluminescent reporters used in chemical biology. *Chemistry & biology* **17**(6): 646-657.
- Tobin AB, Butcher AJ and Kong KC (2008) Location, location, location...site-specific GPCR phosphorylation offers a mechanism for cell-type-specific signalling. *Trends Pharmacol Sci* **29**(8): 413-420.
- Topiol S (2018) New opportunities for GPCR allosteric modulators. *Future Med Chem*.
- Trinquet E, Bouhelal R and Dietz M (2011) Monitoring Gq-coupled receptor response through inositol phosphate quantification with the IP-One assay. *Expert Opin Drug Discov* **6**(10): 981-994.
- Trinquet E, Fink M, Bazin H, Grillet F, Maurin F, Bourrier E, Ansanay H, Leroy C, Michaud A, Durroux T, Maurel D, Malhaire F, Goudet C, Pin JP, Naval M, Hernout O, Chretien F, Chapleur Y and Mathis G (2006) D-myo-inositol 1-phosphate as a surrogate of D-myo-inositol 1,4,5-tris phosphate to monitor G protein-coupled receptor activation. *Analytical biochemistry* **358**(1): 126-135.



- Tsien RY (1980) New calcium indicators and buffers with high selectivity against magnesium and protons: design, synthesis, and properties of prototype structures. *Biochemistry* **19**(11): 2396-2404.
- Tsien RY (1998) The green fluorescent protein. *Annu Rev Biochem* **67**: 509-544.
- Tsvetanova NG and von Zastrow M (2014) Spatial encoding of cyclic AMP signaling specificity by GPCR endocytosis. *Nature chemical biology* **10**(12): 1061-1065.
- Tyagi S and Lemke EA (2015) Single-molecule FRET and crosslinking studies in structural biology enabled by noncanonical amino acids. *Curr Opin Struct Biol* **32**: 66-73.
- van der Westhuizen ET, Breton B, Christopoulos A and Bouvier M (2014) Quantification of ligand bias for clinically relevant beta2-adrenergic receptor ligands: implications for drug taxonomy. *Molecular pharmacology* **85**(3): 492-509.
- van der Westhuizen ET, Valant C, Sexton PM and Christopoulos A (2015) Endogenous allosteric modulators of G protein-coupled receptors. *J Pharmacol Exp Ther* **353**(2): 246-260.
- Van Eps N, Preininger AM, Alexander N, Kaya AI, Meier S, Meiler J, Hamm HE and Hubbell WL (2011) Interaction of a G protein with an activated receptor opens the interdomain interface in the alpha subunit. *Proceedings of the National Academy of Sciences of the United States of America* **108**(23): 9420-9424.
- Van Munster EB, Kremers GJ, Adjobo-Hermans MJ and Gadella TW, Jr. (2005) Fluorescence resonance energy transfer (FRET) measurement by gradual acceptor photobleaching. *J Microsc* **218**(Pt 3): 253-262.
- van Unen J, Stumpf AD, Schmid B, Reinhard NR, Hordijk PL, Hoffmann C, Gadella TW, Jr. and Goedhart J (2016) A New Generation of FRET Sensors for Robust Measurement of Galphai1, Galphai2 and Galphai3 Activation Kinetics in Single Cells. *PLoS one* **11**(1): e0146789.
- Vandame P, Spriet C, Riquet F, Trinel D, Cailliau-Maggio K and Bodart JF (2014) Optimization of ERK activity biosensors for both ratiometric and lifetime FRET measurements. *Sensors (Basel)* **14**(1): 1140-1154.
- Venter JC, Fraser CM and Harrison LC (1980) Autoantibodies to beta 2-adrenergic receptors: a possible cause of adrenergic hyporesponsiveness in allergic rhinitis and asthma. *Science* **207**(4437): 1361-1363.
- Verhaegent M and Christopoulos TK (2002) Recombinant Gaussia luciferase. Overexpression, purification, and analytical application of a bioluminescent reporter for DNA hybridization. *Anal Chem* **74**(17): 4378-4385.
- Verkhusha VV and Lukyanov KA (2004) The molecular properties and applications of Anthozoa fluorescent proteins and chromoproteins. *Nature biotechnology* **22**(3): 289-296.
- Villardaga JP, Bunemann M, Krasel C, Castro M and Lohse MJ (2003) Measurement of the millisecond activation switch of G protein-coupled receptors in living cells. *Nature biotechnology* **21**(7): 807-812.
- Villardaga JP, Nikolaev VO, Lorenz K, Ferrandon S, Zhuang Z and Lohse MJ (2008) Conformational cross-talk between alpha2A-adrenergic and mu-opioid receptors controls cell signaling. *Nature chemical biology* **4**(2): 126-131.
- Villardaga JP, Steinmeyer R, Harms GS and Lohse MJ (2005) Molecular basis of inverse agonism in a G protein-coupled receptor. *Nature chemical biology* **1**(1): 25-28.
- Violin JD and Lefkowitz RJ (2007) Beta-arrestin-biased ligands at seven-transmembrane receptors. *Trends Pharmacol Sci* **28**(8): 416-422.
- Vishnivetskiy SA, Hirsch JA, Velez MG, Gurevich YV and Gurevich VV (2002) Transition of arrestin into the active receptor-binding state requires an extended interdomain hinge. *The Journal of biological chemistry* **277**(46): 43961-43967.
- von Zastrow M and Kobilka BK (1992) Ligand-regulated internalization and recycling of human beta 2-adrenergic receptors between the plasma membrane and endosomes containing transferrin receptors. *The Journal of biological chemistry* **267**(5): 3530-3538.

- Wacker D, Stevens RC and Roth BL (2017a) How Ligands Illuminate GPCR Molecular Pharmacology. *Cell* **170**(3): 414-427.
- Wacker D, Wang S, McCorvy JD, Betz RM, Venkatakrishnan AJ, Levit A, Lansu K, Schools ZL, Che T, Nichols DE, Shoichet BK, Dror RO and Roth BL (2017b) Crystal Structure of an LSD-Bound Human Serotonin Receptor. *Cell* **168**(3): 377-389 e312.
- Wade SM, Lan K, Moore DJ and Neubig RR (2001) Inverse agonist activity at the alpha(2A)-adrenergic receptor. *Molecular pharmacology* **59**(3): 532-542.
- Wang JH, Shao XX, Hu MJ, Wei D, Liu YL, Xu ZG and Guo ZY (2017) A novel BRET-based binding assay for interaction studies of relaxin family peptide receptor 3 with its ligands. *Amino Acids* **49**(5): 895-903.
- Waters CM, Long J, Gorshkova I, Fujiwara Y, Connell M, Belmonte KE, Tigyi G, Natarajan V, Pyne S and Pyne NJ (2006) Cell migration activated by platelet-derived growth factor receptor is blocked by an inverse agonist of the sphingosine 1-phosphate receptor-1. *Faseb J* **20**(3): 509-511.
- Weber M, Ferrer M, Zheng W, Inglese J, Strulovici B and Kunapuli P (2004) A 1536-well cAMP assay for Gs- and Gi-coupled receptors using enzyme fragmentation complementation. *Assay Drug Dev Technol* **2**(1): 39-49.
- Wigdal SS, Anderson JL, Vidugiris GJ, Shultz J, Wood KV and Fan F (2008) A novel bioluminescent protease assay using engineered firefly luciferase. *Current chemical genomics* **2**: 16-28.
- Wild C, Cunningham KA and Zhou J (2014) Allosteric Modulation of G Protein-Coupled Receptors: An Emerging Approach of Drug Discovery. *Austin J Pharmacol Ther* **2**(1).
- Wootten D, Christopoulos A and Sexton PM (2013a) Emerging paradigms in GPCR allostery: implications for drug discovery. *Nat Rev Drug Discov* **12**(8): 630-644.
- Wootten D, Lindmark H, Kadmiel M, Willcockson H, Caron KM, Barwell J, Drmota T and Poyner DR (2013b) Receptor activity modifying proteins (RAMPs) interact with the VPAC2 receptor and CRF1 receptors and modulate their function. *Br J Pharmacol* **168**(4): 822-834.
- Wootten D, Miller LJ, Koole C, Christopoulos A and Sexton PM (2017) Allostery and Biased Agonism at Class B G Protein-Coupled Receptors. *Chem Rev* **117**(1): 111-138.
- Wright PT, Schobesberger S and Gorelik J (2015) Studying GPCR/cAMP pharmacology from the perspective of cellular structure. *Frontiers in pharmacology* **6**: 148.
- Wu B, Chien EY, Mol CD, Fenalti G, Liu W, Katritch V, Abagyan R, Brooun A, Wells P, Bi FC, Hamel DJ, Kuhn P, Handel TM, Cherezov V and Stevens RC (2010) Structures of the CXCR4 chemokine GPCR with small-molecule and cyclic peptide antagonists. *Science* **330**(6007): 1066-1071.
- Wu P and Brand L (1994) Resonance energy transfer: methods and applications. *Analytical biochemistry* **218**(1): 1-13.
- Wurdinger T, Badr C, Pike L, de Kleine R, Weissleder R, Breakefield XO and Tannous BA (2008) A secreted luciferase for ex vivo monitoring of in vivo processes. *Nature methods* **5**(2): 171-173.
- Xia H, Xie K and Zou G (2017) Advances in Spiropyran/Spirooxazines and Applications Based on Fluorescence Resonance Energy Transfer (FRET) with Fluorescent Materials. *Molecules* **22**(12).
- Xu TR, Ward RJ, Pediani JD and Milligan G (2012) Intramolecular fluorescence resonance energy transfer (FRET) sensors of the orexin OX1 and OX2 receptors identify slow kinetics of agonist activation. *The Journal of biological chemistry* **287**(18): 14937-14949.
- Xu Y, Piston DW and Johnson CH (1999) A bioluminescence resonance energy transfer (BRET) system: application to interacting circadian clock proteins. *Proceedings of the National Academy of Sciences of the United States of America* **96**(1): 151-156.
- Yang F, Yu X, Liu C, Qu CX, Gong Z, Liu HD, Li FH, Wang HM, He DF, Yi F, Song C, Tian CL, Xiao KH, Wang JY and Sun JP (2015) Phospho-selective mechanisms of arrestin conformations and functions revealed by unnatural amino acid incorporation and (19)F-NMR. *Nature communications* **6**: 8202.

- Yang L, Jackson E, Woerner BM, Perry A, Piwnica-Worms D and Rubin JB (2007) Blocking CXCR4-mediated cyclic AMP suppression inhibits brain tumor growth in vivo. *Cancer Res* **67**(2): 651-658.
- Yano H, Provasi D, Cai NS, Filizola M, Ferre S and Javitch JA (2017) Development of novel biosensors to study receptor-mediated activation of the G-protein alpha subunits Gs and Golf. *The Journal of biological chemistry* **292**(49): 19989-19998.
- Yao Z and Kobilka B (2005) Using synthetic lipids to stabilize purified beta2 adrenoceptor in detergent micelles. *Analytical biochemistry* **343**(2): 344-346.
- Ye S, Zaitseva E, Caltabiano G, Schertler GF, Sakmar TP, Deupi X and Vogel R (2010) Tracking G-protein-coupled receptor activation using genetically encoded infrared probes. *Nature* **464**(7293): 1386-1389.
- Yin H, Chu A, Li W, Wang B, Shelton F, Otero F, Nguyen DG, Caldwell JS and Chen YA (2009) Lipid G protein-coupled receptor ligand identification using beta-arrestin PathHunter assay. *The Journal of biological chemistry* **284**(18): 12328-12338.
- Zapata-Hommer O and Griesbeck O (2003) Efficiently folding and circularly permuted variants of the Sapphire mutant of GFP. *BMC Biotechnol* **3**: 5.
- Zhang H, Kang D, Huang B, Liu N, Zhao F, Zhan P and Liu X (2016) Discovery of non-peptide small molecular CXCR4 antagonists as anti-HIV agents: Recent advances and future opportunities. *Eur J Med Chem* **114**: 65-78.
- Zhang JH, Chung TD and Oldenburg KR (1999) A Simple Statistical Parameter for Use in Evaluation and Validation of High Throughput Screening Assays. *J Biomol Screen* **4**(2): 67-73.
- Zhang JH, Wu X and Sills MA (2005) Probing the primary screening efficiency by multiple replicate testing: a quantitative analysis of hit confirmation and false screening results of a biochemical assay. *J Biomol Screen* **10**(7): 695-704.
- Zhang R and Xie X (2012) Tools for GPCR drug discovery. *Acta Pharmacol Sin* **33**(3): 372-384.
- Zhang WB, Navenot JM, Haribabu B, Tamamura H, Hiramatsu K, Omagari A, Pei G, Manfredi JP, Fujii N, Broach JR and Peiper SC (2002) A point mutation that confers constitutive activity to CXCR4 reveals that T140 is an inverse agonist and that AMD3100 and ALX40-4C are weak partial agonists. *The Journal of biological chemistry* **277**(27): 24515-24521.
- Zhang WH, Otting G and Jackson CJ (2013a) Protein engineering with unnatural amino acids. *Curr Opin Struct Biol* **23**(4): 581-587.
- Zhang X, Tan F, Brovkovich V, Zhang Y and Skidgel RA (2011a) Cross-talk between carboxypeptidase M and the kinin B1 receptor mediates a new mode of G protein-coupled receptor signaling. *The Journal of biological chemistry* **286**(21): 18547-18561.
- Zhang X, Tan F and Skidgel RA (2013b) Carboxypeptidase M is a positive allosteric modulator of the kinin B1 receptor. *The Journal of biological chemistry* **288**(46): 33226-33240.
- Zhang X, Xiao Y and Qian X (2008) A ratiometric fluorescent probe based on FRET for imaging Hg<sup>2+</sup> ions in living cells. *Angew Chem Int Ed Engl* **47**(42): 8025-8029.
- Zhang Y, Sun B, Feng D, Hu H, Chu M, Qu Q, Tarrasch JT, Li S, Sun Kobilka T, Kobilka BK and Skiniotis G (2017) Cryo-EM structure of the activated GLP-1 receptor in complex with a G protein. *Nature* **546**(7657): 248-253.
- Zhang Z, Liu X, Morgan DA, Kuburas A, Thedens DR, Russo AF and Rahmouni K (2011b) Neuronal receptor activity-modifying protein 1 promotes energy expenditure in mice. *Diabetes* **60**(4): 1063-1071.
- Zhang Z, Winborn CS, Marquez de Prado B and Russo AF (2007) Sensitization of calcitonin gene-related peptide receptors by receptor activity-modifying protein-1 in the trigeminal ganglion. *J Neurosci* **27**(10): 2693-2703.
- Zhao X, Jones A, Olson KR, Peng K, Wehrman T, Park A, Mallari R, Nebalasca D, Young SW and Xiao SH (2008) A homogeneous enzyme fragment complementation-based beta-arrestin translocation

- assay for high-throughput screening of G-protein-coupled receptors. *J Biomol Screen* **13**(8): 737-747.
- Zhou X, Clister TL, Lowry PR, Seldin MM, Wong GW and Zhang J (2015) Dynamic Visualization of mTORC1 Activity in Living Cells. *Cell Rep.*
- Zhou XE, He Y, de Waal PW, Gao X, Kang Y, Van Eps N, Yin Y, Pal K, Goswami D, White TA, Barty A, Latorraca NR, Chapman HN, Hubbell WL, Dror RO, Stevens RC, Cherezov V, Gurevich VV, Griffin PR, Ernst OP, Melcher K and Xu HE (2017a) Identification of Phosphorylation Codes for Arrestin Recruitment by G Protein-Coupled Receptors. *Cell* **170**(3): 457-469 e413.
- Zhou XE, Melcher K and Xu HE (2012) Structure and activation of rhodopsin. *Acta Pharmacol Sin* **33**(3): 291-299.
- Zhou XE, Melcher K and Xu HE (2017b) Understanding the GPCR biased signaling through G protein and arrestin complex structures. *Curr Opin Struct Biol* **45**: 150-159.
- Ziegler N, Batz J, Zabel U, Lohse MJ and Hoffmann C (2011) FRET-based sensors for the human M1-, M3-, and M5-acetylcholine receptors. *Bioorganic & medicinal chemistry* **19**(3): 1048-1054.
- Zimmermann T, Rietdorf J, Girod A, Georget V and Pepperkok R (2002) Spectral imaging and linear unmixing enables improved FRET efficiency with a novel GFP2-YFP FRET pair. *FEBS Lett* **531**(2): 245-249.
- Zurn A, Klenk C, Zabel U, Reiner S, Lohse MJ and Hoffmann C (2010) Site-specific, orthogonal labeling of proteins in intact cells with two small biarsenical fluorophores. *Bioconjug Chem* **21**(5): 853-859.
- Zurn A, Zabel U, Vilardaga JP, Schindelin H, Lohse MJ and Hoffmann C (2009) Fluorescence Resonance Energy Transfer Analysis of alpha(2a)-Adrenergic Receptor Activation Reveals Distinct Agonist-Specific Conformational Changes. *Molecular pharmacology* **75**(3): 534-541.
- Zwier JM, Roux T, Cottet M, Durroux T, Douzon S, Bdioui S, Gregor N, Bourrier E, Oueslati N, Nicolas L, Tinel N, Boisseau C, Yverneau P, Charrier-Savournin F, Fink M and Trinquet E (2010) A fluorescent ligand-binding alternative using Tag-lite(R) technology. *J Biomol Screen* **15**(10): 1248-1259.

## **10. Curriculum vitae**

**Name:**

**Date of Birth:**

**Place of Birth:**

**Nationality:**

**Current address:**

**Email address:**

**Current position:**

**Location:**

**Title of PhD thesis:**

**Supervisors:**

**Academic Background:**

**Internships:**

**Language skills:**

**Publications:**

**Oral presentations at international symposia:**

**Poster presentations at international symposia:**

Date and signature

## 11. Acknowledgements

First, I would like to thank my supervisor, Prof. Dr. Martin J. Lohse, for giving me the opportunity to complete my doctoral studies in such excellent research environment. Our scientific discussions have always been of immense value and his outstanding pharmacological experience, as well as his precious strategic advices helped a lot, especially with the preparation of the publication. During the course of my PhD, I had the chance to participate in three lab retreats hosted by Prof. Lohse and learned how inspiring and motivating such intense scientific exchange in a rather isolated location can be.

Secondly, a huge thank is addressed to Dr. Isabella Maiellaro who was always available for any kind of scientific but also personal support. Under her guidance, I learned to plan and conduct experiments in the most efficient way and to develop a critical and analytical attitude in the interpretation of the results. Even when we held different views in a discussion, we could build on a strong respectful and amicable basis and these conversations became an indispensable practice to learn how to defend my ideas with scientific reasoning.

A special thank you goes to Prof. Dr. Michael Decker for being my second supervisor and for the valuable discussions and experiences we shared during the terrific meetings within the retreats of the international doctorate program "Receptor Dynamics" of the Elite Network of Bavaria.

I want to thank Prof. Dr. Michel Bouvier who also agreed on being part of my thesis committee. Our meeting during the Gordon conference and the subsequent close co-operation in the preparation of our manuscripts were of great help and fastened the whole process.

I want to thank all members of the AG Lohse. In particular, Dr. Sylvie Vandenabeele, who lightened my workload and often served as great reviewer of my english drafts. Furthermore, Dr. Ulrike Zabel and Monika Frank who cloned many of the DNA constructs and allowed me to focus on their experimental testing. Jan Möller, Eugene Grushevskiy, Selma Anton and Ali Isbilir joined the lab shortly after my start of the PhD and they showed me how much easier everything can be when you have friends around you – I am very grateful for this, lab sister and lab bros!

Further thanks go to the staff of the Institute of Pharmacology and Toxicology. Here, I would like to emphasize Christine Salomon who always helped in organizational issues, Nicole Ziegler for her continuous support when I needed exotic consumables, Nadine Yurdagül-Hemmrich for teaching me western blots and Annette Hannawacker who helped me out when my cells did not survive the weekend.

Zu guter Letzt möchte ich mich bei den Menschen bedanken, ohne die diese Arbeit niemals möglich gewesen wäre – meiner Familie in Deutschland und Israel und meiner Partnerin Christina. Ihr habt mich durch diese spannende aber auch sehr herausfordernde Phase meines Lebens begleitet und es gibt für mich kein erfüllenderes Gefühl als euch stolz zu sehen!

اخيراً وليس آخراً يوجب عليّ الإعتراف بالفضل أن أشكر الأشخاص الذين ولولا فضلهم عليّ لعجزت عن إنجاز هذا الهدف.  
شكر خاص لعائلتي الشهمه في إسرائيل وعلى رأسهم جدّتي الحبيبة  
سهام توفيق شحاده.

والشكر الحار لعائلتي في ألمانيا وعلى رأسهم جدّتي

Ilse Hänsch

وكذلك جزيل شكري لشريكة حياتي الحبيبه

Christina Hanfland

لقد كُنتم لي سنداً قوياً ودعماً عظيماً طوال مسيرتي هذه نحو النموّ الفكريّ والمعرفيّ.  
إنها كانت فترة مليئة بالعلم والتشويق والتحدّيات.

لا يمكنني أن أتصوّر شعوراً، يضاهي ذلك الذي يملأ قلبي سعادةً، حين أراكم فخورين بي وبإنجازاتي في هذه الحياة المُزيّنه  
بوجودكم.

دمتم ودامت المحبّة في ربوع هذه العائلة الوفورة.